

## **Copyright Warning & Restrictions**

The copyright law of the United States (Title 17, United States Code) governs the making of photocopies or other reproductions of copyrighted material.

Under certain conditions specified in the law, libraries and archives are authorized to furnish a photocopy or other reproduction. One of these specified conditions is that the photocopy or reproduction is not to be “used for any purpose other than private study, scholarship, or research.” If a user makes a request for, or later uses, a photocopy or reproduction for purposes in excess of “fair use” that user may be liable for copyright infringement,

This institution reserves the right to refuse to accept a copying order if, in its judgment, fulfillment of the order would involve violation of copyright law.

**Please Note: The author retains the copyright while the New Jersey Institute of Technology reserves the right to distribute this thesis or dissertation**

Printing note: If you do not wish to print this page, then select “Pages from: first page # to: last page #” on the print dialog screen

The Van Houten library has removed some of the personal information and all signatures from the approval page and biographical sketches of theses and dissertations in order to protect the identity of NJIT graduates and faculty.

## **ABSTRACT**

### **INFLUENCE OF MATERIAL PROPERTIES ON GRANULES PREPARED BY DRY CO-ROTATING TWIN SCREW EXTRUSION AND COUNTER- ROTATING BATCH MIXING**

**by  
Afstathios Steve Pafiakis**

Recently, the pharmaceutical industry has shown interest in continuous granulating technology because of the flexibility it offers as an option that bypasses the costly scale-up process associated with batch manufacturing. However, the granulation mechanism(s) using twin screw co-rotating hot melt extrusion (HME) has not been fully explored, and it is not yet well understood. This leads to costly experiments during development and process reliability problem in commercial manufacturing. The main objective of this dissertation is to increase the mechanistic understanding of the twin screw granulation process of systems containing an active pharmaceutical ingredient (API) and a polymer excipient. This is accomplished by demonstrating that the onset of granule growth is driven by frictional energy dissipation (FED) and plastic energy dissipation (PED); where FED is the dominating mechanism for granule growth. The work presented here demonstrates how these mechanisms manifest in the evolving and resulting granule structure.

The highlights of this dissertation can be categorized into the following parts:

(i) A proof of concept analysis that looks at the morphological evolution of granules formed inside the extruder, specifically across the kneading zone. (ii) A comprehensive understanding of how PED and FED are influenced by the input material properties and the set-up of the extruder and how these interactions manifest themselves through system

responses and granule growth. And finally, (iii) an understanding that PED and FED are predominantly responsible for the onset of granulation in batch mixing studies.

For the first part, a proof-of-concept trial is explored with a prototype formulation containing approximately 65% (w/w) theophylline and hydroxypropylcellulose (HPC) MF (35% w/w). Granule carcasses collected across the kneading zone reveals the onset of granulation and the morphological differences within the granule, indicating that interacting material properties are playing a part in the granule ensemble processes.

Four blends are prepared to investigate how fine API (micronized theophylline) interacts with a coarse polymer (HPC MF), how coarse API (theophylline) interacts with a fine polymer (HPC EXF), and the effects when both components in the blend are fine and coarse. When each formulation is granulated, the torque, product temperature, and particle size are found to be strongly dependent on heating temperature, screw speed, screw design and, ultimately, the input material properties.

Finally, to elucidate the effects from just the input material, the four formulations are granulated under controlled conditions, in a batch mixer, at room temperature. This provides a “*time-dilating*” effect where the granulation process happened in order of minutes vs. seconds as observed in the extruder. The product temperature and torque traces vary for all four formulations, evident that PED and FED are a function of the formulation. The formulations with theophylline reach the maximum torque limit approximately twice as fast as the formulations containing the micronized theophylline. Particle size growth and rate of densification is also different between all the formulations. All observations correlate that the following input material properties: particle size, cohesion, inter-particle coefficient of friction,  $f$ , influence the ensemble and structure of the granules.

**INFLUENCE OF MATERIAL PROPERTIES ON GRANULES PREPARED BY  
DRY CO-ROTATING TWIN SCREW EXTRUSION AND COUNTER-  
ROTATING BATCH MIXING**

**by  
Afstathios Steve Pafiakis**

**A Dissertation  
Submitted to the Faculty of  
New Jersey Institute of Technology  
In Partial Fulfillment of the Requirements for the Degree of  
Doctor of Philosophy in Materials Science and Engineering  
Interdisciplinary Program in Materials Science and Engineering**

**May 2023**

Copyright © 2023 by Afstathios Steve Pafiakis

ALL RIGHTS RESERVED

**APPROVAL PAGE**

**INFLUENCE OF MATERIAL PROPERTIES ON GRANULES PREPARED BY  
DRY CO-ROTATING TWIN SCREW EXTRUSION AND COUNTER -  
ROTATING BATCH MIXING**

**Afstathios Steve Pafiakis**

DocuSigned by:  
March 28, 2023  
Dr. Piero M. Armenante, Dissertation Co-Advisor Date  
Distinguished Professor of Chemical and Materials Engineering, NJIT

DocuSigned by:  
March 31, 2023  
Dr. Costas G. Gogos, Dissertation Co-Advisor Date  
Distinguished Research Professor of Chemical and Materials Engineering, NJIT

DocuSigned by:  
March 31, 2023  
Dr. Nuggenalli M. Ravindra, Committee Member Date  
Professor of Physics, NJIT

DocuSigned by:  
03/31/2023  
Dr. Nikolaos Ioannidis, Committee Member Date  
Director of the Technology Advancement and Retention Center Pilot Process  
Development Facility, Polymer Processing Institute Fairfield, NJ

DocuSigned by:  
3/31/2023  
Dr. Keun Hyuk Ahn, Committee Member Date  
Associate Professor of Physics, NJIT

DocuSigned by:  
3/31/2023  
Dr. Munir Hussain, Committee Member Date  
Retired Distinguished Research Fellow in Drug Product Science and Technology  
Formulation Development, Bristol Myers Squibb New Brunswick, NJ

## BIOGRAPHICAL SKETCH

**Author:** Afstathios Steve Pafiakis

**Degree:** Doctor of Philosophy

**Date:** May 2023

### **Undergraduate and Graduate Education:**

- Doctor of Philosophy in Materials Science and Engineering  
New Jersey Institute of Technology, Newark, NJ, 2023
- Master of Science in Chemical Engineering  
New Jersey Institute of Technology, Newark, NJ, 2012
- Bachelor of Science in Chemical Engineering  
New Jersey Institute of Technology, Newark, NJ, 2004

**Major:** Materials Science and Engineering

### **Presentations and Publications:**

#### **Peer-reviewed Journals:**

Pafiakis A, Armenante PM, Gogos C. 2022. The influence of input material properties on hot melt granules prepared using a counter-rotating batch mixer, *Pharmaceutical Development and Technology* **27**(9):1-17.

Pandey P, Levins C, Pafiakis S, Zacour B, Bindra DS, Trinh J, Buckley D, Gour S, Sharif S, and Stamato S. 2016. Enhancing tablet disintegration characteristics of a highly water-soluble high-drug-loading formulation by granulation process. *Pharmaceutical Development and Technology* **23**(6):587-595.

#### **Conference Presentation:**

Pafiakis S, Twin Screw Granulation: A Case Study for Enabling an Adaptive Study Plan, American Association of Pharmaceutical Scientist (AAPS) Annual Meeting and Exposition; Denver, CO. November; 2016.



### **Conference Posters:**

Pafiakis S, Jones J, Escotet M, Ioannidis N, Chan S, Won B, Macias K, Keluskar R, Martin K, Trinh J, Remy J, Peng C, Levins C, Stamato H, and Gogos C. Investigation of a suitable lubricant for increasing slip in a continuous, co-rotating twin screw dry granulation process. American Institute of Chemical Engineers (AIChE), Salt Lake City, UT. November 2015

Pafiakis S, Wolfe S, Choi C, Pan D, Xu Y, Mathias N, Saari A, Hemenway J, and Narang A. Formulation and process strategies for preventing form conversion in wet granulation: *A case study*. American Association of Pharmaceutical Scientists (AAPS), San Antonio, TX. November 2013

*For my loving wife, Melissa,  
my dearest children,  
Evangeline and Ioannis,  
and my parents,  
Ioannis and Stavroula*

“If it weren't for the last minute, nothing would get done.”

*Rita Mae Brown*

## ACKNOWLEDGMENT

I would like to begin by thanking my advisors, Professors Piero Armenante and Costas Gogos. It has been an honor and a privilege to work with them both. They have supported my goal, that felt very unrealistic at times, of completing my PhD as a part time student. I appreciate the long days discussing fundamentals and experimental plans, especially when things did not go as planned.

Dr. Armenante has shown me unwavering support throughout my time at NJIT, ever since I was an undergraduate student. Professor Armenante always gave me advice and guidance. I greatly value his honesty, directness, and his attention to detail. I appreciate the countless hours he spent helping me solve practice problems when I was preparing for the qualifier exams; he was always available whenever I needed him. He was a great mentor throughout this journey.

Dr. Gogos welcomed me into the Polymer Processing Institute (PPI) family without hesitation. Professor Gogos helped me visualize the mechanisms discussed in this dissertation. The life lessons that I will take away from Professor Gogos are priceless, and I will always remember and cherish my favorite quote of all, that, “life is long!”

I thank all the committee members, Professor Nuggehalli M Ravindra, Professor Keun Hyuk Ahn, Dr. Nikolaos Ioannidis, and Dr. Munir Hussain, for all their time, patience, guidance, and feedback.

I also owe a very big thank you to Ms. Clarisa Gonzalez-Lenahan and Mr. David Tress from Graduate Studies. They were both there every step of the way answering questions. Ms. Clarisa was there to give me that extra nudge to keep working. Thank you so much for everything, Ms. Gonzalez!

There were so many people who helped me along the way. Completing this work really did take, “*a village!*” This dissertation was partially funded by my employer, Bristol Myers Squibb. I could not have completed this work without the support of my current and previous managers, Mr. Neil Martin, Dr. Ann-Marie Fanning, Dr. Sherif Badawy, Mr. Howard Stamato, Dr. Peter Timmins, Dr. Jatin Patel, Mr. Brian Boland, and Dr. Manisha Desai, who accepted me into the Tuition Reimbursement Program and continued to support me over the duration of this research.

I would like to thank the entire PPI staff for their assistance and for making it a great place to work; they truly are like family. I would like to especially thank Dr. Ming-Wan Young, for granting access to the equipment. Dr. Zohar Ophir who helped me brainstorm along the way. I mostly want to thank Dr. Herman Suwardie, Ms. Prarthana Manoj Rajai, Dr. Chunmeng Lu, Ms. Georgia Stavrakis, and Ms. Arisleidy Reyes Castillo; their contribution were instrumental to the completion of this work.

I give my sincere gratitude to my fellow colleagues at Bristol Myers Squibb who engaged in several discussions and assistance with this work. Ms. Mary Bullock for helping me procure the materials needed for this research. Mr. Neil Martin, Mr. Thomas Carragher, Ms. Jade Trinh, Mr. Kyle Martin, Dr. Yue Schuman, Mr. Dipak Naik, Ms. Helen Hughes, Ms. Ge. Zhang, Mr. Brian Breza, Mr. Michael Chiti, Mr. Zygmund Rodzajewski, Mr. Arthur DiBenedetto, Mr. Xavier Odihirin and Mr. Sanjaykumar Patel for helping me set up equipment and run experiments at the Bristol Myers Squibb facilities in New Brunswick.

Dr. Kurt Seefeldt, Dr. Brian Zacour, Mr. Jonathan Schleifer, Dr. Kevin Macias, Dr. Keirnan LaMarche, Dr. Madhavi Srikoti, Mr. Scott Jennings, Dr. Christopher Zordan, Mrs.

Elizabeth Galella, Dr. Michelle Case, Mr. John Fiske, Mr. John Gawel, and Dr. John Gamble who all took the time to hear my plans, contributed to the design of several experiments, and reviewed my writing.

I am very grateful to the staff at American-Leistritz in Somerville, NJ. To Mr. Charlie Martin, Mr. Stuart Kapp, and Mr. Augie Machado for their hospitality and support, engaging in several technical discussions throughout this entire dissertation as well as letting me use their facility to support studies. I would like to thank Mr. Brian Height for taking time to help me execute several trials in a short time frame.

I would like to also thank Mr. Mitchel Perlstein from Horiba, who invited me to use the CamSizer to measure the particle size data presented in this work. A big thank you goes to Dr. Gert Beckmann, and Ms. Kate Wamsley for helping me run the particle size samples at Verder Scientific Inc.

I thank Dr. Bryan Ennis and his team at PowderNotes who helped with the iShear: Powder Flow Rheometer. Dr. Naseem Jibrin and Dr. Benjamin Ennis who took time out of their schedule to brainstorm experiments with me throughout the execution of this body of work.

I thank my friends, Mr. Steven Miller, Mr. Michael Linderman, Mrs. Joanna Mirsky, Dr. Andrew Illot, Dr. Anuji Abraham, Dr. Thiago Carvalho, Dr. Simone Carvalho, and Mr. John Fiske for all their support throughout this journey.

I also want to thank my family, my parents, Mr. Ioannis, and Mrs. Stavroula Pafiakis, who helped me build a strong work ethic from a young age. They are the hardest working people I know and a perfect example of what perseverance and dedication looks like. I thank my sister, Mrs. Tammy Moore, and brother-in-law Mr. Jason Moore; my aunt

and uncle Mrs. Eleni and Mr. Aristides Manolas; and the best cousins anyone could ever ask for, Mr. Nick Manolas; Mr. Foti, and his wife, Mrs. Jaclyn Manolas; and Mr. Cristos, and his wife, Mrs. Deanna Manolas. I thank everyone for their words of inspiration and reassurance that I could complete this work. I truly appreciate everyone's support.

I'm forever thankful to my wife, Melissa Pafiakis, for her constant unwavering support, patience, and words of encouragement. She had more confidence that I could complete this work than I did. This PhD is as much hers as it is mine. We spent countless hours talking through the different heating mechanisms and reviewing data, proofreading manuscripts, and updating slides. Melissa is my rock, my heart, my soul. Then there's "*KID KREW*" - my children, Evangeline, and Ioannis "Jack" Pafiakis, my best buddies in the whole world, without whom life would be meaningless. There were so many memorable moments. My daughter drew me a heat exchanger to help me visualize material getting hot at the mixing blocks. I remember explaining the concept of "*glue points*" formed by the heated polymer to my son. When I showed him the picture he exclaimed, "It looks like Venom!"

Finally, I want to thank one of my best friends, he was practically my brother, Smokey my cat. I had Smokey for 19 years. Smokey spent long hours keeping me company while I studied or did homework throughout graduate school. During the last few days, before submitting this dissertation, Smokey fell sick and passed away. I wish he was around for when I completed this work. "Thanks for the company all those nights. You will be missed brother!"

## TABLE OF CONTENTS

Chapter	Page
1 INTRODUCTION.....	1
2 LITERATURE REVIEW.....	6
2.1 Traditional Pharmaceutical Granulation Processes.....	6
2.1.1 Wet and dry granulation granulation.....	6
2.2 Mechanism of Interparticle Interaction .....	8
2.2.1 Shear cell.....	9
2.3 Twin Screw Co-Rotating Extruder.....	12
2.4 Description of the Hot Melt Extrusion Process and Mechanisms.....	14
2.5 Description of the Twin Screw Granulation Process and Proposed Mechanisms.....	17
2.5.1 Sintering.....	18
2.5.2 Mixing.....	22
2.5.3 Heating and melting mechanism.....	26
3 EXPERIMENTAL.....	33
3.1 Materials.....	33
3.1.1 Active Pharmaceutical Ingredient (API): micronized and non-micronized theophylline (THF).....	33
3.1.2 Polymers: hydroxypropylcellulose (HPC) MF and EXF.....	34

**TABLE OF CONTENTS**  
**(Continued)**

<b>Chapter</b>	<b>Page</b>
3.2 Sample Preparation.....	36
3.2.1 Preparation of theophylline and hydroxypropylcellulose blends for twin screw granulation .....	36
3.2.2 Preparation of theophylline and hydroxypropylcellulose blends for iShear™ powder flow analysis .....	38
3.2.3 Preparation of theophylline and hydroxypropylcellulose granules.....	39
3.3 Material Characterization.....	44
3.3.1 Bulk and tap density.....	44
3.3.2 Particle size distribution.....	44
3.3.3 iShear™: powder flow rheometer.....	45
3.3.4 Thermogravimetric analysis (TGA).....	45
3.3.5 Modulated Differential Scanning Calorimetry (MDSC).....	45
3.3.6 Dynamic Mechanical Thermal Analysis (DMTA).....	46
3.3.7 Scan Electron Microscope (SEM).....	46
3.3.8 Mercury Intrusion Porosimetry (MIP).....	47
3.3.9 CT X-Ray tomography.....	47
3.3.10 Thermal imaging.....	48
4 RESULTS AND DISCUSSION.....	49



**TABLE OF CONTENTS**  
**(Continued)**

<b>Chapter</b>	<b>Page</b>
4.1 Physical Properties.....	49
4.1.1 Hydroxypropylcellulose (HPC) MF and EXF.....	49
4.1.2 API: micronized and non-micronized theophylline.....	53
4.1.3 Theophylline and hydroxypropylcellulose blends.....	56
4.2 Twin Screw Granulation of Theophylline (THF) and Hydroxypropylcellulose (HPC) Blends.....	63
4.2.1 Granule analysis using the 30 mm Twin Screw Mixing Element Evaluator (TSMEE).....	63
4.2.2 Parametric effects using three 5 mm kneading blocks to granulate in a 27 mm co-rotating twin screw extruder.....	75
4.3 iShear™ Powder Flow Analysis: Mechanical Powder Properties Assessment.....	109
4.3.1 Hydroxypropylcellulose (HPC) MF and EXF.....	110
4.3.2 Micronized and non-micronized theophylline.....	113
4.3.3 Theophylline: hydroxypropylcellulose blends.....	116
4.4 Brabender: Mixing Process Monitoring.....	120
4.4.1 Granulating near room temperature using the Brabender: hot melt batch mixer .....	124
4.4.2 Granulation of Micronized Theophylline (MTHF) blends with Hydroxypropylcellulose MF (HPC MF) and Hydroxypropylcellulose EXF (HPC EXF).....	125

**TABLE OF CONTENTS**  
**(Continued)**

<b>Chapter</b>	<b>Page</b>
4.4.3 Granulation of Theophylline (THF) blends with Hydroxypropylcellulose MF (HPC MF) and Hydroxypropylcellulose EXF (HPC EXF).....	140
4.5 Thermal Analysis: Effect of Material Properties on Calorimetry and Polymer Rheology.....	152
4.5.1 Modulated Differential Scanning Calorimetry (MDSC) on micronized and non-micronized Theophylline (THF) and Hydroxypropylcellulose (HPC) raw materials and blends.....	152
4.5.2 Dynamic Mechanical Thermal Analysis (DMTA) for Hydroxypropylcellulose (HPC) MF and EXF.....	157
5 CONCLUDING REMARKS.....	160
5.1 Summary.....	160
5.2 Suggested Future Work .....	163
5.2.1 Real-time measurement of heat (FED) generation during batch mixing.....	163
5.2.2 Thermal shear cell experiments.....	163
5.2.3 Controlled deformation studies.....	164
5.2.4 Downstream processing of resulting granules.....	164
APPENDIX A BULK AND TAP DENSITY.....	166
APPENDIX B PARTICLE SIZE ANALYSES.....	167
APPENDIX C CONVEYING AND KNEADING BLOCK NOMANCLATURE FOR THE 27 mm CO-ROTATING TWIN SCREW EXTRUDER.....	179

**TABLE OF CONTENTS**  
**(Continued)**

<b>Chapter</b>	<b>Page</b>
APPENDIX D iShear™: POWEDER FLOW RHEOMETER REPORTS.....	183
APPENDIX E MERCURY INTRUSION POROSIMETERY: SUMMARY TABLES.....	188
REFERENCES.....	193

## LIST OF TABLES

Table	Page
2.1	Examples of Drug Products Manufactured by the TSG and HME Process..... 15
3.1	Summary of Selected Properties of Theophylline..... 34
3.2	Summary of Selected Properties of Hydroxypropylcellulose..... 35
3.3	Morphology and Formulation Composition for iShear Analysis..... 38
3.4	Distributive Screw Design Evaluated During 27 mm Leistritz Experiments... 41
4.1	30 mm Twin Screw Mixing Element Evaluator (TSMEE) System Parameters..... 63
4.2	Design of Experiments Used for 27 mm Parametric Study..... 76
4.3	Two Dispersive Kneading Zones Screw Design Evaluated During 27 mm Leistritz Experiments..... 79
4.4	Summary of System Responses for 70:30 Micronized Theophylline (MTHF): Hydroxypropylcellulose MF (HPC MF)..... 84
4.5	Summary of System Responses for 70:30 Micronized Theophylline (MTHF): Hydroxypropylcellulose EXF (HPC EXF)..... 91
4.6	Summary of System Responses for 70:30 Theophylline (THF): Hydroxypropylcellulose MF (HPC MF)..... 97
4.7	Summary of System Responses for 70:30 Theophylline (THF): Hydroxypropylcellulose EXF (HPC EXF)..... 103
4.8	Range of Different Flowability Levels, Flowability Classification for Flow Function Coefficient ( $ffc$ )..... 109
4.9	Range of Different Flowability Levels, Flowability Classification for Relative Flow Index (RFI)..... 110
4.10	Range of Different Flowability Classification for $ffc$ and RFI for Hydroxypropylcellulose MF (HPC MF) and Hydroxypropylcellulose EXF (HPC EXF)..... 112

**LIST OF TABLES**  
**(Continued)**

<b>Table</b>	<b>Page</b>
4.11 Range of Different Flowability Classification for $ffc$ and RFI for Micronized Theophylline (MTHF) and Theophylline (THF).....	115
4.12 Range of Different Flowability Levels, Flowability Classification for $ffc$ and RFI for Formulations Containing Hydroxypropylcellulose MF (HPC MF).....	118
4.13 Range of Different Flowability Levels, Flowability Classification for $ffc$ and RFI for Formulations Containing Hydroxypropylcellulose EXF (HPC EXF)...	119
4.14 Suggested Onset and Significant Granule Growth Across all Formulations is Occurring Within the Ranges of the Endothermic Event Observed for Hydroxypropylcellulose MF (HPC MF) (Coarse Polymer) and Hydroxypropylcellulose EXF (HPC EXF) (Fine Polymer).....	152
4.15 Estimated Endothermic Event Measured by MDSC for: (a) 70% Theophylline: 30% Hydroxypropylcellulose MF (HPC MF); (b) 70% Theophylline: 30% Hydroxypropylcellulose EXF (HPC EXF) (Fine Polymer); (c) 70% Micronized Theophylline: 30% Hydroxypropylcellulose MF (HPC MF); (d) 70% Micronized Theophylline: 30% Hydroxypropylcellulose MF (HPC MF).....	155
4.16 Estimated Endothermic Event Measured by MDSC for (a) As-is Hydroxypropylcellulose MF (HPC MF); (b) Dried Hydroxypropylcellulose MF (HPC MF); (c) As-is Hydroxypropylcellulose EXF (HPC EXF); (d) Dried Hydroxypropylcellulose EXF (HPC EXF).....	157
A.1 Bulk and Tap Density of Raw Material.....	166
A.2 Bulk and Tap Density of Theophylline Blends.....	166
B.1 CamSizer Data for Hydroxypropylcellulose MF (HPC MF).....	168
B.2 CamSizer Data for Hydroxypropylcellulose EXF (HPC EXF).....	169
B.3 CamSizer Data for Micronized Theophylline (MTHF).....	170
B.4 CamSizer Data for Theophylline (THF).....	171

**LIST OF TABLES**  
**(Continued)**

<b>Table</b>	<b>Page</b>
B.5 CamSizer Data for 70% Micronized Theophylline (MTHF) and 30% Hydroxypropylcellulose EXF (HPC EXF).....	172
B.6 CamSizer Data for 70% Micronized Theophylline (MTHF) and 30% Hydroxypropylcellulose MF (HPC MF).....	173
B.7 CamSizer Data for 70% Theophylline (THF) and 30% Hydroxypropylcellulose MF (HPC MF).....	174
B.8 CamSizer Data for 70% Theophylline (THF) and 30% Hydroxypropylcellulose EXF (HPC EXF) .....	175
B.9 Sieve Analysis Data for 70% Micronized Theophylline (MTHF) and 30% Hydroxypropylcellulose EXF (HPC EXF).....	176
B.10 Sieve Analysis Data for 70% Micronized Theophylline (MTHF) and 30% Hydroxypropylcellulose MF (HPC MF).....	177
B.11 Sieve Analysis Data for 70% Theophylline (THF) and 30% Hydroxypropylcellulose MF (HPC MF).....	177
B.12 Sieve Analysis Data for 70% Theophylline (THF) and 30% Hydroxypropylcellulose EXF (HPC EXF).....	178
D.1 iShear Data for Theophylline (THF): Hydroxypropylcellulose EXF (HPC EXF).....	184
D.2 iShear Data for Theophylline (THF): Hydroxypropylcellulose MF (HPC MF).....	185
D.3 iShear Data for Micronized Theophylline (MTHF): Hydroxypropylcellulose EXF (HPC EXF).....	186
D.4 iShear Data for Micronized Theophylline (MTHF): Hydroxypropylcellulose MF (HPC MF).....	187
E.1 Mercury Intrusion Data Summary for Raw Materials.....	188

**LIST OF TABLES**  
**(Continued)**

<b>Table</b>	<b>Page</b>
E.2 Mercury Intrusion Data Summary for Theophylline and Hydroxypropylcellulose Blends Prior to Batch Mixing (t=0).....	189
E.3 Mercury Intrusion Data Summary for Applicable Theophylline and Hydroxypropylcellulose Blends at t=0.30 sec.....	189
E.4 Mercury Intrusion Data Summary for Applicable Theophylline and Hydroxypropylcellulose Blends at t=1 min.....	190
E.5 Mercury Intrusion Data Summary for Applicable Theophylline and Hydroxypropylcellulose Blends at t=1.5 min.....	190
E.6 Mercury Intrusion Data Summary for Applicable Theophylline and Hydroxypropylcellulose Blends at t=2 min.....	191
E.7 Mercury Intrusion Data Summary for Applicable Theophylline and Hydroxypropylcellulose Blends at t=3 min.....	191
E.8 Mercury Intrusion Data Summary for Applicable Theophylline and Hydroxypropylcellulose Blends at t=4 min.....	192
E.9 Mercury Intrusion Data Summary for Applicable Theophylline and Hydroxypropylcellulose Blends at t=5 min.....	192

## LIST OF FIGURES

<b>Figure</b>	<b>Page</b>
2.1 Basic diagram of a high shear wet granulation process.....	7
2.2 Basic diagram of a fluid bed granulation process.....	7
2.3 Basic diagram of a roller compaction dry granulation process.....	8
2.4 Schematic of an iShear™ powder flow rheometer and normal force applied to a powder sample equipped for shear cell testing.....	10
2.5 Example of time series profile for normal force, shear, and density of hydroxypropylcellulose MF from the iShear™ powder flow rheometer.....	10
2.6 Yield loci for consolidated bulk material derived from Mohr circle.....	12
2.7 Intermeshing co-rotating twin screw extruder: 27mm Leistritz extruder.....	13
2.8 Schematic representation of the dissolution mechanism of an API during the HME process carried out at a temperature above the melting point of the API.	16
2.9 Illustration of sintering.....	19
2.10 Schematic representation of the melt granulation using a Co-TSE process.....	19
2.11 Illustration of a particulate cluster of API and “tacky” polymer created via glue points.....	20
2.12 Unconfined compression stress–strain curves and experimentally measured temperature increase $\Delta T_a$ as a function of strain for PS (Dow 685), LDPE (Dow 640), and Soluplus (BASF).....	21
2.13 Schematic representation of random distributive mixing (e.g., a process takes place in a V-blender).....	22
2.14 Illustrating dispersive and distributive kneading elements.....	23
2.15 Schematic representation of striation thickness reduction by stretching and folding a.k.a extensional/ elongation flows.....	24
2.16 Evolution of free-flowing blend to a solid’s rich suspension.....	27



**LIST OF FIGURES**  
**(Continued)**

<b>Figure</b>	<b>Page</b>
2.17 Cross section of the mixing chamber of a Farrel continuous mixer (FCM), illustrating the regions where deformation and flow patterns that lead to melting and mixing.....	29
2.18 Representation of particle-particle interaction under pressure for an ideal, smooth system. and an interlocked, abrasive system under relentless deformation.....	31
3.1 Chemical structure of theophylline.....	33
3.2 Chemical structure of hydroxypropylcellulose.....	34
3.3 Process flow diagram for preparing theophylline: hydroxypropylcellulose blends for twin screw granulation.....	37
3.4 Screw configuration used for 27 mm ZSE Maxx experiments. The mixing zone is comprised of three 5 mm kneading blocks.....	42
3.5 Brabender batch mixer frontal view of all components and mixing screws.....	43
4.1 Particle size distribution of neat hydroxypropylcellulose MF (HPC MF) with a $D_{10}=99.5 \mu\text{m}$ , $D_{50}=306.3 \mu\text{m}$ , and a $D_{90}=599.0 \mu\text{m}$ .....	50
4.2 Particle size distribution of neat hydroxypropylcellulose EXF (HPC EXF) with a $D_{10}=16.1 \mu\text{m}$ , $D_{50}=45.8 \mu\text{m}$ , and a $D_{90}=86.25 \mu\text{m}$ .....	50
4.3 Bulk and tap density of hydroxypropylcellulose MF (HPC MF) and hydroxypropylcellulose EXF (HPC EXF).....	51
4.4 Microscopy image comparison of hydroxypropylcellulose MF (HPC MF) and hydroxypropylcellulose EXF (HPC EXF) at 20x magnification.....	52
4.5 SEM image comparison of hydroxypropylcellulose MF (HPC MF) and hydroxypropylcellulose EXF (HPC EXF).....	52
4.6 Particle size distribution of neat, micronized theophylline (MTHF) with a $D_{10}=3.5 \mu\text{m}$ , $D_{50}=7.0 \mu\text{m}$ , and a $D_{90}=13.9 \mu\text{m}$ .....	53
4.7 Particle size distribution of neat, theophylline 325M (THF) with a $D_{10}=6.3 \mu\text{m}$ , $D_{50}=15.5 \mu\text{m}$ , and a $D_{90}=28.6 \mu\text{m}$ .....	54

**LIST OF FIGURES**  
**(Continued)**

<b>Figure</b>	<b>Page</b>
4.8 Bulk and tap density of micronized and non-micronized theophylline.....	55
4.9 Microscopy image comparison of theophylline 325M (THF) and micronized theophylline (MTHF) at 20x magnification.....	55
4.10 SEM image comparison of theophylline 325M (THF) and micronized theophylline (MTHF).....	56
4.11 Particle size distribution of 70:30 micronized theophylline (MTHF) blended with hydroxypropylcellulose EXF (HPC EXF) with a $D_{10}=4.0\ \mu\text{m}$ , $D_{50}=9.5\ \mu\text{m}$ , and a $D_{90}=76.5\ \mu\text{m}$ .....	57
4.12 Particle size distribution of 70:30 micronized theophylline (MTHF) blended with hydroxypropylcellulose MF (HPC MF) with a $D_{10}=4.3\ \mu\text{m}$ , $D_{50}=16.5\ \mu\text{m}$ , and a $D_{90}=440.6\ \mu\text{m}$ .....	58
4.13 Sieve analysis for particle size distribution of 70:30 micronized theophylline (MTHF) blended with hydroxypropylcellulose EXF (HPC EXF).....	59
4.14 Sieve analysis for particle size distribution of 70:30 micronized theophylline (MTHF) blended with hydroxypropylcellulose MF (HPC MF).....	59
4.15 Particle size distribution of theophylline (THF) blended with hydroxypropylcellulose EXF (HPC EXF) with a $D_{10}=7.4\ \mu\text{m}$ , $D_{50}=19.2\ \mu\text{m}$ , and a $D_{90}=60.4\ \mu\text{m}$ .....	60
4.16 Particle size distribution of theophylline (THF) blended with hydroxypropylcellulose MF (HPC MF) with a $D_{10}=6.6\ \mu\text{m}$ , $D_{50}=17.54\ \mu\text{m}$ , and a $D_{90}=180.50\ \mu\text{m}$ .....	61
4.17 Sieve analysis for particle size distribution of 70:30 theophylline (THF) blended with hydroxypropylcellulose (HPC EXF).....	61
4.18 Sieve analysis for particle size distribution of 70:30 theophylline (THF) blended with hydroxypropylcellulose (HPC MF).....	62
4.19 Bulk and tap density of micronized and non-micronized theophylline.....	62

**LIST OF FIGURES**  
**(Continued)**

<b>Figure</b>	<b>Page</b>
4.20 30 mm Twin Screw Mixing Element Evaluator (TSMEE) with one reverse (1RS) screw configuration.....	64
4.21 Carcass analysis by SEM of the theophylline (THF) formulation granulated with the one reverse (1RS) screw configurations: 8 <sup>th</sup> , 7 <sup>th</sup> , and 6 <sup>th</sup> segments show no morphological change relative to the unprocessed formulation.....	65
4.22 Carcass analysis by SEM of the theophylline (THF) formulation granulated with the one reverse (1RS) screw configurations: between segment 5 and 4...	65
4.23 Carcass analysis by SEM of the theophylline (THF) formulation granulated with the one reverse (1RS) screw configurations: between segment 4 and 3...	66
4.24 Carcass analysis by SEM of the theophylline (THF) formulation granulated with the one reverse (1RS) screw configurations: between segment 2 and 1...	67
4.25 Carcass analysis by SEM of the theophylline (THF) formulation granulated with the one reverse (1RS) screw configurations: final granulation.....	68
4.26 30 mm Twin Screw Mixing Element Evaluator (TSMEE) with five kneading blocks (5KB) and one reverse (1RS) screw configuration.....	69
4.27 Carcass analysis by SEM of the theophylline (THF) formulation granulated with the five kneading blocks (5 KB) and one reverse (1RS) screw configurations: before segment 8.....	69
4.28 Carcass analysis by SEM of the theophylline (THF) formulation granulated with the five kneading blocks (5 KB) and one reverse (1RS) screw configurations: between segment 8 and 7.....	70
4.29 Carcass analysis by SEM of the theophylline (THF) formulation granulated with the five kneading blocks (5 KB) and one reverse (1RS) screw configurations: between segment 7 and 6.....	71
4.30 Carcass analysis by SEM of the theophylline (THF) formulation granulated with the five kneading blocks (5 KB) and one reverse (1RS) screw configurations: between segment 6 and 5.....	71

**LIST OF FIGURES**  
**(Continued)**

<b>Figure</b>	<b>Page</b>
4.31 Carcass analysis by SEM of the theophylline (THF) formulation granulated with the five kneading blocks (5 KB) and one reverse (1RS) screw configurations: between segment 5 and 4.....	72
4.32 Carcass analysis by SEM of the theophylline (THF) formulation granulated with the five kneading blocks (5 KB) and one reverse (1RS) screw configurations: between segment 4 and 3.....	72
4.33 Carcass analysis by SEM of the theophylline (THF) formulation granulated with the five kneading blocks (5 KB) and one reverse (1RS) screw configurations: between segment 3 and 2.....	73
4.34 Carcass analysis by SEM of the theophylline (THF) formulation granulated with the five kneading blocks (5 KB) and one reverse (1RS) screw configurations: between segment 2 and 1.....	73
4.35 Carcass analysis by SEM of the theophylline (THF) formulation granulated with the one reverse (1RS) screw configurations: final granulation.....	74
4.36 System analytical model used for 27 mm twin screw extrusion trials.....	75
4.37 Example of how residence time was determined using micronized theophylline and hydroxypropylcellulose MF blend (MTHF:HPC MF).....	77
4.38 Screw configuration used during scouting studies for 27 mm ZSE Maxx experiments. The mixing zone is comprised of two 15 mm kneading sections. Each kneading block is 5 mm wide.....	80
4.39 Cross sectional area of a portion of the theophylline (THF): Hydroxypropylcellulose EXF (HPC EXF) “plug” approximately 1 mm from the top.....	81
4.40 Cross sectional area of a portion of the theophylline (THF): Hydroxypropylcellulose EXF (HPC EXF) “plug” approximately 1 mm from the left side.....	81
4.41 Cross sectional area of a portion of the tip of the theophylline (THF): Hydroxypropylcellulose EXF (HPC EXF) “plug” from the back.....	82

**LIST OF FIGURES**  
**(Continued)**

<b>Figure</b>	<b>Page</b>
4.42 Cross sectional area of a portion of the theophylline (THF): Hydroxypropylcellulose EXF (HPC EXF) granule approximately 1 mm from the front (plane not shown).....	83
4.43 Granules and particle size distribution of granules for micronized theophylline (MTHF) and hydroxypropylcellulose MF (HPC MF) blend (MTHF:HPC MF) at 4 kg/hr.; 200rpm; 35°C.....	85
4.44 Granules and particle size distribution for micronized theophylline (MTHF) and hydroxypropylcellulose MF (HPC MF) blend (MTHF:HPC MF) at 4 kg/hr.; 400 rpm; 35°C.....	86
4.45 Granules and particle size distribution for micronized theophylline (MTHF) and hydroxypropylcellulose MF (HPC MF) blend (MTHF:HPC MF) at 8 kg/hr.; 200 rpm; 35°C.....	87
4.46 Granules and particle size distribution for micronized theophylline (MTHF) and hydroxypropylcellulose MF (HPC MF) blend (MTHF:HPC MF) at 8 kg/hr.; 400 rpm; 35°C.....	88
4.47 Granules and particle size distribution for micronized theophylline (MTHF) and hydroxypropylcellulose MF (HPC MF) blend (MTHF:HPC MF) at 4 kg/hr.; 200 rpm; 50°C .....	89
4.48 Granules and particle size distribution for micronized theophylline (MTHF) and hydroxypropylcellulose MF (HPC MF) blend (MTHF:HPC MF) at 8 kg/hr.; 200 rpm; 50°C.....	90
4.49 Granules for micronized theophylline (MTHF) and hydroxypropylcellulose EXF (HPC EXF) blend (MTHF:HPC EXF) at 4 kg/hr.; 200 rpm; 35°C .....	92
4.50 Granules for micronized theophylline (MTHF) and hydroxypropylcellulose EXF (HPC EXF) blend (MTHF:HPC EXF) at 4 kg/hr.; 400 rpm; 35°C.....	93
4.51 Granules for micronized theophylline (MTHF) and hydroxypropylcellulose EXF (HPC EXF) blend (MTHF:HPC EXF) at 8 kg/hr.; 200 rpm; 35°C.....	94
4.52 Granules for micronized theophylline (MTHF) and hydroxypropylcellulose EXF (HPC EXF) blend (MTHF:HPC EXF) at 4 kg/hr.; 200 rpm; 50°C.....	95


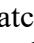
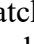
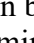
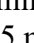
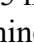


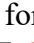
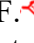
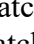

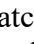
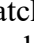
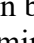
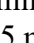
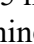


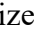
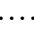

**LIST OF FIGURES**  
**(Continued)**

<b>Figure</b>	<b>Page</b>
4.53 Granules for micronized theophylline (MTHF) and hydroxypropylcellulose EXF (HPC EXF) blend (MTHF:HPC EXF) at 8 kg/hr.; 400 rpm; 50°C.....	95
4.54 Granules for micronized theophylline (MTHF) and hydroxypropylcellulose EXF (HPC EXF) blend (MTHF:HPC EXF) at 4 kg/hr.; 400 rpm; 50°C.....	96
4.55 Granules for theophylline (THF) and hydroxypropylcellulose MF (HPC MF) blend (THF:HPC MF) at 4 kg/hr.; 200 rpm; 35°C.....	98
4.56 Granules for theophylline (THF) and hydroxypropylcellulose MF (HPC MF) blend (THF:HPC MF) at 4 kg/hr.; 400 rpm; 35°C .....	99
4.57 Granules for theophylline (THF) and hydroxypropylcellulose MF (HPC MF) blend (THF:HPC MF) at 8 kg/hr.; 200 rpm; 35°C.....	99
4.58 Granules for theophylline (THF) and hydroxypropylcellulose MF (HPC MF) blend (THF:HPC MF) at 8 kg/hr.; 400 rpm; 35°C .....	100
4.59 Granules for theophylline (THF) and hydroxypropylcellulose MF (HPC MF) blend (THF:HPC MF) at 4 kg/hr.; 200 rpm; 50°C.....	101
4.60 Granules for theophylline (THF) and hydroxypropylcellulose MF (HPC MF) blend (THF:HPC MF) at 8 kg/hr.; 200 rpm; 50°C.....	101
4.61 Granules for theophylline (THF) and hydroxypropylcellulose MF (HPC MF) blend (THF:HPC MF) at 8 kg/hr.; 200 rpm; 50°C.....	102
4.62 Granules for theophylline (THF) and hydroxypropylcellulose EXF (HPC EXF) blend (THF:HPC EXF) at 4 kg/hr.; 200 rpm; 35°C.....	104
4.63 Granules for theophylline (THF) and hydroxypropylcellulose EXF (HPC EXF) blend (THF:HPC EXF) at 8 kg/hr.; 200 rpm; 35°C.....	104
4.64 Granules for theophylline (THF): hydroxypropylcellulose EXF (HPC EXF) blend (THF:HPC EXF) at 4 kg/hr.; 400 rpm; 35°C.....	105
4.65 Granules for theophylline (THF): hydroxypropylcellulose EXF (HPC EXF) blend (THF:HPC EXF) at 8 kg/hr.; 400 rpm; 35°C.....	105

**LIST OF FIGURES**  
**(Continued)**


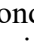
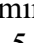
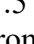
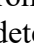




<b>Figure</b>	<b>Page</b>
4.66 Granules for theophylline (THF) and hydroxypropylcellulose EXF (HPC EXF) blend (THF:HPC EXF) at 4 kg/hr.; 200 rpm; 50°C.....	106
4.67 Granules for theophylline (THF) and hydroxypropylcellulose EXF (HPC EXF) blend (THF:HPC EXF) at 8 kg/hr.; 200 rpm; 50°C.....	107
4.68 Granules for theophylline (THF) and hydroxypropylcellulose EXF (HPC EXF) blend (THF:HPC EXF) at 8 kg/hr.; 400 rpm; 50°C.....	108
4.69 Yield loci for hydroxypropylcellulose MF (HPC MF).....	110
4.70 Yield loci for consolidated hydroxypropylcellulose EXF (HPC EXF).....	111
4.71 Cohesion and uniaxial compressive strength for hydroxypropylcellulose MF (HPC MF) and hydroxypropylcellulose (HPC EXF).....	113
4.72 Yield loci for consolidated micronized theophylline (MTHF).....	114
4.73 Yield loci for consolidated theophylline 325M (THF).....	114
4.74 Cohesion and uniaxial compressive strength for micronized theophylline (MTHF) and theophylline (THF).....	115
4.75 Coefficient of friction, $f$ as a function of drug load.....	116
4.76 Cohesion and uniaxial compressive strength for 70% theophylline blends.....	120
4.77 Still frames taken from a thermal imaging video of the theophylline (coarse polymer): hydroxypropylcellulose (HPC) MF (coarse polymer) showing the evolution of FED inside the batch mixer.....	122
4.78 Illustration of the different stages of deformation from consolidated particles to a solid rich suspension via batch mixing. Stage I illustrates the sample loaded into the mixer, stage II is the onset of resistance and increase in sample temperature of the semi-compacted mass, stage III is steady state compaction, stage IV are melt bound particles, and stage V is a completely deformed solid rich suspension.....	122

**LIST OF FIGURES**  
(Continued)


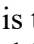

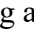

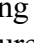

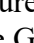
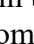
<b>Figure</b>	<b>Page</b>
4.79 Particle size distribution profiles as a function of mixing time for micronized theophylline (MTHF) and hydroxypropylcellulose MF (HPC MF) blend (MTHF:HPC MF).....	125
4.80 Particle size distribution profiles as a function of mixing time for micronized theophylline (MTHF) and hydroxypropylcellulose EXF (HPC EXF) blend (MTHF:HPC EXF).....	126
4.81 Illustrates the torque and temperature traces, as a function of time for the formulations containing 70% w/w MTHF and 30% w/w HPC MF.  is the temperature reading and  is the torque reading from the 1 min batch.  is temperature reading and  is the torque reading from the 2 min batch.  is the temperature reading and  is the torque reading from the 3 min batch.  is the temperature reading and  is the torque reading from the 4 min batch.  is the temperature reading and  is the torque reading from the 5 min batch. The  is the Geometric Mean Diameter of granules determined from the particle size distribution measured at each time point.....	128
4.82 Illustrates the torque and temperature traces, as a function of time for the formulations containing 70% w/w MTHF and 30% w/w HPC EXF.  is the temperature reading and  is the torque reading from the 1 min batch.  is temperature reading and  is the torque reading from the 2 min batch.  is the temperature reading and  is the torque reading from the 3 min batch.  is the temperature reading and  is the torque reading from the 4 min batch.  is the temperature reading and  is the torque reading from the 5 min batch. The  is the Geometric Mean Diameter of granules determined from the particle size distribution measured at each time point.....	129
4.83 Total intrusion volume for the formulations prepared with micronized theophylline (MTHF; fine API).....	131
4.84 X-Ray tomography for 70:30 micronized theophylline (MTHF) and hydroxypropylcellulose MF (HPC MF) blend (MTHF:HPC MF) as a function of time and deformation stage.....	132
4.85 SEM images for 70:30 micronized theophylline (MTHF) and hydroxypropylcellulose MF (HPC MF) blend (MTHF:HPC MF) after one minute of mixing time (Stage II) in the Brabender.....	133



**LIST OF FIGURES**  
(Continued)

<b>Figure</b>	<b>Page</b>
4.86 SEM images for 70:30 micronized theophylline (MTHF) and hydroxypropylcellulose MF (HPC MF) blend (MTHF:HPC MF) after three minutes of mixing time (Stage II/Stage III) in the Brabender.....	134
4.87 SEM images for 70:30 micronized theophylline (MTHF) and hydroxypropylcellulose MF (HPC MF) blend (MTHF:HPC MF) after five minutes of mixing time (Stage III) in the Brabender.....	135
4.88 X-Ray tomography for 70:30 micronized theophylline (MTHF) and hydroxypropylcellulose EXF (HPC EXF) blend (MTHF:HPC EXF) as a function of time and deformation stage.....	136
4.89 SEM images for 70:30 micronized theophylline (MTHF) and hydroxypropylcellulose EXF (HPC EXF) blend (MTHF:HPC EXF) after one minute of mixing time (Stage II) in the Brabender.....	137
4.90 SEM images for 70:30 micronized theophylline (MTHF) and hydroxypropylcellulose EXF (HPC EXF) blend (MTHF:HPC EXF) after three minutes of mixing time (Stage IV) in the Brabender.....	138
4.91 SEM images for 70:30 micronized theophylline (MTHF) and hydroxypropylcellulose EXF (HPC EXF) blend (MTHF:HPC EXF) after five minutes of mixing time (Stage IV) in the Brabender.....	139
4.92 Particle size distribution profiles as a function of mixing time for theophylline (THF) and hydroxypropylcellulose MF (HPC MF) blend (THF:HPC MF).....	140
4.93 Particle size distribution profiles as a function of mixing time for theophylline (THF) and hydroxypropylcellulose EXF (HPC EXF) blend (THF:HPC EXF).....	141
4.94 Illustrates the torque and temperature traces, as a function of time for the formulations containing 70% w/w THF and 30% w/w HPC MF.  is the temperature reading and  is the torque reading from the 30 seconds batch.  is temperature reading and  is the torque reading from the 1 min batch.  is the temperature reading and  is the torque reading from the 1.5 min batch.  is the temperature reading and  is the torque reading from the 2 min batch. The  is the Geometric Mean Diameter of granules determined from the particle size distribution measured at each time point.....	143

**LIST OF FIGURES**  
(Continued)

<b>Figure</b>	<b>Page</b>
4.95 Illustrates the torque and temperature traces, as a function of time for the formulations containing 70% w/w THF and 30% w/w HPC EXF.  is the temperature reading and  is the torque reading from the 30 seconds batch.  is temperature reading and  is the torque reading from the 1 min batch.  is the temperature reading and  is the torque reading from the 1.5 min batch.  is the temperature reading and  is the torque reading from the 2 min batch. The  is the Geometric Mean Diameter of granules determined from the particle size distribution measured at each time point.....	144
4.96 Total intrusion volume for the formulations prepared with theophylline (THF; coarse API).....	146
4.97 X-Ray tomography for 70:30 theophylline (THF) and hydroxypropylcellulose MF (HPC MF) blend (THF:HPC MF) as a function of time and deformation stage.....	147
4.98 X-Ray tomography for 70:30 theophylline (THF) and hydroxypropylcellulose EXF (HPC EXF) blend (THF:HPC EXF) as a function of time and deformation stage.....	148
4.99 SEM images for 70:30 theophylline (THF) and hydroxypropylcellulose EXF (HPC EXF) blend (THF:HPC EXF) after 30 seconds of mixing time (Stage II) in the Brabender.....	149
4.100 SEM images for 70:30 theophylline (THF) and hydroxypropylcellulose EXF (HPC EXF) blend (THF:HPC EXF) after 1.5 minutes of mixing time (Stage II/III) in the Brabender.....	150
4.101 SEM images for 70:30 theophylline (THF) and hydroxypropylcellulose EXF (HPC EXF) blend (THF:HPC EXF) after two minutes of mixing time (Stage II/III) in the Brabender.....	151
4.102 Endothermic event measured by MDSC for As-is (a) 70% theophylline (THF): 30% hydroxypropylcellulose MF (HPC MF); (b) 70% theophylline (THF): 30% hydroxypropylcellulose EXF (HPC EXF); (c) 70% micronized theophylline (MTHF) : 30% hydroxypropylcellulose MF (HPC MF); (d) 70% micronized theophylline (MTHF): 30% hydroxypropylcellulose MF (HPC MF).....	154

**LIST OF FIGURES**  
**(Continued)**

<b>Figure</b>	<b>Page</b>
4.103 Endothermic event measured by MDSC for (a) as-is hydroxypropylcellulose MF (HPC MF); (b) dried hydroxypropylcellulose (HPC MF); (c) as-is hydroxypropylcellulose EXF (HPC EXF); (d) dried hydroxypropylcellulose (HPC EXF).....	156
4.104 Dynamic temperature ramp of hydroxypropylcellulose MF (HPC MF).....	158
4.105 Dynamic temperature ramp of hydroxypropylcellulose (HPC EXF).....	158
C.1 Screw elements and kneading block names.....	180
C.2 Screw conveying element names.....	181
C.3 Conveying and kneading block naming convention.....	182

## LIST OF ACRONYMS/ABBREVIATIONS

API	Active Pharmaceutical Ingredient
Co-TSE	Co-rotating Twin Screw Extruder
DSC	Differential scanning calorimetry
DMM	dissipative mix-melting
EYL	Effective yield locus
HDPE	High Density Polyethylene
HME	Hot Melt Extrusion
HPC MF	Coarse Hydroxypropylcellulose
HPC EXF	Fine Hydroxypropylcellulose
LDPE	Low Density Polyethylene
LIW	Loss in Weight
MIP	Mercury Intrusion Porosimetry
MPB	Milled Pre-blend
MTHF	Micronized Theophylline
PB	Pre-blend
PP	polypropylene
PE	Polyethylene
PED	Plastic Energy Dissipation
PMMA	Polymethyl methacrylate
PS	Polystyrene
PSD	Particle Size Distribution

FCM	Farrel continuous mixer
FED	Frictional Energy Dissipation
SEM	Scanning electron microscopy
$T_{\text{Barrel}}$	Barrel Temperature of the extruder
THF	Coarse Theophylline 325M
TGA	Thermogravimetric analysis
TM	Trademark
_TSG	Twin Screw Granulation
_TSMEE	Twin Screw Mixing Element Evaluator
_VED	viscous energy dissipation
_YL	Yield locus

## NOMENCLATURE

A	Cross sectional area
C	Intensity of the tracer
C	Cohesion Intercept
$C_p$	Heat Capacity
$E^*$	Complex Young's Modulus
$E'$	Storage (Elastic) Modulus
$E''$	Loss (Viscous) Modulus
$E(t)$	Cumulative residence time distribution
$F$	Interparticle friction coefficient
$F_C$	Cap line
$f_c$	Uniaxial compressive yield stress
$F_N$	Normal force
$F_s$	Shear Failure
$F_T$	Tangential force
L	Length
N	Normal force
P	hydrostatic stress
$\dot{q}$	Heat flux
$\dot{Q}$	Volumetric Flow Rate
R	Particle Radius
t	time
$T_g$	Glass transition temperature

$T_m$	Melt temperature
$u$	Internal energy
$v$	Particle velocity
$V$	Volume
$x$	Neck radius
$B$	Interparticle friction coefficient
$\Gamma$	Surface Tension
$\Delta$	Effective angle of internal friction
$\dot{\gamma}$	Shear rate
$\rho$	Density
$E$	Strain
$\varepsilon$	Porosity
$\varepsilon_{min}$	Minimum achievable porosity
$\varepsilon_0$	Initial porosity
$K$	Exponential consolidation rate
$T$	Shear stress
$\tau_0$	Cohesion
$\Delta t$	Change in time
$\Delta v$	Change in velocity
$\Delta H_{sp}$	Specific Enthalpy
$\Delta T_a$	adiabatic specific enthalpy
$D/Dt$	Substantial derivative
$\nabla$	Vector operator “del” or “nabla”

# CHAPTER 1

## INTRODUCTION

Granulation processing is a routine method used in the development and manufacture of goods in the food, plastic, and pharmaceutical industries. Granulation is also the primary unit operation used in the manufacture of oral solid dosage forms in the pharmaceutical industry. The goal with granulation is to transform fine, poor flowing powders into enlarged, free-flowing agglomerates to enhance handling and improve subsequent processing. Most granulations are batch type systems or, at best, semi-continuous.

In recent years, pharmaceutical companies have taken strong interest in continuous manufacturing. This stems from the demand that the number of patients who need treatment is constantly increasing and the industry is obligated to deliver quality medicines to meet this need. Combined with the everchanging political and regulatory landscape, companies must evolve and adapt to remain relevant. This necessity has led the way for new granulation unit operations. Many equipment manufacturers have devoted more attention to continuous processing.

The concept of continuous processing has many advantages for the industry. Scale-up and manufacturing time are significantly reduced using this approach. Many institutions are also taking advantage of equipment readily available within their network. For this reason, co-rotating twin screw hot melt extruders (HME) are currently being investigated more intensively because of their versatility; they can be efficient continuous granulators. While amorphous dispersion is obtained from dissolution of API in polymer at elevated temperature during HME process, twin screw mixing can also be utilized for granulation of particulates.



In this work, the powder-to-granule evolution during Twin Screw Granulation (TSG) in the extruder, at the kneading zone, was studied using two sets of binary crystalline dispersion systems. Each set containing theophylline (THF) and micronized theophylline (MTHF), and each API was blended with hydroxypropylcellulose (HPC) MF and HPC EXF at various concentrations, resulting in four different formulations.

A literature review is presented in Chapter 2, beginning with a description of common granulating unit operations used in the pharmaceutical industry. This is followed by a review of available literature on interparticle interactions. Since the powder flow properties were measured using the iShear<sup>TM</sup>: Powder Flow Rheometer for this research, the theory behind this instrument was discussed. A mechanistic description of amorphous solid dispersion prepared using HME is briefly described and complimented with a proposed mechanism for TSG.

In the TSG section, four major mechanisms are discussed as the main contributors to ensure granule growth via TSG: mixing, heating, melting, and sintering. These all occurred simultaneously, while the material is in the compacted state. Ultimately, experimental evidence shows that plastic energy dissipation (PED) and *excessive* frictional energy dissipation (FED) are the dominant drivers for obtaining a suitable granulation.

Chapter 3 summarizes the experimental methods that are used throughout this work. These experiments used novel and popular methods to elucidate the influence which these material properties had on the granulating mechanism. Microscopy is used to evaluate the asperities and to help visualize the morphological contribution towards the melting mechanisms. The friction coefficient was measured experimentally using the iShear<sup>TM</sup> powder flow analyzer. Mercury Intrusion Porosimetry (MIP) was also used to assess the

densification and pore distribution of granules prepared at different conditions across the different formulations.

Chapter 4 begins with the measured physical properties of the “as-is” raw materials and blends. Particle size distribution (PSD), morphology and density are introduced for micronized and non-micronized THF, HPC MF and HPC EXF, and the four THF/HPC Blends.

This was followed by a feasibility assessment of preparing granules using a 30 mm TSG. For this study only non-micronized THF, at 65% drug loading, and HPC MF was evaluated. Initial assessment suggested that this formulation was appropriate for TSG.

Given the success of the feasibility assessment, the following four formulations were prepared: micronized and non-micronized THF with HPC MF (coarse polymer) and micronized and non-micronized THF with HPC EXF (fine polymer) consisting mixture of different particle sizes of the API (70% w/w) and polymer (30% w/w). Milled theophylline (MTHF; fine API) was blended with coarse hydroxypropylcellulose (HPC MF; coarse polymer), theophylline (THF; coarse API) with fine hydroxypropylcellulose (HPC EXF, fine polymer), and the other two formulations consisted of both components in the blend being fine or coarse.

These formulations were evaluated on a Leistritz 27 mm co-rotating TSE, equipped with three custom 5 mm dispersive kneading blocks. The influence particle size differences had on the system parameters (e.g., torque, product temperature power, specific energy, residence time, and heat generation at the mixing block) as a function of feed rate, barrel temperature, screw speed are presented here. The resulting granules give a closer look at the complex, simultaneous mechanisms occurring in the kneading zone of the Co-TSE.

The granule particle size distribution data qualitatively show the evidence of sintering as well as the relentless extensional and elongations flow regimes the powders undergo during granule formation.

To better understand what was observed from the TSG trials, the iShear<sup>TM</sup>: Powder Flow Rheometer was used to measure the interparticle properties of the raw materials and the blends. The following mechanical properties were determined from consolidated and unconsolidated Mohr Circles. The Mohr Circles were determined from the measured uniaxial compressive strength ( $\sigma_c$ ), major consolidation stress ( $\sigma_1$ ) and the minor consolidation stress ( $\sigma_2$ ). The coefficient of friction,  $f$  was determined from the associated yield loci as a function of drug load. Theophylline for these experiments ranged from 25-75 % w/w; a total of 16 formulations were evaluated.

The Brabender was used to explore a novel method that enabled granulation in a counter-rotating batch mixer to minimize large scale granulation trials. Reproducibility using this method was investigated while studying the implications when the particle sizes of the API and Polymer were varied and what these differences had on the system parameters (e.g., product temperature and torque) as a function of input formulation. The resulting granules gave a deeper understanding of the complex, simultaneous mechanisms that are occurring in the kneading zone of the Co-TSE being emulated in the batch mixer. This study assessed the influence particle sizes differences between the API and the Polymer had on understanding the PED and FED mechanisms.

This was accomplished by tracking processability and the evolution of granule growth and densification rate. In parallel, a thermal analysis was used to characterize the rheological properties of the blends and the polymers to determine the onset of granulation.

Scan Electron Microscopy (SEM), Modulated Dynamic Scan Calorimetry (MDSC) and Dynamic Mechanical Thermal Analysis (DMTA) were used to assess localized polymer melting and on-set of Polymer softening.

## **CHAPTER 2**

### **LITERATURE REVIEW**

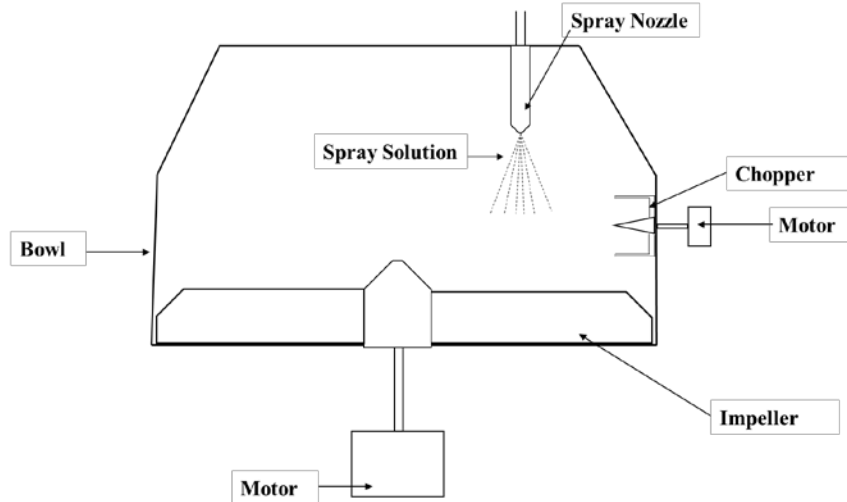
#### **2.1 Traditional Pharmaceutical Granulation Processes**

Granulating technology is used as a size enlargement process for small particles by which a process or procedure forces them to agglomerate into larger free flowing particles. There is a variety of unit-operations and processing techniques dedicated to particle agglomeration. Agglomeration is the formation of aggregates, where the agglomerates are bound together by selective ingredients and processes. The processes can be described by a series of agitating and compressing techniques (Ennis 1996, Palzer 2011). For oral solid dosage forms, a heterogeneous particulate system is fed into a granulating unit operation and is agglomerated, or granulated, either batch wise (i.e., High Shear Wet Granulation) or semi-continuously (i.e., Roller Compaction), to form a granulated product (Freeman 2016).

The feed typically consists of a mixture of solid ingredients, referred to as the formulation. These include an active pharmaceutical ingredient (API), binders, diluents, flow aids, surfactants, wetting agents, lubricants, fillers, or end-use aids (e.g., sintering aids, colors or dyes, taste modifiers). The agglomeration can be induced in several ways.

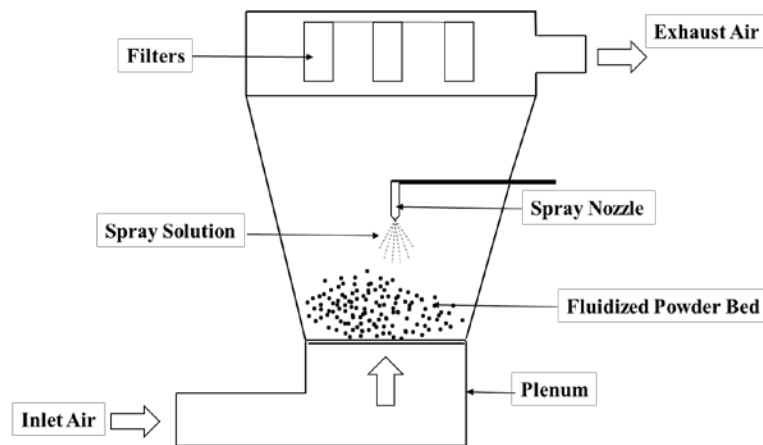
##### **2.1.1 Wet and dry granulation**

Wet granulations employ a spray flux, sometimes comprised of a binder solution on top of a fixed, cross-section, agitated powder bed. The powder blend is agitated by an impeller, which helps provide an equal distribution of the binder solution. Most high shear wet granulators are equipped with a chopper that facilitates the break-up of larger agglomerates and the distribution of a uniform binder.



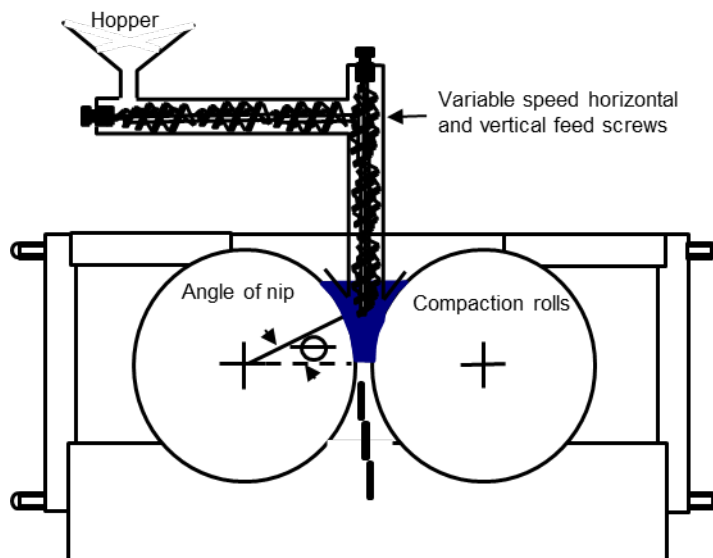
**Figure 2.1:** Basic diagram of a high shear wet granulation process.  
 (Source: Oulahna, Cordier et al. 2003)

Some APIs are known to be shear sensitive, meaning a low shear wet granulation process would be employed. For this case, the same fundamentals are present but can be carried out in a fluid bed dryer, as illustrated in Figure 2.2. The powder blend in this case is agitated by a pre-treated stream of air at a set inlet temperature and due point. Agglomeration in this case occurs when particles are gently stacked together via liquid bridges. Fines generated during the process are arrested in the exhaust filters.



**Figure 2.2** Basic diagram of a fluid bed granulation process.  
 (Source: Xinhui, 2008)

A dry granulation is commonly referred to as roller compaction. This is a semi-continuous granulations process. The formulation, made up of a homogenous blend of excipients and the API, is fed through two counter rotating rolls where the roll force presses the powders, pre-mixed with a dry binder, to form ribbons to a specified solid fraction that is subsequently milled downstream into granules.



**Figure 2.3** Basic diagram of a roller compaction dry granulation process.

## 2.2 Mechanism of Interparticle Interaction

The study of powder is often broken into two categories: dynamic and static. Some materials will demonstrate the same characteristics as a liquid, while others will behave like a solid, and some will be unique particulate-interface dominant. The differences between particulate and liquid are observed when a powder is either static or dynamic. For example, powders take the shape of the container it is held in, similar to a liquid. However, powders do support shearing stresses and, as a result, form a pile similar to solids. Another similarity to solids is that the shearing stress is proportional to the normal load rather than the rate of deformation. Particulates deviate from solid-like behavior because the

magnitude of the shearing stress is unknown. The following inequality holds:

$$\tau \leq f' \sigma \quad (2.1)$$

where  $f'$  is the interparticle static coefficient of friction and  $\sigma$  is the range of normal forces that can be applied to the powder before the shear stress,  $\tau$  is large enough to cause the particles to slide past one another and begin to flow (Tadmor and Gogos 2006, p.146).

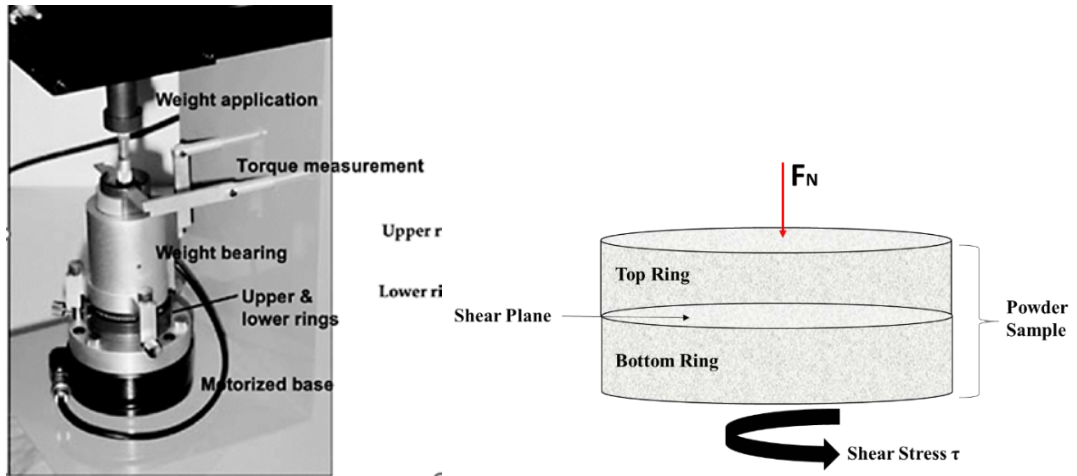
Adhesion forces between particles heavily influence the handling of powder material. The three major forces that affect interparticle interactions for bulk powders are: Van der Waals force, electrostatic force, and capillary force due to liquid bridges. All three are the main source of the adhesive force (Okuyama, Higashitani 1997).

### **2.2.1 Shear cell**

Shear cell testing gained its reputation as a reliable powder flow analysis for soil mechanics. The Shear cells were used to determine simple flow indices and measure the forces required to initiate flow. This is defined as powder failure based on measurements of cohesive strength, powder friction, and wall friction, where applicable (Ennis, 2008).

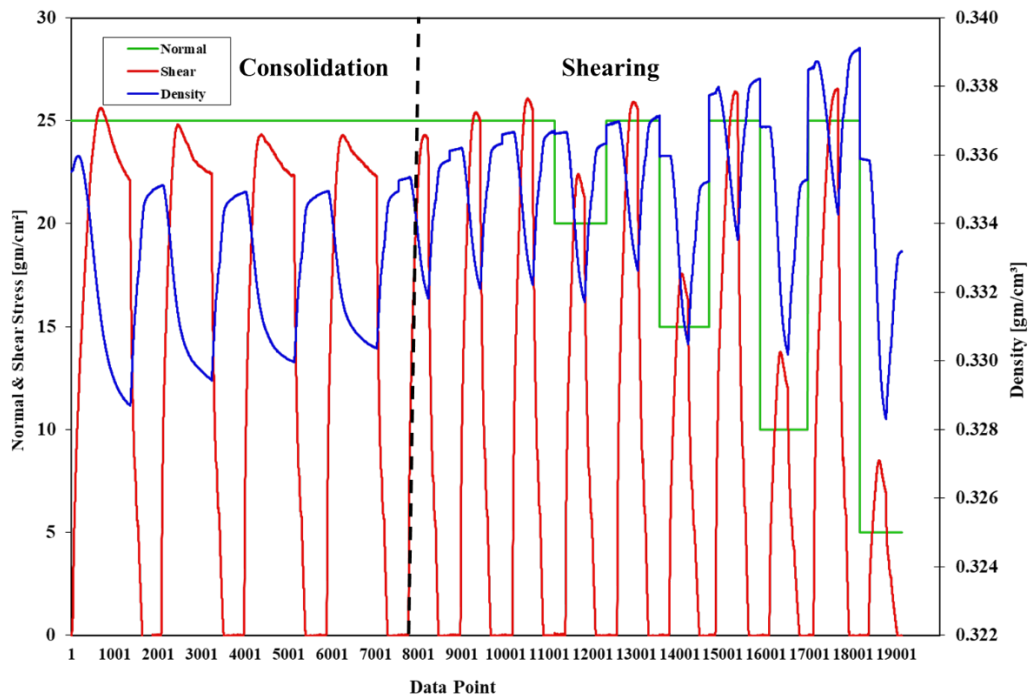
The same principles which apply to soils, are also relevant to pharmaceutical powder systems. The shear cell is used to quantify the flowability of a powder by applying a normal force ( $F_N$ ) on a powder contained within two rings, one on top of the other. The portion of the powder contained in the bottom ring would slowly rotate against the powder in the fixed top ring. The shearing interface is known as the shear plane (Freeman 2007, Ennis, 2007).





**Figure 2.4** Schematic of an iShear™ powder flow rheometer and normal force applied to a powder sample equipped for shear cell testing.  
 (Source: Emnis et al. 2008, Powder Systems 2022)

This assembly translates the torque experienced at the shearing interface as a function of time and is known as the shear stress ( $\tau$ ) time series. The time series is developed at variable normal Forces while the sample is being sheared.



**Figure 2.5** Example of time series profile for normal force, shear, and density of hydroxypropylcellulose MF from the iShear™ powder flow rheometer.

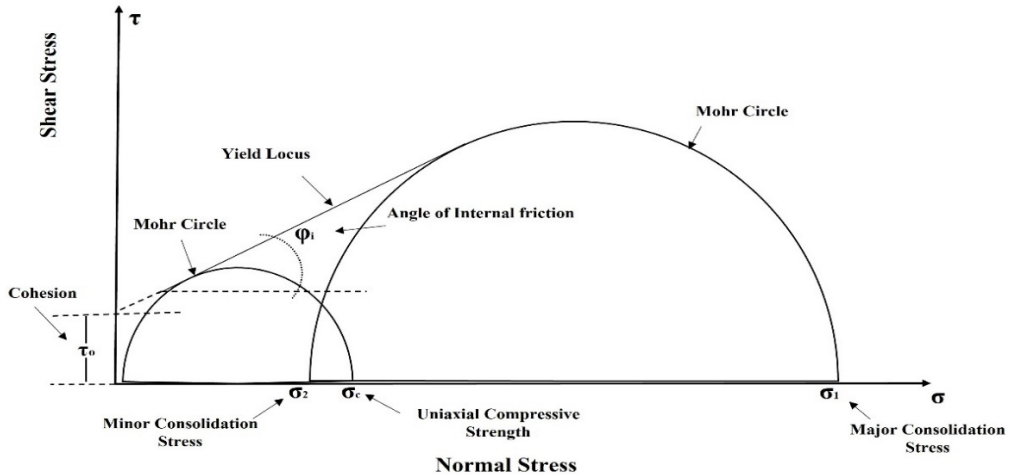
The yield characterization of the powder is a function of the consolidation it undergoes prior to shearing. In the consolidation stage, the torque is applied for each shear step until the sample fails (i.e., flows). The cell is then counter-rotated to remove the torque applied. This step is repeated until the shear stress reaches steady state ( $\tau$ ). At steady state, the sample reaches critical porosity ( $\epsilon_c$ ), which is a function of the consolidation normal stress. The sample is then ready for shearing. In the shearing stage, a smaller normal force is applied to the sample in the rings. Prior to each shearing step, the sample is sheared with the original normal stress before applying the next normal load. In addition, the shear stress is increased so that the sample can reach the maximum shear stress. At this point the powder will flow. The function of shear stress as a function of normal force is known as the yield locus. A common equation known as the Mohr-Coulomb is used to estimate the yield locus (Ennis 2007).

Where:

$$\tau = \tau_o + f\sigma = \tau_o + \sigma \tan(\varphi_i) \quad (2.2)$$

The coefficient of friction,  $f$ , is the slope of the resulting yield locus (YL) as described in Equation 2.2.

The coefficient of friction,  $f$ , can be derived from consolidated and unconsolidated Mohr Circles. The Mohr Circles are determined from the measured uniaxial compressive strength ( $\sigma_c$ ), major consolidation stress ( $\sigma_1$ ) and the minor consolidation stress ( $\sigma_2$ ) as presented in Figure 2.6.

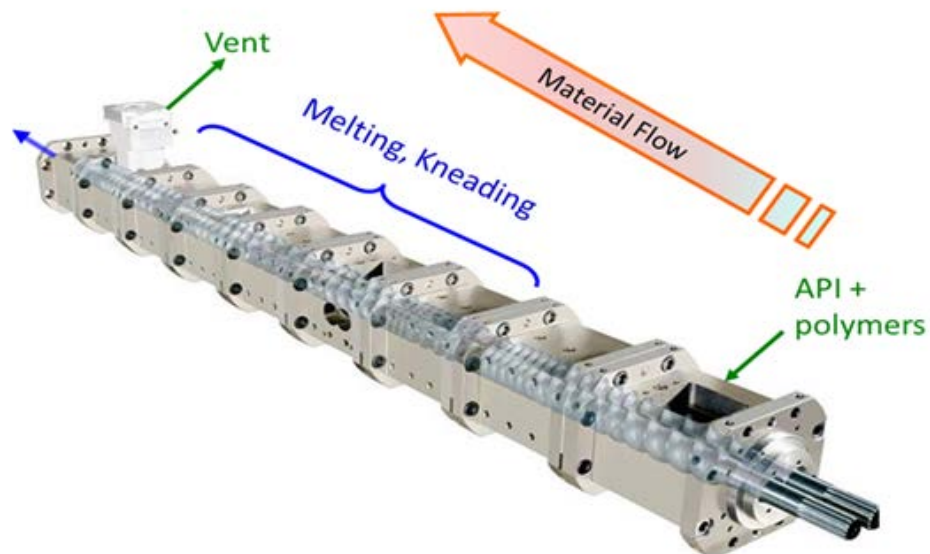


**Figure 2.6** Yield loci for consolidated bulk material derived from Mohr Circle.  
 (Source: Carson and Pittenger 1998; Roberts 2005, Freeman 2007)

### 2.3 Twin Screw Co-Rotating Extruder

Twin-Screw Extruders are equipped with two screws in a Figure-eight barrel. This design takes advantage of the material interacting between the screws, primarily the kneading or mixing section, as well as the interaction of the material between the inner barrel wall and the screw. These twin-screw extruders are used in the continuous melting, mixing, and homogenizing of different polymers with various additives. Twin screw extruders implement intimate mixing, which is essential for reactions in which at least one of the materials has high visco-elastic properties. The screws can either be tangential or intermeshing, where the intermeshing design can either be co or counter rotating. Tangential designs provide a wide range of channel depth and can accommodate longer lengths. Counter rotating intermeshing screws exert a dispersive mixing action on the material between the screws. These behave like a positive displacement device, with the ability to generate pressure more efficiently than any other extruder. (Perry, Green and Maloney 1997).

The most common type of twin-screw mixing extruder is the co-rotating intermeshing variety (APV, Berstorff, Davis Standard, Leistritz, Werner and Pfleiderer). The shafts for these machines are splined and are fitted with matching pairs of conveying elements and kneading disks as shown in Figure. 2.7. The configuration of these elements can be tuned to accommodate the compounding needs of different materials, including pharmaceutical formulations. The twin screw extruder has been used in the pharmaceutical industry primarily to manufacture solid dispersions for poorly soluble APIs. Vanhoorne et al. (2016) and Kallakunta et al. (2019) discusses applications of preparing crystalline API in a polymer matrix for controlled release oral solid dosage forms.



**Figure 2.7** Intermeshing co-rotating twin screw extruder: 27mm Leistritz extruder.  
(Source: Martin, 2011)

## 2.4 Description of the Hot Melt Extrusion Process and Mechanisms

A working design space and control strategy is established around the processing temperature (PT) for pharmaceutically relevant HME application. The product temperature is controlled between 50°- 100°C above the glass transition temperature ( $T_g$ ) of the polymer (or above the melting point for semi-crystalline polymer excipients) and below the melting point of the active if it is not thermally labile (Terife, 2013). This expression takes the form of:

$$P_T \approx T_{g\ polymer} + 50^\circ - 100^\circ \quad (2.3)$$

Terife (2013) has listed several products that have been developed and commercialized in Table 2.1. The listed products are made using extrusion technology. It can be assumed that all these products consist of a homogenous blend made up of an API in its crystalline or amorphous form. These are mixed with a polymer excipient to serve as a carrier and to provide the desired quality attributes. The API is dependent on the excipient to keep the product stable in the amorphous or a crystalline state. For crystalline formulation, the crystalline API is dispersed in what can be referred to as a solid rich suspension. Solid rich suspensions are typically used for the manufacture of controlled release oral solids like Kalitra<sup>®</sup>, which is an example of a commercial product manufactured via twin screw granulation (Breitenbach 2006).

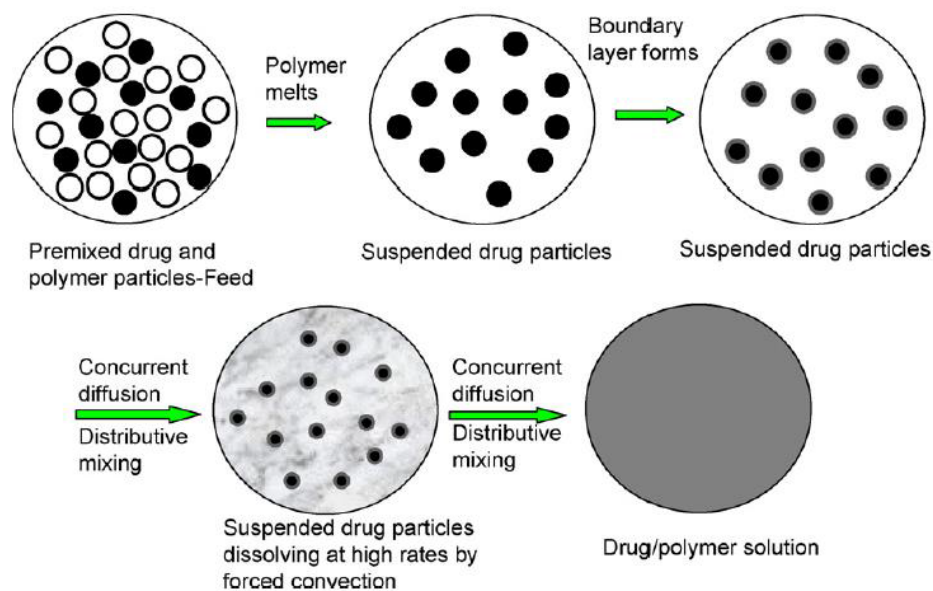
**Table 2.1** Examples of Drug Products Manufactured by the TSG and HME Process

Name	API	Polymer Excipient*	Delivery Form	Indication	Status	HME Purpose
Lacrisert®	None	HPMC	Implant	Dry eye syndrome	M	Shape
NuvaRing	Etonogestrel + Ethinyl Estradiol	EVAa	Implant	Contraceptive	M	Shape
Zoladex	Goserelin acetate	PLGA	Implant	Prostate cancer	M	Shape
Implanon	Etonogestrel	EVA	Implant	Contraceptive	M	Shape
Ozurdex®	Dexamethasone	PLGA	Implant	Macular Edema	M	Shape
Kaletra®	Lopinavir + Ritonavir	PVP-VA	Tablet	Anti-Viral (HIV)	M	Amorphous solution
Norvir®	Ritonavir	PVP-VA	Tablet	Anti-Viral (HIV)	M	Amorphous solution
Eucreas®	Vildagliptin +Metformin	HPMC	Tablet	Diabetes	M	Melt granulation
Rukobia®	Fostemsavir	HPMC+HPC	Tablet	Anti-Viral (HIV)	M	Melt granulation
Zithromax®	Azithromycin	HPMC	Tablet	Antibiotic	M	Taste Masking
Gris-PEG®	Griseofulvin	PEG	Tablet	anti-fungal	M	Crystalline
Rezulin®	Troglitazone	PVP	Tablet	Diabetes	W	Amorphous solution
Palladone™	Hydrophone	EC + ERS	Tablet	Pain	W	Controlled release
Posaconazole	Posaconazole	-	Tablet	Anti-fungal	D	Amorphous solution
Anacetrapib	Anacetrapib	-	-	Cardiovascular disease	D	Amorphous solution

\*EVA: Ethyl Vinyl Acetate, HPMC: Hydroxypropyl methylcellulose, PLGA: Poly(lactic-co-glycolic acid), PVP-VA: Polyvinyl pyrrolidone co-vinyl acetate, PEG: Polyethylene glycol, PVP: Polyvinyl pyrrolidone, EC: Ethyl cellulose, ERS: Eudragit® RS.

Source:(Terife, 2013) c D: Development, M: Marketed product, and W: Withdrawn from the market

The HME process can be broken up into four elementary steps: conveying, melting, mixing/kneading, and pressurization (Dreiblatt 2007, Gogos 2012 ). The API and polymer(s) can be fed into the extruder as individual components. However, they are typically introduced as premixed homogeneous blends. Materials are generally fed into the extruder using a loss in weight (LIW) feeder. The LIW controller adjusts feeder screw speed to produce a rate of weight loss equal to the desired feed rate. The blend is conveyed by the screws where it is heated. The polymer melts primarily by heat generated by volume-wise reduction through plastic energy dissipation (PED) and frictional energy dissipation (FED). PED and FED are created by the action of the kneading blocks deforming fully filled stream regions (Tadmor, Gogos 2006 p 219). The PED and FED mechanisms facilitate the dissolution of the API into the molten polymer via elongation and extensional flows. Figure 2.8 shows the mechanism of the API dissolving in the molten polymer for a miscible mixture.



**Figure 2.8** Schematic representation of the dissolution mechanism of an API during the HME process carried out at a temperature above the melting point of the API.

*Source: (Liu et al. 2010)*

Lastly, devolatilization sections are incorporated into the setup of the process to allow volatiles to vent from the extruder while they are melting (Todd 1998). Pressurization is the last mechanism observed. This occurs when the molten mixture is pushed through the die by the rotating screws. Initially, the material builds up at the die until enough mass accumulates to push the melt through the die. The extrudate is then rapidly cooled below the  $T_g$  and the API-Polymer mixture is locked in an amorphous state, retarding the mobility of the API for a finite duration of time (Terife 2013).

### **2.5 Description of the Twin Screw Granulation Process and Proposed Mechanisms**

Like traditional granulation, two types of processes can be considered with TSG: a wet or dry. The elementary steps for a wet process are as follows: conveying, spraying, and drying. Powder is fed into the extruder and conveyed towards the kneading blocks by the two co-rotating screws. A binder solution is used to facilitate granulation upon compaction, usually at the kneading zone. The granules are subsequently dried either down the barrel of the extruder after mixing or externally by some other method (e.g., drying oven or fluidized bed). The granule attributes are strongly dependent on the binder addition rate, barrel temperature, screw speed, and screw design. Barrel temperature may not be a critical parameter when a wet method is employed.

In the case for dry twin screw granulation, a polymer binder is added to the premix prior to granulation. While the pre-blend is conveyed down the barrel of the extruder, the polymer is softened using the external heating mechanism. In this case, granulation is facilitated by the compaction that is occurring in the fully filled kneading section. Here, the API is folded and kneaded into the softened binder. The granule attributes are strongly dependent on barrel temperature, screw speed, chilling capacity of the cooling media, as



well as the screw design and the pressure profile (Ebube, Hikal, Wyandt et al 1997, Bravo, Hrymak, and Wright, 2000, Gogos 2012, Trinh 2015, Pafiakis 2016, Shah, Karde, Ghoroi et al 2017). Dry twin screw granulation lends itself to a narrow processing window. This is due to the variability of the input material properties, making it difficult to design a robust process (Peeters 2015).

### 2.5.1 Sintering

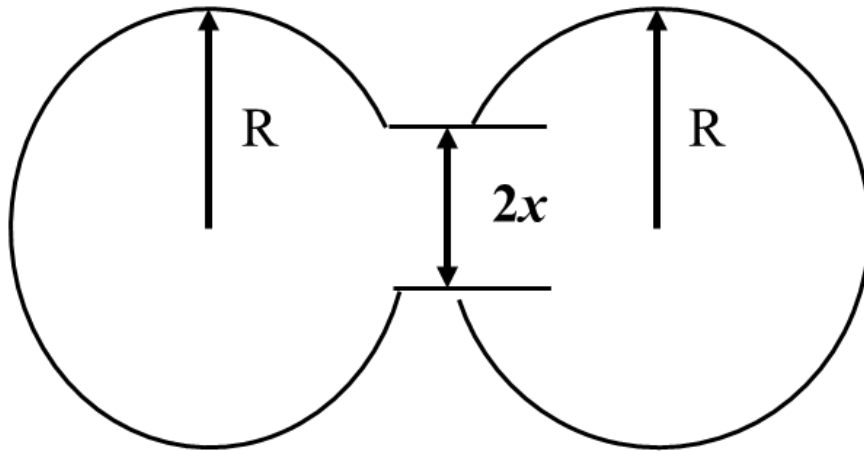
Sintering occurs when particulates stick to each other when they come in contact at high temperatures. Surface tension is the driving force for sintering. Since the particles coalesce, the surface area decreases and because of this, the total volume of the particulate bed decreases. A decrease in the surface area also decreases the surface energy. There are two different stages for sintering. The first stage consists of the formation of bridges between particles small enough to not change the density. The second stage consists of densifying, where the voids between the particles decrease. This causes an increase in density. This sintering occurs locally between particles due to viscous flow. This means the rate of densification is driven by the local temperature between particles (Liu, Thompson, and O'Donnell 2017, Alvarez, Snijder, Vaneker et al. 2022.)

Frenkel has presented the following equation for viscous sintering.

$$\frac{x^2}{R} = \frac{2 \Gamma}{3 \eta} t \quad (2.4)$$

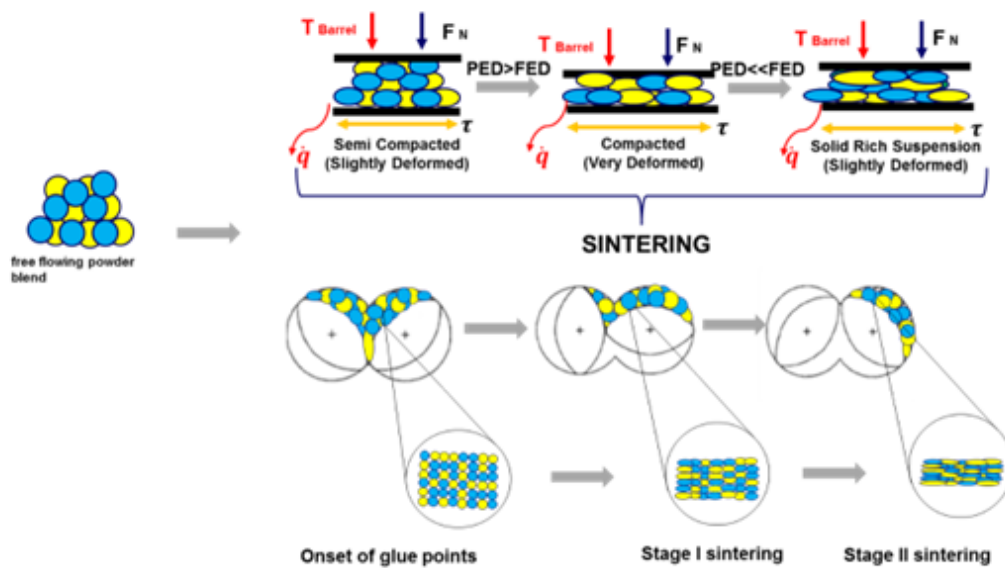
Where  $x/R < 0.3$ ,  $x$  is the radius of the neck and  $R$  is the radius of the particulate,  $\Gamma$  is the surface tension,  $\eta$  is viscosity and  $t$  is sintering time.

An illustration of Frenkel's model is presented in Figure 2.9.



**Figure 2.9** Illustration of sintering.  
(Source: Tadmor and Gogos p. 200)

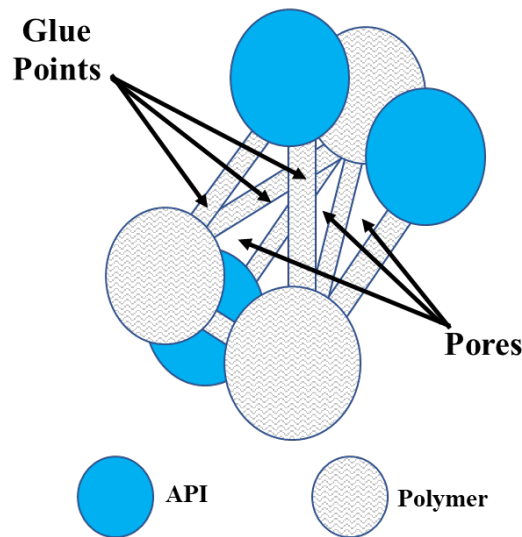
A TSG granulation is a process by which particulates are agglomerated using polymers, pre-mixed in a homogeneous mixture. The polymers become tacky during the process and suspend non-meltable materials via the sintering mechanism. Figure 2.10 illustrates this granulation mechanism.



**Figure 2.10:** Schematic representation of the melt granulation using a Co-TSE process.

The top half of the cartoon in Figure 2.10 illustrates the relentless expansion and contraction of the polymer and non-melting component mixture. The cartoon shows the deformations the particles are experiencing in the fully filled kneading section of the HME. The onset of glue points and the multi-stage sintering process phenomena is shown. The bottom half of the cartoon shows a more generalized case of the rapid volume-wise heating phenomenon that is taking place due to the deformation. This shows the simultaneous nature of the PED and FED mechanisms that drive softening of the polymers.

For granulation of particulates, melting of the API is undesired. Instead, the intent of the process is to bind the API to the polymer matrix. This is achieved by operating in a regime where Tadmor and Gogos show that polymer particulates can create glue points or particulate clusters. This regime is FED dominant. These glue points are generated by the FED mechanism. This leads to binding and granule growth.



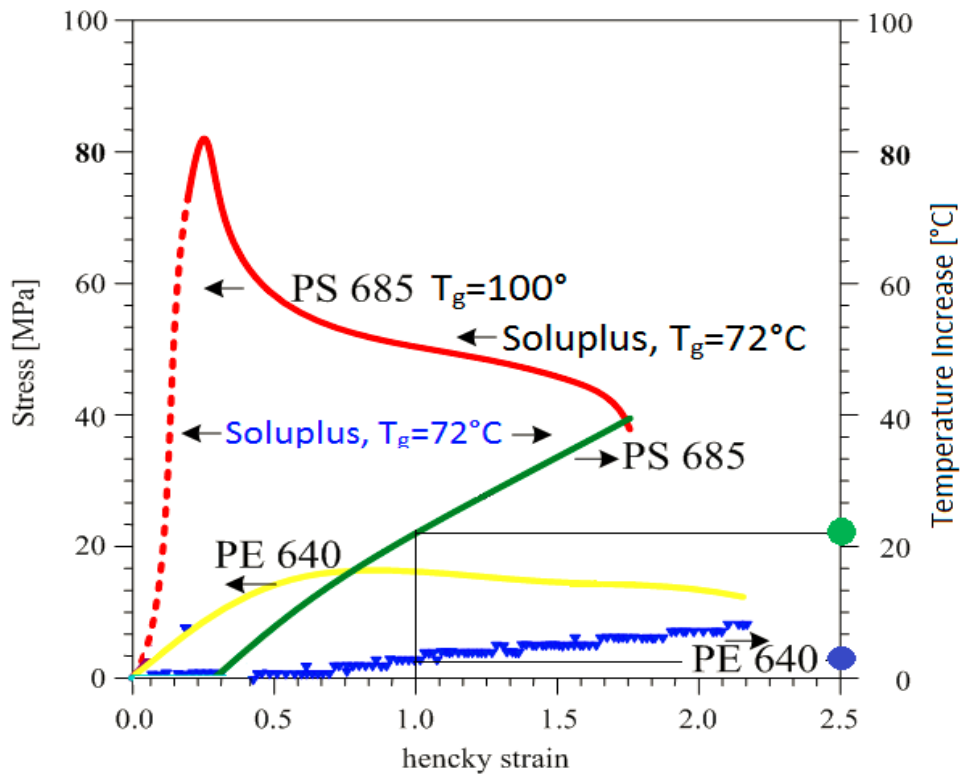
**Figure 2.11** Illustration of a particulate cluster of API and “tacky” polymer created via glue points.  
*(Source Pafiakis, Armenante and Gogos 2022)*

Kim et al. analyzed the melting of molded polymer discs that were subjected to rapid and cyclic deformation. These experiments defined Plastic Energy Dissipation (PED)

caused by the viscous component of the viscoelastic properties of polymer solids (Tadmor, Gogos 2006 p.222).

$$PED = \int_{\epsilon_e}^{\epsilon} \sigma d\epsilon = \rho C_p \Delta T_a \quad (2.5)$$

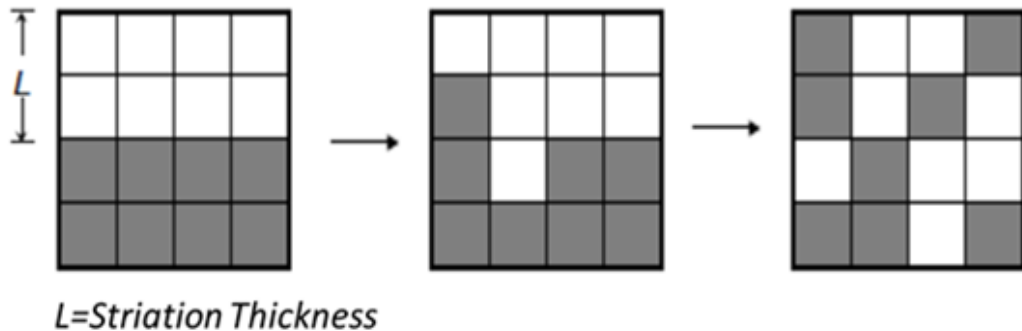
The area under the stress–strain curve with the adiabatic specific enthalpy  $\Delta T_a$  increase during compression as shown in Figure 2.12.



**Figure 2.12** Unconfined compression stress–strain curves and experimentally measured temperature increase  $\Delta T_a$  as a function of strain for PS (Dow 685), LDPE (Dow 640), and Soluplus (BASF).  
(Source Ioannidis 2014)

### 2.5.2 Mixing

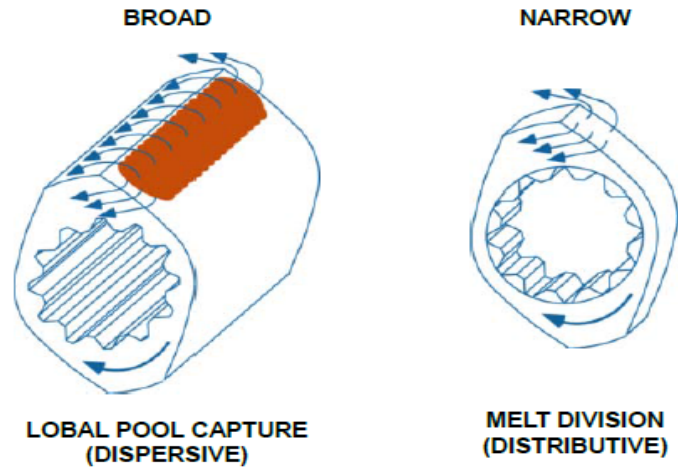
Mixing is a physical process that reduces heterogeneity when two or more components are blended for a length of time. For immiscible fluids, it requires mechanical energy in the form of laminar, turbulent, or bulk flow creating phase dispersion and distribution. For polymers, only laminar flow is needed. The goal for extrusion polymer systems is to reduce the thickness of a striation and, as a direct result increase the interfacial area. Figure 2.13 illustrates the same mechanism for mixing observed in a V-blender.



**Figure 2.13** Schematic representation of random distributive mixing (e.g., a process takes place in a V-blender).

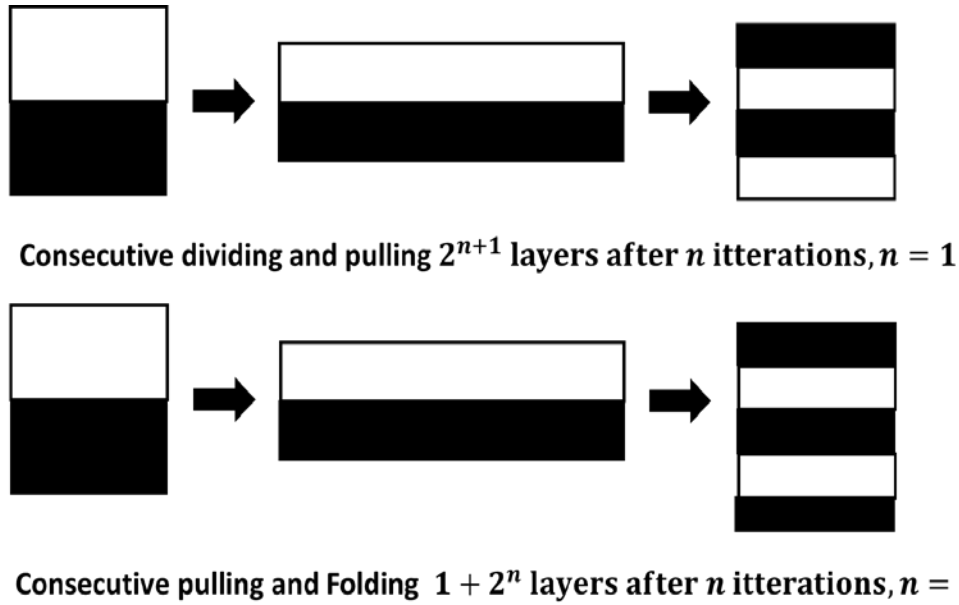
*(Source Gogos 2011)*

Co-rotating twin screw extruders use the fully filled mixing sections to provide uniform and rapid mixing. The screw and kneading configuration provide the holdup required to enable the axial mixing (Gogos 2011). There are several types of kneading elements that are available. However, they all are based on two basic designs. One design facilitates dispersive mixing and the other distributive mixing.



**Figure 2.14** Illustrating dispersive and distributive kneading elements  
 (Source: Thiele 2007, Martin 2011)

The wider disk provides extensional shear or dispersive mixing. The thinner disk provides melt divisions or distributive mixing (Thiele 2007, .Martin, 2011). Bakers' transformation describes these phenomena where the striation thickness is reduced by stretching and folding. This is also referred to as extensional and elongational flows. These are like that of kneading a dough (Gogos 2011).



**Figure 2.15** Schematic representation of striation thickness reduction by stretching and folding a.k.a extensional/ elongation flows.  
*(Source Gogos 2011)*

The density of the resulting granulation is proportional to the extensional and elongational flows. Furthermore, for pre-blends that are highly cohesive and poor flowing, fast screw speeds are required to convey the powder to the kneading zone. It is typically expected that faster screw speeds may result in excessive temperature generation that causes a FED dominant melting mechanism. PED and FED melting sources provide an effective deformation/frictional-melting mechanism. Repeated deforming stress induced by both PED and FED will simultaneously act as heat sources (Tadmor, Gogos 2006, p. 324).

Other system parameters used to characterize different formulations during development or scale-up are product temperature, residence time, power, and specific energy (SE). Power is a system parameter monitored and used in the scaling of fluid system. Sirasitthichoke (2022) explains that power dissipation depends on the impeller

geometry and location within the vessel, as well as how the agitator interacts with the fluid. The same holds for screw configurations and the interaction with the powder. This is important, especially as it transitions from a free-flowing powder to viscous melt in the extruder.

The cumulative residence time distribution is given by the equation:

$$F(t) = \int_0^{\infty} E(t)dt = \sum_0^t E(t)\Delta t = \frac{\sum_0^t c \Delta t}{\sum_0^{\infty} c \Delta t} \quad (2.6)$$

Where:

$$\int_0^{\infty} E(t)dt = \frac{c}{\int_0^{\infty} c dt} = \frac{c}{\sum_0^{\infty} c \Delta t} = 1 \quad (2.7)$$

is the exit age distribution,  $c$  is the intensity of the tracer at time  $t$ .

The mean residence time is given by the expression:

$$\bar{t} = \int_0^{\infty} t \cdot E(t)dt = \frac{\int_0^{\infty} t c dt}{\int_0^{\infty} c dt} = \frac{\sum_0^t t c \Delta t}{\sum_0^{\infty} c \Delta t} \quad (2.8)$$

Where  $\bar{t}$  is the mean residence time (Kolter et al., 2010).

$\bar{t}$  can simply be determined by the volume,  $V$  and  $\dot{Q}$  is the volumetric flow rate using the following equation (Dankwerts 1953).

$$\bar{t} = \frac{V}{\dot{Q}} \quad (2.9)$$



The Specific Energy (SE) is calculated by the power per amount processed per time. Steiner (2007) defines Power (KW) and SE in two steps using the following equations:

$$\text{KW (applied)} = \frac{\text{KW (motor rating)} \times \% \text{ torque} \times \text{RPM running}}{\text{Max. RPM} \times 0.97 \text{ (gearbox efficiency)}} \quad (2.10)$$

$$\text{Specific Energy} = \frac{\text{KW(applied)}}{\text{kg/hr}} \quad (2.11)$$

### 2.5.3 Heating and melting mechanism

Heating and melting of any substance can be described by the thermal energy balance:

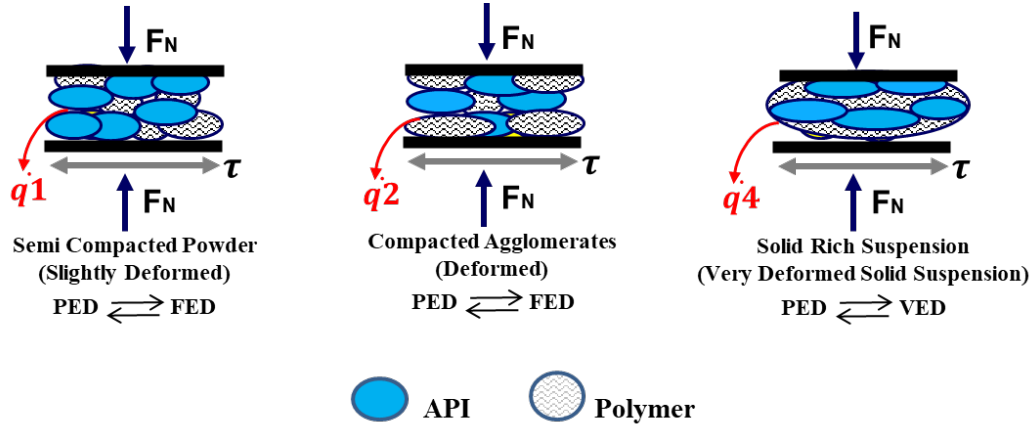
$$\rho \frac{Du}{Dt} = -\nabla \cdot \mathbf{q} - P(\nabla \cdot \mathbf{v}) - (\boldsymbol{\tau} : \nabla \mathbf{v}) + \dot{S} \quad (2.12)$$

Where  $-\nabla \cdot \mathbf{q}$  is the net rate of the internal energy increase per unit volume from an outside source.  $P(\nabla \cdot \mathbf{v})$  is the rate of internal energy increase per unit volume by compression.  $-(\boldsymbol{\tau} : \nabla \mathbf{v})$  is the rate of internal energy increase by flow and deformation.  $\dot{S}$  is an external source for homogeneous internal energy increase such as chemical reaction (Tadmor and Gogos 2006, p. 179).

For melting polymer systems in co-TSEs, the mechanisms can be qualitatively described as deformation/ frictional melting.  $-(\boldsymbol{\tau} : \nabla \mathbf{v})$  can be described by two different mechanisms of physical phenomena.

The first is when individual particles are exposed to repeated deformations, heat ( $\dot{q}$ ) is generated inside the particle; this is PED. The second is when the mechanical energy exerted on the material is dissipated into heat through particle-particle friction under the pressure of compaction, in the kneading zone of the particulate bed; this is FED. FED is

the dominating melting mechanism in Co-TSE that leads to the desirable downstream granules. Figure 2.16 illustrates the PED and FED mechanisms.



**Figure 2.16:** Evolution of a free-flowing blend to a solid rich suspension

The overall internal thermal energy balance is simplified to the following equation presenting in Equation 2.13.

$$\rho \frac{D_u}{D_t} = -\nabla \cdot q + PED + FED \quad (2.13)$$

At this point it is difficult to form mathematical expression for the PED and FED terms because of the non-homogeneity of the source systems (i.e., the compacted powder bed and particulate assembly). However, these two mechanisms are the most important when it comes to melting polymer powders and pellets in Co-TSE's (Tadmor , Gogos 2006, p. 182).

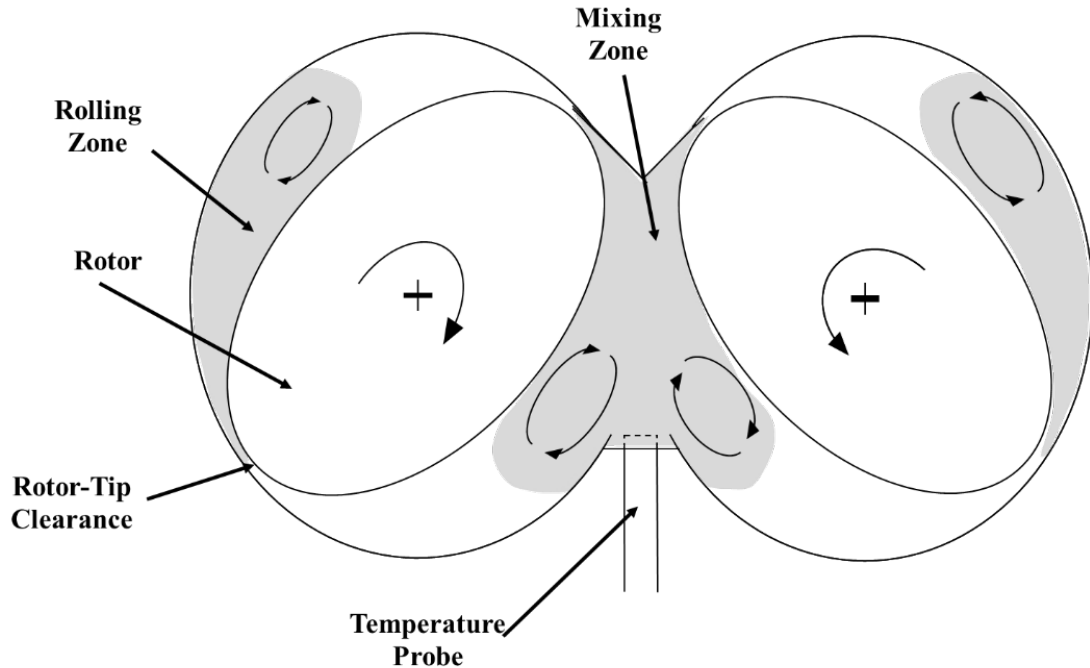
A simplification of the overall heating mechanism can be summarized by the following expression

$$\text{Rate of Heating} = \left\{ \begin{array}{l} \text{Rate of Conductive} \\ \text{Surface Heating} \\ \text{(Barrel)} \end{array} \right\} + \left\{ \begin{array}{l} \text{Rate of Dissipative} \\ \text{Volume - wise Heating} \\ \text{(Motor)} \end{array} \right\} \quad (2.14)$$

Where the motor term is the mechanical energy given off as heat. The packed solids in the fully filled kneading section of the co-TSE is undergoing simultaneous PED and FED (Ioannidis 2016).

Kim et al. (1999) found that when melting pellets in a Co-TSE, the PED mechanism fades along the length of the partially filled region of the screw and transitions to the next dominating mechanism, FED. FED occurs in the fully filled region at the kneading block, this leads to melting.

Elements of a possible melting mechanism in continuous mixers can be qualitatively described from the Valsamis–Canedo experiments. In this body of work, it was proposed that significant amount of melting may occur sooner than previously expected in the mixing section of the co-TSE. The energy dissipated at the entry of the mixing section was large enough to sinter and partially melt the particulates. This causes them to fuse to one another and agglomerate via sintering. Again, the fusing and the partial melting were caused by the two melting mechanisms that involve polymer particulates, FED and PED (Tadmor, Gogos 2006, p. 559).



**Figure 2.17** Cross section of the mixing chamber of a Farrel continuous mixer (FCM), illustrating the regions where deformation and flow patterns that lead to melting and mixing.

(Source: Pafiakis, Armenante and Gogos 2022)

In counter rotating batch mixers, solids are pulled by the rotors toward the mixing zone, as illustrated in Figure 2.17. In the rolling zone, the solids get compacted and sheared. When they reach the rotor-tip clearance region, there is nowhere else for the particles to go. Therefore, the compacted particulates undergo excessive shear deformation at a high rate of the order of  $\dot{\gamma}_{app} \sim \pi D_{max}/h$  where  $h$  is the rotor tip–barrel clearance and  $D_{max}$  is the rotor tip rotor diameter. (Tadmor and Gogos 2006, p.560)

It can be assumed that the particulate solids in the mixing chamber fill the “rolling zone” up to the minimum rotor diameter. The particulate bed is densified and compacted as the bed is forced through the rotor-tip clearance. This region can be defined as  $h = H_0$ , where  $H_0$  is the maximum and  $h$  is the minimum clearance between the barrel and the rotors. Due to the tight tolerance, the particulate bed is experiencing significant

compression and shear, causing the particulates to deform. This deformation, driven by PED, is softening interparticle contact and increasing their effective friction coefficient,  $f$  (Tadmor, Gogos 2006, p. 560).

The shear deformation experienced by the particulate in the converging mixing zone will cause particle to particle velocity differences. This will lead to the particles excessively rubbing. Since the polymer particles are in a compacted state, each particle will experience a normal force,  $F_N$  by the particle next to it. The velocity difference between the surface of the rotor-tip that is moving, and the stationary barrel surface is  $\pi D_{max} N$  (Tadmor, Gogos 2006 p. 560).

The difference in velocity of one circumferential layer of particles to the next one in the radial direction is:

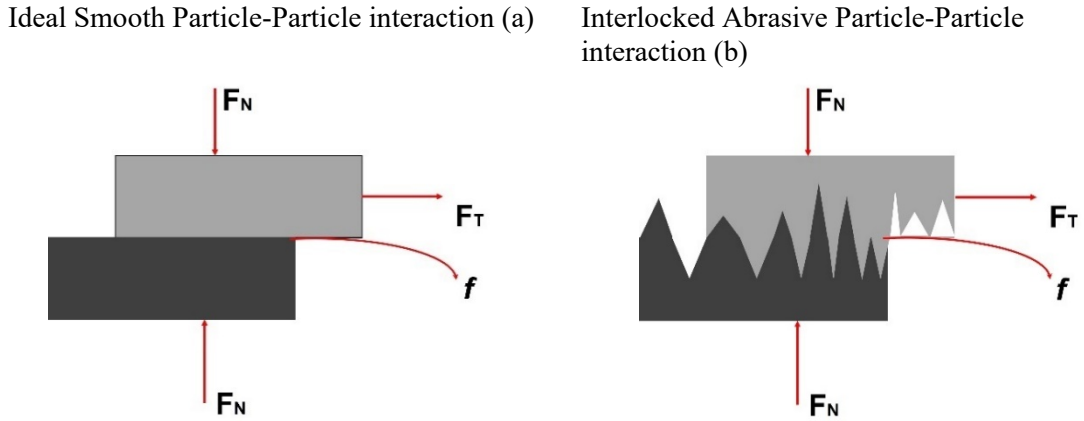
$$\Delta v = \pi D_{max} N \left( \frac{d_p}{h} \right) \quad (2.15)$$

Where  $d_p$  is the average particulate diameter, and  $\frac{d_p}{h} \sim 10^{-2}$ . The power dissipated locally by the FED is of the order of:

$$W_{FED} \sim \pi D_{max} N \left( \frac{d_p}{h} \right) f F_N \quad (2.16)$$

Where  $f$  is the interparticle friction coefficient (Tadmor, Gogos 2006 p. 560).

Particle- particle friction can be characterized using the following illustration.



**Figure 2.18** Representation of particle-particle interaction under pressure for an ideal, smooth system. and an interlocked, abrasive system under relentless deformation.  
(Source: Pafiakis, Armenante, Gogos 2022)

When powders are loosely packed, the cohesive forces are the most influential, highlighting each discrete particle. When powders are consolidated, the frictional forces and those due to mechanical locking are far more dominant because the particles are forced together. The contact pressure and the contact area will increase (Cohen and Tabor 1966). Cohesion still exists in the compacted state but only represents a fraction of the forces that restrict independent particle – particle movement (Freeman Technologies 2017). This is overcome by the rotors in the blender, forcing particles to grind against each other. A contrast of a smooth vs. abrasive particle-particle interacting system is illustrated in Figures 2.18, highlighting the relative velocities formed between particles (Pafiakis, Armenante and Gogos 2022).

Where  $F_N$  is the normal force,  $F_T$  is the tangential force, and  $f$  is the coefficient of friction. Furthermore, the top particle is moving with a different velocity ( $V_{el}$ ) in reference to the adjacent particle, represented as a displaced length ( $L$ ) over time ( $t$ ) as shown in Equation 2.17 and Equation 2.18.

$$Power = F_T \cdot V_{el} = (F_T \cdot L)/t \quad (2.17)$$

$$\text{Where } F_T = f \cdot F_N \quad (2.18)$$

Valsamis–Canedo experiments demonstrated that the energy dissipated in the mixing section was large enough to sinter and partially melt the particulates. This random deforming mechanism in turn caused the particles to agglomerate. The fusing and the partial melting were attributed to the two melting mechanisms that involve polymer particulates PED and FED (Valsamis and Canedo 1994). PED and FED cause enough melting that leads to the formation of a solids-rich suspension. The solid-rich suspension experiences excessive dissipative mix-melting in the “mixing zone”, where complex flows are caused by the rotor-tip design. (Tadmor and Gogos 2006).

Lastly, little has been investigated on the roles of PED and FED in the initiation of rapid volume-wise melting in mixers with respect to input material properties. Gogos et al. investigated the agglomeration rate of powder blends containing three different amounts of fine polypropylene (PP) powder. It was concluded that the blend with the highest level of fines demonstrated the fastest onset of growth (Gogos, Esseghir, Yu, Todd, and Curry 1994).

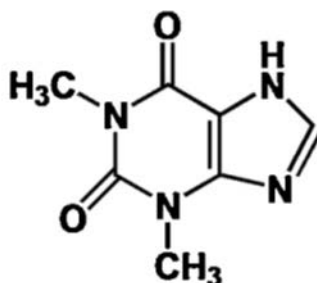
## CHAPTER 3

### EXPERIMENTAL

#### 3.1 Materials

##### 3.1.1 Active Pharmaceutical Ingredients (API): micronized and non-micronized theophylline (THF)

Micronized anhydrous theophylline (MTHF) and non-micronized anhydrous theophylline (THF) were used as the model active pharmaceutical ingredients (API). Both were purchased from BASF (Minden, Germany) The chemical structure for THF is presented in Figure 3.1 and a summary of some of its properties are listed in Table 3.1.



**Figure 3.1** Chemical structure of theophylline.  
(Source: Wang, Randviir and Banks 2000)

Theophylline is a bronchodilator used to treat asthma chronic obstructive pulmonary disease for the past several decades (Sullad 2010). In the solid state, it exists in three anhydrous polymorphs (Forms I, II, and IV) and one crystalline monohydrate (Form M). Forms I, II, and IV are kinetically stable at room temperature. No solid-state transition of any anhydrous form was observed when stored in a desiccator with anhydrous silica (Mahlin and Bergström, 2013).



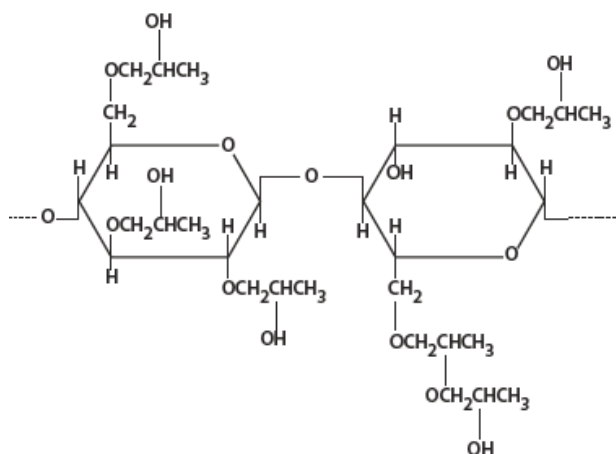
**Table 3.1** Summary of Selected Properties of Theophylline

Property	THF	MTHF
Chemical Formula	$C_7H_8N_4O_2^a$	
Melt Temperature [ $^{\circ}C$ ]	273.0	
Glass Transition Temperature [ $^{\circ}C$ ]	94.0 <sup>a</sup>	
MW [g/mol]	180.167 <sup>b</sup>	
Solubility parameter [ $MPa^{1/2}$ ]	24.4-29.8 <sup>c</sup>	
LogP	-0.02 <sup>b</sup>	

Source: (a-Hancock, York, and Rowe, 1997; b- Mahlin and Bergström 2013, c-Kim, lee Change et al. 2014)

### 3.1.2 Polymers: Hydroxypropylcellulose (HPC) MF and EXF

Two different grades of Klucel<sup>TM</sup> or hydroxypropylcellulose (HPC) were used in this study. Klucel<sup>TM</sup> MF and Klucel<sup>TM</sup> EXF (or HPC MF and HPC EXF) were purchased from Ashland (Hopewell, VA). The chemical structures for HPC are presented in Figure 3.2 and a summary of some properties for each grade are presented in Table 3.2.

**Figure 3.2** Chemical structure of hydroxypropylcellulose.

(Source Klucel<sup>TM</sup> Physical and Chemical Properties).

HPC is a nonionic water-soluble cellulose ether. It is manufactured by facilitating a reaction between alkali cellulose and propylene oxide at high temperatures and pressures. Propylene oxide is substituted on the cellulose through an ether linkage at the three reactive hydroxyls present on each hydroglucose monomer unit of the cellulose chain. Furthermore, etherification takes place in such a way that hydroxypropyl substituent groups contain almost entirely secondary hydroxyls. The secondary hydroxyl present in a side chain is available for additional reactions with the oxide to facilitate chaining out to form side chains that can have more than one mole of propylene oxide (Klucel™ Physical and Chemical Properties).

All grades of HPC are thermoplastic and are amenable to plastic manufacturing unit operations including HME. For pharmaceutical application, lower molecular weight grades of HPC (e.g., EXF) are recommended for thermal labile drugs. Medium to higher molecular weight HPC grades (e.g., MF) are recommended when harder material is warranted like controlled release tablets (Klucel™ Physical and Chemical Properties).

**Table 3.2** Summary of Selected Properties of Hydroxypropylcellulose

Property	HPC MF	HPC EXF
Glass Transition Temperature $T_g$ [°C]		130
Softening Temperature [°C]		100-150
MW [KDa]	850	80

Source: (Klucel™ Physical and Chemical Properties, )

## 3.2 Sample Preparation

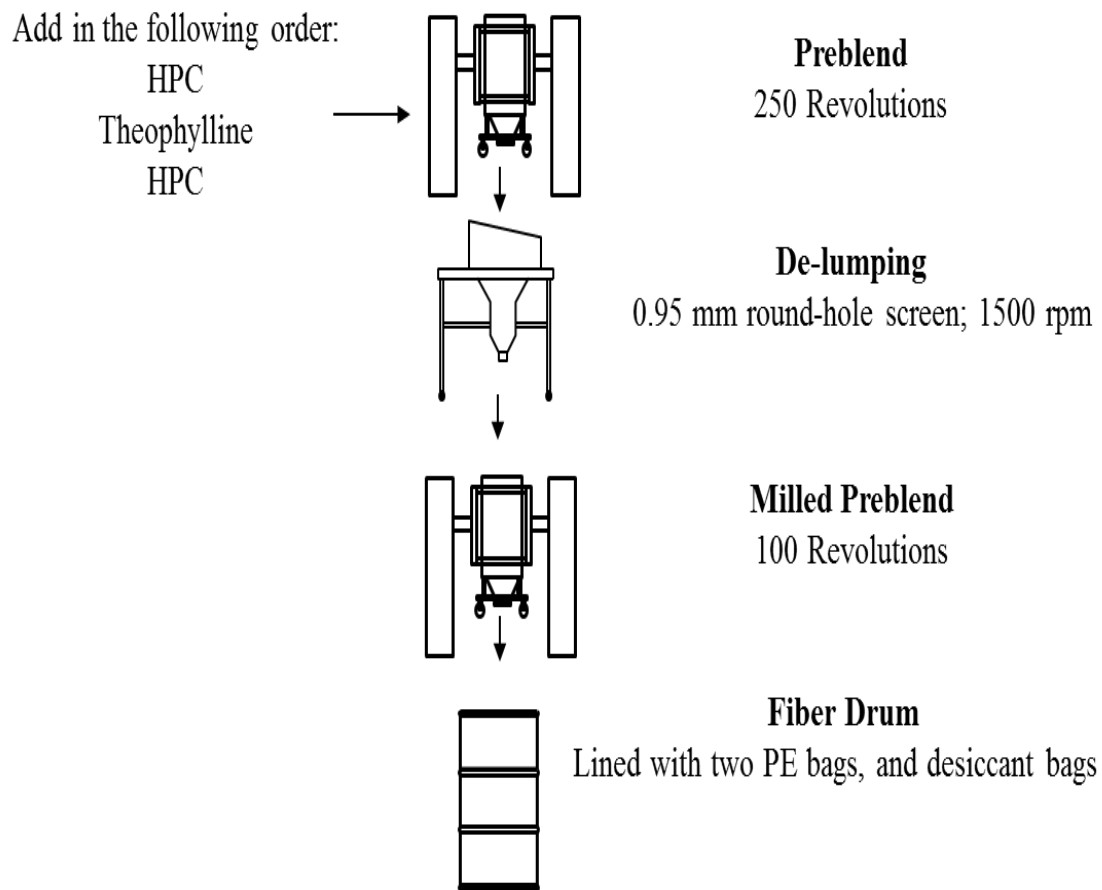
### 3.2.1 Preparation of theophylline and hydroxypropylcellulose blends for twin screw granulation

Four different blends were prepared using micronized and non-micronized THF at 70 % drug load. Each was blended with HPC MF and HPC EXF. Approximately 80 kg were prepared for each formulation.

A 454 L diffusion blender (SERVOLiFT, Randolph, NJ) was initially charged with approximately half the required amount of HPC, followed by the entire required amount of THF, and finally the remaining amount of HPC. The API was “*sandwiched*” between the two halves of the polymer, a common practice used for blending in industry.

Each blend was rotated for 25 minutes at 10 rpm for a total of 250 revolutions. The 454L bin containing pre-blend (PB) was then raised over, and gravity fed through, a U-10 Quadro Comil (Quadro, Waterloo, Ontario CA) with a round impeller at 1500 rpm and round 0.037” (0.94 mm) screen.

The milled pre-blend (MPB) was collected in a second 454 L diffusion blender. The MPB was rotated for 25 minutes at 10 rpm for a total of 250 revolutions. The final blend (FB) was collected and stored in fiber drums, doubled line with polyethylene (PE) bags, with desiccant pouches in between the two PE bags. Figure 3. 3 shows a flow diagram of this blending process.



**Figure 3.3** Process flow diagram for preparing theophylline: hydroxypropylcellulose blends for twin screw granulation.

### 3.2.2 Preparation of theophylline and hydroxypropylcellulose blends for iShear™ powder flow analysis

100 g blends were prepared for iShear™ analysis where the level of theophylline for each formulation was 25 %, 50 %, 70 % and 75 % w/w as listed in Table 3.3.

**Table 3.3** Morphology and Formulation Composition for iShear Analysis

Formulation	Ingredients	Morphology	% (w/w)					
I	THF	Coarse	--	25	50	70	75	100
	HPC MF	Coarse	100	75	50	30	25	--
II	MTHF	Fine	--	25	50	70	75	100
	HPC MF	Coarse	--	75	50	30	25	--
III	THF	Coarse	--	25	50	70	75	--
	HPC EXF	Fine	100	75	50	30	25	--
IV	MTHF	Fine	--	25	50	70	75	--
	HPCEXF	Fine	--	75	50	30	25	--

The blends were prepared by adding each material to suitably sized jar. The blend was tumbled using a turbula mixer (Glen Mills Inc., Clifton, NJ) at 45 rev<sup>-1</sup> for ten minutes. The resulting blend was passed through an 18mesh (0.0394", 1mm) screen (Newark Wire Cloth Company, Clifton, NJ). The screened blend was added back to the original jar and tumbled in the turbula mixer for another ten minutes. The final blend was collected and stored in doubled lined polyethylene (PE) bags, with desiccant pouches in between the two PE bags.

### **3.2.3 Preparation of theophylline and hydroxypropylcellulose granules**

**3.2.3.1 Twin screw granulation using the 30 mm (TSMEE).** A feasibility assessment for preparing granules using a Co-rotating 30 mm Twin Screw Mixing Element Evaluator (TSMEE). For this study only non-micronized THF, at approximately 65% drug loading with HPC MF was evaluated. Literature review suggested that this formulation was appropriate for TSG (Nkere 1997, Breighenbach 2006, Mohammed, Majumdar, Singh et al. 2012). There are 3 zones of 160 mm length, totaling 480 mm on the extruder. Two screw configurations were evaluated. The first screw configuration consisted of one reverse conveying element at the discharge of the extruder. The second screw configuration was made up of five kneading blocks followed by one reverse section, also at the discharge of the extruder. There was no die plate equipped for these experiments.

For each screw configuration granulation was stopped after steady state was achieved for ~15-20 minutes. The barrels of the 30 mm extruder can open like a clam shell and carcass samples, like those described by Maddock (1959), were collected from the mixing sections of both configurations and assessed using scan electron microscopy (SEM).

### **3.2.3.2 Twin screw granulation using the ZSE Maxx 27 mm co-rotating extruder.**

The 70% THF blends were granulated using the Leistritz ZSE Maxx 27 mm extruder (Somerville, NJ) fitted with a loss in weight feeder set in gravimetric mode. There are 9 zones of 120 mm length totaling 1080 mm on the extruder. The screw configuration was equipped with three, 5 mm distributive, broad lobed, kneading blocks at the end of Zone 7. Screw configuration is presented in Table 3.4. Not all the formulations were processable,

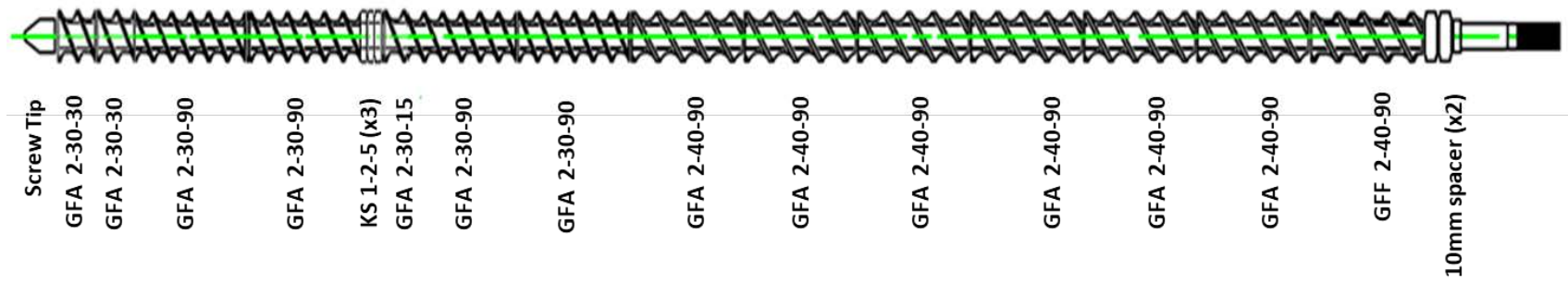
but this configuration was ideal for characterizing the extent of granulation for each formulation as a function of process temperature, feed rate and screw speed.

**Table 3.4** Distributive Screw Design Evaluated During 27 mm Leistritz Experiments

<b>Order</b>	<b>Element</b>	<b>Function</b>	<b>Elements along the shaft (mm)</b>
1	10 mm spacer	Spacer	N/A
2	10 mm spacer	Spacer	N/A
3	GFF-2-40-90	Conveying	90
4	GFA-2-40-90	Conveying	90
5	GFA-2-40-90	Conveying	90
6	GFA-2-40-90	Conveying	90
7	GFA-2-40-90	Conveying	90
8	GFA-2-40-90	Conveying	90
9	GFA-2-40-90	Conveying	90
10	GFA-2-30-90	Conveying	90
11	GFA-2-30-90	Conveying	90
12	GFA-2-30-15	Conveying	15
13	<b>KS1-2-5-90-E</b>	<b>Kneading</b>	<b>5</b>
14	<b>KS1-2-5-90-A</b>	<b>Kneading</b>	<b>5</b>
15	<b>KS1-2-5-90-M</b>	<b>Kneading</b>	<b>5</b>
<b>16</b>	GFA-2-30-90	Conveying	90
<b>17</b>	GFA-2-30-90	Conveying	90
18	GFA-2-30-30	Conveying	30
19	GFA-2-30-30	Conveying	30
20	Screw Tip	Total	1080

The screw configuration is also presented in Figure 3.4.

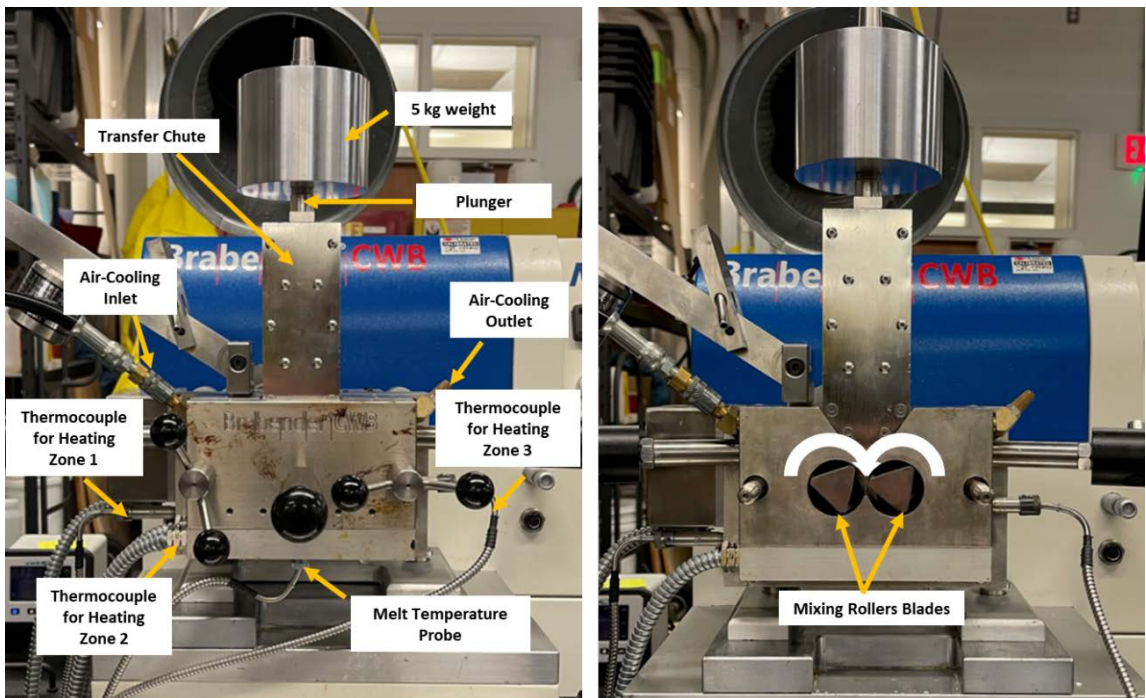




**Figure 3.4** Screw configuration used for 27 mm ZSE Maxx experiments. The mixing zone is comprised of three 5 mm kneading blocks.

The system parameters were recorded automatically by the data logger on the Co-TSE every 2 seconds for each run. The temperatures set for the study were 35°C and 50°C. These low temperatures were ideal because the screw configuration allowed for any heat generation to be primarily driven by the frictional energy dissipation (FED) mechanism between the two particles. Product temperature was measured manually with an IR gun when the equipment reached steady state.

**3.2.3.3 Brabender: batch mixing evaluation.** Batch mixer granulation was performed using a Brabender MetaTorque batch mixer (C.W. Brabender Instruments Inc., South Hackensack, NJ) equipped with 60cc bowl and two counter-rotating roller blades. Approximately 45 g of blend was loaded into the Brabender through a transport shoot while the blades were in motion at a 2-5 rpm. The mixer needed to be filled such that the mixer was fully filled for all the formulations despite the density differences.



**Figure 3.5** Brabender batch mixer frontal view of all components and mixing screws.  
(Source: Pafiakis, Armenante and Gogos 2022)

After mixing was completed for each time point, the sample was completely removed from the mixer and cooled down to room temperature for further analysis.

### **3.3 Materials Characterization**

#### **3.3.1 Bulk and tap density**

Bulk density was determined by pouring approximately 50 mL of powder into a 100 mL graduated cylinder. The graduated cylinder was tared prior to loading and the mass was recorded. A precise reading of the volume was recorded. The mass was divided by the volume to obtain the bulk density. The tap density was measured by placing the sample into the Vankel<sup>®</sup> tap density tester (Agilent, Santa Clara, CA) and measuring the volume after 500 taps.

#### **3.3.2 Particle size distribution**

*For the raw material:* the CamSizer<sup>®</sup> X2 (MICROTRAC MRB, Montgomeryville, PA) was performed using MICROTRAC MRB's standard settings. All measurements were performed using the X-Dry module with the X-Jet air pressure dispersion cartridge. MTHF and THF were measured using a dispersion pressure of 20kPa. The HPC MF and HPC EXF, were measured using a dispersion pressure of 250kPa. The 70% w/w theophylline preblends were also evaluated using the CamSizer<sup>®</sup>.

*For the preblends and the granulations:* The 70% w/w theophylline preblends and resulting granules, from the 27 mm TSG experiments, were measured by sieve analysis using an ATM Sonic Sifter (ATM, Corporation, Milwaukee, WI) with 6 screens and a fine collecting pan. The screen sizes used for analysis were as follows: 20 (840  $\mu\text{m}$ ), 40 (420  $\mu\text{m}$ ), 60 (250  $\mu\text{m}$ ), 80 (180  $\mu\text{m}$ ), 140 (105  $\mu\text{m}$ ), and 270 mesh (53  $\mu\text{m}$ ) and Pan. Approximately 5 g of sample was tested with a total sifting time of 5 minutes. The percent

retained was calculated from the amount retained on each screen divided by the sample size.

The 70% w/w theophylline preblends and resulting granules, from the Brabender experiments, were measured by sieve analysis using a Meinzer II Sieve Shaker (CSC Scientific, Fairfax, VA) with seven screens and a fine collecting pan. The screen sizes used for analysis were as follows: 8 (2360  $\mu\text{m}$ ), 20 (840  $\mu\text{m}$ ), 40 (420  $\mu\text{m}$ ), 60 (250  $\mu\text{m}$ ), 80 (180  $\mu\text{m}$ ), 140 (105  $\mu\text{m}$ ), and 270 mesh (53  $\mu\text{m}$ ) and Pan. Approximately 40 g of sample was tested with a total sifting time of 10 minutes. The percent retained was calculated from the amount retained on each screen divided by the sample size. The geometric mean diameter (GMD) was determined using the methods described by Wilcox and Deyoe (1970).

### **3.3.3 iShear<sup>TM</sup>: powder flow rheometer**

The iShear<sup>TM</sup> Rotary Split Cell (E&G Associates, Inc; Chattanooga TN) was used to measure the flow properties. Each sample was loaded into the standard 30 cc shear cell. The sample was pre-consolidated using a 600 g weight for 5 minutes. The sample was initially conditioned at a normal stress of 25 g/m<sup>2</sup>. The analysis was operated at the following normal stress 25, 20, 15, 10, and 5 g/m<sup>2</sup> with a 25g/m<sup>2</sup> normal stress conditioning between each operating normal stress.

### **3.3.4 Thermogravimetric Analysis (TGA)**

A TGA 5500 thermogravimetric analyzer was used to determine the loss of water for the two polymers before and after drying. Nitrogen was used as a purge gas at a flow rate of 25mL/ min; samples of approximately 10 mg were heated in open platinum pans to 300°C.

### **3.3.5 Modulated Differential Scanning Calorimetry (MDSC)**

A DSC 2500 apparatus was used to analyze the 70% drug load formulations and the two

polymers (“as-is” and dried). Approximately 3.0-6.0 mg samples in an aluminum pan. the samples were equilibrated at -20°C before heating. The heating rate was set at 2.00°C/ min up to 200°C and modulated at  $\pm 1.00^\circ\text{C}$  every 60 seconds.

### **3.3.6 Dynamic Mechanical Thermal Analysis (DMTA)**

Dynamic mechanical thermal analysis (DMTA) was conducted using a Rheometric Scientific DMTA-IV (Rheometric Scientific Inc., NJ) to characterize the onset of molecular mobility of the polymers similar to Monteyene et al. (2016). Measurements were performed using a dual cantilever with medium size clamp for testing. The samples were molded using compression molding at 70°C. The sample dimensions were approximately 16 mm (L) x 12.5 mm (w) x 1.8 mm (h). The sample was heated from 25°C to 160°C with a slow ramp rate of 2°C/min at frequency of 1Hz (6.28 rad/s) and 0.15% strain within linear viscoelastic (LVE) region of the samples. The run was terminated when the  $E''$ (viscous modulus) was higher than  $E'$ ( elastic modulus) since the sample became soft and would buckle.

### **3.3.7 Scan Electron Microscope (SEM)**

***Polymer and API:*** Scanning electron microscope (SEM) images were collected on samples staged on aluminum stubs prepared with adhesive carbon conductive tabs. The sample was sputter coated using a Cressington 208 HR Auto Sputter Coater® equipped with a platinum target (Ted Pella, Inc., Redding, CA). SEM images were acquired using 1.5kV-3kV using a field emission FEI Quanta 250 Field Emission Gun (FEG) SEM. (FEI Company, Hillsboro, OR, 97124).

***Granules:*** Scanning electron microscopy was performed using a JEOL JSM- 5510 (Japan Electron Optics Laboratory LTD) scanning electron microscope and were scanned at 10–

20 kV. From the foam material, transverse or tangential slices were made with a scalpel. These slices were mounted on a double-sided tape. The powdery samples were affixed on the stub with adhesive tape. The mounted samples were coated with a layer of gold using a Blazers sputtering device. Samples were placed in a multiple specimen holder of the scanning electron microscope. Digital images were processed in Adobe Photoshop.

### **3.3.8 Mercury Intrusion Porosimetry (MIP)**

Porosity was measured by mercury intrusion porosimetry (MIP) using an AutoPore IV instrument (Micromeritics, Inc., Norcross, GA). Approximately 200 mg of the granules were loaded into the MIP porosimeter. Granule porosity was determined using the following parameters: evacuation pressure of 50 mm Hg, mercury filling pressure of 0.5 psi, and equilibration time of 5 seconds for each of incremental pressure values from 0 to 30,000 psi. Data were generated at the 1-10  $\mu\text{m}$  range and were analysed to quantitate maximum intrusion volume and the pore size distribution within 1–5  $\mu\text{m}$  range to assess intra-granular porosity differences between different samples.

### **3.3.9 CT X-Ray tomography**

Data was acquired on a Nikon XT H 225ST X-Ray CT Scanner with a beam energy of 120 kV and 108  $\mu\text{A}$  beam current. The exposure time was 0.5 s, with 3142 separate image projections used to recreate the volumetric image, each a single scan for a total scan time of approximately 25 mins. Images were acquired using the Inspect X (Nikon Metrology) software. Raw image projections were processed using CT Pro 3D Version XT 4.4.2 (Nikon Metrology) to recover the volumetric image data, which was visualized using VGStudio MAX 2.2 (Volume Graphics GmbH).

### **3.3.10 Thermal imaging**

Thermal imaging was obtained using a Flir T440 thermal imaging camera (Flir Wilsonville, OR). Thermal distribution is captured in real-time with heat map superimposed on the image being measured. Spot temperature was recorded by the crosshair and a temperature-color scale was used to capture the temperature distribution in the image. A zinc selenide (ZnSe) window was used to collect thermal imaging spectra. The ZnSe window has a 68 mm diameter, thickness of 2 mm, and a band gap of 2.82 eV. The window was encased in a stainless steel 316 flange and mounted onto the front face of the Brabender.

## CHAPTER 4

### RESULTS AND DISCUSSION

#### 4.1 Physical Properties

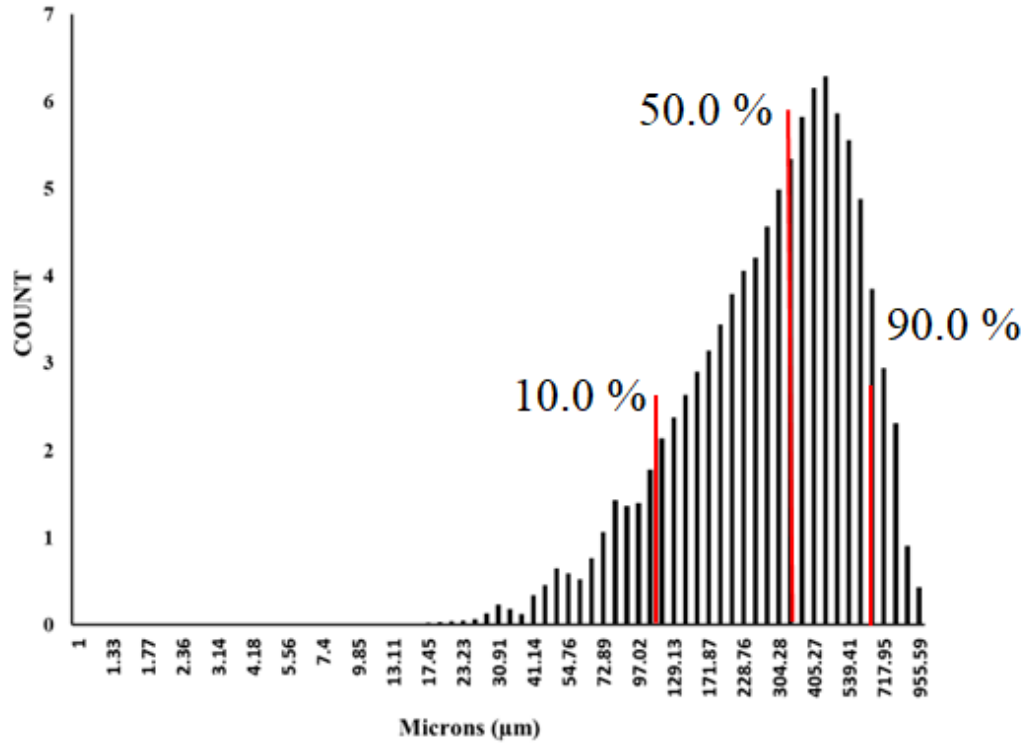
The characterization and manipulation of powders is complex. Many properties are interacting synergistically, dictating particle-particle, bulk, and ultimately, granulating behaviour. Most of these competing material parameters include morphology, long-range interactions, and contact mechanics. Morphological attributes consist of roughness, friction, and particle size intrinsic to that material. Some long-range interactions may consist of surface energy and electrical properties. Contact mechanics consist of toughness, rigidity, and the different moduli (Ennis 2008, Shah, Karde , Ghoroi and Heng 2017).

##### 4.1.1 Hydroxypropylcellulose (HPC) MF and EXF

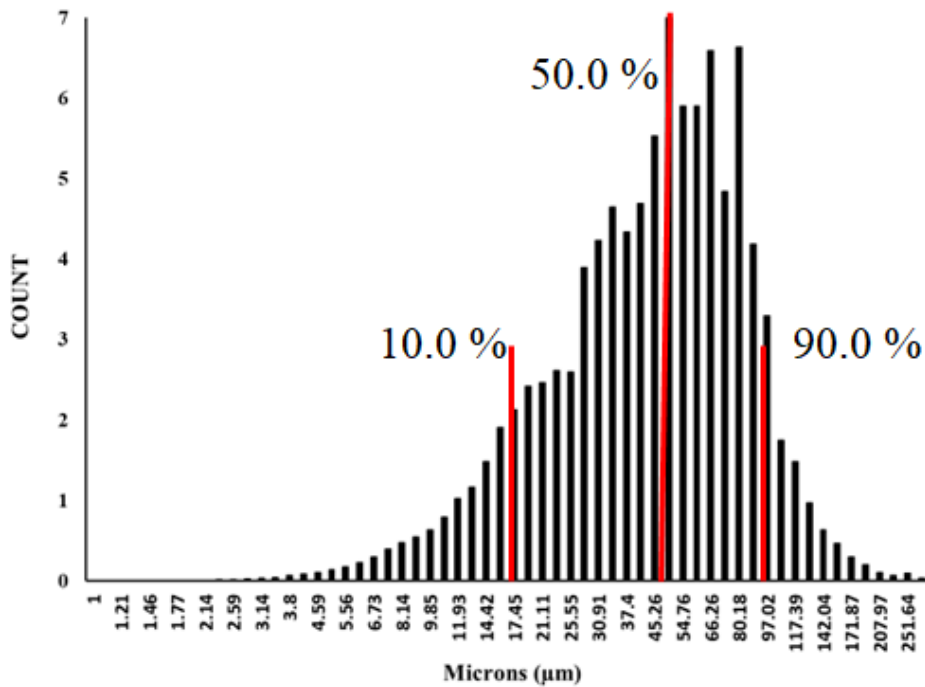
HPC MF and HPC EXF were the granulating polymers used for this work. The thermoplastic characteristics of these polymers made them amenable to extrusion work, but in this work, it was the morphological characteristics of the polymers and their interaction with the API as a function of particle size that were heavily investigated.

The particle size distributions for neat HPC MF and HPC EXF are presented in Figures 4.1 and 4.2 respectively.





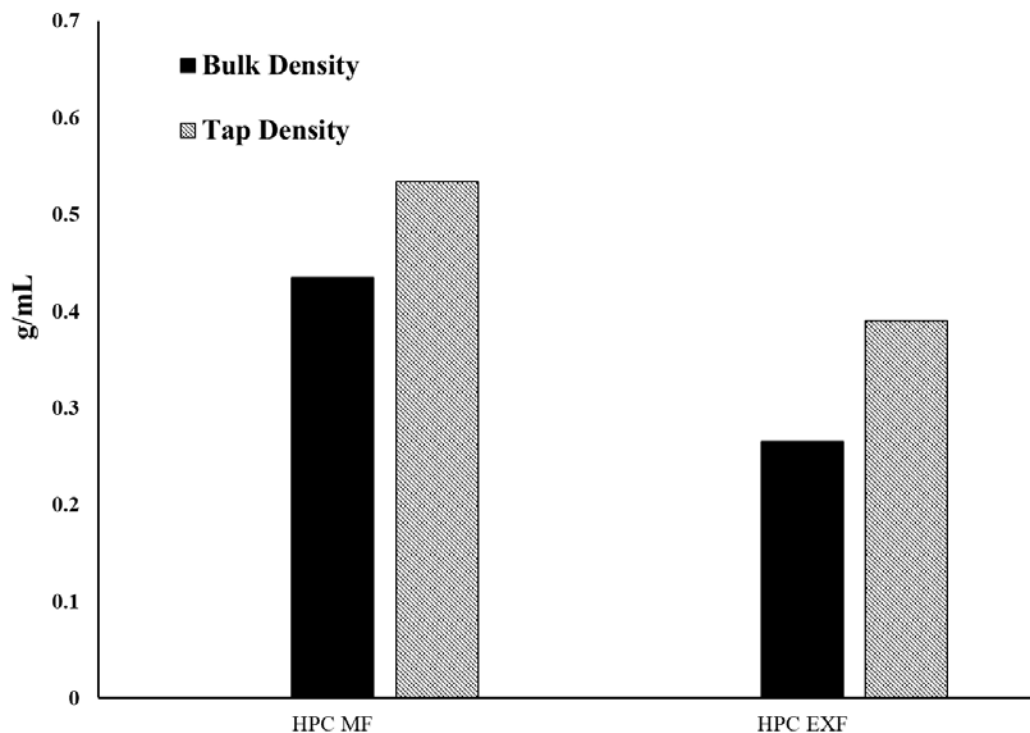
**Figure 4.1** Particle size distribution of neat hydroxypropylcellulose MF (HPC MF) with a  $D_{10}=99.5\mu\text{m}$ ,  $D_{50}=306.3\mu\text{m}$ , and a  $D_{90}=599.0\mu\text{m}$ .



**Figure 4.2** Particle size distribution of neat hydroxypropylcellulose EXF (HPC EXF) with a  $D_{10}=16.1\mu\text{m}$ ,  $D_{50}=45.8\mu\text{m}$ , and a  $D_{90}=86.25\mu\text{m}$ .

Figure 4.1 shows that HPC MF has a larger median particle size ( $D_{50}$ ) when compared to HPC EXF in Figure 4.2. Both polymer grades used have uniform distribution.

HPC MF also has a greater bulk and tap density compared to HPC EXF as shown in Figure 4.3.



**Figure 4.3** Bulk and tap density of hydroxypropylcellulose MF (HPC MF) and hydroxypropylcellulose EXF (HPC EXF).

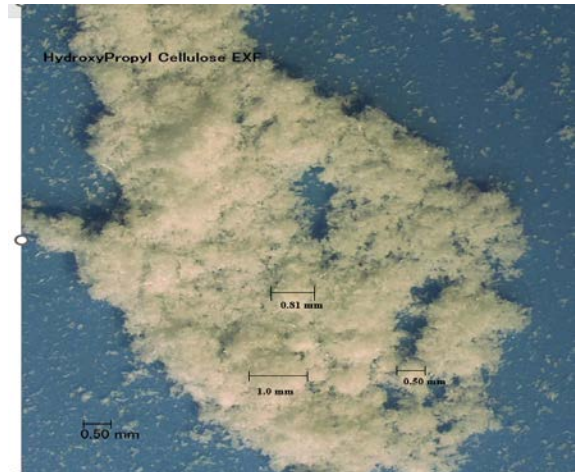
*(Source: Pafiakis, Armenante and Gogos 2022)*

One of the most critical material properties in this work are the material asperities and surface roughness of the particles. These characteristics correlate with the friction coefficient,  $f$  of the particle. These morphological disparities can be observed between HPC MF and HPC EXF in the microscopy and SEM images in Figures 4.4 and 4.5, respectively.

**HPC MF**



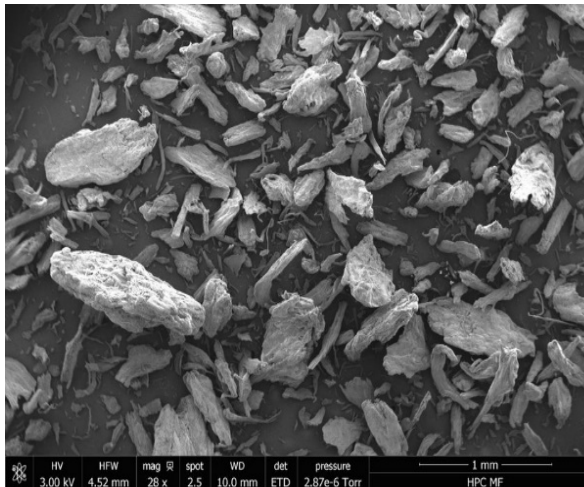
**HPC EXF**



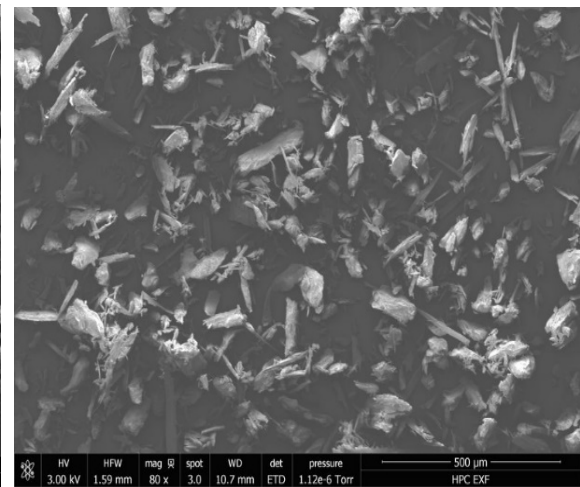
**Figure 4.4** Microscopy image comparison of hydroxypropylcellulose MF (HPC MF) and hydroxypropylcellulose EXF (HPC EXF) at 20x magnification.

The bulk properties of HPC MF show clear discrete particulates. The bulk characteristic of HPC EXF shows several agglomerates. This may be due to tribol effects, cohesion, or moisture content.

**HPC MF**



**HPC EXF**

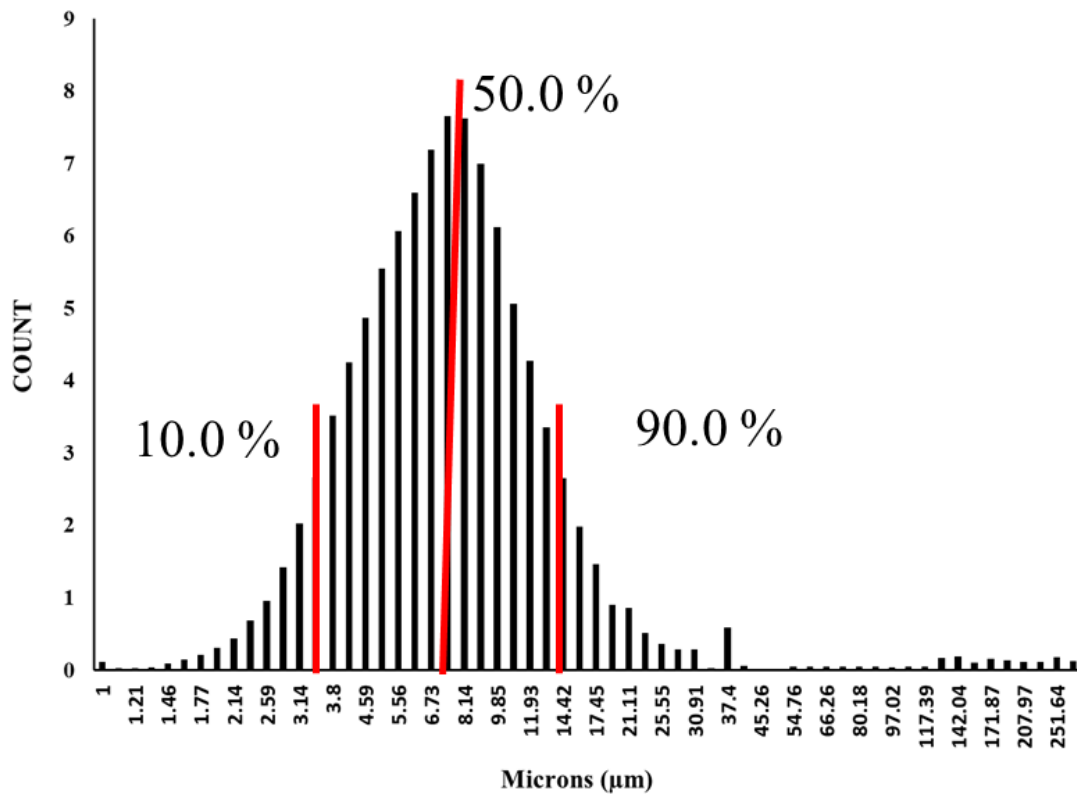


**Figure 4.5** SEM image comparison of hydroxypropylcellulose MF (HPC MF) and hydroxypropylcellulose EXF (HPC EXF).  
(Source: Pafiakis, Armenante and Gogos 2022)

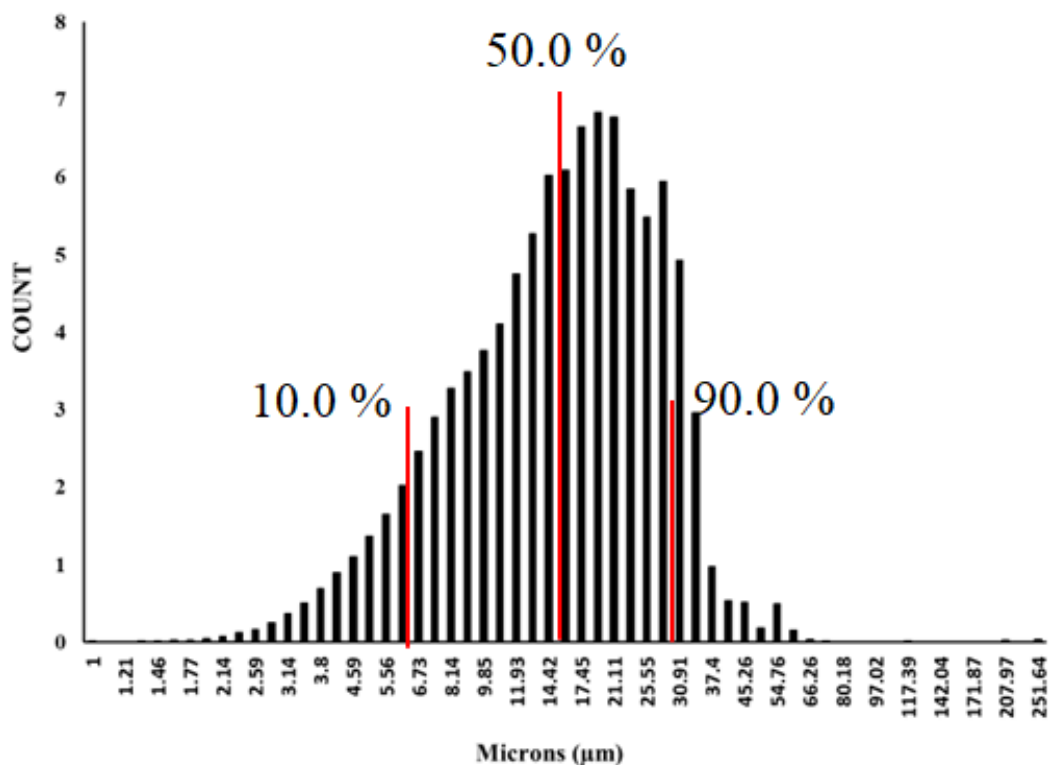
The HPC MF appears “chunky”, coarse, and abrasive in the SEM whereas the HPC EXF particles are fine, thin fibers. The criticality of these morphological characteristics and correlation to the materials friction coefficient,  $f$  will be explained in subsequent sections.

#### 4.1.2 API: Micronized and Non-Micronized Theophylline

The API used for this work was theophylline. Two different grades were used, micronized theophylline (MTHF) and theophylline 325M (THF). The particle size distribution for MTF is presented in Figure 4.5 and THF is presented in Figure 4.6.

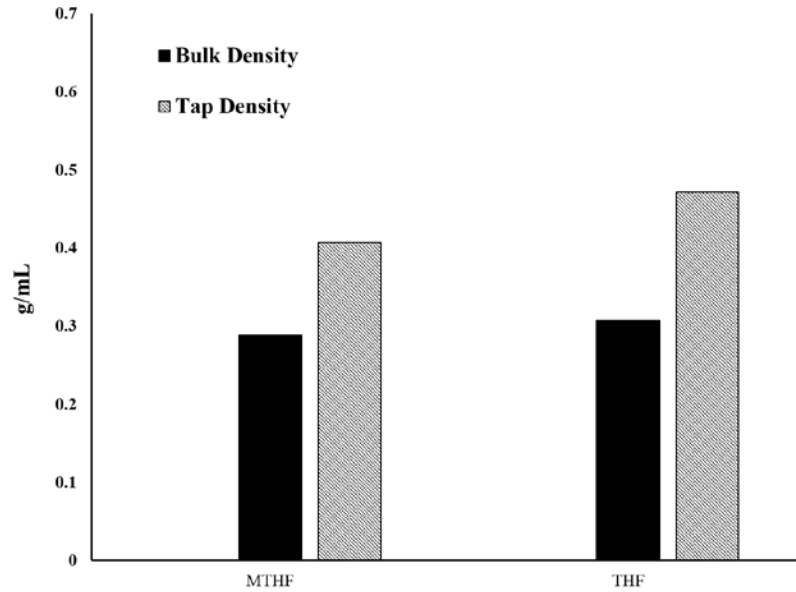


**Figure 4.6** Particle size distribution of neat, micronized theophylline (MTHF) with a  $D_{10}=3.5 \mu\text{m}$ ,  $D_{50}=7.0 \mu\text{m}$ , and a  $D_{90}=13.9 \mu\text{m}$



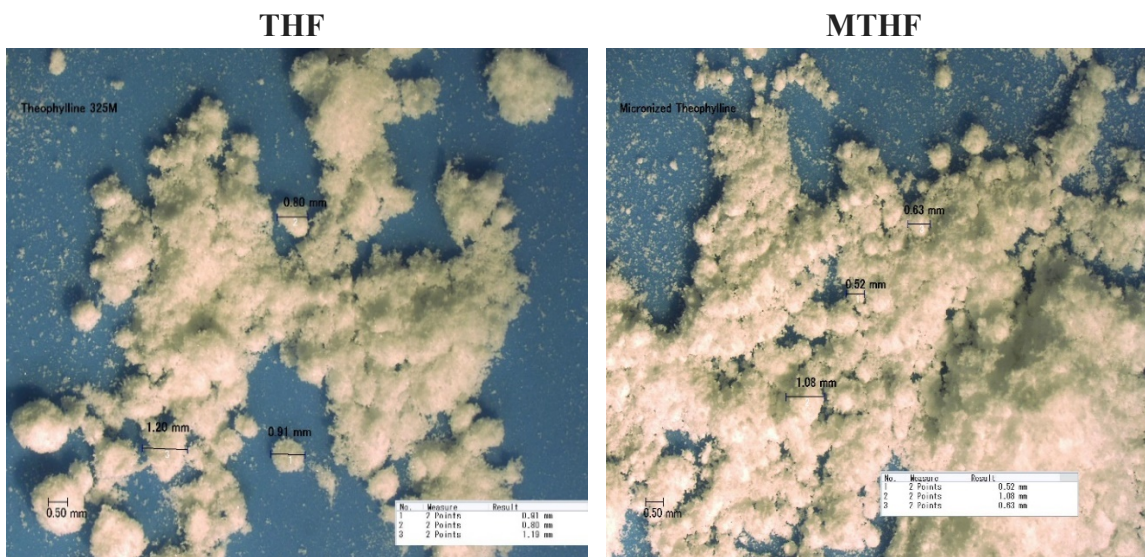
**Figure 4.7** Particle size distribution of neat, theophylline 325M (THF) with a  $D_{10}=6.3\mu\text{m}$ ,  $D_{50}=15.5\mu\text{m}$ , and a  $D_{90}=28.6\mu\text{m}$ .

Figure 4.5 shows that MTHF has a smaller mean particle size ( $D_{50}$ ) when compared to THF. Both API samples also showed to have uniform distribution. The bulk and tap density for both API samples was comparable where THF had a slightly higher tap density than the micronized sample. The bulk and tap density are presented in Figure 4.8.

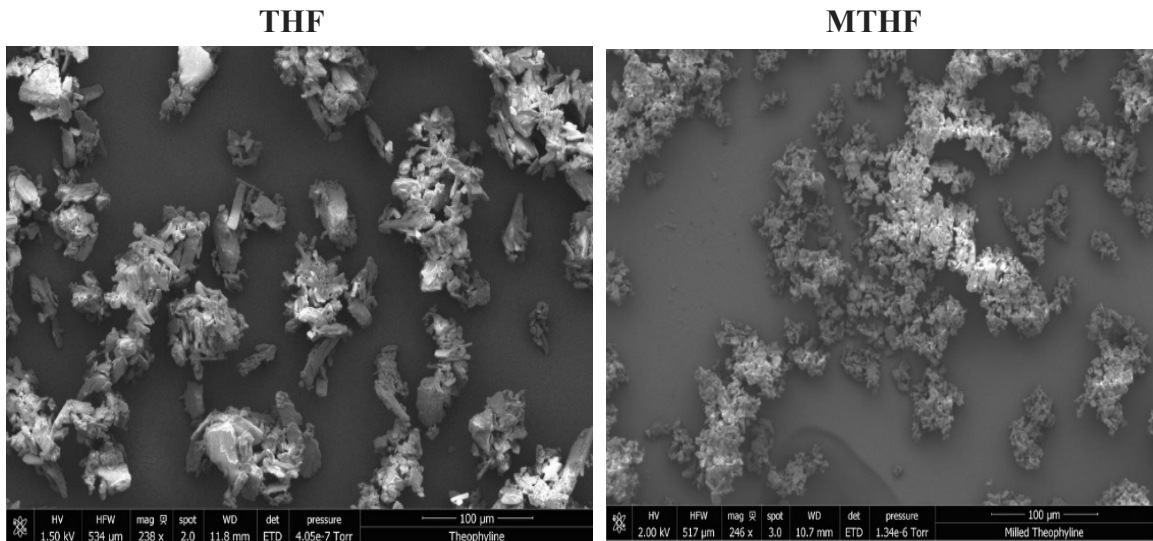


**Figure 4.8** Bulk and tap density of micronized and non-micronized theophylline. (Source: Pafiakis, Armenante and Gogos 2022)

Like the polymers, the morphology of the API was also critical in this work. The morphological disparities can be observed between THF and MTHF in Figure 4.9 of the Bulk component and SEMs in Figure 4.10



**Figure 4.9** Microscopy image comparison of theophylline 325M (THF) and micronized theophylline (MTHF) at 20x magnification.



**Figure 4.10** SEM image comparison of theophylline 325M (THF) and micronized theophylline (MTHF).

(Source: Pafiakis, Armenante and Gogos 2022)

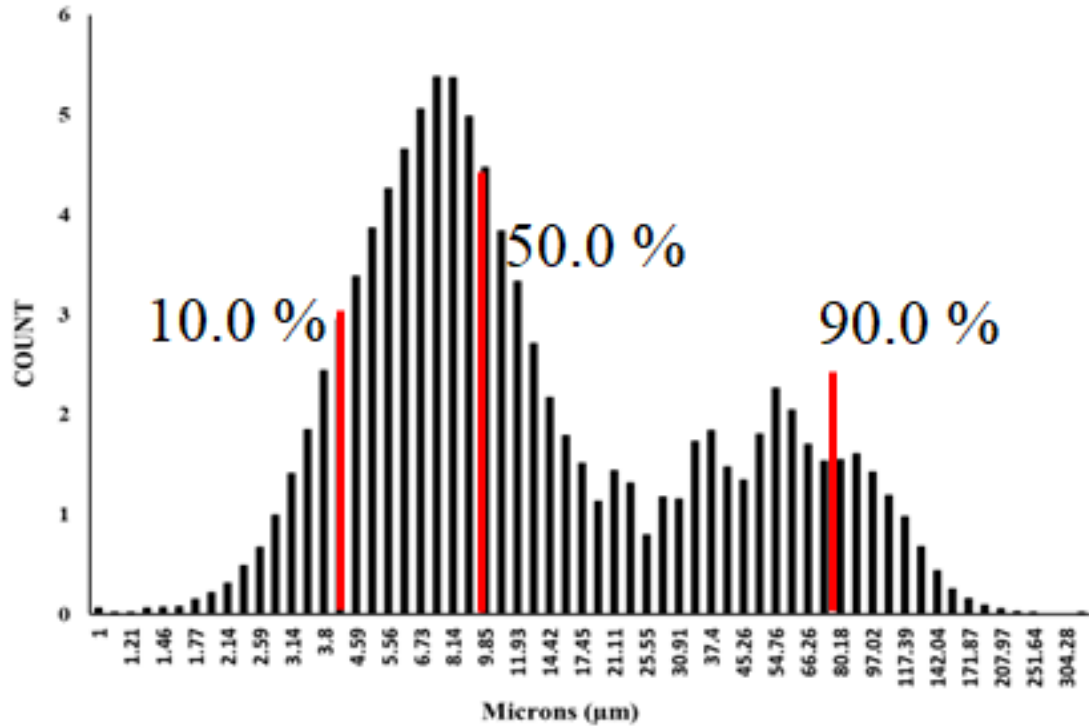
THF consist of thicker elongated particulate clusters while MTHF consist of a mixture of both fine spheres and some thicker block-like particle, also in clusters.

#### 4.1.3 Theophylline: Hydroxypropylcellulose Blends

Four blends were prepared for iShear<sup>TM</sup> analysis, twin screw granulation, and counter rotating batch mixing. These formulations contained a mixture of the different particle sizes presented where the API (70% w/w) and polymer (30% w/w). micronized (or milled) theophylline (MTHF; fine API) was blended with coarse hydroxypropylcellulose (HPC MF; coarse polymer), theophylline (THF; coarse API) with fine hydroxypropylcellulose (HPC EXF, fine polymer), and the other two formulations consisted of both components in the blend being fine or coarse.

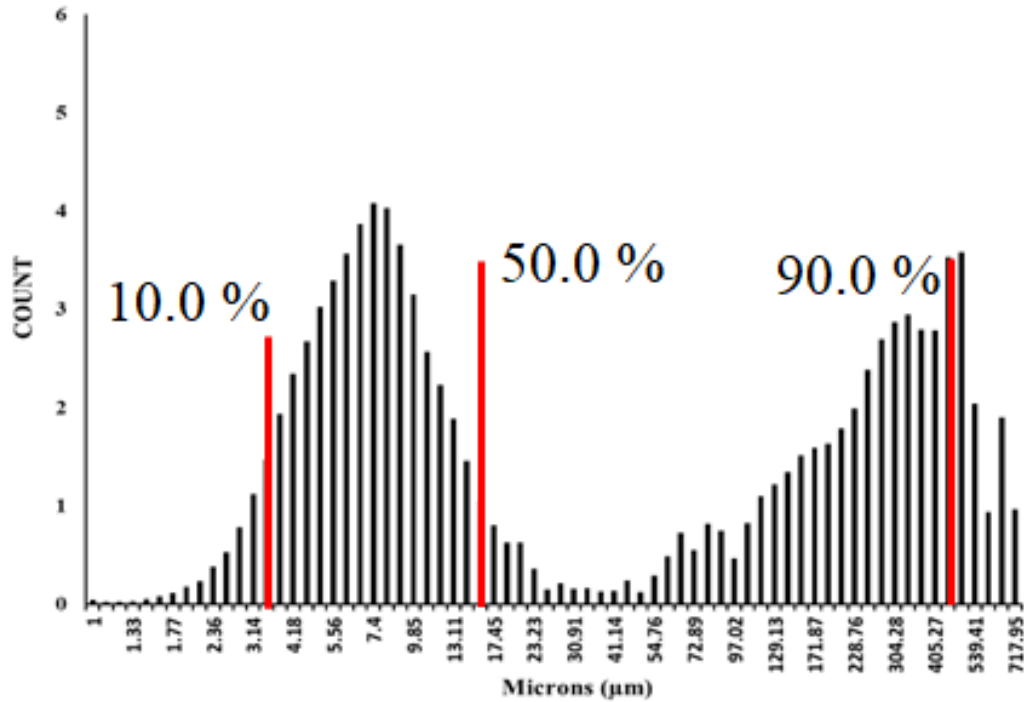
Particle size distribution was measured using the CamSizer and with traditional sieve analysis for the 70:30 theophylline: polymer blends since the CamSizer was not readily available during this work.

The particle size distribution taken by the CamSizer showed a bimodal distribution for the 70:30 MTHF:HPC EXF formulation and the 70:30 MTHF:HPC MF formulation, as expected. The particle size distributions are presented in Figures 4.11 and 4.12, respectively. The distributions show that the blend of the two fine components, MTHF and HPC EXF, were closer in size when compared to the blend with the MTHF and HPC MF.



**Figure 4.11** Particle size distribution of 70:30 micronized theophylline (MTHF) blended with hydroxypropylcellulose EXF (HPC EXF) with a  $D_{10}=4.0 \mu\text{m}$ ,  $D_{50}=9.5 \mu\text{m}$ , and a  $D_{90}=76.5 \mu\text{m}$ .

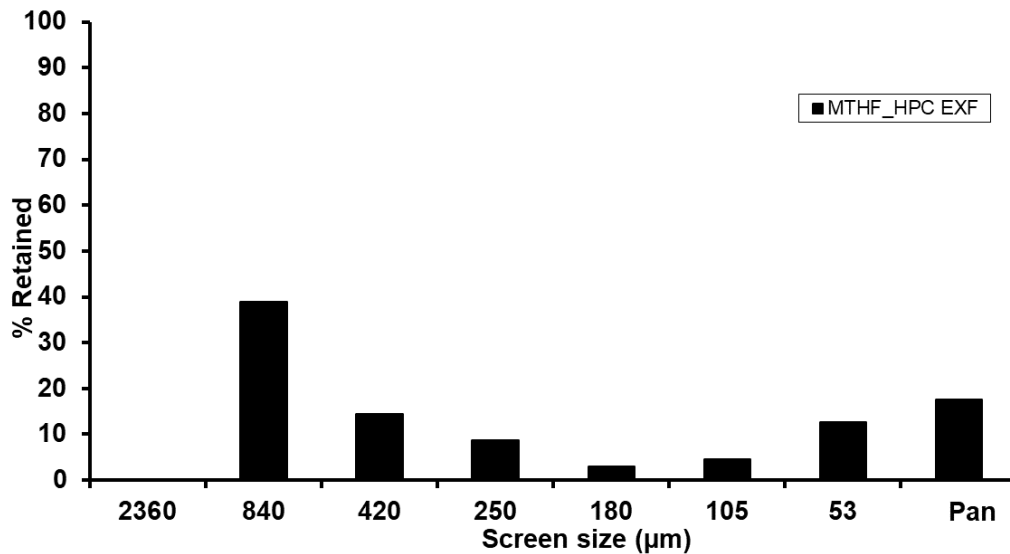




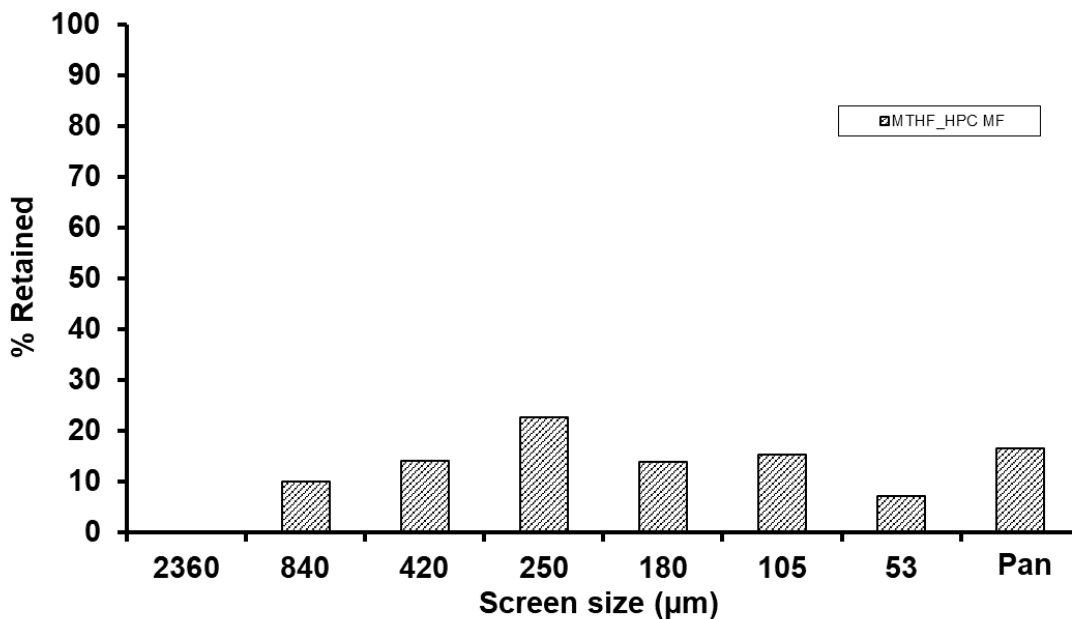
**Figure 4.12** Particle size distribution of 70:30 micronized theophylline (MTHF) blended with hydroxypropylcellulose MF (HPC MF) with a  $D_{10}=4.3 \mu\text{m}$ ,  $D_{50}=16.5 \mu\text{m}$ , and a  $D_{90}=440.6 \mu\text{m}$ .

Sieve Analysis for the 70:30 MTHF blends are presented in Figure 4.13 and 4.14.

A bimodal distribution is also observed for both MTHF formulations. This method was developed to enable a way to track the particle size growth as a function of time. This will be discussed more when the Brabender batch mixer is introduced.

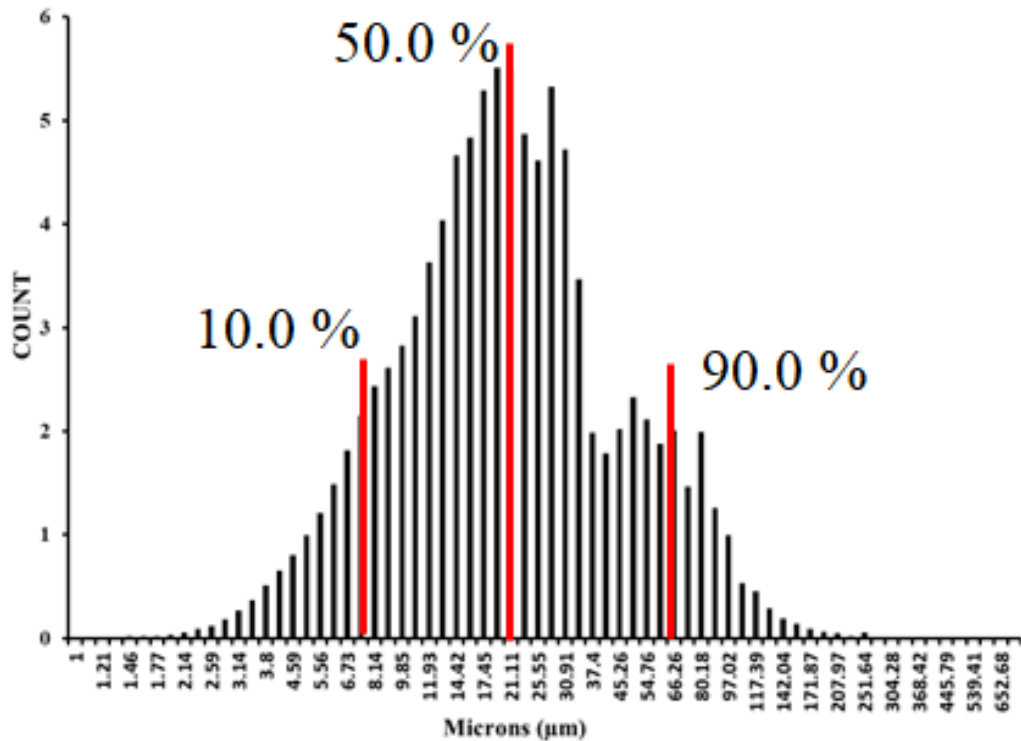


**Figure 4.13** Sieve analysis for particle size distribution of 70:30 micronized theophylline (MTHF) blended with hydroxypropylcellulose EXF (HPC EXF).

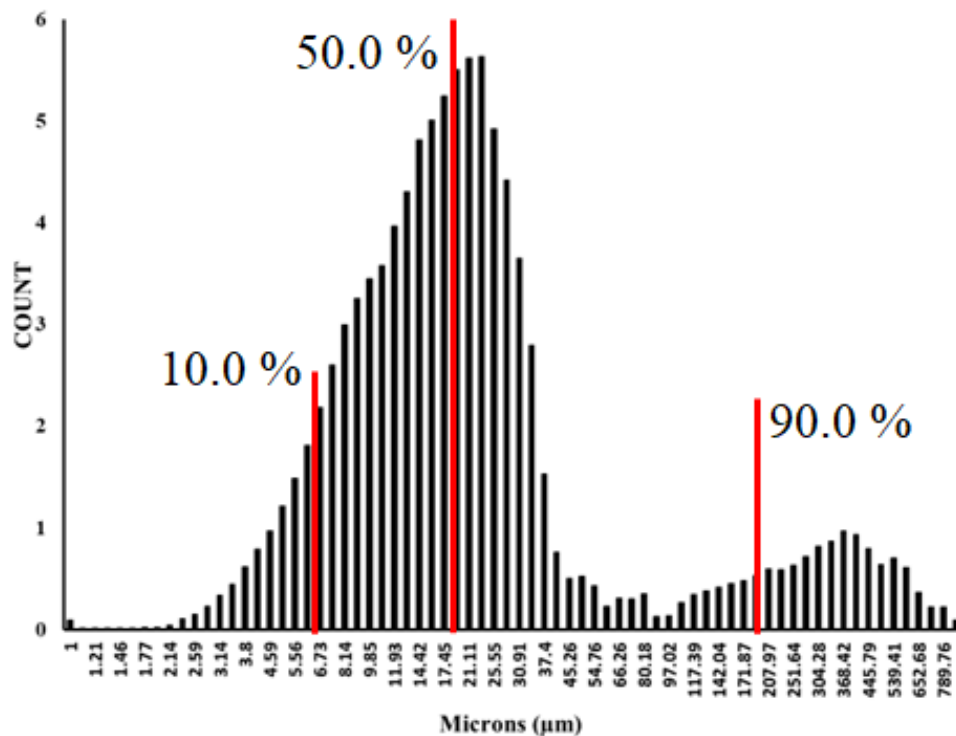


**Figure 4.14** Sieve analysis for particle size distribution of 70:30 micronized theophylline (MTHF) blended with hydroxypropylcellulose MF (HPC MF).

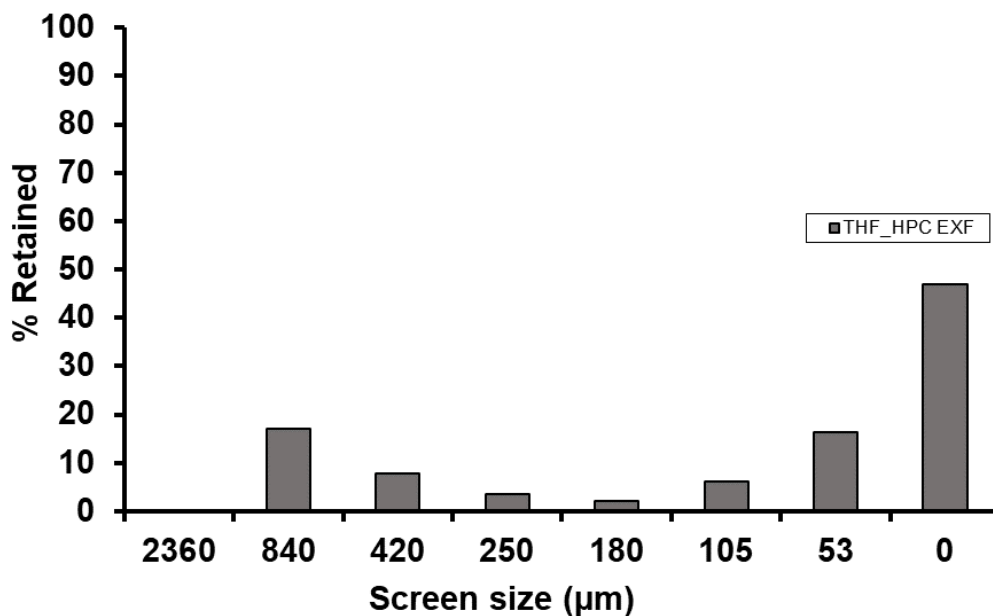
The Camsizer data for the 70:30 THF:HPC EXF formulation shows a unimodal distribution, suggesting a more homogeneous distribution of particles in the bulk blend. This behavior can lead to specific packing orientation. This will be further discussed in subsequent section when the coefficient of friction,  $f$  is introduced.



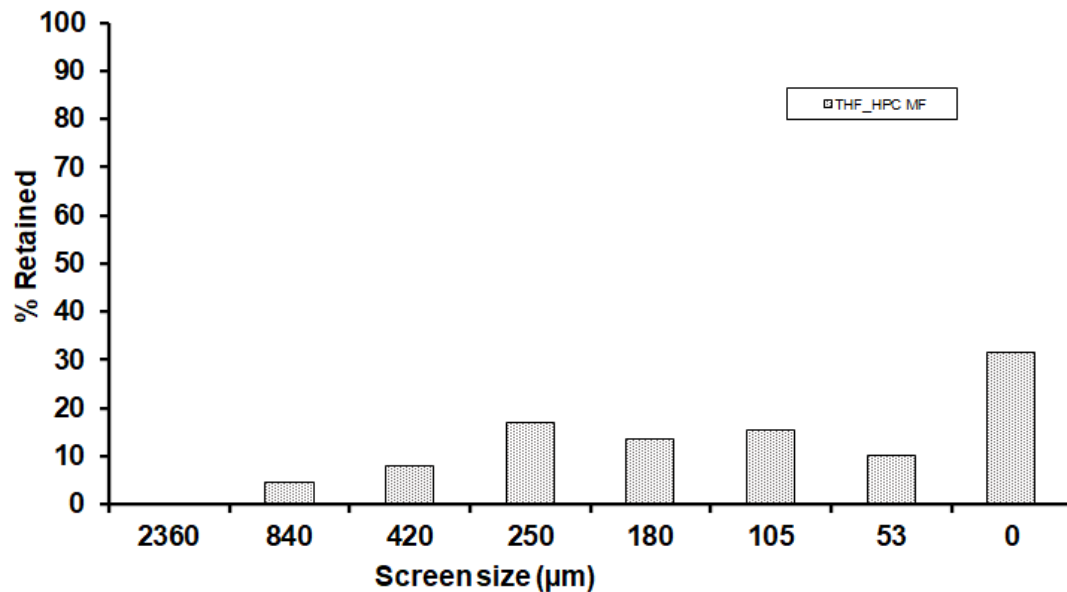
**Figure 4.15** Particle size distribution of theophylline (THF) blended with hydroxypropylcellulose EXF (HPC EXF) with a  $D_{10}=7.4 \mu\text{m}$ ,  $D_{50}=19.2 \mu\text{m}$ , and a  $D_{90}=60.4 \mu\text{m}$ .



**Figure 4.16** Particle size distribution of theophylline (THF) blended with hydroxypropylcellulose MF (HPC MF) with a  $D_{10}=6.6 \mu\text{m}$ ,  $D_{50}=17.54 \mu\text{m}$ , and a  $D_{90}=180.50 \mu\text{m}$ .

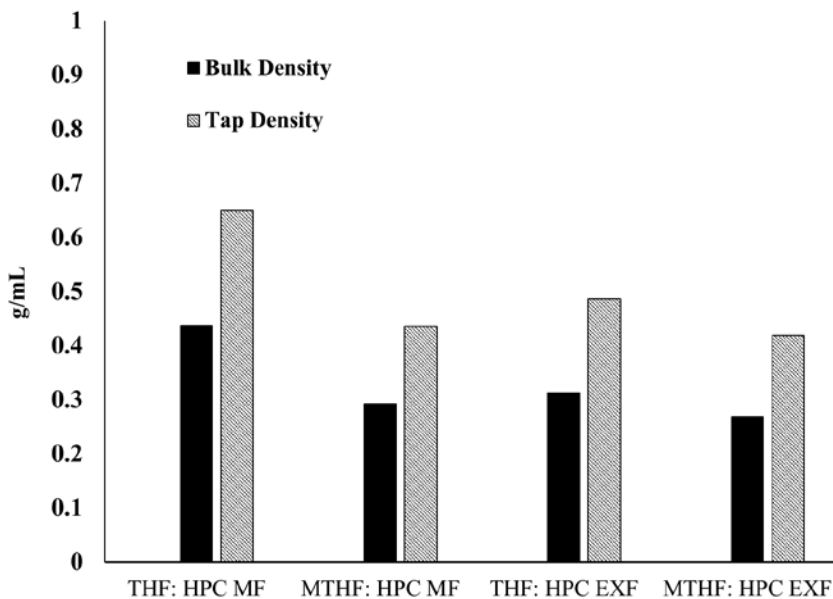


**Figure 4.17** Sieve Analysis for Particle Size Distribution of 70:30 Theophylline (THF) blended with Hydroxypropylcellulose (HPC EXF)



**Figure 4.18** Sieve analysis for particle size distribution of 70:30 theophylline (THF) blended with hydroxypropylcellulose (HPC MF).

The bulk and tap density for all 70:30 samples were comparable where the 70:30 THF:HPC MF blend had slightly higher bulk and tap density than the other three samples.



**Figure 4.19** Bulk and tap density of micronized and non-micronized theophylline. (Source: Pafiakis, Armenante and Gogos 2022)

## 4.2 Twin Screw Granulation of Theophylline and Hydroxypropylcellulose Blends

### 4.2.1 Granule analysis using the 30 mm Twin Screw Mixing Element Evaluator (TSMEE)

For this study only non-micronized theophylline (THF), at approximately 65% drug loading with HPC MF was evaluated. The minimum processing barrel temperature was determined experimentally by ramping the temperature in Zone 1 and Zone 2 (Data not available). Zone 3 was kept constant at 20°C. The feed rate was constant at 4.5 kg/hr. at a screw speed of 105 rpm.

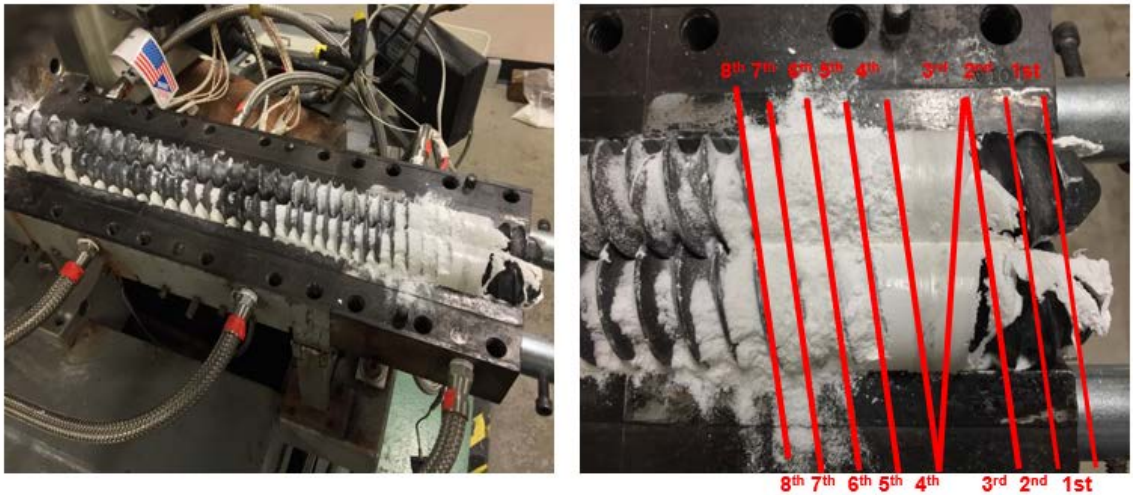
**4.2.1.1 System Parameters for 30mm Twin Screw Mixing Element Evaluator (TSMEE).** The minimum processing barrel temperature was found to be 90°C for both screw configurations. Table 4.1 presents the following parameters and response (product temperature and torque).

**Table 4.1** 30 mm Twin Screw Mixing Element Evaluator (TSMEE) System Parameters

Screw Configuration	Feed Rate (kg/hr.)	Screw Speed (rpm)	Zone 1 Temp °C (set/actual)	Zone 2 Temp °C (set/actual)	Zone 3 Temp °C (set/actual)	Product Temp °C	Torque (%)
1 x Rev. Conveyor (1RS)			90/90	90/90	20/35	95	28
5 x Kneading Blocks + 1 x Reverse Conveyor (5KB1RS)	4.5	105	90/90	90/90	20/40	90	35

FED and PED are occurring because of the temperature recorded in Zone 3. From the temperature ramping trials, it was observed that the temperature in Zone 3 would climb extremely fast. There was a 15°C and 20°C temperature increase between the reverse (1RS) conveying set up and the one with the five kneading blocks (5KB+1RS), respectively.

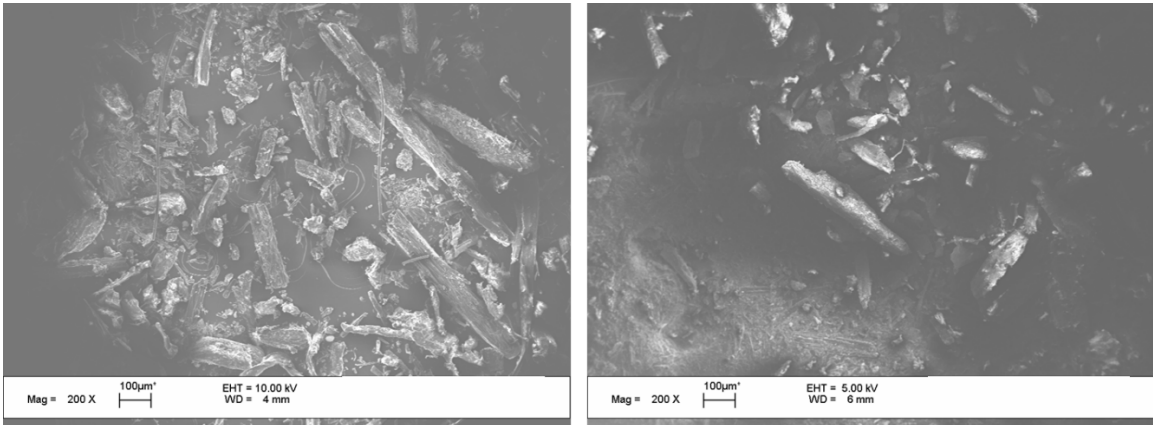
**4.2.1.2 Carcass Analysis Using the 30 mm Twin Screw Mixing Element Evaluator (TSMEE) for the One Reverse Section Screw Configuration.** Carcass samples were collected from the extruder after it was opened from the segments identified in Figure 4.20 for the screw configuration with one reverse section (1RS).



**Figure 4.20** 30 mm Twin Screw Mixing Element Evaluator (TSMEE) with one reverse (1RS) screw configuration.

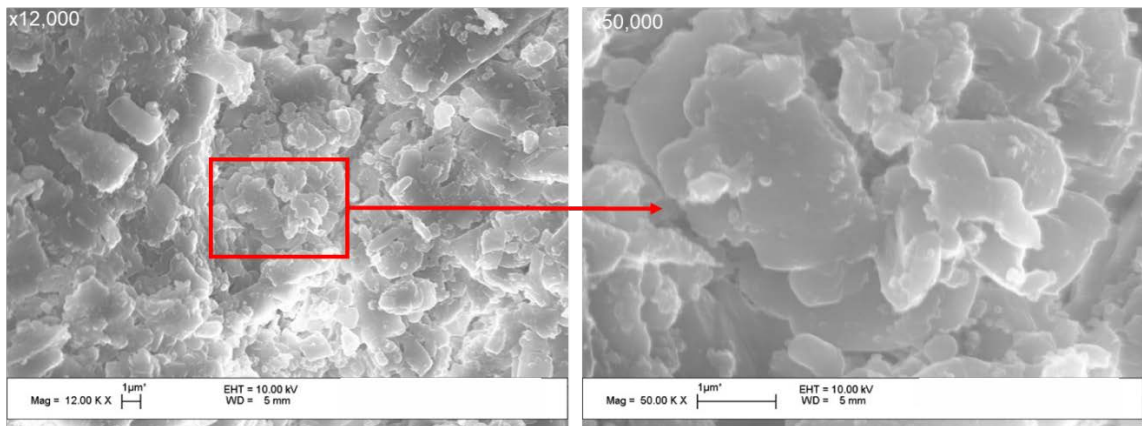
Figure 4.20 shows that the extruder is running starved. The powder begins to build up at segment 8. This is due to the reverse (1RS) screw element that was used for this configuration. From segment 8 and forward, there is powder build up that accumulates from the mixing/ granulating that is occurring between segment 5 and 1.

Figure 4.21 shows carcass samples from segments 8, 7 and 6 show that there were no morphological changes relative to the unprocessed formulations.



**Figure 4.21** Carcass analysis by SEM of the theophylline (THF) formulation granulated with the one reverse (IRS) screw configurations: 8<sup>th</sup>, 7<sup>th</sup> and 6<sup>th</sup> segments show no morphological change relative to the unprocessed formulation.

Figure 4.22 shows carcass samples between segment 5 and 4.



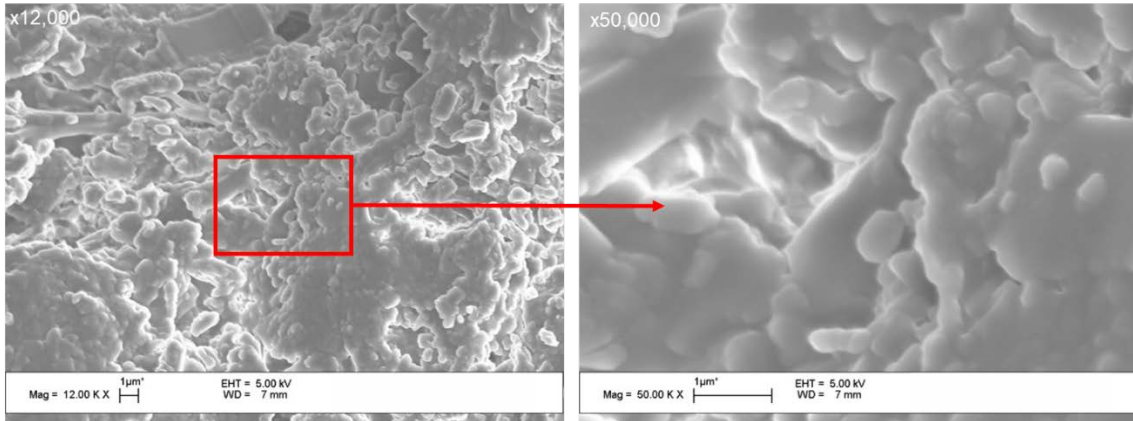
**Figure 4.22** Carcass analysis by SEM of the theophylline (THF) formulation granulated with the one reverse (IRS) screw configurations: between segment 5 and 4.

Material collected between segment 5 and 4 are not in a particulate form and show that they are slightly deformed. The particles do appear to be in “chunks” composed of many fused or sintered particles in the range of 1-10µm. The segment between 5 and 4 is



the first segment, moving downstream in the extruder screw, that the material appears to be in one solid plug rather than free flowing powder.

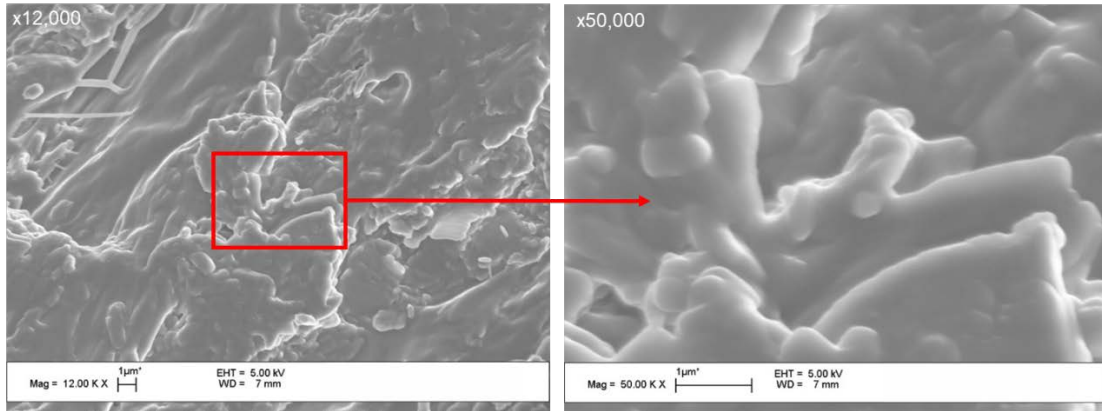
Figure 4.23 shows carcass samples between segment 4 and 3.



**Figure 4.23:** Carcass analysis by SEM of the Theophylline (THF) formulation granulated with the one reverse (1RS) screw configurations: between segment 4 and 3.

Material collected between segment 4 and 3, still appears to be fused particulates (or sintered), however, areas that resemble a polymer melt begin to appear. This may be indicative that the heat generated locally is going beyond the PED and FED melting mechanisms and approaching or entering the viscous energy dissipation (VED). The extent that particulates are fused together also seems to be noticeably greater, compared to material collected from the previous lobe.

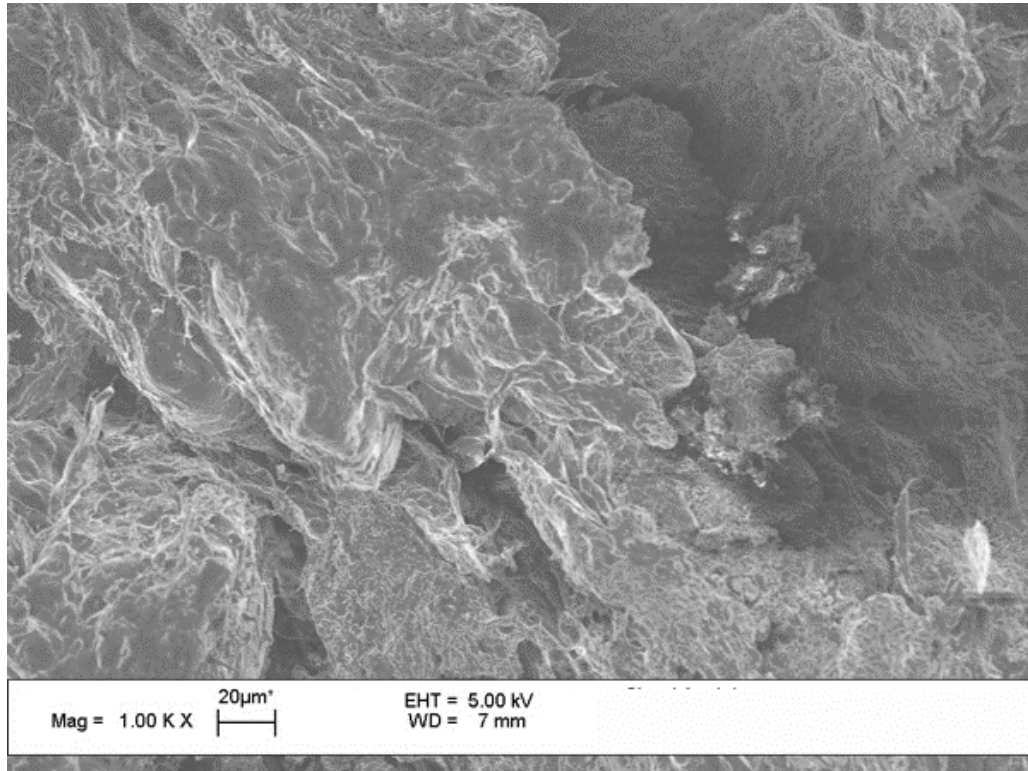
Samples between segment 3 and 2 were not collected. Figure 4.24 shows carcass samples between 2 and 1.



**Figure 4.24** Carcass analysis by SEM of the theophylline (THF) formulation granulated with the one reverse (IRS) screw configurations: between segment 2 and 1.

Material collected between segment 2 and 1 have a strong resemblance to a solid rich suspension and polymer melt vs. a granulation and the extent that the particles are fused is clear, but the mass is approaching one single phase. Discrete particulates are no longer visible.

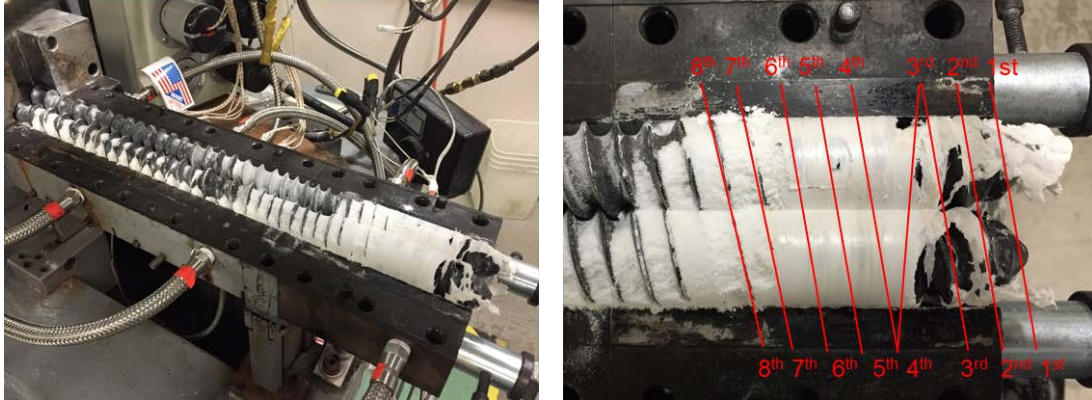
Figure 4.25 shows the morphology of the final product.



**Figure 4.25** Carcass analysis by SEM of the theophylline (THF) formulation granulated with the one reverse (1RS) screw configurations: final granulation.

The final product is not very different than the morphology observed between segment 2 and 1. All the mass building seemed to occur between segment 4 and 1. It is possible that that the blend was one solid rich suspension by segment 2.

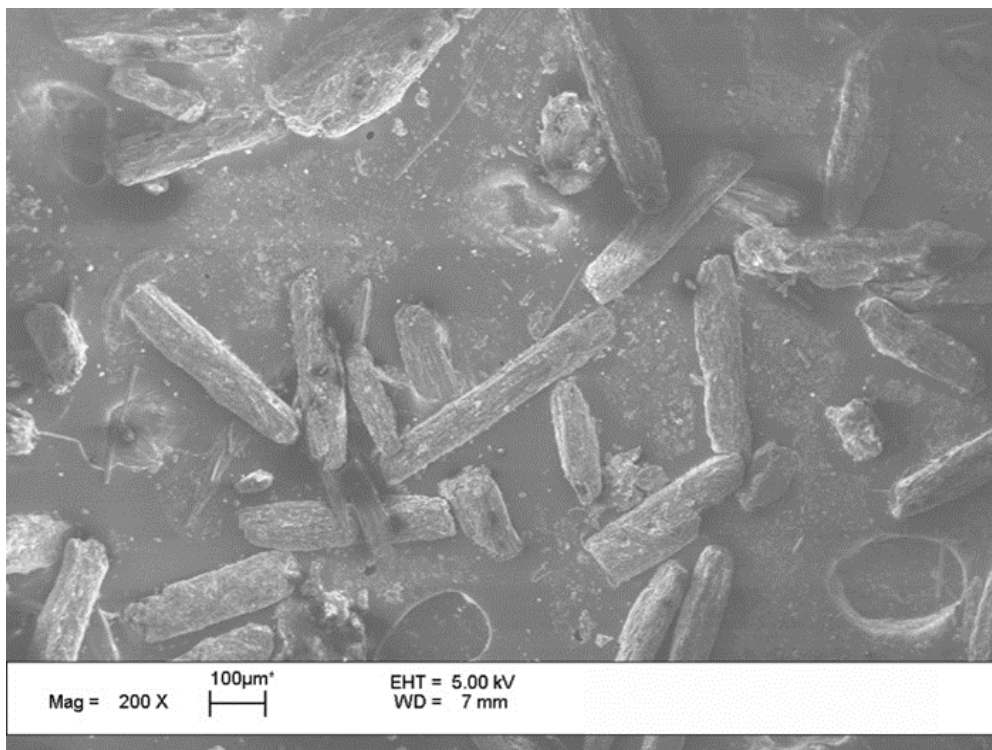
**4.2.1.3 Carcass analysis using the 30 mm Twin Screw Mixing Element Evaluator (TSMEE) for the one reverse and five kneading block section screw configurations (5KB+1RS).** figure 4.26 shows the filled extruder for the screw configuration with the five kneading elements followed by the one reverse section. (5KNB+1RS).



**Figure 4.26** 30 mm Twin Screw Mixing Element Evaluator (TSMEE) with five kneading blocks (5KB) and one reverse (1RS) screw configuration.

Like Figure 4.20, Figure 4.26 shows that the extruder is also running starved with this configuration. There is more powder build up prior to segment 8, but the morphology of this material was found to be equivalent to that taken between segment 8 and 7.

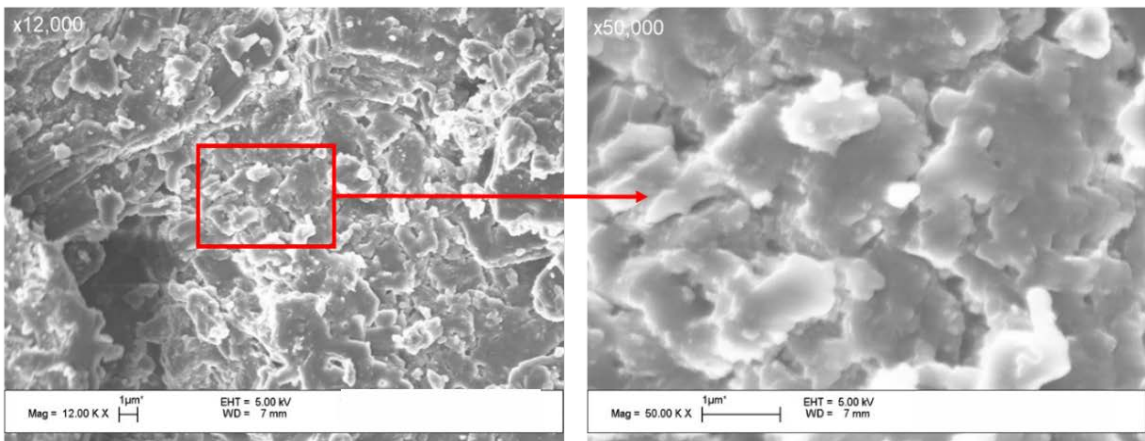
Figure 4.27 shows carcass samples before segment 8.



**Figure 4.27** Carcass analysis by SEM of the theophylline (THF) formulation granulated with the five kneading blocks (5 KB) and one reverse (1RS) screw configurations: before segment 8.

It is also clear that granulation is occurring much sooner using the 1RS configuration, due to the addition of the five kneading blocks. Only the segment between 8 and 7 are powder and granulation begin between segment 7 and 6.

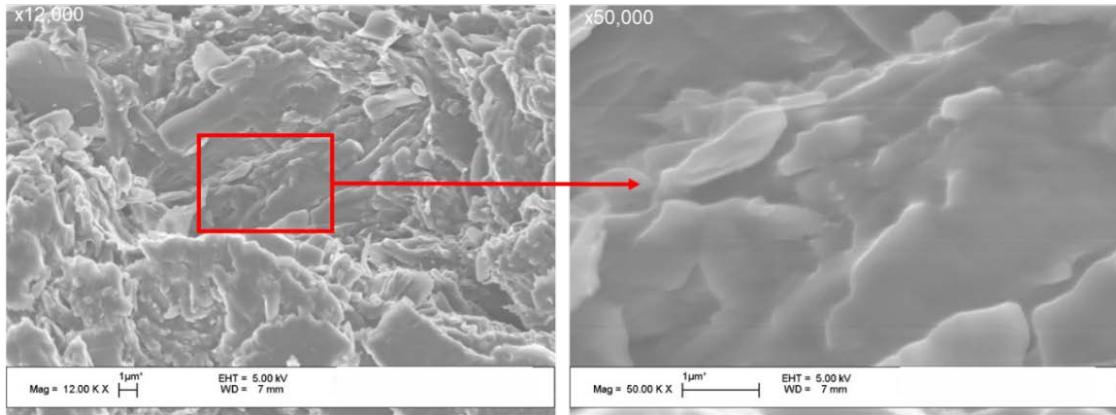
Figure 4.28 shows the granulation between segment 7 and 6.



**Figure 4.28** Carcass analysis by SEM of the theophylline (THF) formulation granulated with the five kneading blocks (5 KB) and one reverse (1RS) screw configurations: between segment 8 and 7.

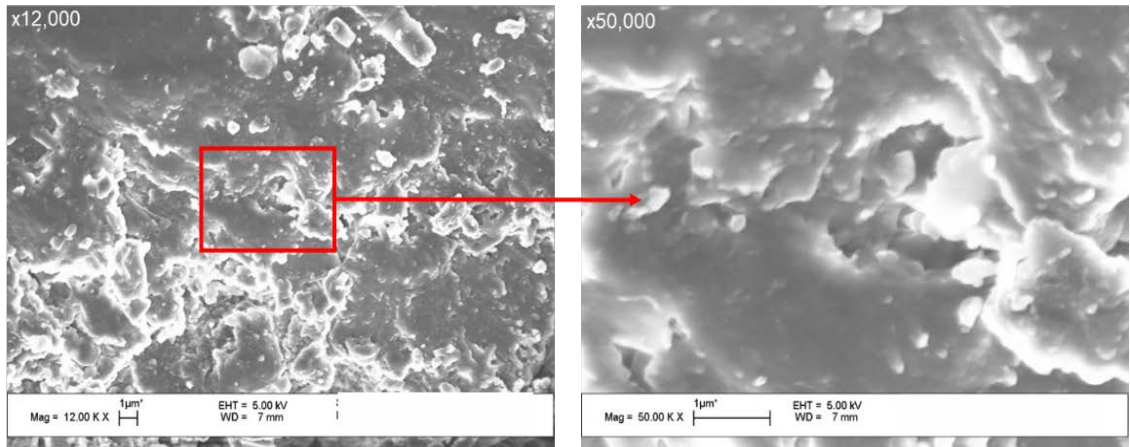
In this segment, the blend is no longer in free-flowing particulate form but rather in a granulated or sintered state. Note that, with the 1 RS screw configuration, this morphology was observed in the segment between 5 and 6, further down the extruder. Until then, the only changes for this granulation is the change in the product temperature.

Figure 4.29 shows the granulation between segment 7 and 6.



**Figure 4.29** Carcass analysis by SEM of the theophylline (THF) formulation granulated with the five kneading blocks (5 KB) and one reverse (1RS) screw configurations: between segment 7 and 6.

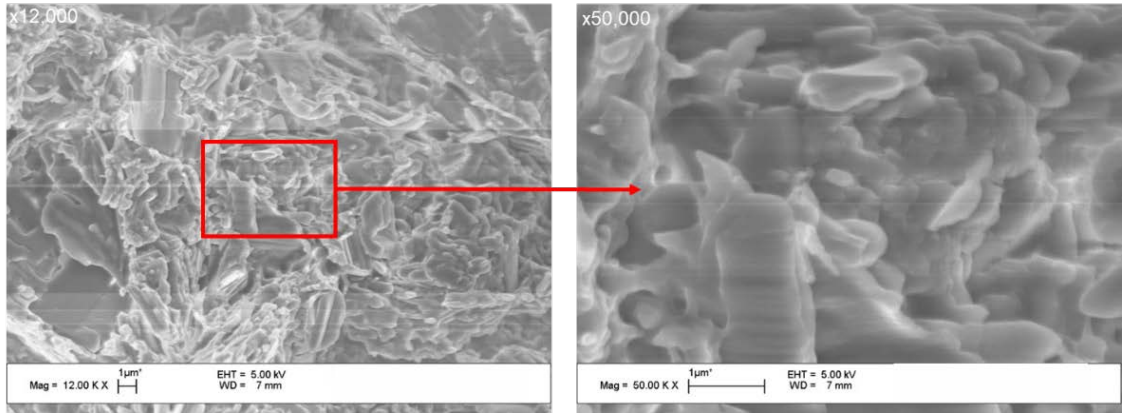
The samples collected from the first neutral kneading block consist of sintered particulates with occasional areas that resemble a polymer melt. Figure 4.30 shows the granulation between segment 6 and 5.



**Figure 4.30** Carcass analysis by SEM of the theophylline (THF) formulation granulated with the five kneading blocks (5 KB) and one reverse (1RS) screw configurations: between segment 6 and 5.

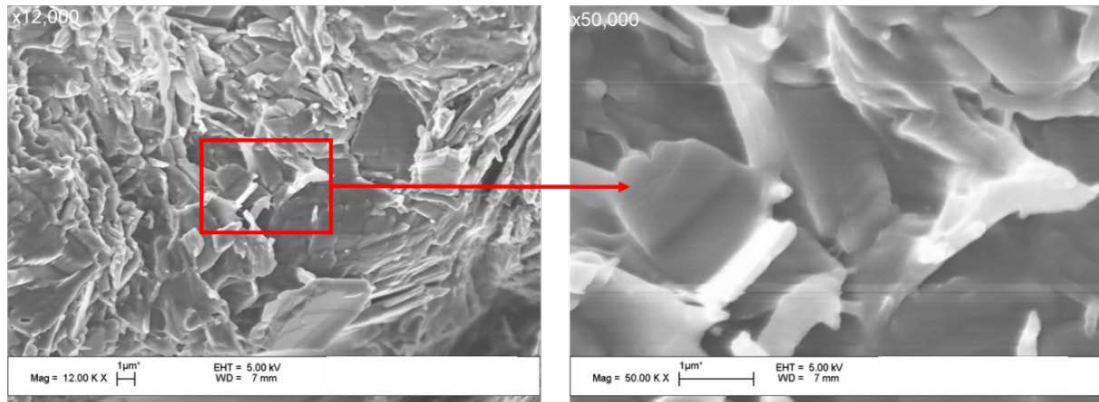
The granules collected between segment 6 and 5 now show strong evidence of agglomeration and sintering (or granulation). These images also show that the morphology

from segment 7 and 6 is maintained with this configuration. There does not seem to be an increase in the extent of polymer melting. Figure 4.31 shows the granulation between segment 5 and 4.



**Figure 4.31** Carcass analysis by SEM of the theophylline (THF) formulation granulated with the five kneading blocks (5 KB) and one reverse (1RS) screw configurations: between segment 5 and 4.

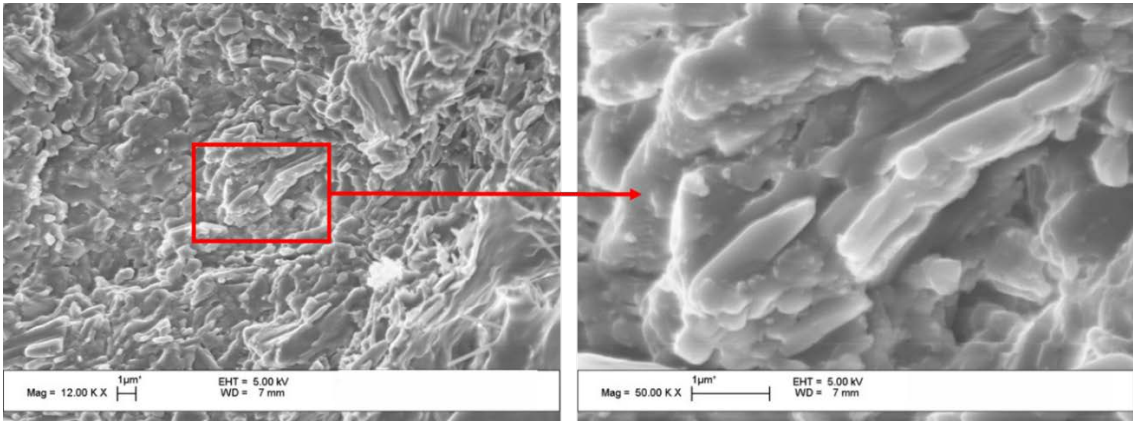
The granule morphology continues to show the fusing of discrete particles vs. a solid rich suspension. Figure 4.32 shows the granulation between segments 4 and 3.



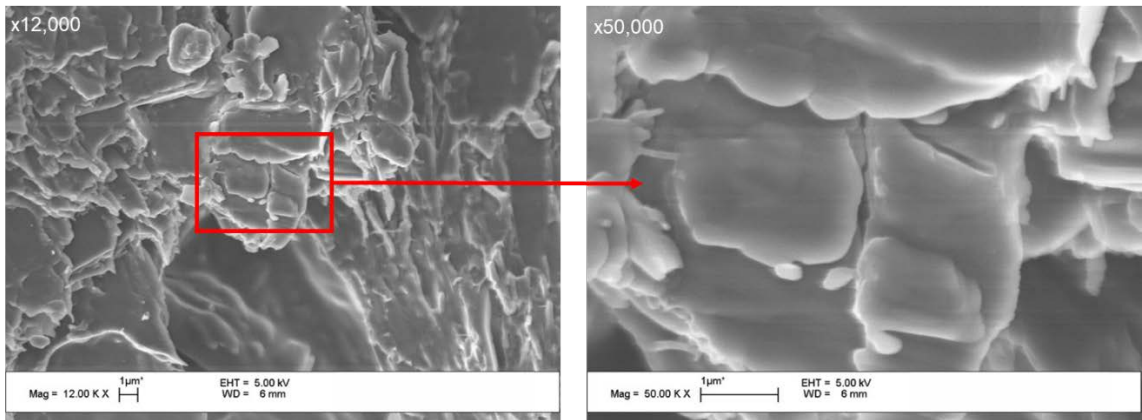
**Figure 4.32** Carcass analysis by SEM of the theophylline (THF) formulation granulated with the five kneading blocks (5 KB) and one reverse (1RS) screw configurations: between segment 4 and 3.

The segment between 4 and 3 still shows discrete particles fused together. By this stage it may be possible that the API particles (and some polymers particles) are held

together by the polymer glue points. Figure 4.33 shows the granulation between segment 3 and 2. Figure 4.34 shows the granulation between segment 2 and 1.



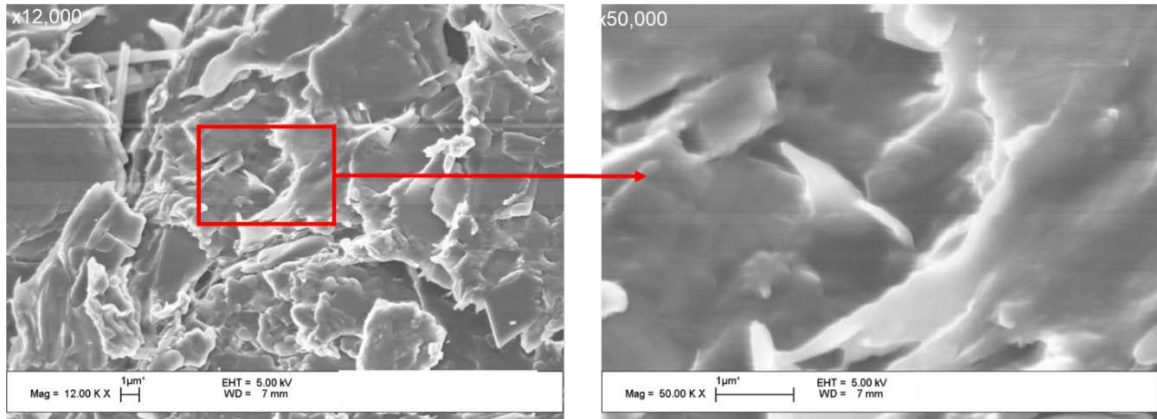
**Figure 4.33** Carcass analysis by SEM of the theophylline (THF) formulation granulated with the five kneading blocks (5 KB) and one reverse (1RS) screw configurations: between segment 3 and 2.



**Figure 4.34** Carcass analysis by SEM of the theophylline (THF) formulation granulated with the five kneading blocks (5 KB) and one reverse (1RS) screw configurations: between segment 2 and 1.



Figure 4.35 shows the morphology of the final product.



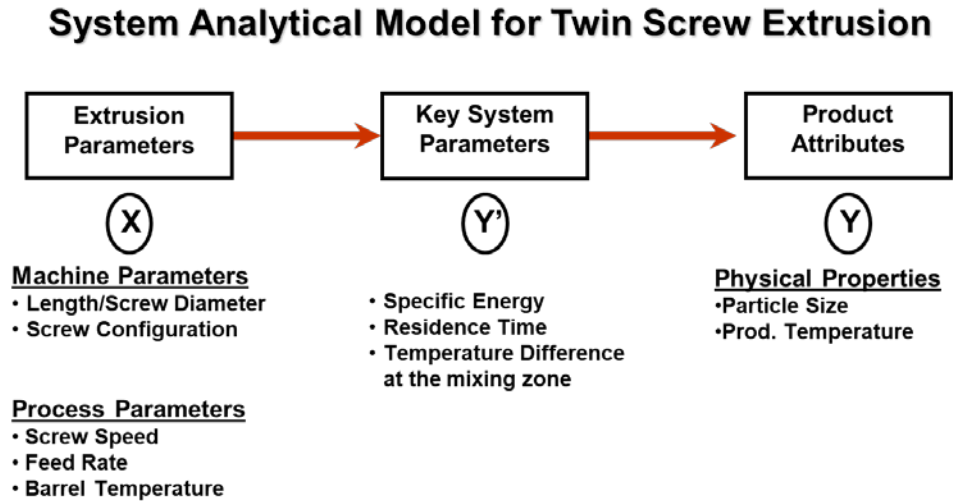
**Figure 4.35** Carcass analysis by SEM of the theophylline (THF) formulation granulated with the one reverse (1RS) screw configurations: final granulation.

The segments between 3 and 2, 2 and 1, and the final product do not show any morphological difference. On the contrary, the morphology continues to be maintained throughout the mixing section.

Based on this carcass analysis and the limited temperature data collected during processing, the kneading blocks alleviate some of the PED and FED that may have been more aggressive with the 1RS configuration alone. This may seem counterintuitive but the blend with the 5KB and the 1RS conveyor had a “*metering*” effect. The material in the mixing section was controlled in a way for this configuration that did not lead to VED and, hence, a solid suspension.

#### 4.2.2 Parametric Effects using three 5mm Kneading Blocks to Granulate in a 27 mm Co-Rotating Twin Screw Extruder.

A system analytical model was used for analyzing the parametric effects for each formulation. The model is presented in Figure 4.36.



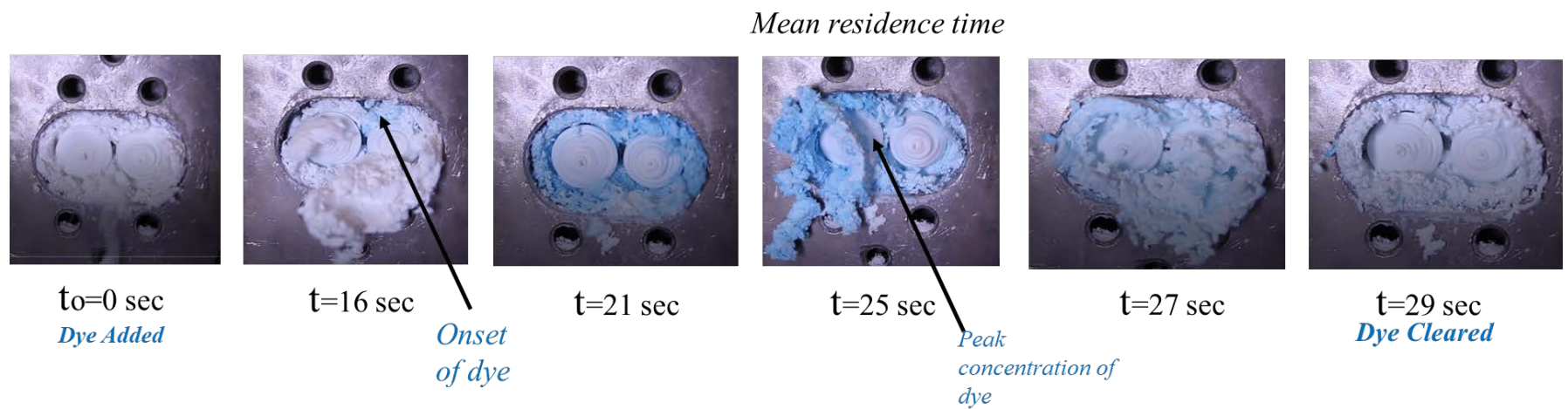
**Figure 4.36** System analytical model used for 27 mm twin screw extrusion trials.  
(Source: Dreiblatt 2013)

Table 4.2 list the set points of all the parameters that were evaluated.

**Table 4.2** Design of Experiments Used for 27 mm Parametric Study.

FEED RATE (kg/hr.)	SCREW SPEED (rpm)	TEMPERATUE (°C)
4	200	35
		50
	400	35
		50
8	200	35
		50
	400	35
		50

The mean residence time and residence time distribution was qualitatively captured by injecting approximately 100 g of blend died with blue food coloring and recording the time it took for the tracer to peak and to clear the extruder (Kolter 2010). This was performed for all formulations that were processable at the given temperature, feed rate, and screw speed. Figure 4.37 shows an example of the onset of the blue die and the time it takes to clear the extruder.



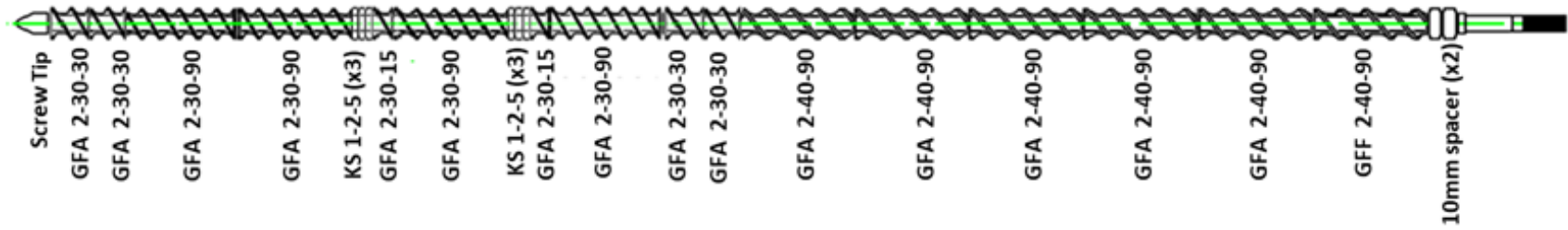
**Figure 4.37** Example of how residence time was determined using the micronized theophylline and hydroxypropylcellulose MF blend (MTHF:HPC MF).

#### **4.2.2.1 Screw configuration evaluation for the 27 mm granulation experiments.**

Two scouting assessments were used to identify the screw configuration and the processing temperature for the screening experiments. Only the 70% theophylline: 30% HPC EXF formulation was used for these assessments. The first screw configuration evaluated is presented in Table 4.3 and Figure 4.38. This screw configuration was evaluated at 50°C only.

**Table 4.3** Two Dispersive Kneading Zones Screw Design Evaluated During 27 mm Leistritz Experiments

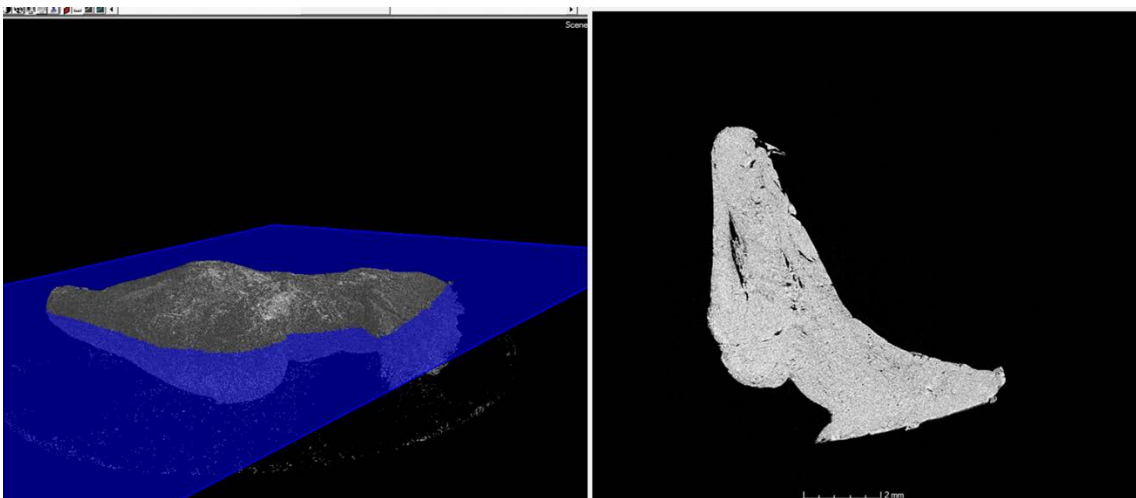
Order	Element	Function	Elements along the shaft (mm)
1	10 mm spacer	Spacer	N/A
2	10 mm spacer	Spacer	N/A
3	GFF-2-40-90	Conveying	90
4	GFA-2-40-90	Conveying	90
5	GFA-2-40-90	Conveying	90
6	GFA-2-40-90	Conveying	90
7	GFA-2-40-90	Conveying	90
	GFA-2-40-90	Conveying	90
	GFA-2-30-30	Conveying	30
	GFA-2-30-30	Conveying	30
8	GFA-2-40-90	Conveying	90
9	GFA-2-30-15	Conveying	15
10	<b>KS1-2-5-90-E</b>	<b>Kneading</b>	<b>5</b>
11	<b>KS1-2-5-90-A</b>	<b>Kneading</b>	<b>5</b>
12	<b>KS1-2-5-90-M</b>	<b>Kneading</b>	<b>5</b>
13	GFA-2-30-90	Conveying	90
14	GFA-2-30-15	Conveying	15
15	<b>KS1-2-5-90-E</b>	<b>Kneading</b>	<b>5</b>
16	<b>KS1-2-5-90-A</b>	<b>Kneading</b>	<b>5</b>
17	<b>KS1-2-5-90-M</b>	<b>Kneading</b>	<b>5</b>
18	GFA-2-30-90	Conveying	90
19	GFA-2-30-90	Conveying	90
20	GFA-2-30-30	Conveying	30
21	GFA-2-30-30	Conveying	30
22	Screw Tip	Total	1080



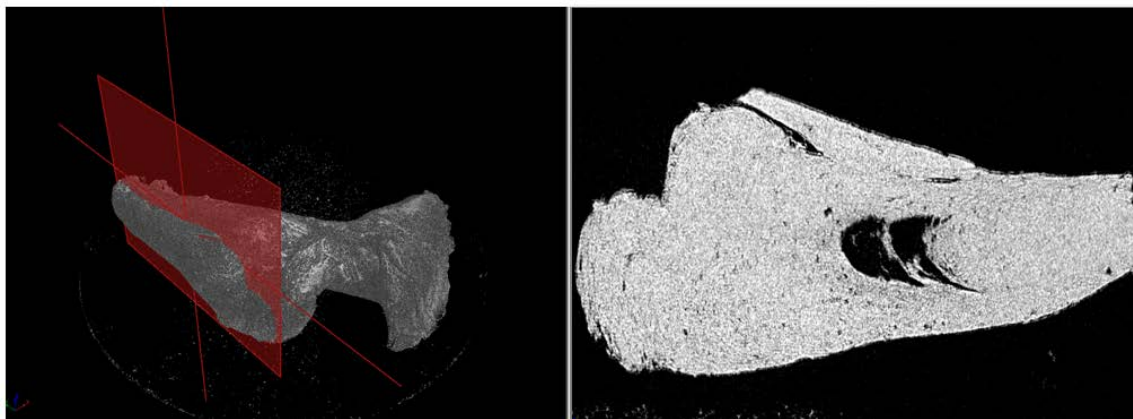
**Figure 4.38** Screw configuration used during scouting studies for 27 mm ZSE Maxx experiments. The mixing zone is comprised of two 15 mm kneading sections. Each kneading block is 5 mm wide.

The resulting product had a high product temperature of approximately 215-223°C and the product was not a granulation, but rather more of a solid plug (photo not available). Samples that were collected were X-rayed to assess the density distribution in the solid mass.

Figures 4.39 through 4.40 show the cross-section from various angles of a piece of the resulting plug.

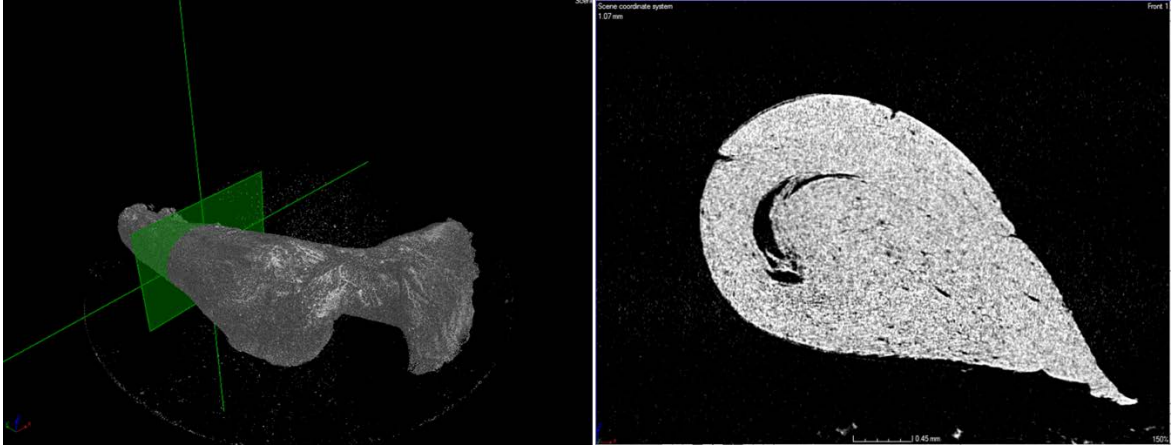


**Figure 4.39:** Cross sectional area of a portion of the theophylline (THF): hydroxypropylcellulose EXF (HPC EXF) “plug” approximately 1 mm from the top.



**Figure 4.40** Cross sectional area of a portion of the theophylline (THF): hydroxypropylcellulose EXF (HPC EXF) “plug” approximately 1 mm from the left side.

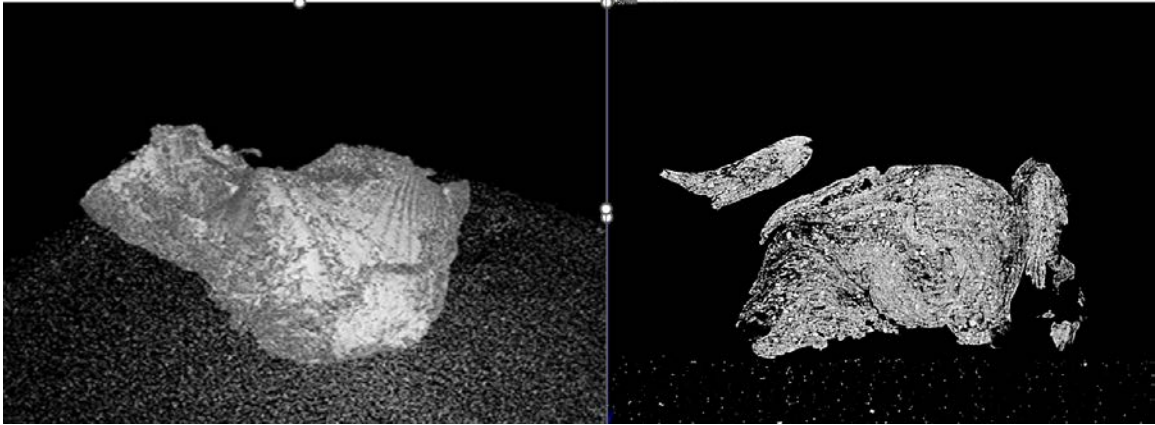




**Figure 4.41** Cross sectional area of a portion of the tip of the theophylline (THF): hydroxypropylcellulose EXF (HPC EXF) “plug” from the back.

The images show the pore (or density) distribution which is proportional to the sintering that is occurring between the particulates. The extensional and elongational flows are also evident. The swirl can be seen in the center of the granule around a large void. This phenomenon indicates that the two dispersive kneading blocks may be experiencing excessive FED and PED leading to viscous energy dissipation (VED).

Granules were successfully collected from the screw configuration with one dispersive kneading zone. The granules were clearly dense, and they did reach a product temperature of approximately 180°C. However, the product was indeed a granulation (photos available in the next section). Granules from this trial were also X-rayed. Figures 4.42 shows the cross-sectional area of the front of the resulting granules.



**Figure 4.42** Cross sectional area of a portion of the theophylline (THF): hydroxypropylcellulose EXF (HPC EXF) granule approximately 1mm from the front (plane not shown).

Like the screw configuration with the two dispersive kneading section, this image shows the pore distribution between the particulates within the granule. The extensional and elongational flows are also evident for this configuration in the granule. The swirl again is observed in the center of the granule around a much smaller cluster of voids. Several channels can be seen throughout the granule with this configuration that were not observed in the configuration with two kneading sections, suggesting the local temperature was low enough for the granulation to be in a predominate PED and FED regime.

#### **4.2.2.2 Temperature evaluation for the 27 mm granulation experiments.** A

temperature profile was evaluated on the screw configuration with one dispersive kneading zone for the THF:HPC EXF formulation. The temperatures evaluated were 35°C, 50°C, 65°C and 100°C. It was found that it was not possible to produce granules at 65°C and 100°C with this screw configuration and formulation. The run times were too short to record any meaningful data, therefore, samples were not collected since steady state was never achieved.

**4.2.2.3 Micronized Theophylline (MTHF) with Hydroxypropylcellulose MF (HPC MF) and Hydroxypropylcellulose EXF (HPC EXF).** Parametric effects for the micronized (milled) theophylline and HPC MF are summarized in Table 4.4.

**Table 4.4** Summary of System Responses for 70:30 Micronized Theophylline (MTHF): Hydroxypropylcellulose MF (HPC MF)

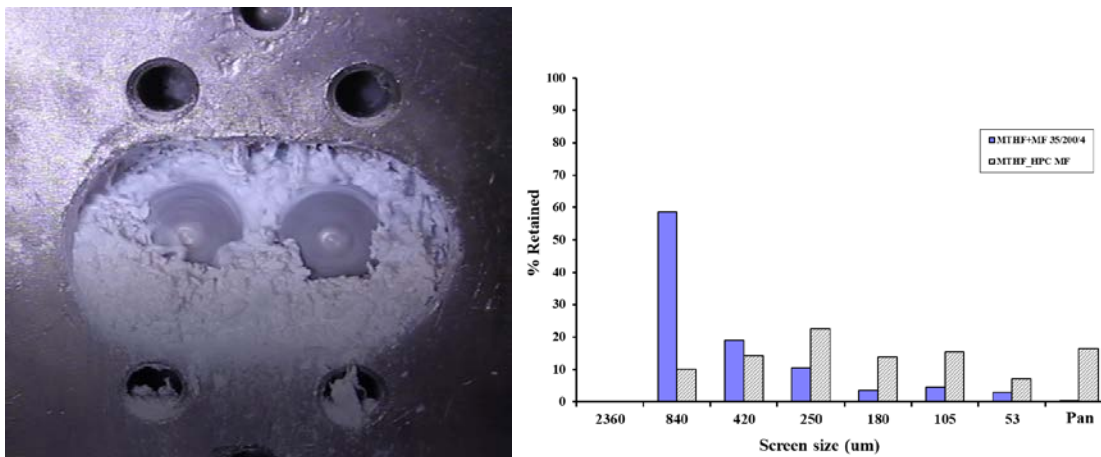
Blend	FEED RATE (kg/hr.)	SCREW SPEED (rpm)	Average Barrel Temp. (°C)	Avg. Torque (%)	Avg. Product Temp (°C)	Mean Residence Time (sec)	Avg. Power (KW)	Avg. Spec. Energy (Kw·hr/Kg)	Avg. ΔT (°C)
MTHF HPC MF	4	200	35	8.7	76.7	25	0.5	0.13	7.9
			50	9.6	103.0	19	0.5	0.14	8.3
		400	35	10.1	130.0	21	1.1	0.29	15.0
			50	10.5	150.0	12	1.2	0.30	7.9
	8	200	35	13.2	102.3	25	0.7	0.10	14.4
			50	11.4	110.7	26	0.6	0.08	8.2
		400	35	10.8	138.0	10	1.2	0.16	14.9
			50	13.1	165.6	NA	1.4	0.19	8.3

a-Residence time not measured.

The torque was comparable across all the runs for the MTHF:HPC MF Formulation. The product temperature was the highest for both feed rates, at the faster screw speed, for both temperatures. The highest product temperature observed was for the 8 kg/hr.; 400 rpm; 50°C run at 167°C. The lowest product temperature reading was for the 4 kg/hr.; 400 rpm; 35°C run at 76.7°C suggesting that particle to particle interactions may be sensitive to feed rate and temperature.

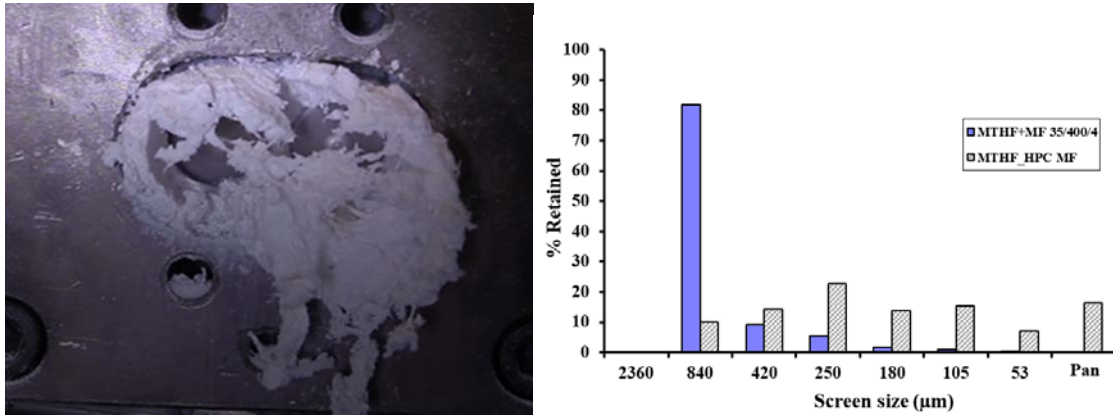
The residence times were similar between feed rates and screw speeds, where the slower screw speed had the longer residence time, as expected. Excessive heat at the mixing block was consistent for each feed rate at the faster screw speed and lower temperature, indicating that the particles were rubbing against each other in the kneading zone creating heat via PED and FED, predominantly FED considering the granules were loose and relatively free flowing. All runs produced acceptable granules and showed a distributive growth in particle size instead of forming a plug or excessively large particles.

Figure 4.43 illustrates the particle size distribution for granules from the 4 kg/hr.; 200 rpm; 35°C. Particle size growth is indicated by the blue columns. The gray columns are the particle size of the blend before granulation.



**Figure 4.43** Granules and particle size distribution of granules for micronized theophylline (MTHF) and hydroxypropylcellulose MF (HPC MF) blend (MTHF:HPC MF) at 4 kg/hr.; 200 rpm; 35°C.

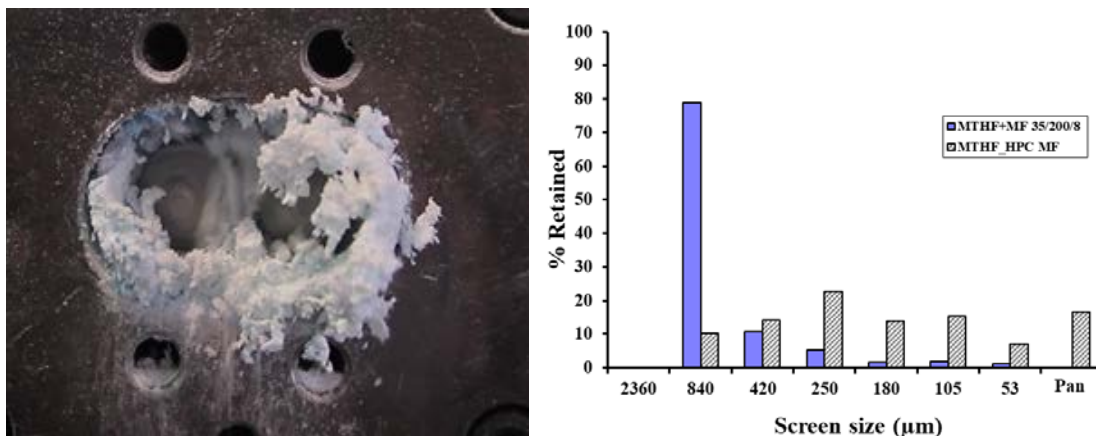
Figure 4.44 illustrates the particle size distribution for granules from the 4 kg/hr.; 400 rpm; 35°C.



**Figure 4.44** Granules and Particle Size Distribution for micronized theophylline (MTHF) and hydroxypropylcellulose MF (HPC MF) blend (MTHF:HPC MF) at 4 kg/hr.; 400rpm; 35°C.

The effect of the screw speed is evident in the particle size distribution. There are less fines between the 420 µm and 53 µm for the granules produced at the faster screw speed. Furthermore, the granules have a "fluffy" appearance, suggesting that they were not over-densified. This is also confirmed from the low torque readings.

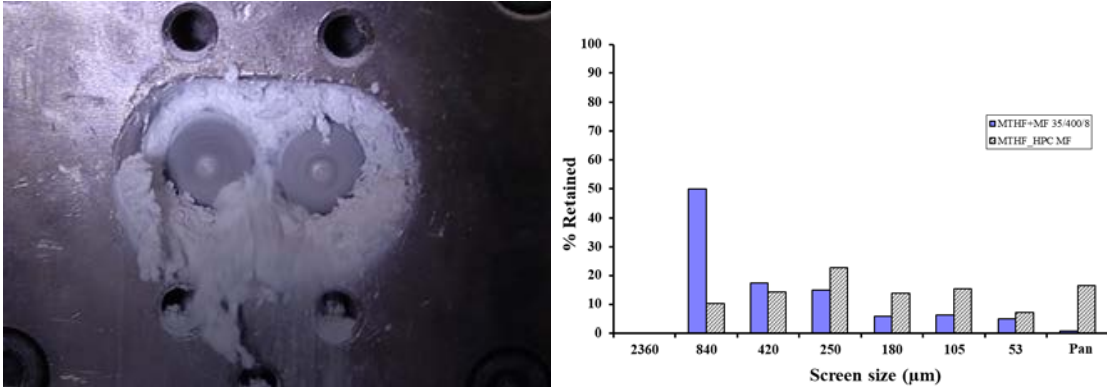
Figure 4.45 illustrates the particle size distribution for granules from the 8 kg/hr.; 200 rpm; 35°C.



**Figure 4.45** Granules and particle size distribution for micronized theophylline (MTHF) and hydroxypropylcellulose MF (HPC MF) blend (MTHF:HPC MF) at 8 kg/hr.; 200rpm; 35°C.

The granules prepared with these conditions have a similar particle size distribution to the granules prepared at 4 kg/hr.; 400rpm; 35°C. Decreasing the screw speed and increasing the feed rate seemed to create the same compacting dynamics in the kneading zone. The product temperature is higher for the granules taken at the lower feed rate and faster screw speed, but the  $\Delta T$  between the set point and the temperature at the kneading block is similar between the two runs suggesting the same heat generation is occurring in the kneading zone.

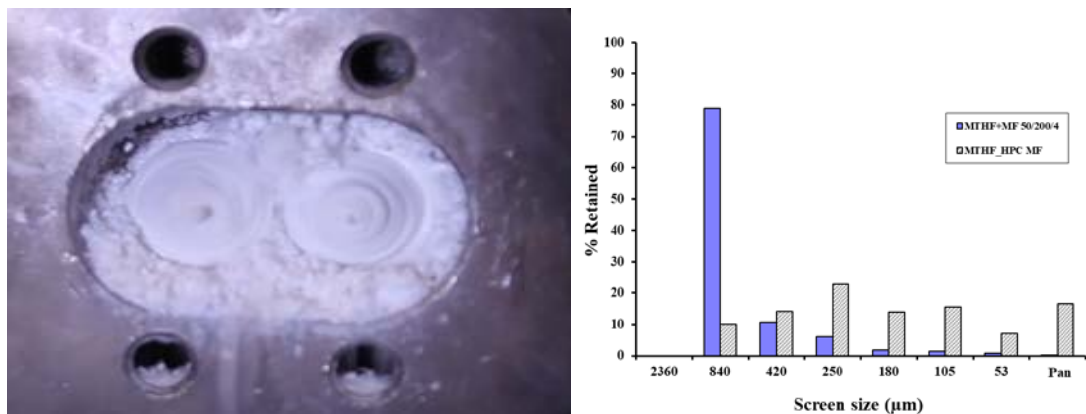
Figure 4.46 illustrates the particle size distribution for granules from the 8 kg/hr.; 400 rpm; 35°C.



**Figure 4.46** Granules and particle size distribution for micronized theophylline (MTHF) and hydroxypropylcellulose MF (HPC MF) blend (MTHF:HPC MF) at 8 kg/hr.; 400rpm; 35°C.

These conditions resulted in the finest granulation for this set. It seemed that there was not enough particle to particle interaction in the kneading block to initiate significant granule growth. Particulates did agglomerate but not to the extent of the other conditions. The energy dissipated in the mixing section was not great enough to sinter and fuse all the particulates, especially at the high feed rate.

Granules for the 4 kg/hr.; 200 rpm were the only granules collected for particle size analysis at 50°C.



**Figure 4.47** Granules and particle size distribution for micronized theophylline (MTHF) and hydroxypropylcellulose MF (HPC MF) blend (MTHF:HPC MF) at 4 kg/hr.; 200rpm; 50°C.

There were noticeably less fines for these granules compared to the ones taken at 35°C. This can be expected since the polymer is softened at the higher temperature, there is more “*kneading capacity*,” meaning it is easier for the material to stretch and fold more API into the polymer.



Figure 4.48 shows the granules for the 8 kg/hr.; 200 rpm; 50°C (particle size data not collected).



**Figure 4.48** Granules and particle size distribution for micronized theophylline (MTHF) and hydroxypropylcellulose MF (HPC MF) blend (MTHF:HPC MF) at 8 kg/hr.; 200rpm; 50°C.

The granules here appear to no longer resemble the discrete agglomerates from the previous runs. Since there is more material available at the kneading block and the polymer is softer, the material is being compacted into a ribbon made up of larger agglomerates, because of the higher temperature.

Overall, all the granules presented at the parameters evaluated are acceptable. It seems that the formulation with the fine API and coarse polymer provides a mean of controlling the velocity differences between adjacent particles, perhaps keeping the melting mechanism in the PED and FED regime. There was no evidence of any solid rich suspension to indicate the mechanism transitioned to VED.

The parametric effects for the micronized theophylline (MTHF) and HPC EXF are captured in Table 4.5.

**Table 4.5** Summary of System Responses for 70:30 Micronized Theophylline (MTHF): Hydroxypropylcellulose (HPC EXF)

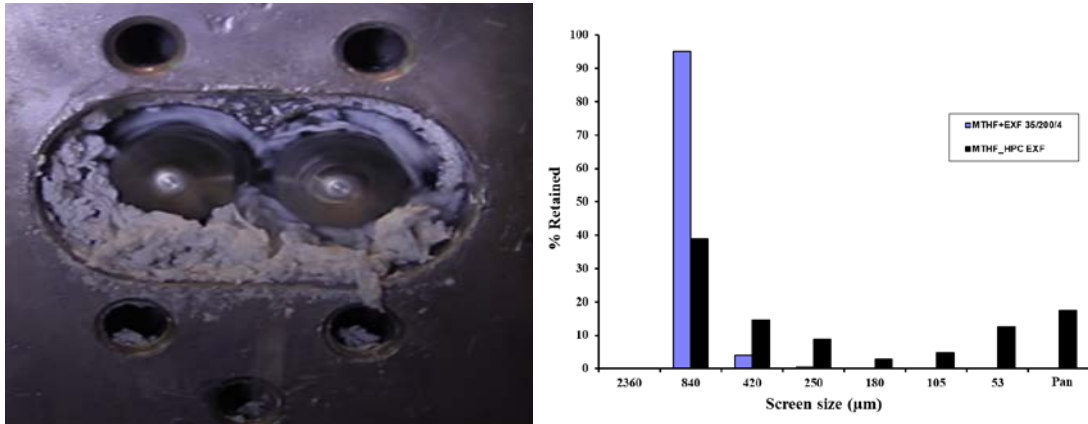
Blend	FEED RATE (kg/hr.)	SCREW SPEED (rpm)	Average Barrel Temp. (°C)	Avg. Torque (%)	Avg. Product Temp (°C)	Mean Residence Time (sec)	Avg. Power (KW)	Avg. Spec. Energy (Kw·hr/Kg)	Avg. ΔT (°C)
MTHF HPC EXF	4	200	35	18.9	126.9	17	1.0	0.27	22.8
			50	18.6	134.6	29	1.0	0.27	11.9
		400	35	14.5	167.0	16	1.6	0.42	24.0
			50 <sup>a</sup>	14.2	156.5	NA	1.6	0.41	13.4
	8	200	35 <sup>b</sup>	NA	NA	NA	NA	NA	NA
			50 <sup>b</sup>	NA	NA	NA	NA	NA	NA
		400	35	15.8	155.1	10	1.7	0.23	28.3
			50	16.3	165.0	10	1.8	0.24	13.4

a-Residence hard to read since solid plug was formed.

b-Run was not processable at 8 kg/hr. The powder would back up in the feed zone.

The data shows that the torque is slightly higher for both temperatures at the 4 kg/hr.; 200 rpm settings. PED and FED are evident from the product temperature readings. Product temperature is highest for both feed rate conditions at the faster screw speeds. The residence time is approximately two times slower at the slower feed rate. The difference between the set point temperature and increase in temperature at the mixing block is greatest for both feed rates and both screw speeds at the lowest temperature. This may be because the particles are not softened enough to granulate, hence, there is less lubrication in the extruder, making the rubbing between the particle more aggressive. This in turn drives up the temperature via FED.

Granules were collected at 4 kg/hr.; 35°C for both screw speeds, as shown in Figure 4.49 along with the corresponding particle size distribution. Particle size growth is indicated by the blue columns. The black columns are the particle size of the blend before granulation.



**Figure 4.49** Granules for micronized theophylline (MTHF) and hydroxypropylcellulose EXF (HPC EXF) blend (MTHF:HPC EXF) at 4 kg/hr.; 200 rpm; 35°C.

Particle size distribution was not measured on the sample collected at 400 rpm since it consisted of several solid “*crescent*” shaped plugs, greater than 30 mm width. As shown in Figure 4.50.



**Figure 4.50** Granules for micronized theophylline (MTHF) and hydroxypropylcellulose EXF (HPC EXF) blend (MTHF:HPC EXF) at 4 kg/hr.; 400 rpm; 35°C.

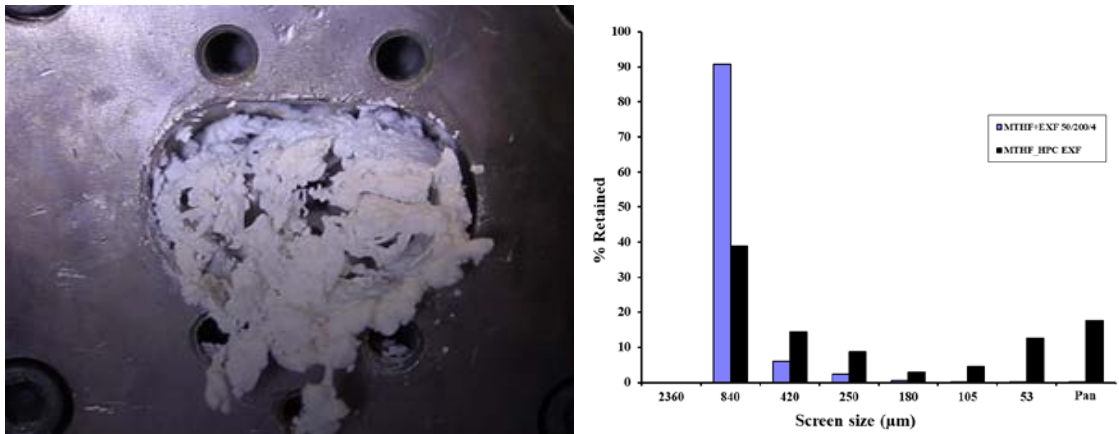
The fast screw speed and high product temperature indicate that the melting mechanism transitioned from FED and PED and entered VED, creating a solid rich suspension.



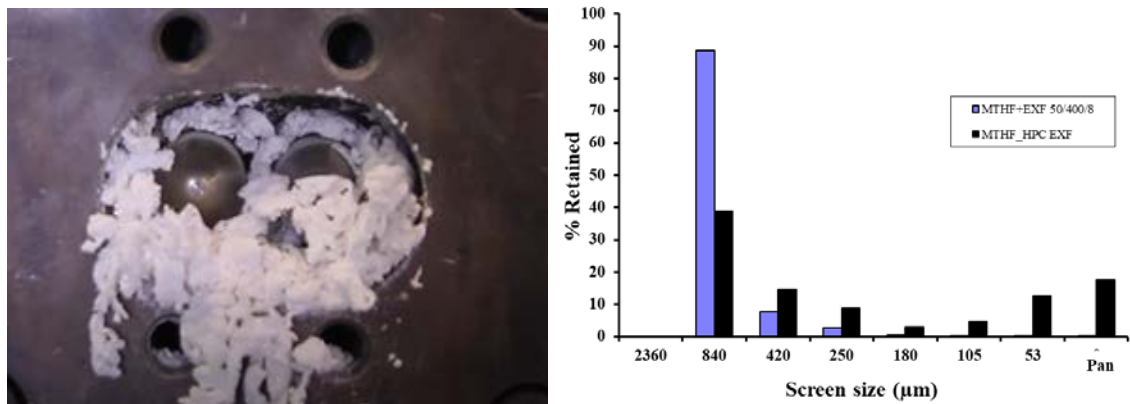
**Figure 4.51** Granules for micronized theophylline (MTHF) and hydroxypropylcellulose EXF (HPC EXF) blend (MTHF:HPC EXF) at 8 kg/hr.; 200 rpm; 35°C.

Since more material was available at the mixing zone and the materials were closer in particle size, the material formed a solid rich suspension. This is indicative of being in a VED dominant melting mechanism.

Granules prepared at 50°C with MTHF: EXF formulation were only collected from the 4 kg/hr.; 200 rpm and 8 kg/hr.; 400 rpm. The granules and their respective particle size distribution are presented in Figure 4.52 and Figure 4.53.



**Figure 4.52** Granules for micronized theophylline (MTHF) and hydroxypropylcellulose EXF (HPC EXF) blend (MTHF:HPC EXF) at 4 kg/hr.; 200 rpm; 50°C.



**Figure 4.53** Granules for micronized theophylline (MTHF) and hydroxypropylcellulose EXF (HPC EXF) blend (MTHF:HPC EXF) at 8 kg/hr.; 400 rpm; 50°C.

The granules prepared at 50°C appear to be connected by “threads” of softened polymer. The system parameters and particle size distribution are similar between these two sets of granules. The product temperature was approximately 165°C for the MTHF:HPC EXF at 8 kg/hr.; 400rpm; 50°C granules; 30°C greater than the MTHF:HPC EXF at 4 kg/hr.; 200rpm; 50°C granules. This difference could be attributed to the synergistic effect of the feed rate and screw speed. Essentially, there is material being compacted at a faster rate, exacerbating the deformation mechanism. Because of the

homogenous distribution of particles for this formulation, these granules were more likely in an FED and PED dominant melting mechanism, but close to transitioning to VED.

The 4 kg/hr.; 400 rpm; 50°C sample demonstrated very interesting behavior. It was not possible to measure particle size for this sample, but it is evident in Figure 4.54 that at the slower feed rate, coupled with higher barrel temperature and fast screw speed, the melting mechanism transitions from FED and PED to VED very quickly. The extreme deformative mixing that is occurring on a smaller mass of softened material eliminates the chance for granulation and drives the blend to form a tube-shaped solid rich suspension.



**Figure 4.54** Granules for micronized theophylline (MTHF) and hydroxypropylcellulose EXF (HPC EXF) blend (MTHF:HPC EXF) at 4 kg/hr.; 400 rpm; 50°C.

There are significant differences between the data collected for the 4 kg/hr.; 200rpm; 35°C for the MTHF:HPC EXF formulation and the MTHF:HPC MF formulation.

It may be possible that the smaller particles of the MTHF coat the larger polymer particles (HPC MF) creating a lubricating effect and delaying the transition from FED and PED to VED. However, since the fine material are closer in size, the energy dissipated in the mixing section causes the polymer particle to soften and granulate sooner because there are more available surfaces.

**4.2.2.4 Theophylline (THF) with Hydroxypropylcellulose MF (HPC MF) and Hydroxypropylcellulose EXF (HPC EXF).** Parametric effects for the THF and HPC MF are summarized in Table 4.6.

**Table 4.6** Summary of System Responses for 70:30 Theophylline (THF): Hydroxypropylcellulose MF (HPC MF)

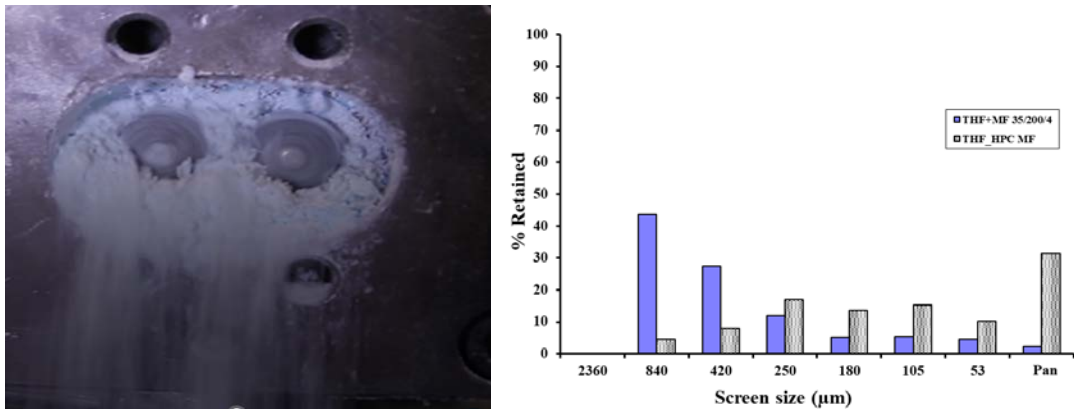
Blend	FEED RATE (kg/hr.)	SCREW SPEED (rpm)	Average Barrel Temp. (°C)	Avg. Torque (%)	Avg. Product Temp (°C)	Mean Residence Time (sec)	Avg. Power (KW)	Avg. Spec. Energy (Kw·hr/Kg)	Avg. ΔT (°C)
THF HPC MF	4	200	35	9.8	85.0	20	0.54	0.14	6.1
			50	9.5	110.0	30	0.52	0.14	6.3
		400	35	10.5	100.0	15	1.15	0.30	9.4
			50 <sup>a</sup>	10.1	137.5	NA	1.1	0.29	6.9
	8	200	35	14.9	94.0	16	0.82	0.11	8.0
			50	13.1	113.0	25	0.72	0.09	7.2
		400	35	10.9	125.6	12	1.2	0.19	11.5
			50	13.7	157.9	15	1.5	0.20	7.9

a-Residence time not measured-

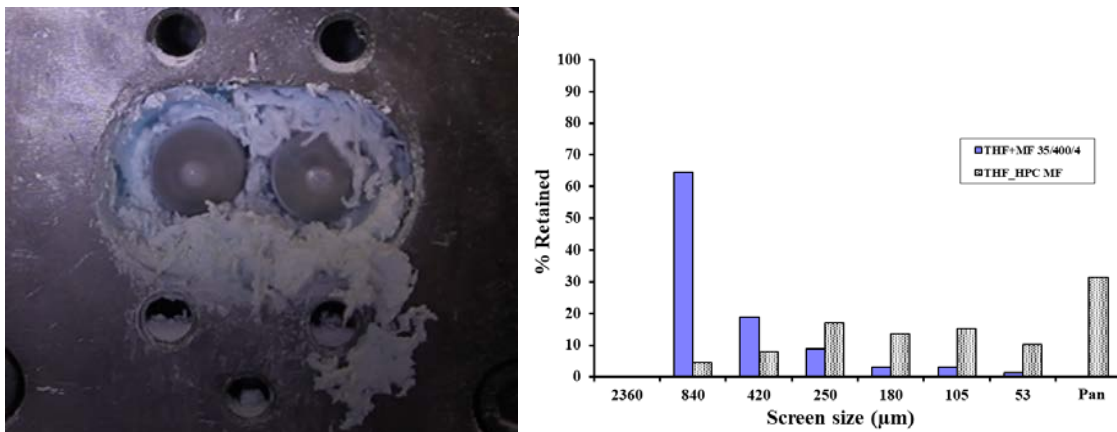
The data shows that the torque is similar between all the runs. The product temperature was lowest for the 4 kg/hr.; 200 rpm; 35°C at 85°C and highest at the 8 kg/hr.;



400 rpm; 50°C at approximately 158°C. This response in product temperature was like the MTHF:HPC MF formulation. Unlike the MTHF:HPC MF formulation, the  $\Delta T$  between the set point and the temperature at Zone 7 was comparable for all runs. It is still slightly higher for both feed rates at the faster screw speeds, but the difference is not as large as it was for MTHF:HPC MF. This suggests that the powder properties of the polymer are influencing the degree of granulation. The particle size difference is creating a control mechanism, keeping the local softening of the polymer in check between PED and FED, predominantly in FED. This is further evident and justified from the particle size analysis presented in Figures 4.55 and 4.56 for the THF:HPC MF granules prepared at 35°C.

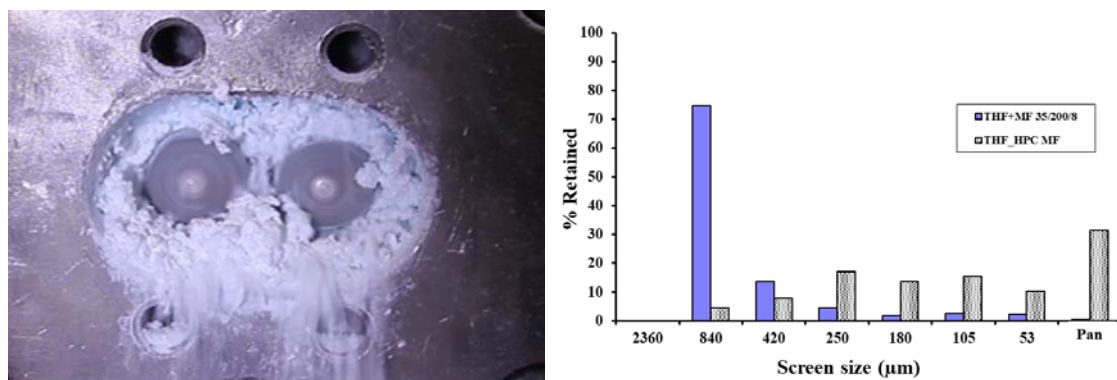


**Figure 4.55** Granules for theophylline (THF) and hydroxypropylcellulose MF (HPC MF) blend (THF:HPC MF) at 4 kg/hr.; 200rpm; 35°C.

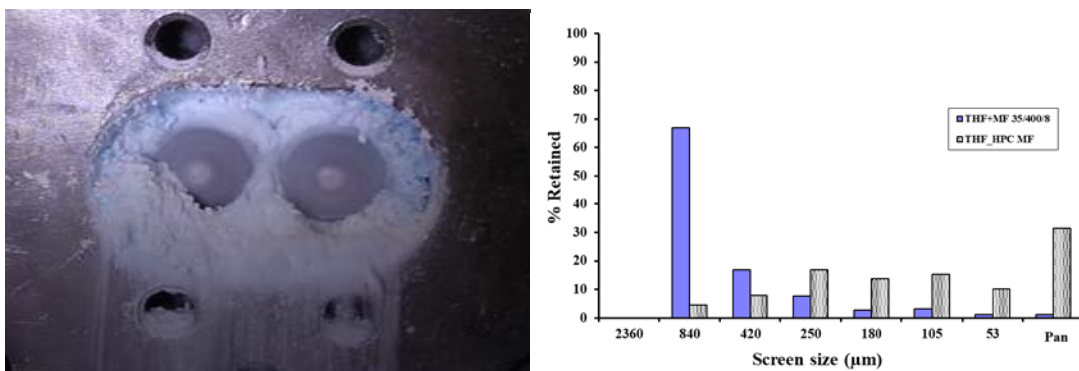


**Figure 4.56** Granules for theophylline (THF) and hydroxypropylcellulose MF (HPC MF) blend (THF:HPC MF) at 4 kg/hr.; 400rpm; 35°C.

Granules prepared at 4 kg/hr.; 35°C show that the screw speed influences the particle size morphology and distribution. The granules at 200 rpm are finer and more like free-flowing spheres. The granules prepared at 400 rpm are coarser but appear to be rolled and flattened. This could be attributed to the rate of mixing on a small volume of material in the kneading zone. It is shown and explained in the next set of Figures that the rolling effect is eliminated at both screw speeds by increasing the feed rate.



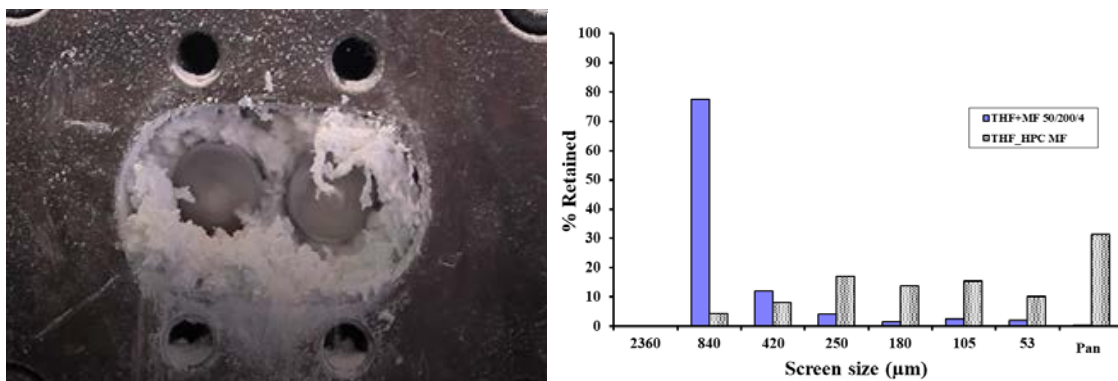
**Figure 4.57** Granules for theophylline (THF) and hydroxypropylcellulose MF (HPC MF) blend (THF:HPC MF) at 8 kg/hr.; 200rpm; 35°C.



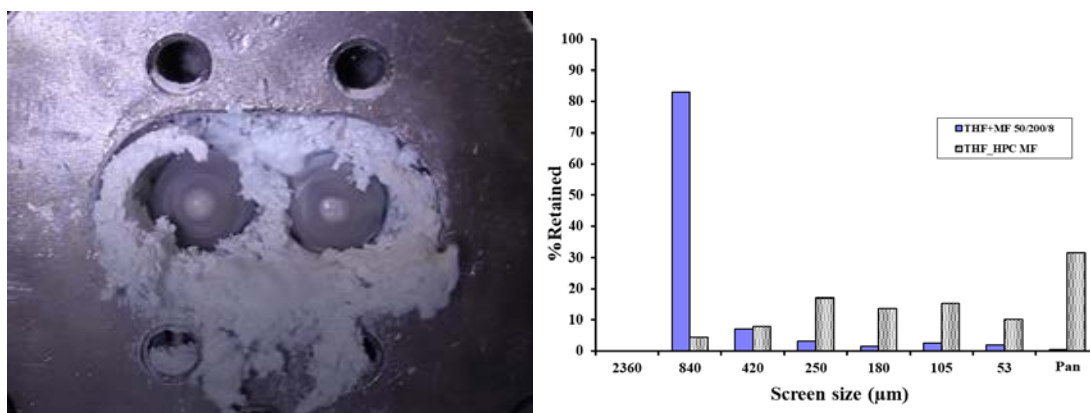
**Figure 4.58** Granules for theophylline (THF) and hydroxypropylcellulose MF (HPC MF) blend (THF:HPC MF) at 8 kg/hr.; 400rpm; 35°C.

The particle sizes are similar for the granules prepared at the faster feed rate despite the screw speeds. The larger particle size is evident from the decrease in fines from 425 μm to sub-53 μm and the drastic increase coarser particles at 850 μm. The increase in feed rate could be promoting additional compaction in the mixing section. It did not seem that there is any excessive FED since the product temperature and  $\Delta T$  are relatively low.

Granules prepared at 50°C with the THF:HPC MF formulation were only collected from the two feed rates at 200 rpm. The granules and their respective particle size distribution are presented in Figure 4.59 and Figure 4.60.



**Figure 4.59** Granules for theophylline (THF) and hydroxypropylcellulose MF (HPC MF) blend (THF:HPC MF) at 4 kg/hr.; 200rpm; 50°C.



**Figure 4.60** Granules for theophylline (THF) and hydroxypropylcellulose MF (HPC MF) blend (THF:HPC MF) at 8 kg/hr.; 200rpm; 50°C.

The granules prepared with these parameters appear to have a similar particle size, torque, product temperature and  $\Delta T$  between the temperature at the mixing block vs. the set point, are comparable. The granules prepared at the faster feed rate do show that there may be some extra compaction by forming “crescent” shaped granules. The granules also look like smaller agglomerates that are weakly binding into a larger agglomerated mass. Granules prepared at the two different feed rates at 400 rpm and 50°C produced a flat solid rich suspension that were not suitable for particle size distribution analysis. The image is provided in Figure 4.61.



**Figure 4.61** Granules for theophylline (THF) and hydroxypropylcellulose MF (HPC MF) blend (THF:HPC MF) at 8 kg/hr.; 200rpm; 50°C.

The melting mechanisms PED and FED were overcome by the softened polymer at this temperature. The particles experience less work and were incorporated in a solid rich suspension much faster. The granules presented in Figure 4.61 reached the highest product temperature despite the  $\Delta T$  being low. The granules for these set of conditions are at the onset of the VED melting mechanism.

The Parametric effects for the theophylline (THF) and HPC EXF are captured in Table 4.7.

**Table 4.7** Summary of System Responses for 70:30 Theophylline (THF): Hydroxypropylcellulose EXF (HPC EXF)

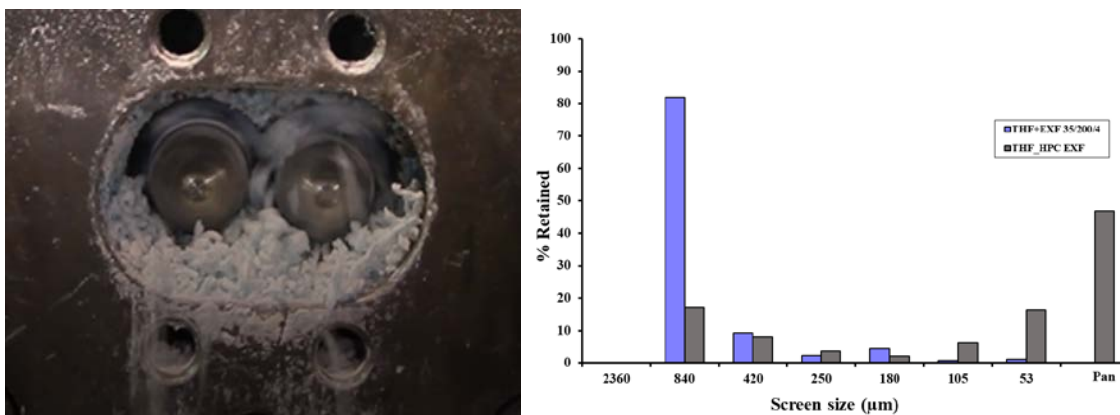
Blend	FEED RATE (kg/hr.)	SCREW SPEED (rpm)	Average Barrel Temp. (°C)	Avg. Torque (%)	Avg. Product Temp (°C)	Mean Residence Time (sec)	Avg. Power (KW)	Avg. Spec. Energy (Kw·hr/Kg)	Avg. ΔT (°C)
THF HPC EXF	4	200	35	57.5	163	24	3.16	0.83	22.4
			50	15.15	115.8	25	0.83	0.22	8.0
	4	400	35	58.9	160.6	15	6.5	1.7	36.7
			50	50.3	162.3	11	6.5	1.7	18.3
	8	200	35	70.8	113	26	3.9	0.51	27.8
			50	62.0	130.9	25	3.4	0.45	14.34
		400	35 <sup>a</sup>	NA	NA	NA	NA	NA	NA
			50 <sup>b</sup>	63.3	212	NA	7.0	0.92	40.1

a-Run was aborted since the equipment would over torque and shut down.

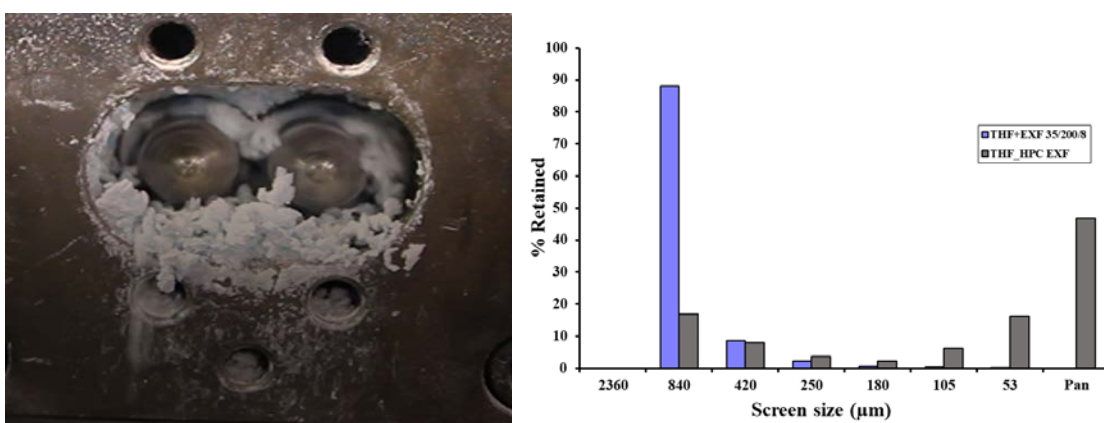
b-Residence time was not measured.

The torque data collected shows that all the conditions evaluated for this formulation were the highest for all the formulations. The only exception was for granules prepared at 4 kg/r; 200 rpm; 50°C. The product temperature and ΔT were also high across the same runs. The ΔT for this formulation was the highest for all formulations observed. The extruder workload was the highest of any of the formulation evaluated as shown by the power readings taken at each data set. The packing efficiency for this formulation may have affected the processability. The higher workload and temperatures observed suggest PED and FED were short lived during the preparation of these granules.

Suitable granules for particle size analysis were collected for the 200 rpm; 35°C at both feed rates.



**Figure 4.62** Granules for theophylline (THF) and hydroxypropylcellulose EXF (HPC EXF) blend (THF:HPC EXF) at 4 kg/hr.; 200rpm; 35°C.



**Figure 4.63** Granules for theophylline (THF) and hydroxypropylcellulose EXF (HPC EXF) blend (THF:HPC EXF) at 8 kg/hr.; 200 rpm; 35°C.

For these granules, the heat generated locally was high. This promoted sintering and fusing of particulates more efficiently like the previous HPC EXF containing formulations. The granules appeared dense and the large particles at 850 μm and the lack of fines suggests that the PED and FED melting mechanisms is in a narrow operating window. This formulation would transition to a full VED driven melting regime. Figures 4.64 and 4.65 support this where at 400 rpm at the two feed rates the material produced are sheets of solid rich suspensions.



**Figure 4.64** Granules for theophylline (THF): hydroxypropylcellulose EXF (HPC EXF) blend (THF:HPC EXF) at 4 kg/hr.; 400rpm; 35°C.



**Figure 4.65** Granules for theophylline (THF): hydroxypropylcellulose EXF (HPC EXF) blend (THF:HPC EXF) at 8 kg/hr.; 400rpm; 35°C.

Granules prepared at 50°C did not perform any better than those evaluated at 35°C.

None of the granules collected were suitable for particle size analysis. All agglomerates



were too large. The resulting granules are presented in Figure 4.66 and 4.67 for those made at the two different feed rates at 200 rpm.



**Figure 4.66** Granules for theophylline (THF) and hydroxypropylcellulose EXF (HPC EXF) blend (THF:HPC EXF) at 4 kg/hr.; 200rpm; 50°C.



**Figure 4.67** Granules for theophylline (THF) and hydroxypropylcellulose EXF (HPC EXF) blend (THF:HPC EXF) at 8 kg/hr.; 200rpm; 50°C.

Excessive deformation is occurring in the mixing zone for this formulation at both feed rates. Given the low temperature of the granules in Figure 4.66, 4 kg/hr.; 200rpm; 50°C and the cleanliness of the extruder (i.e., lack of fines buildup), it may be that the onset of VED occurred in the mixing zone immediately. The low torque reading could be that the extruder was starved at the low feed rate and the molten mass was lubricating the extruder. Once the feed rate went up like for the granules in Figure 4.67, 8 kg/hr.; 200rpm; 50°C. The torque, product temperature, and  $\Delta T$  all increase as well.

The 8 kg/hr.; 400 rpm; 50°C granulation for THF:HPC EXF demonstrated very similar behavior to the MTHF:HPC EXF formulation. It was not possible to measure particle size for this sample, but it is evident from Figure 4.68 that at the faster feed rates, screw speed, and high temperature, that the melting mechanism was dominated by VED.

The heat generated by the extreme deformative mixing drove the blend to form a solid rich suspension plug.



**Figure 4.68** Granules for theophylline (THF) and hydroxypropylcellulose EXF (HPC EXF) blend (THF:HPC EXF) at 8 kg/hr.; 400rpm; 50°C.

The formulations containing HPC EXF processed poorly. It can be concluded that the particle size of the polymer influenced the degree of granulation. The particle size difference for the formulations containing the HPC MF was creating a control mechanism, keeping the melting in the required PED and FED regime. Most of the formulations that were processed into free-flowing granules with a wide particle size distribution were at 35°C. The HPC EXF containing blend were not an ideal formulation suitable for twin screw granulation. Extended run times may lead to fouling or buildup on the inner wall of the extruder, leading to processing difficulties.

The granules for MTHF and THF with HPC EXF were acceptable at the low feed rate, screw speed, and temperature. The granulating mechanism worked better if the

particles had to reach the polymer softening temperature by being deformed at a lower temperature (e.g., processing temperature set point of 35°C) verses being prewarmed (e.g., processing temperature set point of 50°C). The formulations containing HPC MF processed much better despite the API used. All conditions evaluated for THF:HPC MF at 35°C and 50°C produced nice granules with a broad particle size distribution.

#### 4.3 iShear™ Powder Flow Analysis: Mechanical Powder Properties Assessment

The mechanical powder properties were measured for the neat polymers and the neat API's. The flow properties of the neat material and 16 formulations were measured using an iShear® powder flow rheometer.

Neat HPC MF and low drug load formulations for both API's overlap with what is conventionally defined as free flowing according to the flow function coefficient (*ffc*) and the Relative Flow Index (RFI) presented in Table 4.8 (Zegzulka, Gelnar, Jezerska, et al., 2020) and Table 4.9 (iPowder Systems, 2022), respectively.

**Table 4.8** Range of Different Flowability Levels, Flowability Classification for Flow Function Coefficient (*ffc*)

<i>ffc</i> Range	Description
0< <i>ffc</i> <1	Non-Flowing
1< <i>ffc</i> <2	Very Cohesive
2< <i>ffc</i> <4	Cohesive
4< <i>ffc</i> <10	Easy Flowing
10< <i>ffc</i> <∞	Free Flowing

(Source: Pafiakis, Armenante, Gogos 2022)

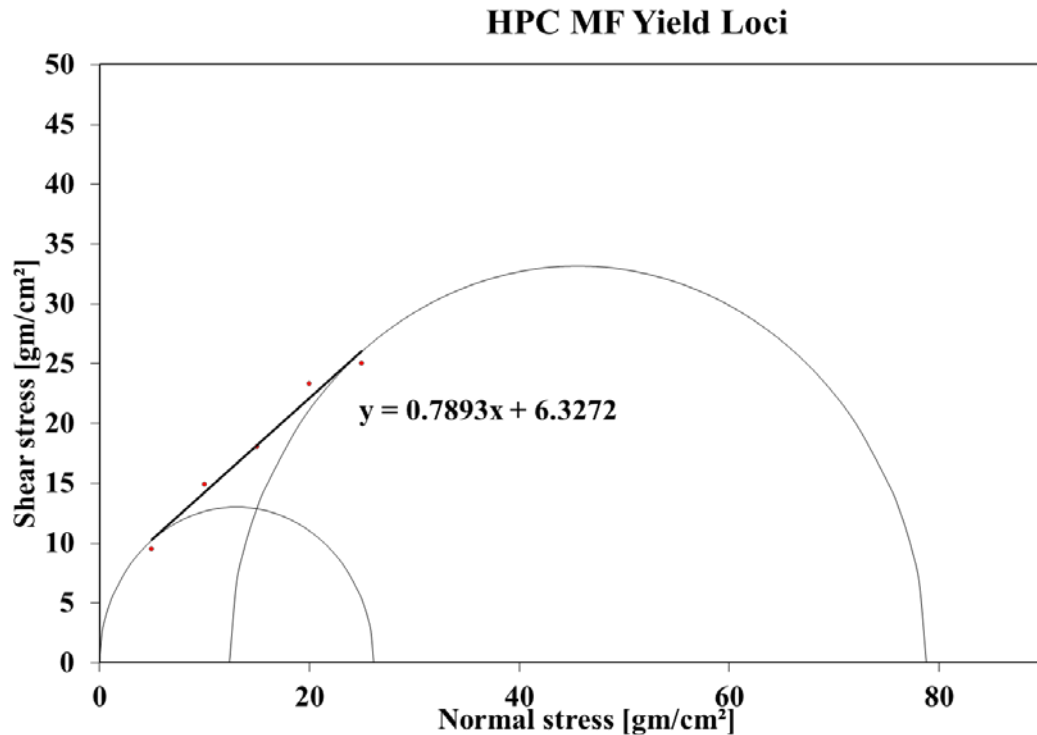
**Table 4.9** Range of Different Flowability Levels, Flowability Classification for Relative Flow Index (RFI)

RFI	Description
<2	Difficult to handle
1.5-4	Cohesive Powders
3-6	Granules
5-10	Harder Excipients
10-15	Sand
>20	If fine, floodable

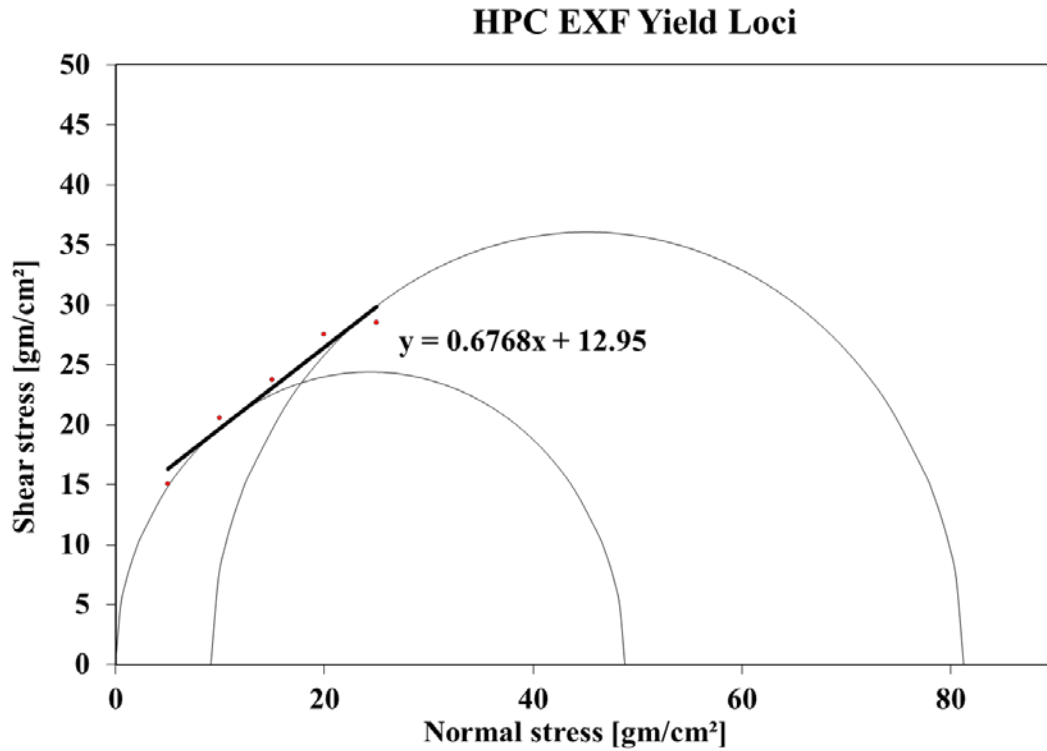
(Source: Pafiakis, Armenante, Gogos 2022)

### 4.3.1 Hydroxypropylcellulose (HPC) MF and EXF

Figures 4.69 and 4.70 show the Mohr circles with the yield loci of the consolidated HPC MF and HPC EXF samples. The slope of the yield locus is defined as the coefficient of friction,  $f$  and the intercept of the yield is the cohesion. The cohesion and the uniaxial strength are summarized and presented in Figures 4.71



**Figure 4.69** Yield loci for hydroxypropylcellulose MF (HPC MF).



**Figure 4.70** Yield loci for consolidated hydroxypropylcellulose EXF (HPC EXF).

The flow function coefficient (*ffc*) is calculated from the Mohr circles generated for each raw material and each formulation at the specified drug load from the following equation:

$$\frac{\sigma_1}{\sigma_c} = \frac{\text{Major Consolidation Stress}}{\text{Uniaxial Compressive Strength}} = \text{flow function coefficient} \quad (4.1)$$

The Relative Flow Index (RFI) is also calculated from the Mohr circles generated for each raw material and each formulation at the specified drug load from the following equation:

$$\frac{\sigma_2 - \sigma_1}{\sigma_c} = \frac{\text{Minor Consolidation Stress} - \text{Major Consolidation Stress}}{\text{Uniaxial Compressive Strength}} = \text{Relative Flow Index} \quad (4.2)$$

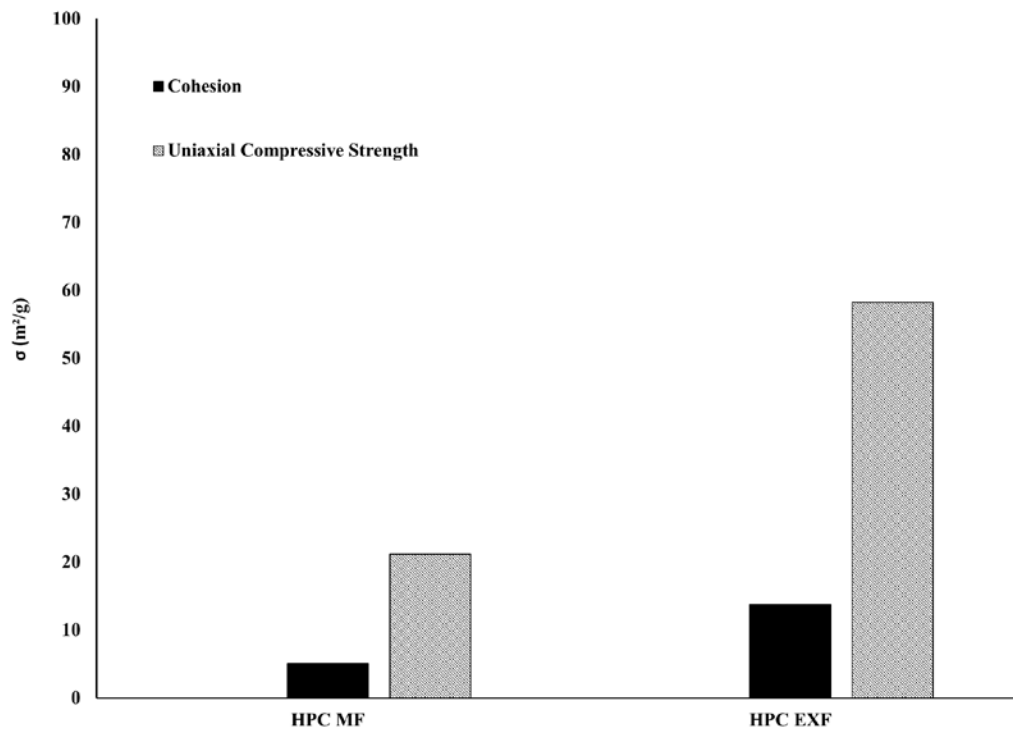
The  $ffc$  and RFI for the neat polymers are presented in Table 4.10

**Table 4.10** Range of Different Flowability Classification for  $ffc$  and RFI For Hydroxypropylcellulose MF (HPC MF) and Hydroxypropylcellulose MF (HPC EXF)

HPC MF		HPC EXF	
$ffc$	RFI	$ffc$	RFI
3.69	3.08	1.69	1.54

(Source: Pafiakis, Armenante, Gogos 2022)

HPC EXF (fine polymer) has a uniaxial compressive strength ( $\sigma_c$ ) of approximately 60 m<sup>2</sup>/g, three times greater than HPC MF (coarse polymer). HPC EXF is also two times more cohesive than HPC MF.



**Figure 4.71** Cohesion and uniaxial compressive strength for hydroxypropylcellulose MF (HPC MF) and hydroxypropylcellulose EXF (HPC EXF).

### 4.3.2 Micronized and non-micronized theophylline

Figures 4.72 and 4.73 show the Mohr circles with the yield loci of the consolidated micronized and non-micronized theophylline samples. The slope of the yield locus is defined as the coefficient of friction,  $f$  and the intercept of the yield is the cohesion. The cohesion and the uniaxial strength are summarized and presented in Figure 4.74.



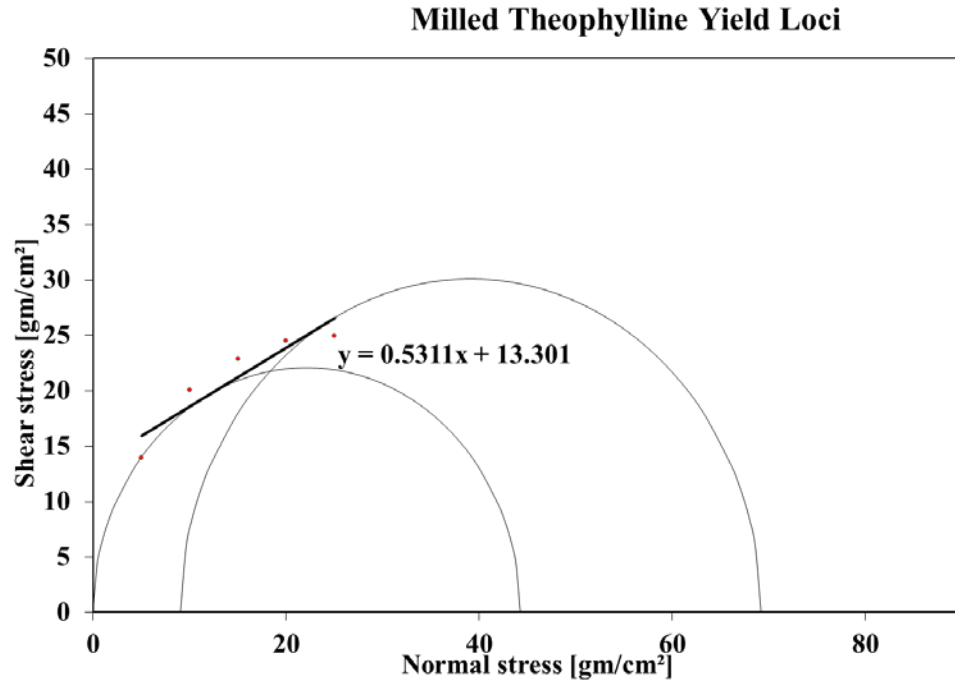


Figure 4.72 Yield loci for consolidated micronized theophylline (MTHF).

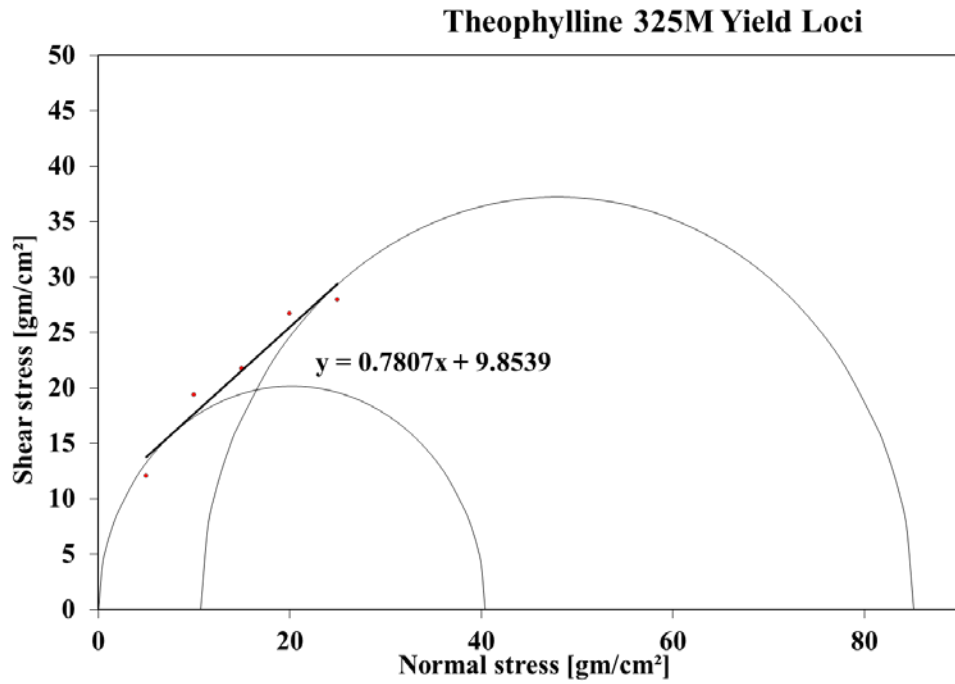


Figure 4.73 Yield loci for consolidated theophylline 325M (THF).

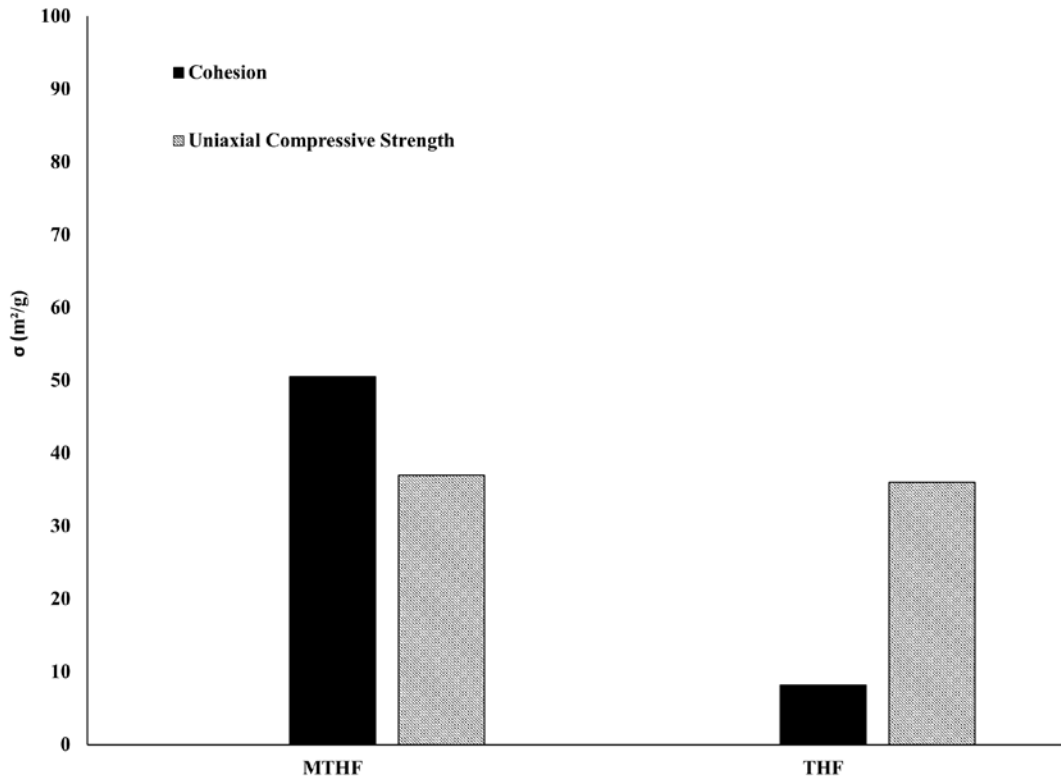
The  $ffc$  and RFI for the neat API's are presented in Table 4.11

**Table 4.11** Range of Different Flowability Classification for  $ffc$  and RFI for Micronized Theophylline (MTHF) and Theophylline (THF)

MTHF		THF	
$ffc$	RFI	$ffc$	RFI
2.26	2.06	2.56	2.28

(Source: Pafiakis, Armenante, Gogos 2022)

At 50 m<sup>2</sup>/g, MTHF (fine API) is approximately five times more cohesive than THF (coarse API). The cohesiveness of the polymers is less than MTHF (fine API) and is comparable to the THF (coarse API). The uniaxial compressive strength ( $\sigma_c$ ) is approximately the same for both API's.



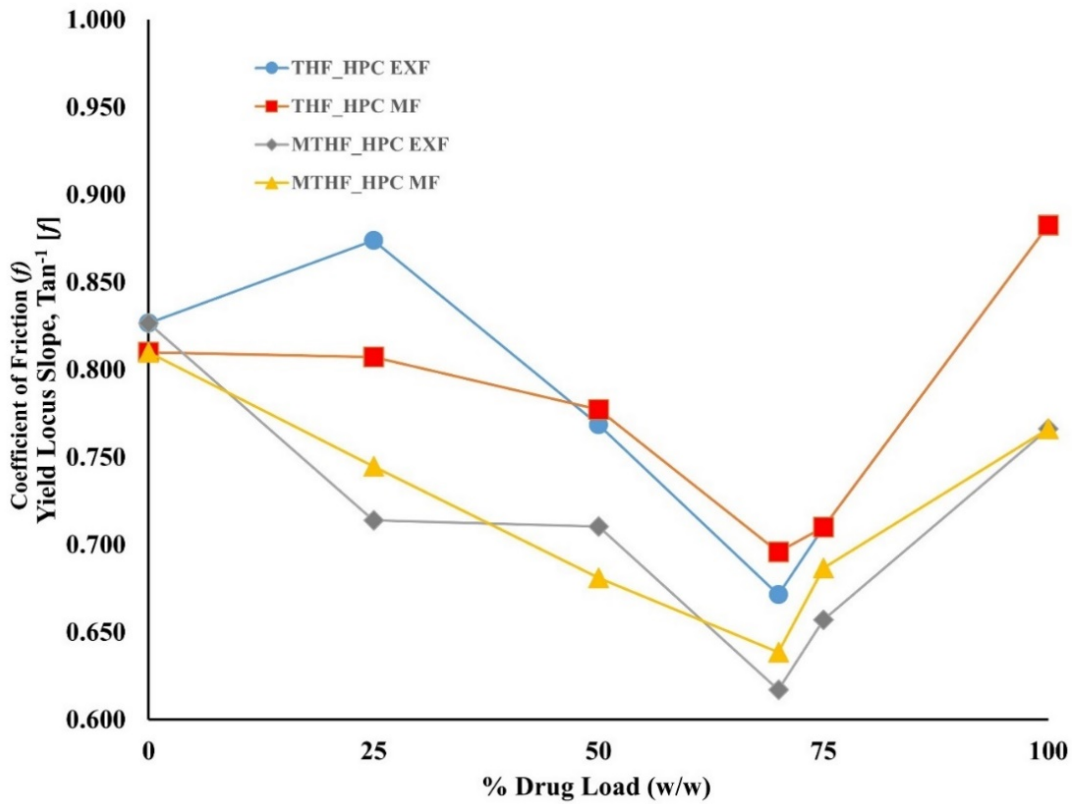
**Figure 4.74** Cohesion and uniaxial compressive strength for micronized theophylline (MTHF) and theophylline (THF).

(Source: Pafiakis, Armenante, Gogos 2022)

### 4.3.3 Theophylline: Hydroxypropylcellulose Blends

The mechanical powder properties were measured for the four formulations prepared at the four different drug loads by varying the level of theophylline at 25%, 50%, 70% and 75% w/w, where 0% is neat polymer and 100% is neat API.

The profiles in Figure 4.75 illustrate the coefficient of friction,  $f$ , as a function of drug load for all four formulations.



**Figure 4.75** Coefficient of friction,  $f$  as a function of drug load.  
(Source: Pafiakis, Armenante, Gogos 2022)

As the concentration of API increase, the coefficient of friction,  $f$ , decreases, except initially for the 25% DL THF:HPC EXF formulation. The smaller particles of the MTHF coat the polymer particles and fill the interstices and other MTHF particles allowing the

particles to slip past one another; essentially lubricating and minimizing the abrasive morphological effects.

The coefficient of friction,  $f$ , is greater for the formulations that contain the coarse API, THF ( $D_{50}=15.5\ \mu\text{m}$ ) vs. the fine API, MTHF ( $D_{50}=6.8\ \mu\text{m}$ ). This difference in coefficient of friction,  $f$ , is attributed to particle morphology and the particle size differences and packing orientation of API. When the sample experiences any shear, the fine API particles roll over API coated polymer.

Figure 4.75 shows that the coefficient of friction,  $f$  for THF is greater than the coefficient of friction,  $f$  for the polymers, where the coefficient of friction,  $f$  of the MTHF is significantly less than THF and less than the polymers, respectively. This is attributed to morphological and random packing effects of the material.

The coarse elongated particle shape of theophylline THF adds an element of entanglement and a random “stacking”, or a “weaving” effect could be expected from these types of particles. Adding THF to HPC MF or HPC EXF, accompanied with low compression (e.g., during the consolidation step of the sample preparation for the shear cell experiments) or high compression (e.g., loading of the batch mixer) locks this network of theophylline needle particles in place. This results in a coarse network of particles that would abrade against the adjacent particle surfaces.

Lubricity was observed across both sample sets, with respect to the polymer, until a minimum is reached at approximately 70 % w/w drug load. Beyond this concentration, the coefficient of friction,  $f$ , began to increase as the profile became more API dominant. The coefficient of friction,  $f$ , profiles correlate well with Furnas’s Estimation of void

fraction (Suzuki 1997), emphasizing that much smaller particles are filling the interstices between the coarse particles.

The coefficient of friction,  $f$ , the cohesion ( $\tau_0$ ) and uniaxial compressive strength ( $\sigma_c$ ) each have a direct effect on the overall blend properties.

**Table 4.12** Range of Different Flowability Levels, Flowability Classification for  $ffc$  and RFI for Formulations Containing Hydroxypropylcellulose MF (HPC MF)

Drug Loading (%)	MTHF:HPC MF	
	$ffc$	RFI
0	3.69	3.08
25	3.33	2.74
50	2.45	2.05
70	2.30	2.03
75	1.67	1.49
100	2.26	2.06
Drug Loading (%)	THF:HPC MF	
	$ffc$	RFI
0	3.69	3.08
25	3.34	2.81
50	2.96	2.51
70	2.36	1.99
75	2.33	1.84
100	2.56	2.28
0%-is neat polymer		
100% -is neat API		

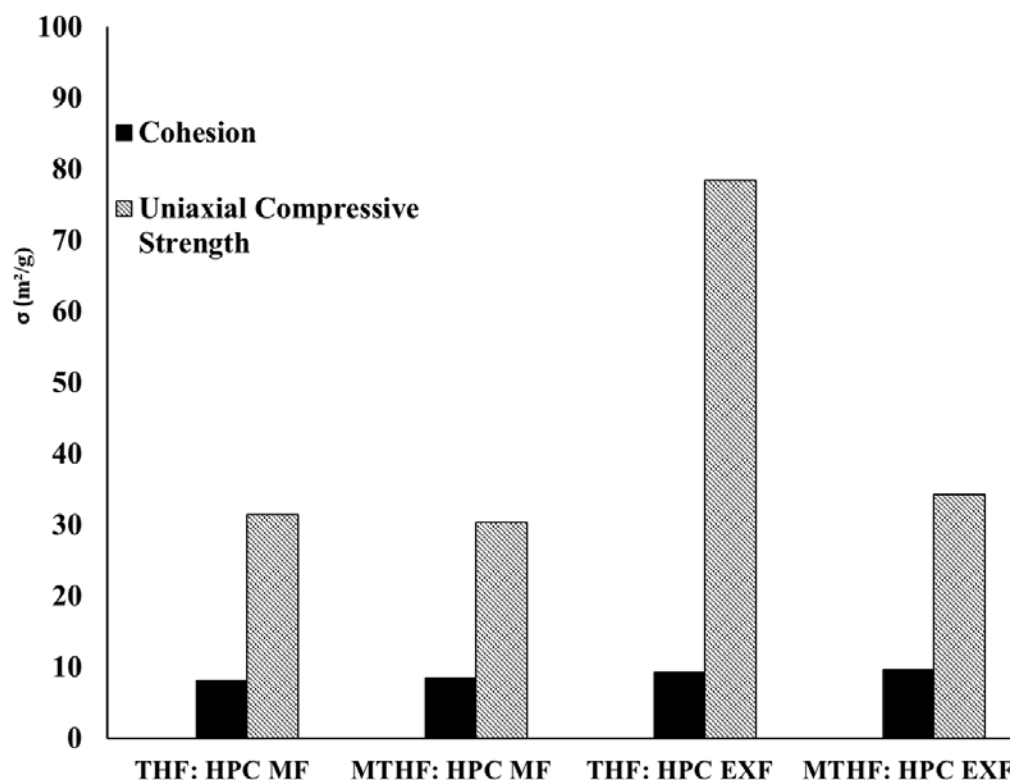
(Source: Pafiakis, Armenante, Gogos 2022)

**Table 4.13** Range of Different Flowability levels, Flowability Classification for ffc and RFI for Formulations Containing HPC EXF

Drug Loading (%)	MTHF:HPC EXF	
	<i>ffc</i>	RFI
0	1.69	1.54
25	1.80	1.59
50	1.89	1.66
70	2.04	1.71
75	2.00	1.71
100	2.26	1.97
Drug Loading (%)	THF:HPC EXF	
	ffc	RFI
0	1.69	1.59
25	2.27	2.02
50	2.25	1.95
70	1.22	1.16
75	2.14	1.84
100	2.56	2.28
0%-is neat polymer		
100% -is neat API		

(Source: Pafiakis, Armenante, Gogos 2022)

Both MTHF (fine API) formulations and the THF:HPC MF (coarse-coarse) formulation have comparable cohesion and uniaxial compressive strength. However, the THF:HPC EXF (course-fine) formulation has a uniaxial compressive strength of approximately 80 m<sup>2</sup>/g. The inherently high uniaxial compressive strength ( $\sigma_c$ ) of the HPC EXF (fine polymer) was the dominating characteristic of this blend. The opposite can be inferred for the MTHF HPC EXF (fine-fine) formulation, where the high uniaxial compressive strength ( $\sigma_c$ ) of the HPC EXF (fine polymer) was diluted by the high cohesion of the MTHF (fine API).



**Figure 4.76** Cohesion and uniaxial compressive strength for 70% theophylline blends. (Source: Pafiakis, Armenante, Gogos 2022)

#### 4.4. Brabender: Mixing Process Monitoring

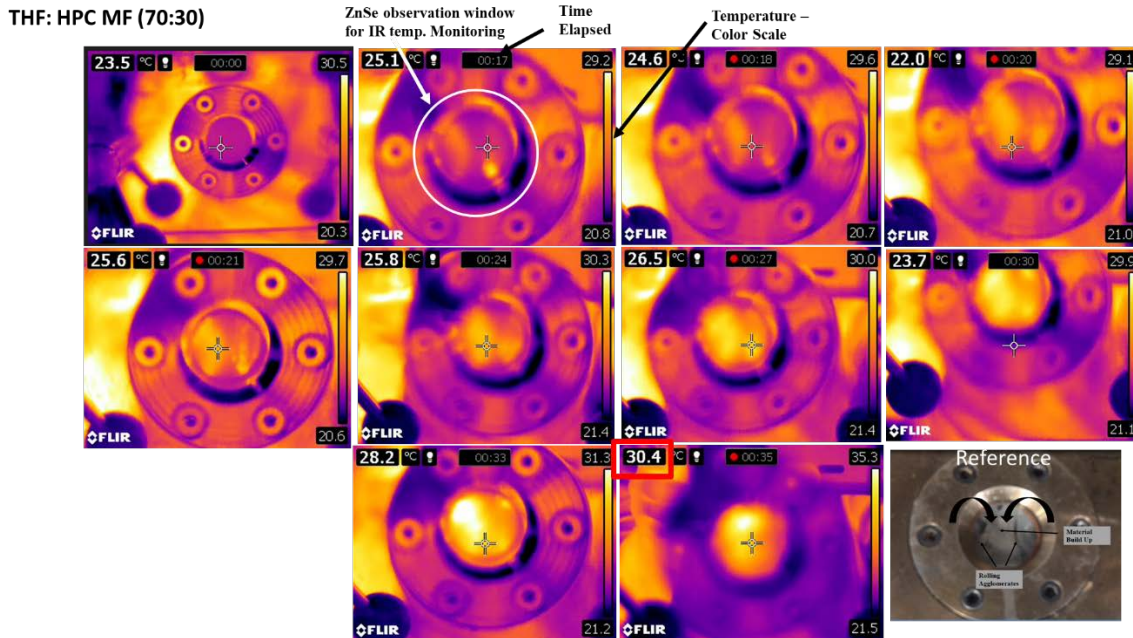
The 70% w/w API formulations used for TSG evaluation had the lowest coefficient of friction,  $f$ , among all the iShear™ formulation. Since it had the lowest coefficient, this drug load provided enough slip in the Brabender where the experiments could be carried out near room temperature, enabling PED and FED to be measured as product temperature. Previous experiments using the batch mixer showed that lower concentrations granulated too quickly due to rapid onset of viscous energy dissipation (VED). Higher drug loads also led to the seizing of the mixer (data not shown). The Brabender batch mixer also gave a qualitative assessment on the mixing intensity across the kneading zone.

Xanthos (1992) was the first to establish the methodology of using the evolution/time dependence of the torque and melt temperature during Brabender Batch Processing. This was established for reactive or morphology-changing polymer systems to predict at what axial positions in continuous processors, such as twin-screw extruders, these changes would take place. This methodology was used in combination with the work of Valsamis and Condedo.

Valsamis et al. (1994) explained that the mixing screws in a batch mixer creates velocity differences between compacted particles in locations of the batch mixer with tighter tolerances (e.g., between the mixing screws and mixer walls), as illustrated in Figure 2.17. These velocity differences convert mechanical energy from the motor to heat as the particles rub against one another. Both the magnitude of the heat liberated, as well as the work required to move the granulation, are dependent on the materials' friction coefficient,  $f$  (Valsamis, Canedo, 1994). The different combinations of particle sizes between the API and the polymer cause different degrees of deformation during granulation.

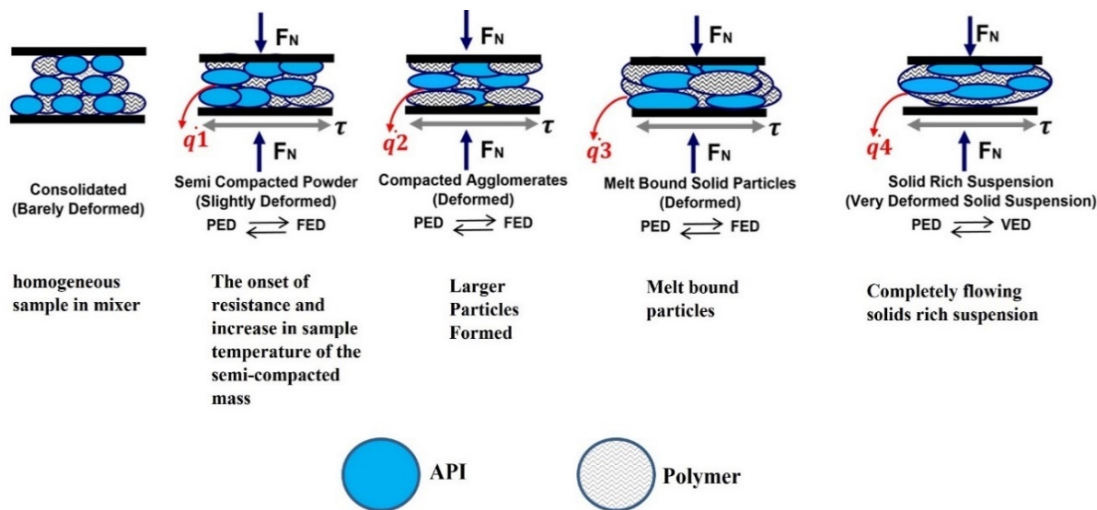
Preliminary studies explored the use of thermal imaging as a function of time in an attempt to model the evolution of heat being liberated due to FED. Figure 4.77 shows still-frames from a recording taken with a thermal imaging camera of a 70:30 THF: MF (coarse API: Coarse Polymer) blend where the onset of FED was observed at approximately 17 seconds from the beginning of mixing. Images continue to show the increase in temperature as a function of time. At 35 seconds into the run, the agglomerates created enough force against the ZnSe sight window that caused it to break. The images do show that after 35 seconds, an increase of approximately  $7^{\circ}\text{C}$  in product temperature was recorded.





**Figure 4.77** Still frames taken from a thermal imaging video of the theophylline (coarse polymer): hydroxypropylcellulose (HPC) MF (coarse polymer) showing the evolution of FED inside the batch mixer.

Figure 4.78 defines the different stages of deformation along with the proposed melting mechanism in a counter rotating batch mixer.



**Figure 4.78** Illustration of the different stages of deformation from consolidated particles to a solid rich suspension via batch mixing. Stage I illustrates the sample loaded into the mixer, Stage II is the onset of resistance and increase in sample temperature of the semi-compacted mass, Stage III is steady state compaction, Stage IV are melt bound particles, and Stage V is a completely deformed solid rich suspension.

(Source: Pafiakis, Armenante, Gogos 2022)

Stage I ( $t \geq 0$  minutes) illustrates when the blend is loaded into the mixer. Stage II is the onset of granulation. This is identified by a slight increase in temperature and torque. The initiation of two simultaneous phenomena is occurring in Stage II. First, the polymer particles are squeezed together. This begins the shear deforming mechanisms, plastic and frictional energy dissipation (PED and FED), and work is being given off as heat ( $\dot{q}_1$ ). This heat is proportional to the mechanical energy of the motor. Secondly, the particles in the mixer begin to coalesce due to compaction, compression for polymer in the melted state, and sintering between the API and mobile polymer as the polymer reaches the softening temperature as it approaches the glass transition temperature ( $T_g$ ).

In Stage III, the compacted mass continues to give off heat ( $\dot{q}_2$ ). The temperature increases on the surface of the particles, driven by FED, melts the polymer, causing more local viscous flow. This allows the adjacent particles to fuse via “*glue points*” (Tadmor and Gogos 2006, p. 221).

The workload needed to move the larger agglomerates increases as indicated by the torque profile. At the maximum of Stage III, the compacted mass requires significant work to mix due to the agglomerates increased strength. This relentless mixing promoted the formation of localized hydrogen bonds between adjacent API and Polymer particles (Breitenbach 2002, Bhugra and Pikal 2008). The work required to mix the sample increased exponentially along with the heat generated ( $\dot{q}_2$ ). The high amplitudes in the torque profile are attributed to non-uniform chaotic agglomeration, where the larger agglomerates require more power to move through the tighter regions of the mixer.

At the onset of Stage IV, the heat given off ( $\dot{q}_3$ ) was greater than those generated in Stages III ( $\dot{q}_2$ ) and II ( $\dot{q}_1$ ) and continued to climb as it approaches viscous energy

dissipation (VED). The granulation reached a maximum torque. Since the particles were still being deformed, the phenomena described in Stage II and III were still present. FED now approached VED. The agglomerates become softer due to the relentless stretching and pulling through the shear intense sections of the batch mixer. Inevitably, the material succumbed to the extreme deformation and relaxed. This was indicated by a decrease in the torque profile and steady increase in temperature. Since the theophylline and micronized theophylline were measured to have high melting temperatures ( $T_m$ ) of 272.6°C and 273.20, respectively, it was far from melting and became suspended in the molten polymer in Stage V. Stage V can be characterized by a plateau in the torque and temperature, where PED and VED became the dominant heating mechanisms (Valsamis and Canedo 1991,1994; Kim 1999)

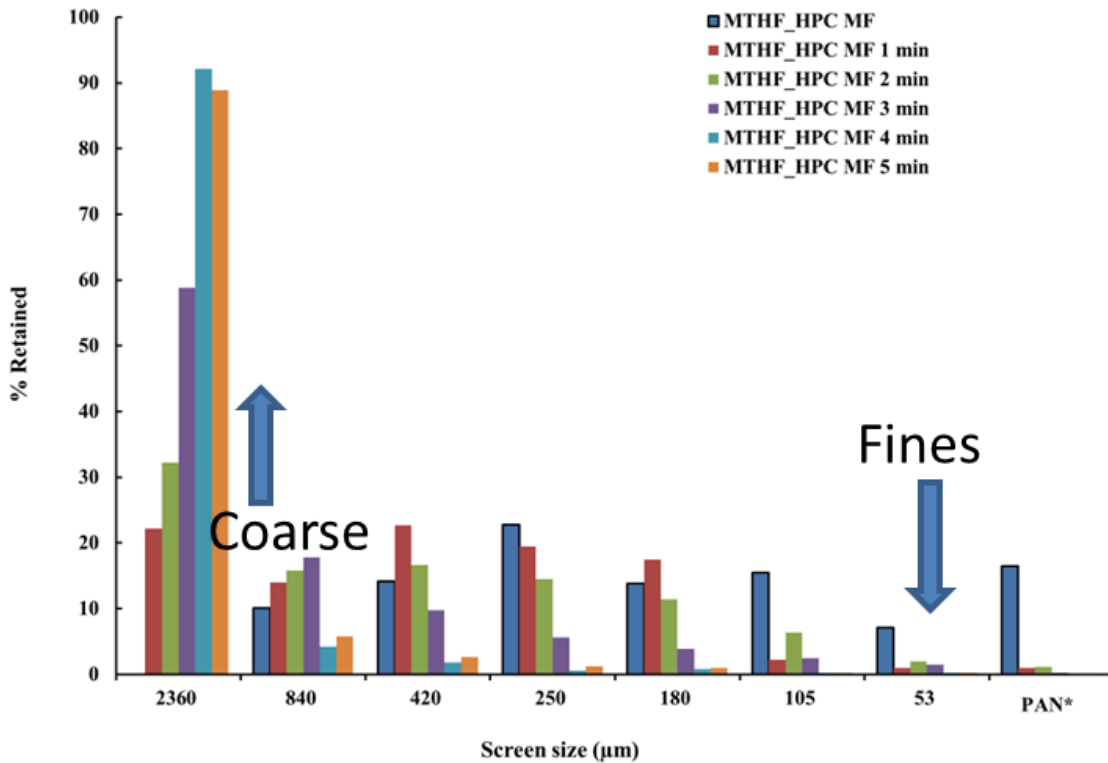
#### **4.4.1 Granulating near room temperature using the Brabender: hot melt batch mixer**

The formulations that contained the coarse API, THF reached the maximum torque limit in approximately two minutes. The formulations that contained the fine API, MTHF reached the maximum torque limit in approximately five minutes. This difference in residence time is attributed to morphological and random packing effects of the material; hence varying the coefficient of friction,  $f$ .

The THF formulations had a higher coefficient of friction,  $f$ , than the formulations containing the MTHF. It can be inferred that the particle-particle interaction for the THF formulations were more abrasive. Since the material was compacted, interparticle “stacking” or “weaving” expected from these particles can intensify this effect (Tadmor and Gogos 2006 p. 154).

#### 4.4.2 Granulation of Micronized Theophylline (MTHF) blends with Hydroxypropylcellulose MF (HPC MF) and Hydroxypropylcellulose EXF (HPC EXF)

4.4.2.1 Particle size analysis of Micronized Theophylline (MTHF) blends with Hydroxypropylcellulose MF (HPC MF) and Hydroxypropylcellulose EXF (HPC EXF). The MTHF:HPC MF (fine-coarse) formulation demonstrated a bimodal particle size distribution at 250  $\mu\text{m}$  and 2360  $\mu\text{m}$  as shown in Figures 4.79 and 4.80 for MTHF:HPC EXF (fine-fine) formulation, respectively.

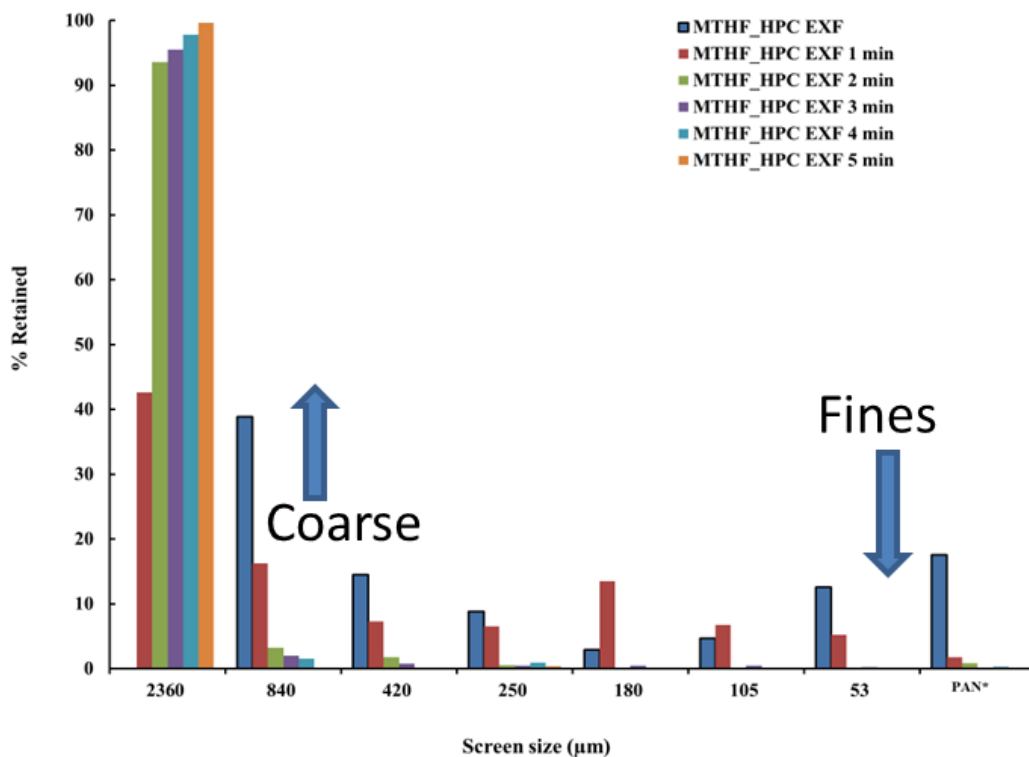


**Figure 4.79** Particle size distribution profiles as a function of mixing time for micronized theophylline (MTHF) and hydroxypropylcellulose MF (HPC MF) blend (MTHF:HPC MF).

(Source: Pafiakis, Armenante, Gogos 2022)

The particle size distribution for the MTHF:HPC EXF (fine-fine) formulation showed that most of the granulation was occurring at 2360  $\mu\text{m}$ . Over the course of the

five minutes, MTHF:HPC MF (fine-coarse) granulated steadily. It can be hypothesized that the differences between the particle size of the API and polymer allowed the API to create a protective coating layer around the polymer. This delayed the onset of glue points, and controlled granule growth in a steady fashion. However, in less than two minutes, the MTHF:HPC EXF (fine-fine) formulation was essentially one solid mass.



**Figure 4.80** Particle size distribution profiles as a function of mixing time for micronized theophylline (MTHF) and hydroxypropylcellulose EXF (HPC EXF) blend (MTHF:HPC EXF).

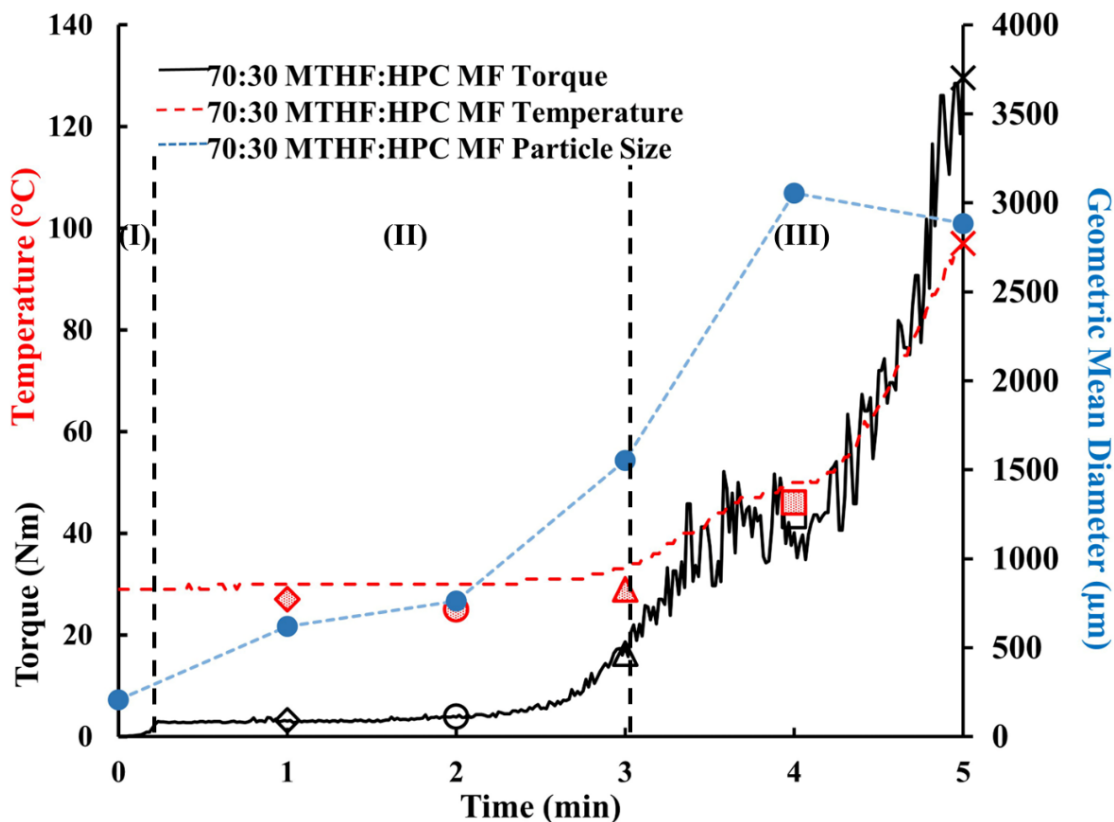
(Source: Pafiakis, Armenante, Gogos 2022)

The high binding efficiency for the MTHF:HPC EXF (fine-fine) formulation is attributed to the packing of more uniformly distributed particles. Despite this formulation having the lowest coefficient of friction,  $f$ , this blend has the highest surface area. The fine API particles were homogeneously distributed between the fine polymer particles. The

high surface area facilitated enough particle-particle interaction in the compacted state to allow PED and FED to occur uniformly. This induced localized melting pools of the polymer on surfaces, thereby promoting sintering and rapidly facilitating more “*glue points*” (Okayama 1997; Esseghir, Yu, Gogos, and Todd 1997).

**4.4.2.2 Granule growth and system parameter correlation of micronized theophylline (MTHF) blends with hydroxypropylcellulose MF (HPC MF) and hydroxypropylcellulose EXF (HPC EXF).** Figure 4.81 highlights the strong correlation between the geometric mean diameter (GMD), product temperature as a result of PED and FED, and torque (mechanical work) measured during granulation for the formulations containing MTHF (Fine API) along with the proposed stages of deformation.

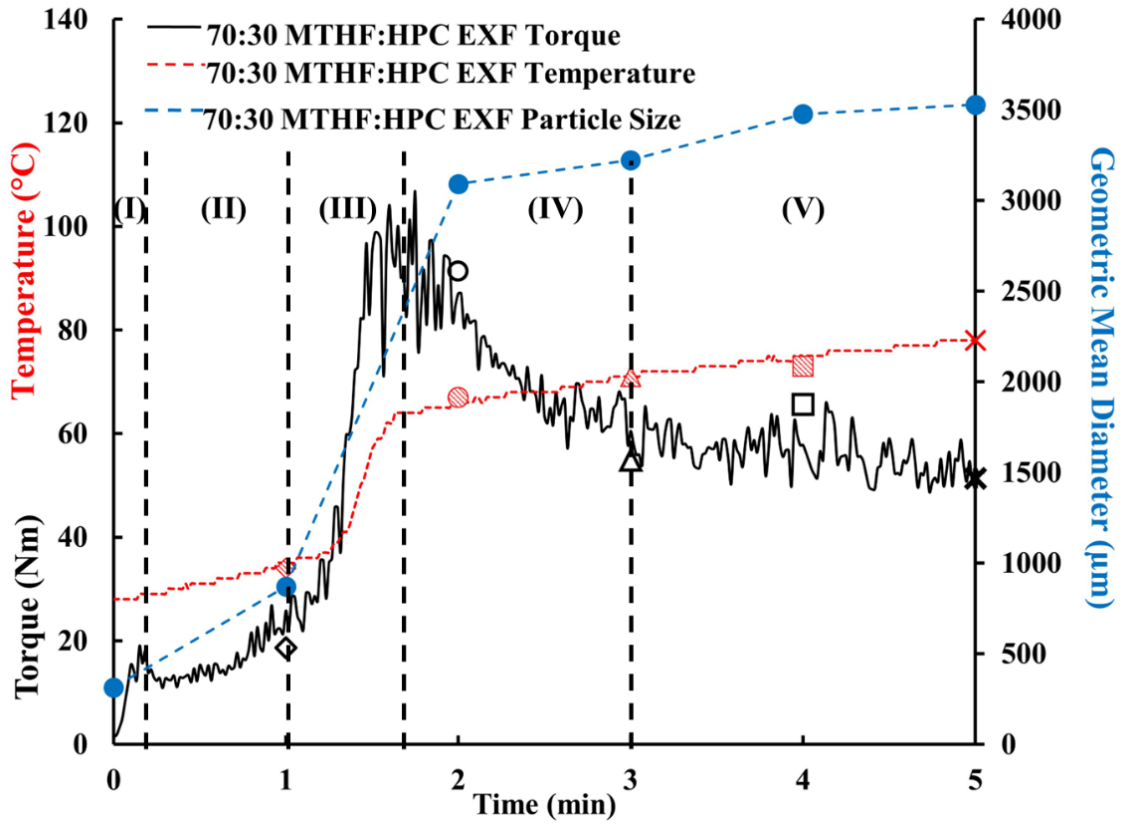
Granulation activity from Stage I to Stage II can be attributed to compaction of the powders for both formulations.



**Figure 4.81** illustrates the torque and temperature traces, as a function of time for the formulations containing 70% w/w MTHF and 30% w/w HPC MF.  $\blacklozenge$  is the temperature reading and  $\blacklozenge$  is the torque reading from the 1 min batch.  $\bullet$  is temperature reading and  $\circ$  is the torque reading from the 2 min batch.  $\blacktriangle$  is the temperature reading and  $\triangle$  is the torque reading from the 3 min batch.  $\blacksquare$  is the temperature reading and  $\square$  is the torque reading from the 4 min batch.  $\blacktimes$  is the temperature reading and  $\times$  is the torque reading from the 5 min batch. The  $\bullet$  is the Geometric Mean Diameter of granules determined from the particle size distribution measured at each time point.

(Source: Pafiakis, Armenante, Gogos 2022)

The MTHF:HPC MF (fine-coarse) formulation had the longest Stage II, lasting for approximately three minutes. Since temperature and torque were constant, the increase in GMD is dominated by compaction of the formulation. This further supports the hypothesis that the API is lubricating the polymer, allowing limited API-Polymer surface interaction that translate to a slower granulation. The lubricating effect of the API, coupled with a high surface area, explains why Stage II is slow.



**Figure 4.82** Illustrates the torque and temperature traces, as a function of time for the formulations containing 70% w/w MTHF and 30% w/w HPC EXF.  $\diamond$  is the temperature reading and  $\diamond$  is the torque reading from the 1 min batch.  $\circ$  is temperature reading and  $\circ$  is the torque reading from the 2 min batch.  $\triangle$  is the temperature reading and  $\triangle$  is the torque reading from the 3 min batch.  $\square$  is the temperature reading and  $\square$  is the torque reading from the 4 min batch.  $\times$  is the temperature reading and  $\times$  is the torque reading from the 5 min batch. The  $\bullet$  is the Geometric Mean Diameter of granules determined from the particle size distribution measured at each time point.

(Source: Pafiakis, Armenante, Gogos 2022)

The granule growth in Stage II may contain small pockets of local pools of molten polymer, facilitating some sintering and agglomeration. Stage II for the MTHF:HPC EXF (fine-fine) is much faster and is only observed for approximately one minute. The GMD for this formulation is greater than that observed for THF:HPC EXF (coarse-fine).



In Stage III, the MTHF:HPC EXF (fine-fine) formulation experienced a large increase in particle size. The temperature was approximately 60°C and the torque was approximately 100Nm. Both formulations show gradual granule growth.

The MTHF:HPC EXF (fine-fine) formulation was the only formulation of the four that was able to go through all five stages of deformation in the Brabender. At the onset of Stage IV, the temperature leveled off at approximately 65°C. The torque decreased and plateaued at approximately 60 Nm. At three minutes, the process transitioned into Stage V and remained there for two more minutes.

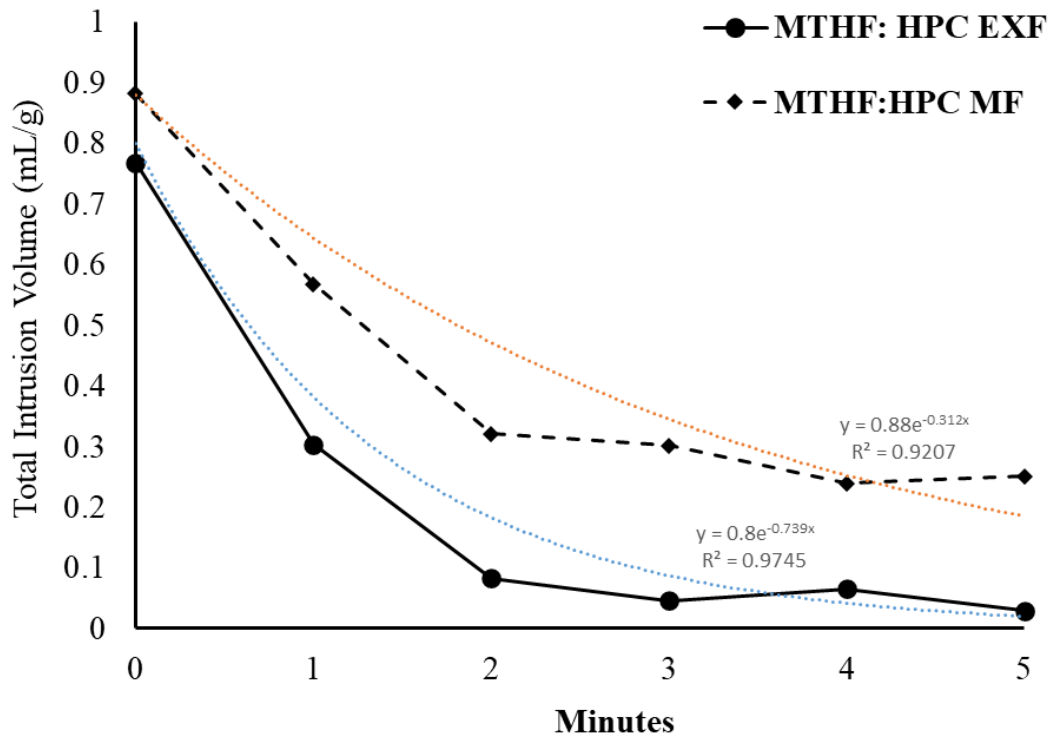
Very little mass building occurred in Stage IV. Negligible changes in the torque and GMD were strong indicators that the entire batch was essentially one solid rich suspension. The oscillations observed in the torque reading indicated the material was being stretched, cut, and reattached, like kneading dough. The high surface area of this formulation may have increased the efficiency of PED and FED, leading to sintering and agglomeration (Okuyama and Higashitani 1997; Esseghir, Yu, Gogos, and Todd 1997).

**4.4.2.3 Consolidation rate and granule evolution as a function of batch mixing time for Micronized Theophylline (MTHF) formulations.** The interaction of the coefficients of friction,  $f$ , between the API and the polymer dictate the rate of densification or consolidation rate for each formulation. Compaction and locally occurring sintering create molten polymer pools facilitating compression of the tacky polymer. The polymers pools cause particles to agglomerate, creating voids between granulated clusters. These voids are measured as pores. Figure 4.83 show the granule consolidation kinetics as a function of mixing time for the formulations prepared with MTHF (fine API).

The following exponential decay model can be used to characterize the consolidation rate as a function of batch mixing time and formulation.

$$\frac{\varepsilon - \varepsilon_{min}}{\varepsilon_o - \varepsilon_{min}} = e^{-kt} \quad (4.1)$$

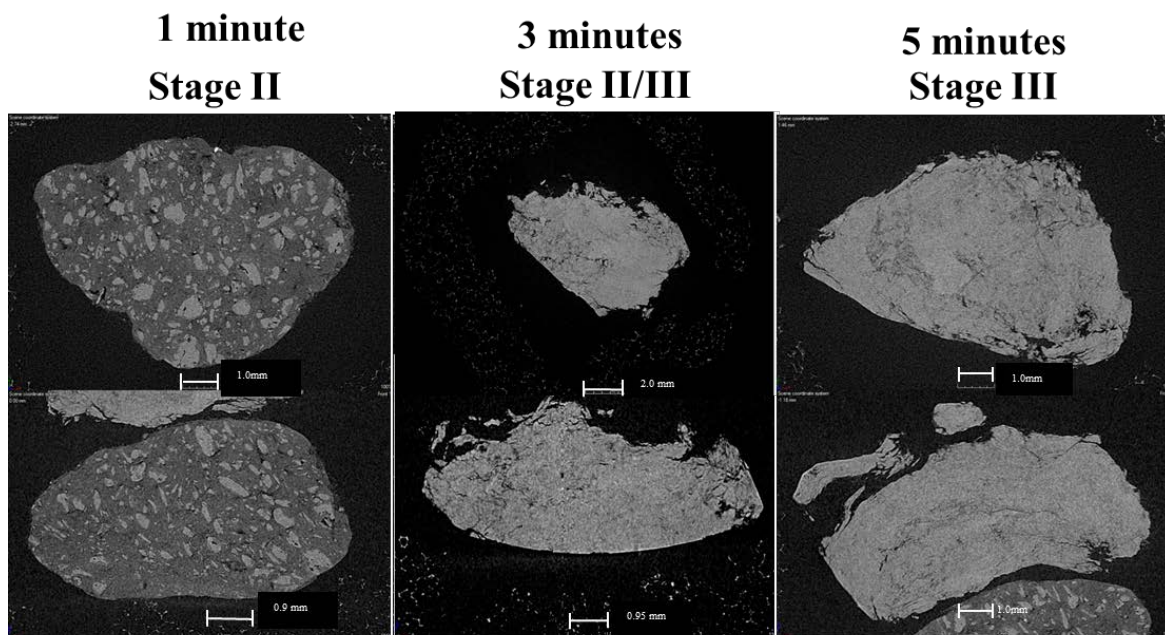
Where  $\varepsilon_{min}$  is the minimum achievable porosity,  $k$  is the exponential consolidation rate constant,  $\varepsilon$  is the granule porosity at time  $t$ , and  $\varepsilon_o$  is the initial porosity (Narang et al. 2019).



**Figure 4.83** Total intrusion volume for the formulations prepared with micronized theophylline (MTHF; fine API).

(Source: Pafiakis, Armenante, Gogos 2022)

The MTHF:HPC EXF (fine-fine) formulation showed the greatest extent of densification, where the other MTHF (and two THF formulations) were similar in pore intrusion volume. Figure 4.84 shows X-ray Tomography images of granules made using the MTHF:HPC MF (fine-coarse) formulation.

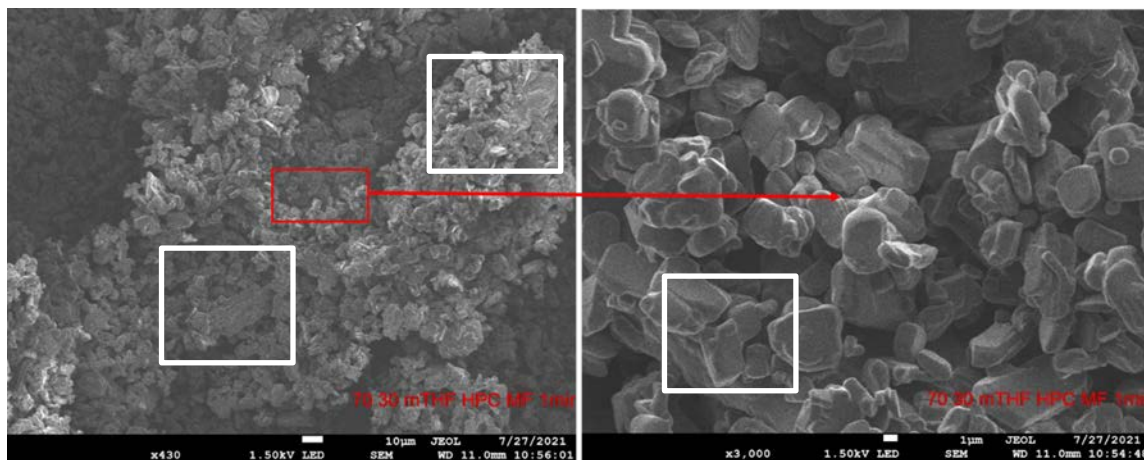


**Figure 4.84** X-Ray tomography for 70:30 micronized theophylline (MTHF) and hydroxypropylcellulose MF (HPC MF) blend (MTHF:HPC MF) as a function of time and deformation stage.

*(Source: Pafiakis, Armenante, Gogos 2022)*

The images show that after one minute of mixing, the HPC MF particles (the brighter particulates) are fully intact and surrounded by the API. This indicates that the polymer is not fully dispersed until the end of granulation. The sample taken at one minute indicates that most of the agglomeration is occurring due to compression. This is supported by the image showing the polymer. The onset of granulation due to molten polymer most likely occurred at the inflection point of temperature and torque; this is the onset of Stage III. The three-minute sample shows that the polymer has just become incorporated into the granule.

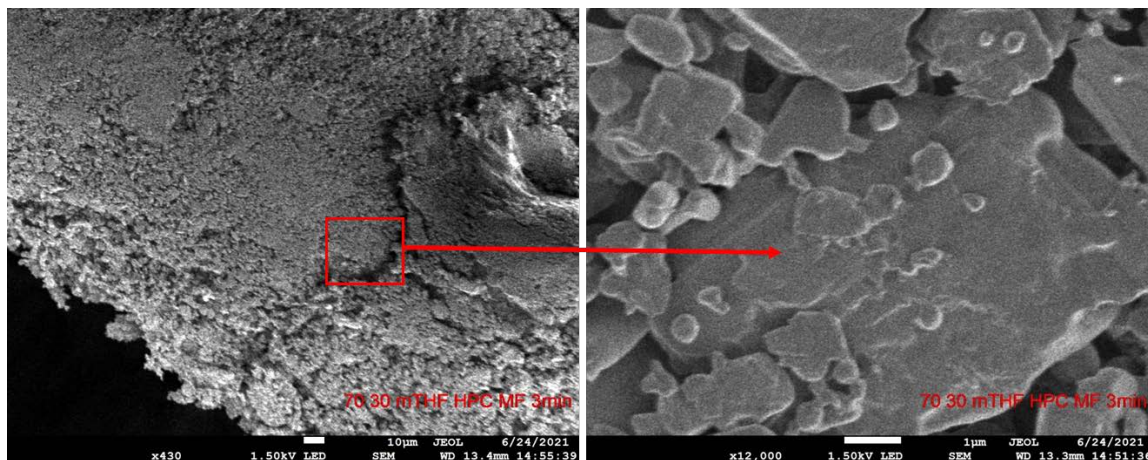
SEM images were also collected from available samples for the MTHF:HPC MF formulation. The SEMs for this formulation show the evolution of agglomeration and the onset of local polymer flow. Figure 4.85 shows SEM taken after one minute of mixing in the Brabender.



**Figure 4.85** SEM images for 70:30 micronized theophylline (MTHF) and hydroxypropylcellulose MF (HPC MF) blend (MTHF:HPC MF) after one minute of mixing time (Stage II) in the Brabender.

The SEM shows sintered discrete particles fused together to form a larger agglomerate after one min of mixing. This is primarily due to compaction of the powder blend and some softening of the polymer due to FED. The temperature of the powder blend at this time point was approximately 27°C. The white squares show HPC MF coated with API. It was discussed earlier that the API coating the polymer may be the control mechanism for maintaining the FED melting mechanism to facilitate granulation. This may be why a steady granule growth and finer granules were observed for the HPC MF formulations during the batch mixing and 27 mm trials, respectively.

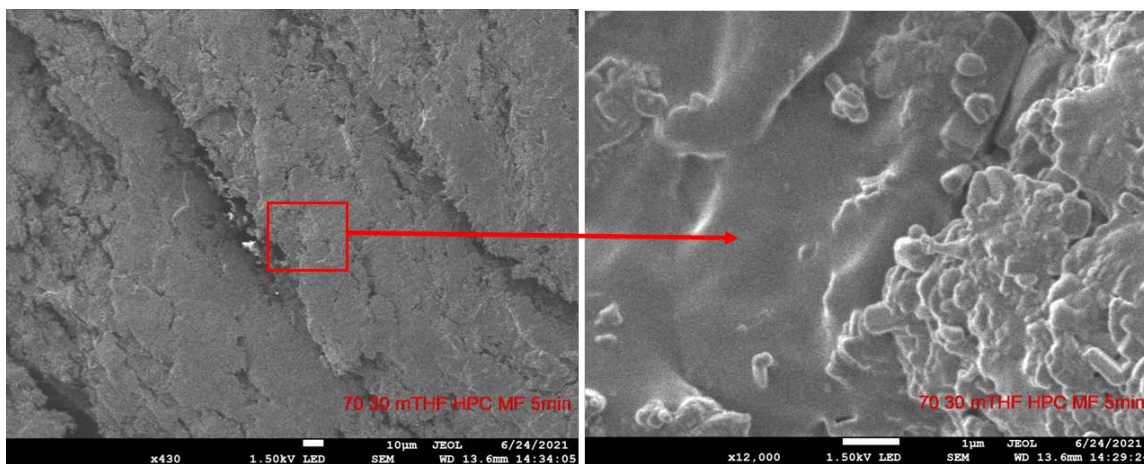
This sample in Figure 4.86 was taken after three minutes of batch mixing. For the MTHF:HPC MF formulation. Three minutes was the onset of granulation. The figure shows that despite the low product temperature of 29°C, the particles are beginning to fuse and sinter.



**Figure 4.86** SEM images for 70:30 micronized theophylline (MTHF) and hydroxypropylcellulose MF (HPC MF) blend (MTHF:HPC MF) after three minutes of mixing time (Stage II/Stage III) in the Brabender.

The SEM shows that after three minutes of batch mixing a transition from discrete particles to the formation of a smooth surface occurred. This is clear in the magnified image on the right showing particles fused together and sections appear like polymer melt where the polymer is losing its particulate shape.

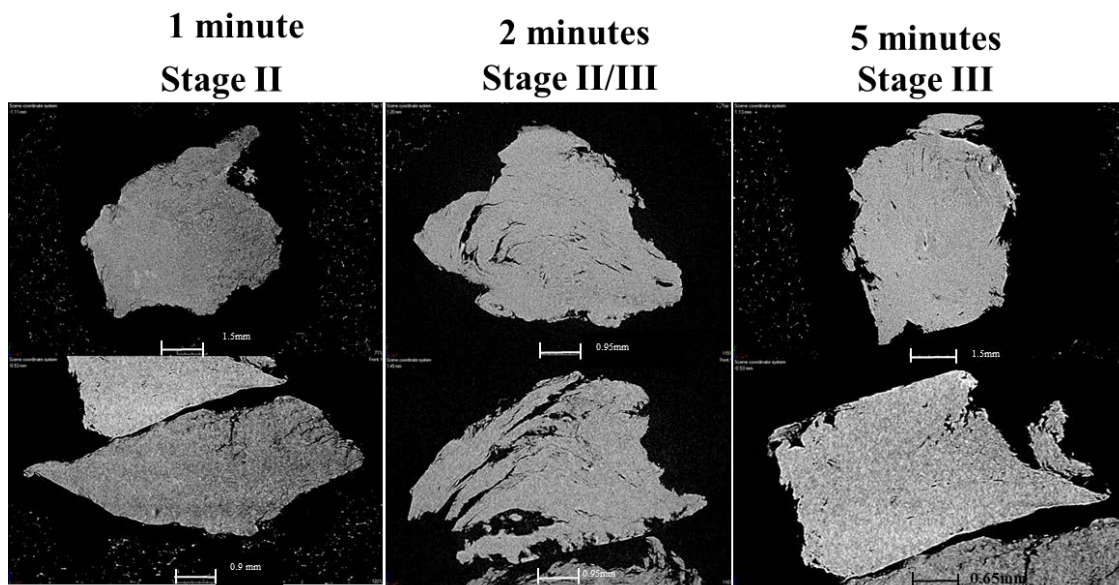
The SEM images at five minutes in Figure 4.87 show that for the MTHF:HPC MF formulation there were a few discrete particles left and locally the polymer has completely coated whatever particulates were left on the surface of the granule. The product temperature at five minutes was 97°C.



**Figure 4.87** SEM images for 70:30 micronized theophylline (MTHF) and hydroxypropylcellulose MF (HPC MF) blend (MTHF:HPC MF) after five minutes of mixing time (Stage III) in the Brabender.

The SEM shows that after five minutes of batch mixing the powder blend developed several smooth surfaces. The FED and PED melting mechanisms reached temperatures that initiated significant localized polymer flow. This formulation may have been on the transition from FED and PED to PED and VED. The magnified image on the right shows complete localized polymer flow coating the surface of the granule.

Figure 4.88 shows X-ray Tomography images of granules made using the MTHF:HPC EXF (fine-fine) formulation. The MTHF:HPC EXF (fine-fine) formulation shows a uniform blend at one minute.

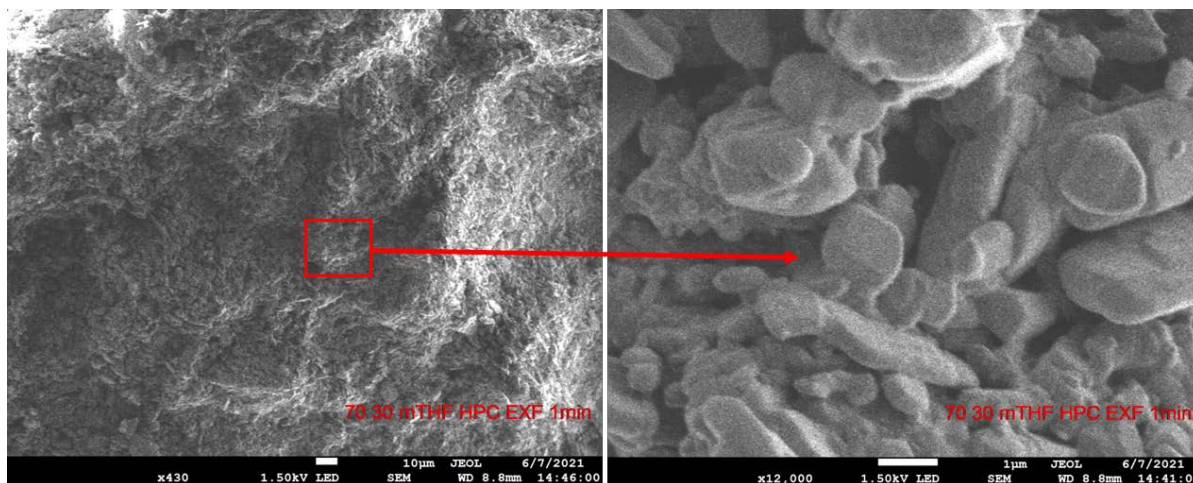


**Figure 4.88** X-Ray tomography for 70:30 micronized theophylline (MTHF) and hydroxypropylcellulose EXF (HPC EXF) blend (MTHF:HPC EXF) as a function of time and deformation stage.

*(Source: Pafiakis, Armenante, Gogos 2022)*

By two minutes, this sample is showing evidence of voids with a swirl profile. These are the extensional and elongational flow profiles trapped within the granule (Agassant et al. 2002). At five minutes, the pores are very small, indicating that the formulation is essentially a solid rich suspension.

SEM images were collected from available samples for the MTHF:HPC EXF formulation. The SEMs for this formulation show the evolution of agglomeration and the onset of local polymer flow. Figure 4.89 shows SEM taken after one minute of mixing in the Brabender.

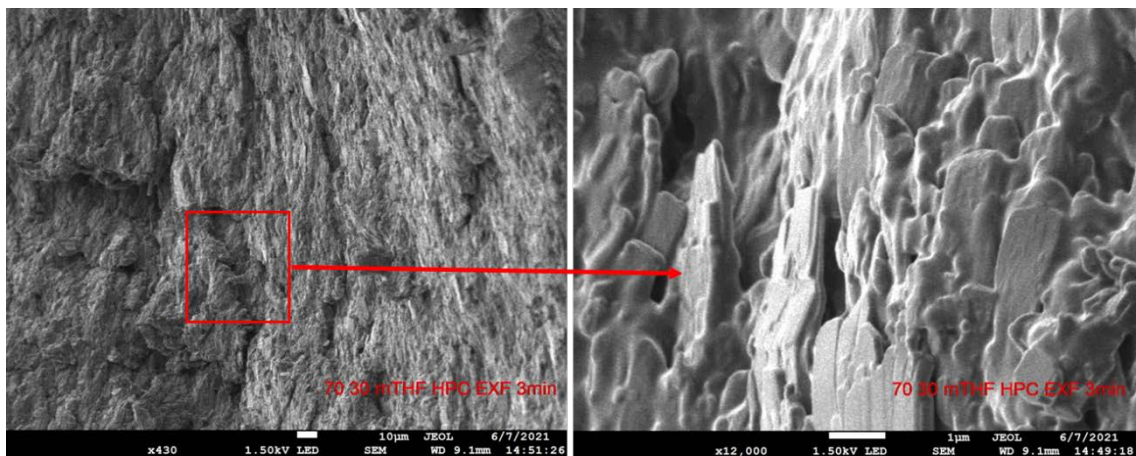


**Figure 4.89** SEM images for 70:30 micronized theophylline (MTHF) and hydroxypropylcellulose EXF (HPC EXF) blend (MTHF:HPC EXF) after one minute of mixing time (Stage II) in the Brabender.

The SEM images after one minute of batch mixing for the MTHF:HPC EXF formulation show a granule made up of discrete particulates. The API and polymer for this formulation were very similar in particle size between the two as seen from the SEM on the left. The higher magnified image on the right shows several discrete structures. It also shows the onset of fusing and sinter or “*glue points*” between particulates indicating localized polymer flow. The product temperature for this batch was approximately 34°C when the sample was collected.



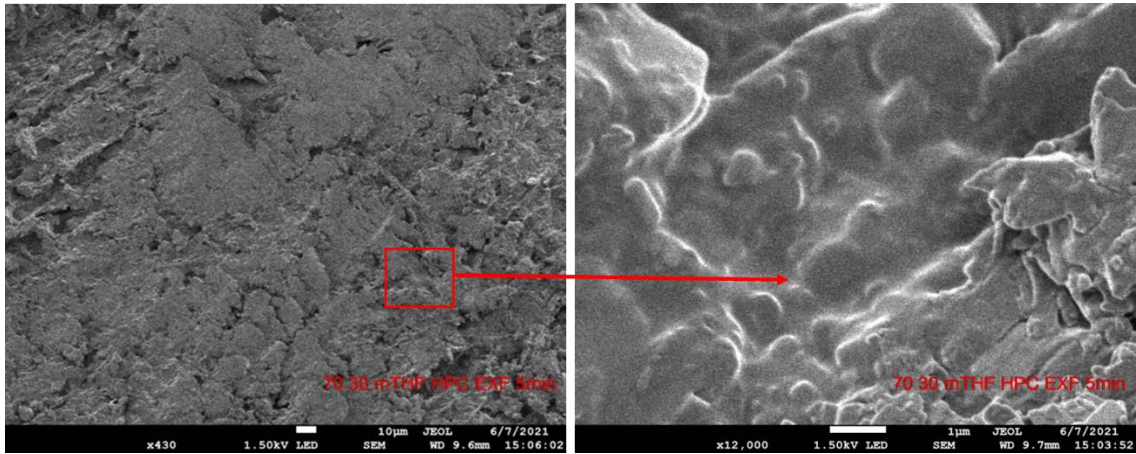
The SEM images after three minutes (one minute after the torque peaked) of batch mixing in Figure 4.90 show that with more mixing the product temperature rapidly increased to 71°C. At this point, the melt mechanisms are transitioning from FED and PED to PED and VED.



**Figure 4.90** SEM images for 70:30 micronized theophylline (MTHF) and hydroxypropylcellulose EXF (HPC EXF) blend (MTHF:HPC EXF) after three minutes of mixing time (Stage IV) in the Brabender.

The SEM suggests that after three minutes of batch mixing the granules transitioned from granules comprised of discrete particulates to granules with smooth rigid surfaces. This is clear in both low and high magnification SEM images. Individual particles are no longer observed and local polymeric flow is clear in the SEM on the right with higher magnification. This is similar to the SEMs of the granules evaluated in Subsection 4.2.1 Granule Analysis Using the 30 mm Twin Screw Mixing Element Evaluator (TSMEE) on page 63.

The SEM images after five minutes of batch mixing in Figure 4.91 show that for the MTHF:HPC EXF formulation, more mixing caused the temperature to increase steadily to 78°C. At this point the melting mechanism was dominated by VED and the particles have become a solid rich suspension.

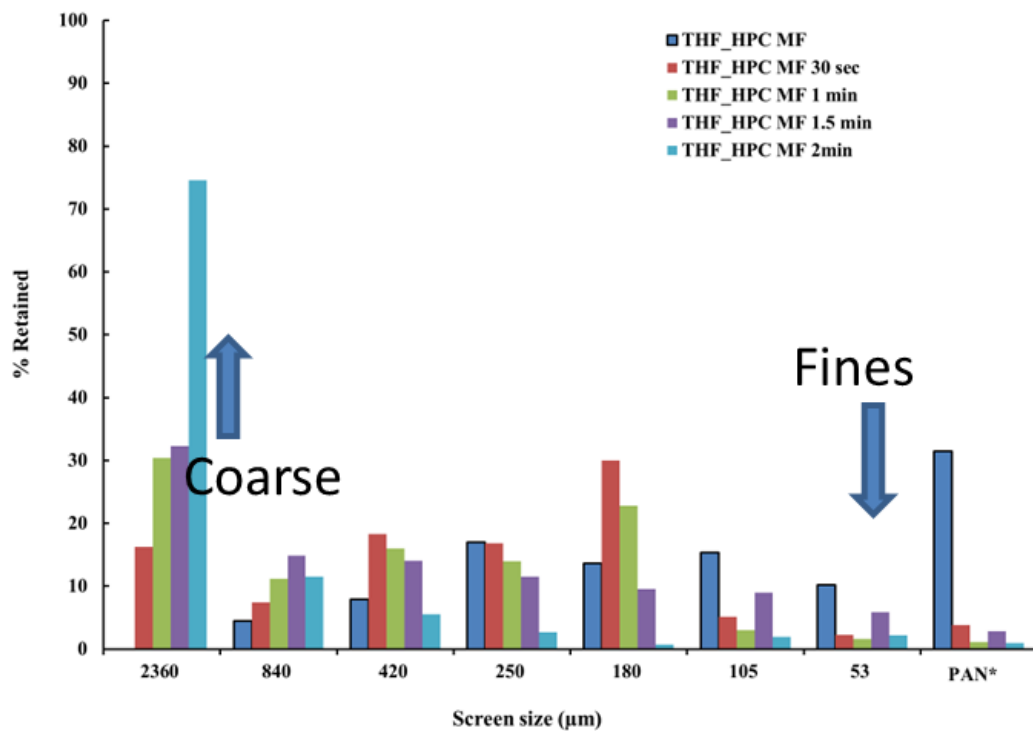


**Figure 4.91** SEM images for 70:30 micronized theophylline (MTHF) and hydroxypropylcellulose EXF (HPC EXF) blend (MTHF:HPC EXF) after five minutes of mixing time (Stage IV) in the Brabender.

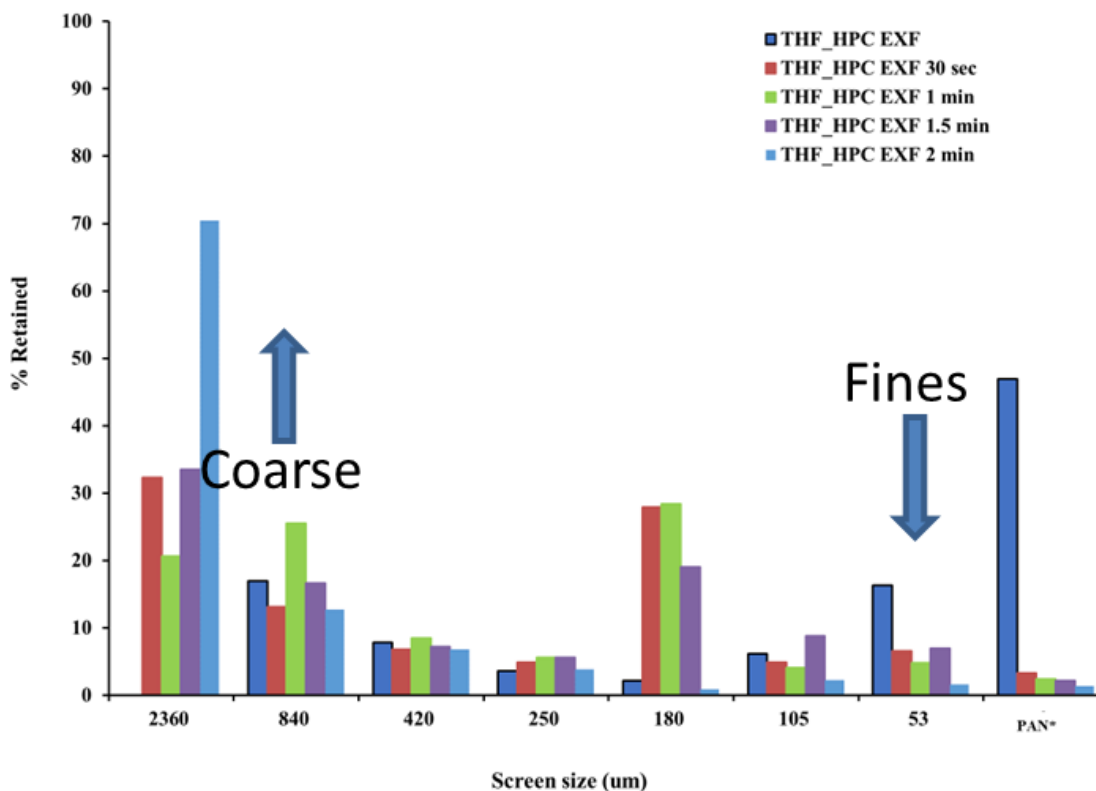
The SEM shows that after five minutes of batch mixing the powder blend developed a smoother surface. This is because the melting has fully transitioned to VED. The additional mixing provided extensive deformative melting through the extensional and elongation forces of repeated folding and cutting in the mixing and rolling zone in the batch mixer. The magnified image on the right shows complete localized polymer flow coating the surface solid rich suspension.

### 4.4.3 Granulation of Theophylline (THF) blends with Hydroxypropylcellulose MF (HPC MF) and Hydroxypropylcellulose EXF (HPC EXF)

4.4.3.1 Particle size analysis of theophylline (THF) blends with Hydroxypropylcellulose MF (HPC MF) and Hydroxypropylcellulose EXF (HPC EXF). Comparison of the particle size distribution (PSD) for the THF formulations are presented in Figures 4.92 and 4.93 as a function of mixing time.



**Figure 4.92** Particle size distribution profiles as a function of mixing time for theophylline (THF) and hydroxypropylcellulose MF (HPC MF) blend (THF:HPC MF).  
(Source: Pafiakis, Armenante, Gogos 2022)



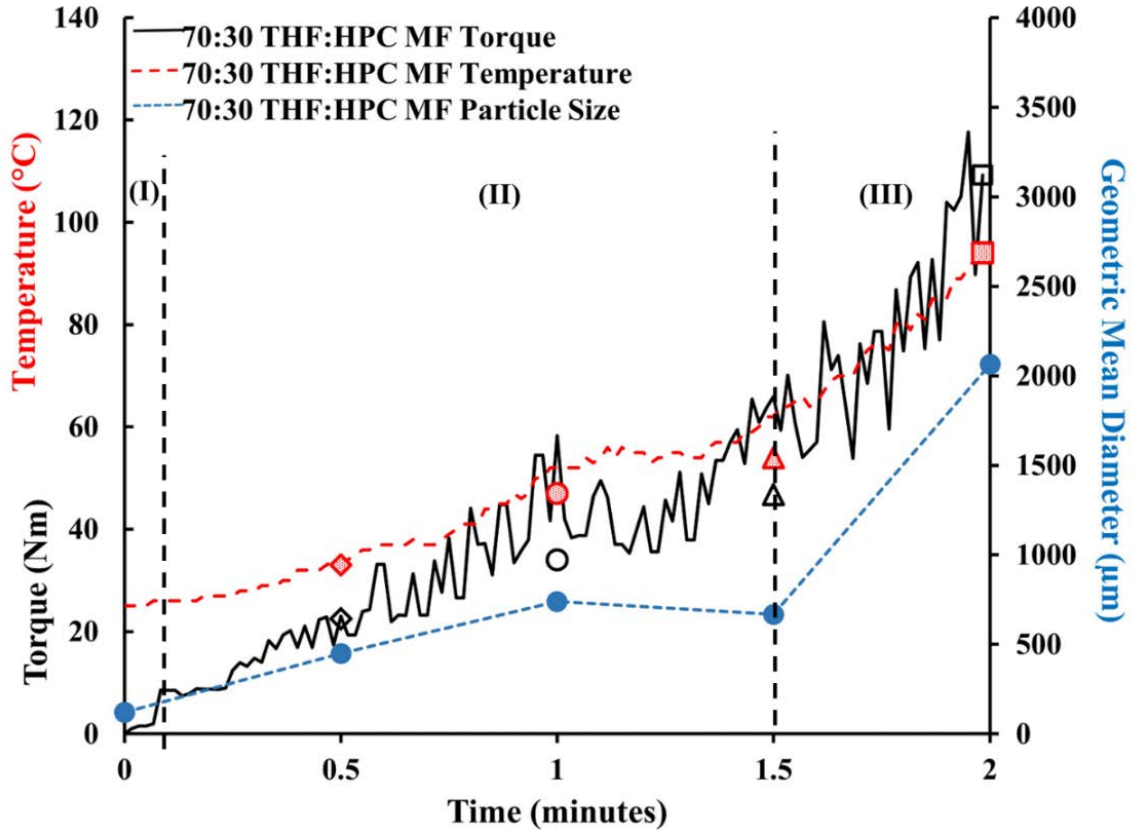
**Figure 4.93** Particle size distribution profiles as a function of mixing time for theophylline (THF) and hydroxypropylcellulose EXF (HPC EXF) blend (THF:HPC EXF).  
 (Source: Pafiakis, Armenante, Gogos 2022)

The fines ( $\leq 105 \mu\text{m}$ ) for both THF (coarse API) formulations agglomerated within the first thirty seconds. Both formulations showed a bimodal distribution at  $180 \mu\text{m}$  and  $2360 \mu\text{m}$ . Divergence between the two became noticeable after one minute. A steady decline in granule growth was observed at  $180 \mu\text{m}$  for the THF:HPC MF (coarse-coarse) formulation, indicating that these granules were growing and fusing with other particulates.

The particle size data for the THF:HPC EXF (coarse-fine) formulation indicated that the agglomerates were breaking and rebuilding. This is evident at the  $53 \mu\text{m}$ ,  $105 \mu\text{m}$ ,  $180 \mu\text{m}$  and  $2360 \mu\text{m}$ , from thirty seconds to a minute and a half. At a minute and a half, the particle size increases for the remainder of the run. This indicated that enough API-Polymer surfaces were available for PED and FED to facilitate effective binding. The

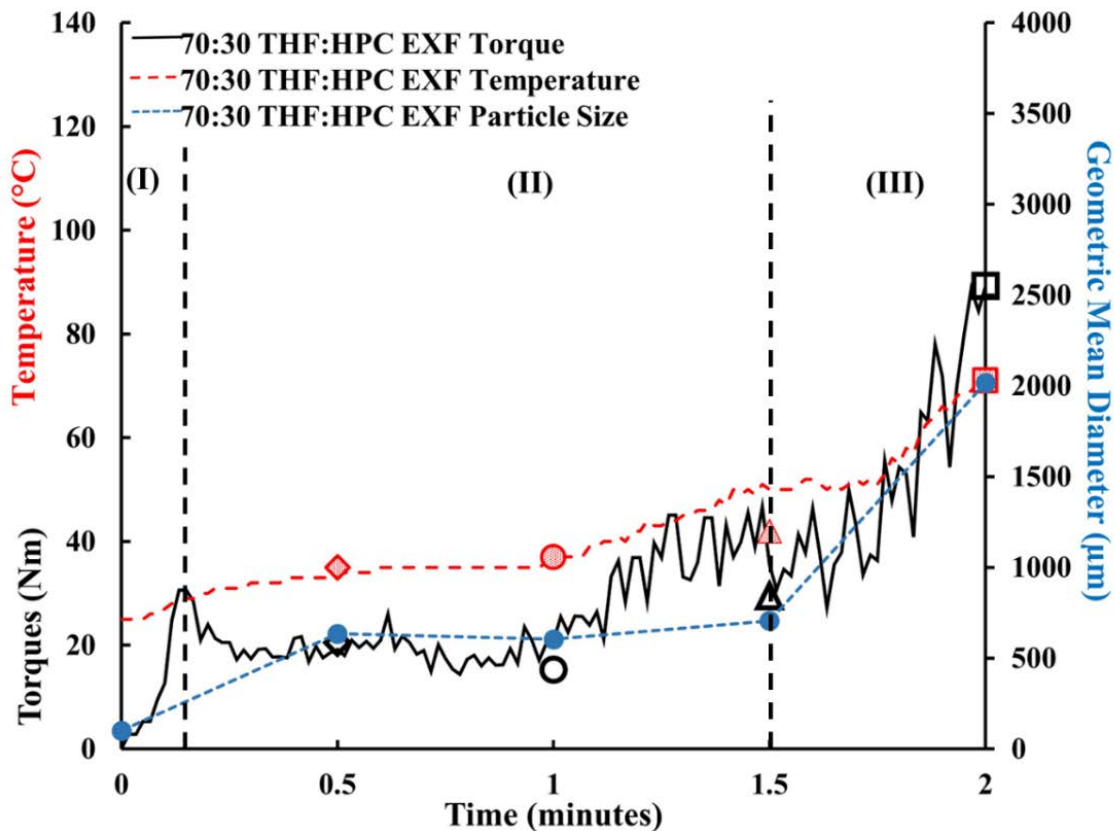
breaking may be attributed to the high uniaxial compressive strength ( $\sigma_c$ ) that was measured for this formulation; the deformation induced heating can be expected to be much lower, due to the inherently high strength of the compressed powder bed ((Pafiakis, Armenante, Gogos 2022)).

**4.4.3.2 Granule growth and system parameter correlation of Theophylline (THF) Blends with Hydroxypropylcellulose MF (HPC MF) and Hydroxypropylcellulose EXF (HPC EXF).** Figures 4.94 and 4.95 highlight the strong correlation between the geometric mean diameter (GMD), product temperature (PED and FED) and torque (mechanical work) measured during granulation for the formulations containing THF (Fine API) along with the proposed stages of deformation.



**Figure 4.94** Illustrates the torque and temperature traces, as a function of time for the formulations containing 70% w/w THF and 30% w/w HPC MF.  $\diamond$  is the temperature reading and  $\diamond$  is the torque reading from the 30 seconds batch.  $\circ$  is temperature reading and  $\circ$  is the torque reading from the 1 min batch.  $\triangle$  is the temperature reading and  $\triangle$  is the torque reading from the 1.5 min batch.  $\square$  is the temperature reading and  $\square$  is the torque reading from the 2 min batch. The  $\bullet$  is the Geometric Mean Diameter of granules determined from the particle size distribution measured at each time point.

(Source: Pafiakis, Armenante, Gogos 2022)



**Figure 4.95** Illustrates the torque and temperature traces, as a function of time for the formulations containing 70% w/w THF and 30% w/w HPC EXF.  $\blacklozenge$  is the temperature reading and  $\blacklozenge$  is the torque reading from the 30 seconds batch.  $\bullet$  is temperature reading and  $\circ$  is the torque reading from the 1 min batch.  $\blacktriangle$  is the temperature reading and  $\blacktriangle$  is the torque reading from the 1.5 min batch.  $\blacksquare$  is the temperature reading and  $\blacksquare$  is the torque reading from the 2 min batch. The  $\bullet$  is the Geometric Mean Diameter of granules determined from the particle size distribution measured at each time point.

(Source: Pafiakis, Armenante, Gogos 2022)

Stage I is the loading and consolidation of the blend. The torque increases for both formulations. For the THF:HPC MF (coarse-coarse) formulation, the torque plateaus at approximately 10 Nm and for THF:HPC EXF (coarse-fine) it is approximately 30 Nm. The formulation with the HPC EXF (fine polymer) has a higher initial load because it is the finer system; hence, it is more compactable (Yohannes et al. 2015). More particles were loaded in the blender, requiring more work to move the solid mass. Stage I shows the response to loading the mixer. The THF:HPC EXF (coarse-fine) formulation is two times

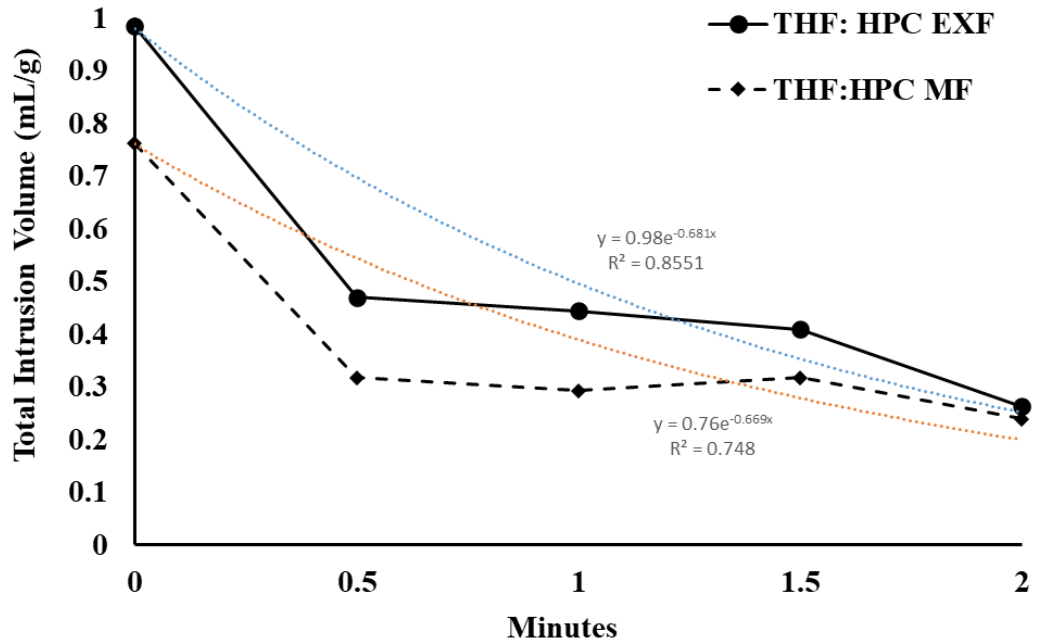
less compactable than the MTHF:HPC EXF (fine-fine) ((Pafiakis, Armenante, Gogos 2022)).

Stage II for the THF:HPC MF (coarse-coarse) formulation shows a shallow linear increase in torque and temperature, as well as a slight increase in the GMD. For the THF:HPC MF (coarse-coarse) formulation, the torque and temperature are both flat. This is further evidence that there is little particle-particle interaction promoting PED and FED, leading to very little granule growth at this stage. At one and a half minutes, the two THF formulations enter Stage III, where both showed rapid granule growth rates. Both THF formulations formed granules and, despite the independent paths that each took, the GMD was similar at the end of granulation (Pafiakis, Armenante, Gogos 2022).

The THF:HPC EXF (coarse-fine) formulation enters STAGE III at three minutes and was stopped at five minutes. The temperature in Stage III climbed exponentially from approximately 30°C to 100°C in just two minutes.

**4.4.3.3 Consolidation rate and granule evolution as a Function of batch mixing time for theophylline (THF) formulations.** Figure 4.96 show the granule consolidation kinetics as a function of mixing time for the formulations prepared with for the formulations prepared with THF (coarse API).

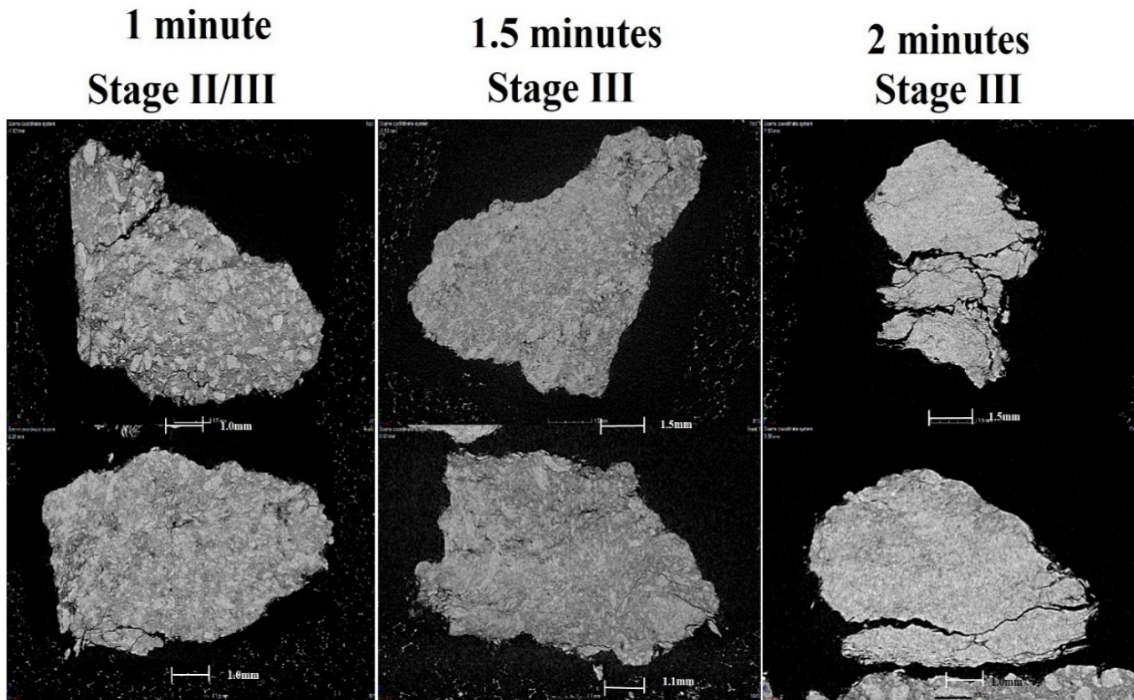




**Figure 4.96** Total Intrusion Volume for the formulations prepared with theophylline (THF; coarse API).  
 (Source: Pafiakis, Armenante, Gogos 2022)

Pore formation for the THF (coarse API) formulations plateaued during Stage II. THF:HPC EXF (coarse-fine) may have had the slowest densification due to the high uniaxial compressive strength ( $\sigma_c$ ).

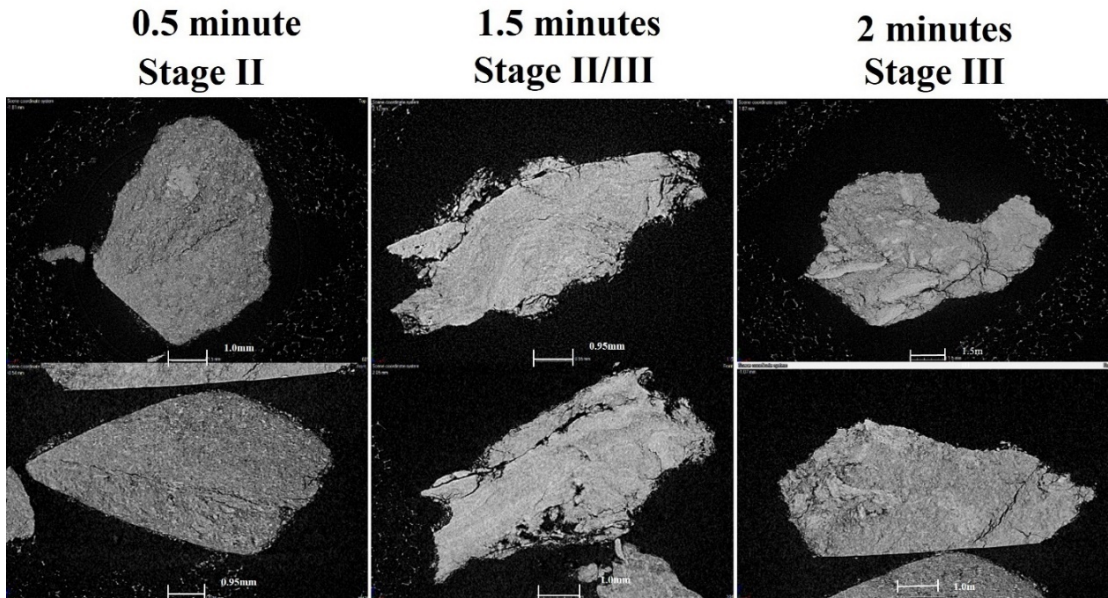
Figures 4.97 and 4.98 shows X-ray Tomography images of granules made from the THF:HPC MF (coarse-coarse) and THF:HPC EXF (coarse-fine) formulation, respectively.



**Figure 4.97** X-Ray tomography for 70:30 theophylline (THF) and hydroxypropylcellulose MF (HPC MF) blend (THF:HPC MF) as a function of time and deformation stage.  
(Source: Pafiakis, Armenante, Gogos 2022)

The images show that after one minute of mixing, the HPC MF particles (i.e., the brighter particulates) are integrating into the granulation. This indicates that the polymer is dispersing earlier at a much lower product temperature (Pafiakis, Armenante, Gogos 2022).

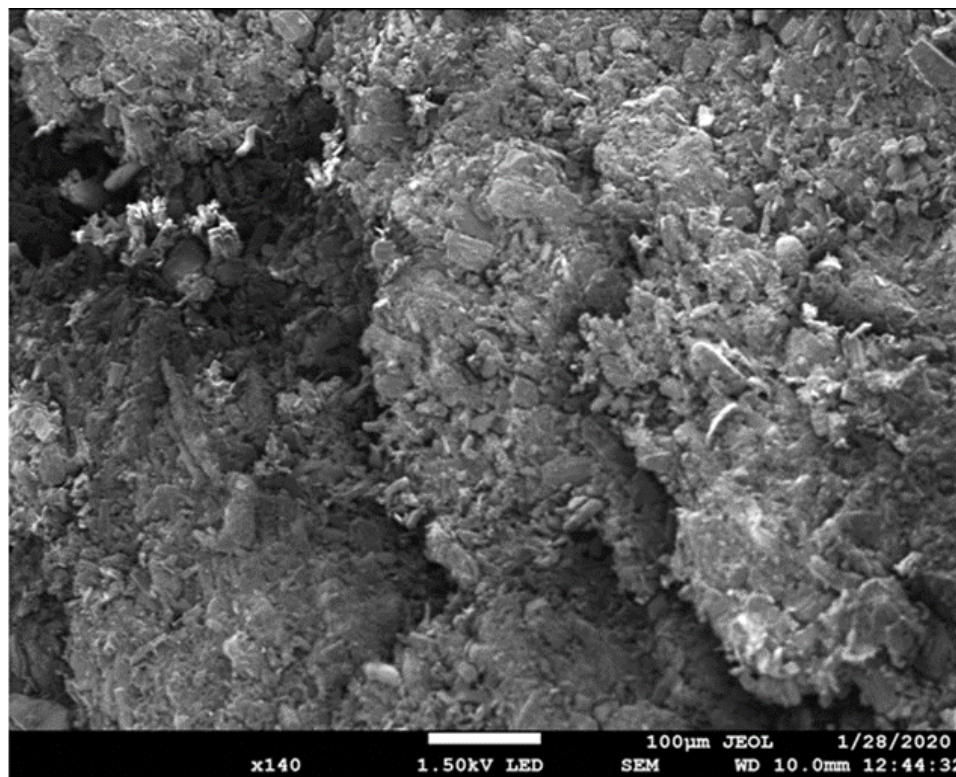
Figure 4.98 shows THF:HPC EXF (coarse-fine) formulation.



**Figure 4.98** X-Ray tomography for 70:30 theophylline (THF) and hydroxypropylcellulose EXF (HPC EXF) blend (THF:HPC EXF) as a function of time and deformation stage. (Source: Pafiakis, Armenante, Gogos 2022)

The images show the particles homogeneously dispersed within thirty seconds. As previously suggested, the figure also illustrates that breaking is observed. The image at one and a half minutes shows several cracks within the granule. These could be the new surfaces needed for PED and FED to ramp up agglomeration (Pafiakis, Armenante, Gogos 2022).

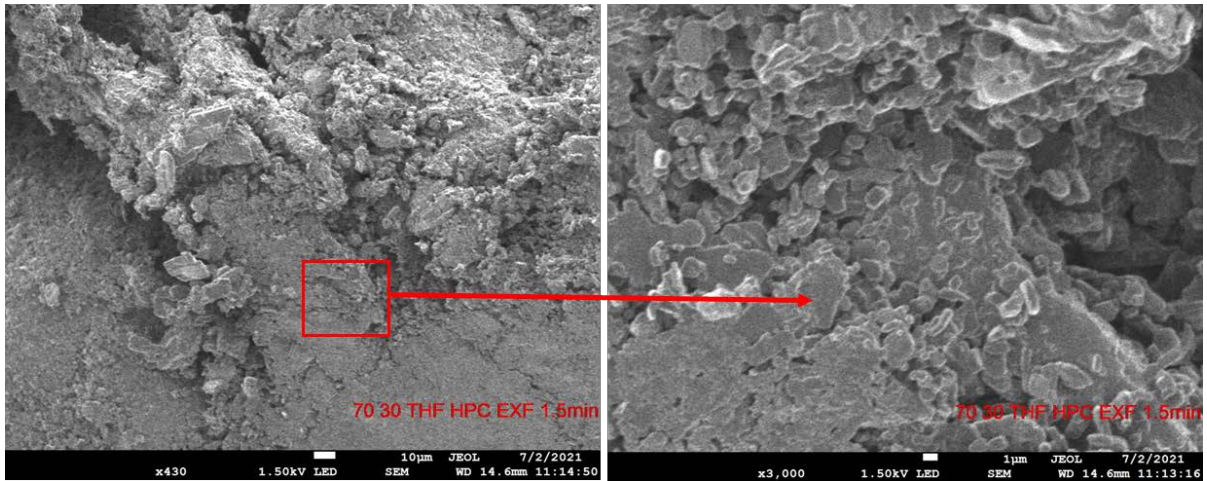
SEM images were also collected from available samples for the THF:HPC EXF formulation. The SEMs for this formulation show the evolution of agglomeration and the onset of local polymer flow. Figure 4.99 shows SEM taken after 30 seconds of mixing in the Brabender.



**Figure 4.99** SEM images for 70:30 theophylline (THF) and hydroxypropylcellulose EXF (HPC EXF) blend (THF:HPC EXF) after 30 seconds of mixing time (Stage II) in the Brabender.

The SEM after 30 seconds of mixing shows discrete particles agglomerated together. This is primarily due to compaction of the powder blend and some softening of the polymer due to FED. The temperature of the powder blend at this time point was approximately 35°C.

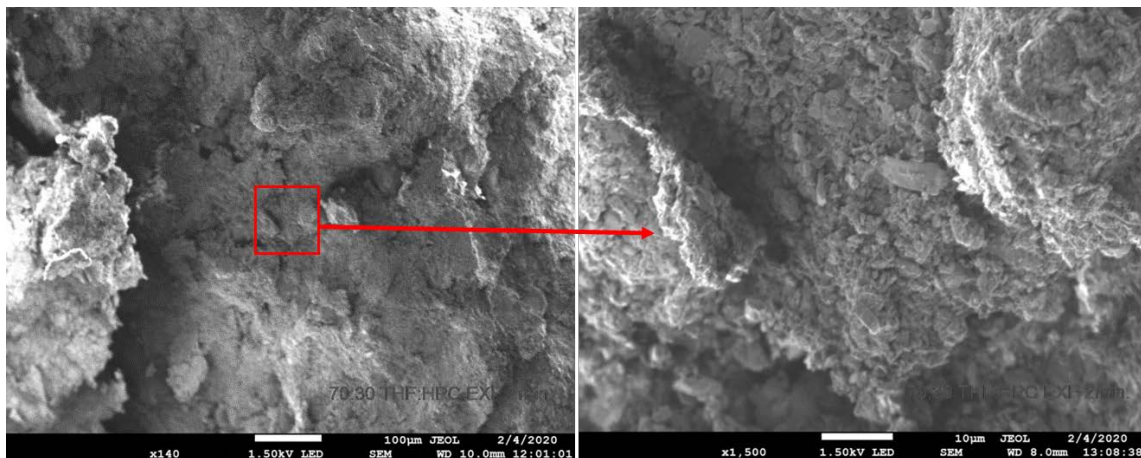
The SEM images at 1.5 min in Figure 4.100 show that with more mixing at slightly elevated temperature of 42°C, the particles begin to fuse and sinter. There is also evidence of local polymeric flow at higher magnification.



**Figure 4.100** SEM images for 70:30 theophylline (THF) and hydroxypropylcellulose EXF (HPC EXF) blend (THF:HPC EXF) after 1.5 minutes of mixing time (Stage II/III) in the Brabender.

The SEM shows that after 1.5 minutes of batch mixing a subtle transition from discrete particles to the formation of a smoother surface becomes apparent. This is clear on the bottom half of the image on the left at the lower magnification. The magnified image on the right shows particles fused together and sections are beginning to appear like melts and that the polymer is losing shape and appears to be “*spreading*”, similar to the SEMs of the granules evaluated in Subsection 4.2.1 Granule Analysis Using the 30 mm Twin Screw Mixing Element Evaluator (TSMEE) on page 63.

The SEM images at two minutes in Figure 4.101 show that for this formulation the particles are part of larger agglomerates and maintain a discrete particulate profile at a temperature of 71°C. In addition to the particle size data and X-Ray images for this formulation, there is additional evidence that this formulation may have been breaking and rebuilding during batch mixing.



**Figure 4.101** SEM images for 70:30 theophylline (THF) and hydroxypropylcellulose EXF (HPC EXF) blend (THF:HPC EXF) after two minutes of mixing time (Stage II/III) in the Brabender.

The SEM shows that after two minutes of batch mixing the powder blend transitioned from a partially smooth surface back to a discrete particulate granulated structure. It may be with more mixing time the smoother surface is folded back into the center of the granule in the mixing zone of the Brabender. A large crack in is also visible in the image on the left at the lower magnification. The magnified image on the right shows particles fused together and a section appears as if it is folding over itself; not fully integrated with the rest of the granule.

#### 4.5 Thermal Analysis: Effect of Material Properties on Calorimetry and Polymer Rheology

The data presented from the Brabender studies suggested that the onset and significant granule growth across all formulations is occurring within the ranges of this endothermic event observed from the MDSC measurement. The temperature ranges of significant granule growth are presented in Table 4.14.

**Table 4.14** Suggested Onset and Significant Granule Growth Across all Formulations is Occurring Within the Ranges of the Endothermic Event Observed for Hydroxypropylcellulose MF (HPC MF) (Coarse Polymer) and Hydroxypropylcellulose EXF (HPC EXF) (Fine Polymer)

Formulation	Temperature Range with Significant Granule Growth
70% theophylline: 30% HPC MF	55°C-95°C
70% theophylline: 30% HPC EXF	42°C-71°C
70% micronized theophylline: 30% HPC MF	30°C -97°C
70% micronized theophylline: 30% HPC EXF	35°C-78°C

(Source: Pafiakis, Armenante, Gogos 2022)

##### 4.5.1 Modulated Differential Scanning Calorimetry (MDSC) on micronized and non-micronized Theophylline (THF) and Hydroxypropylcellulose (HPC) raw materials and blends

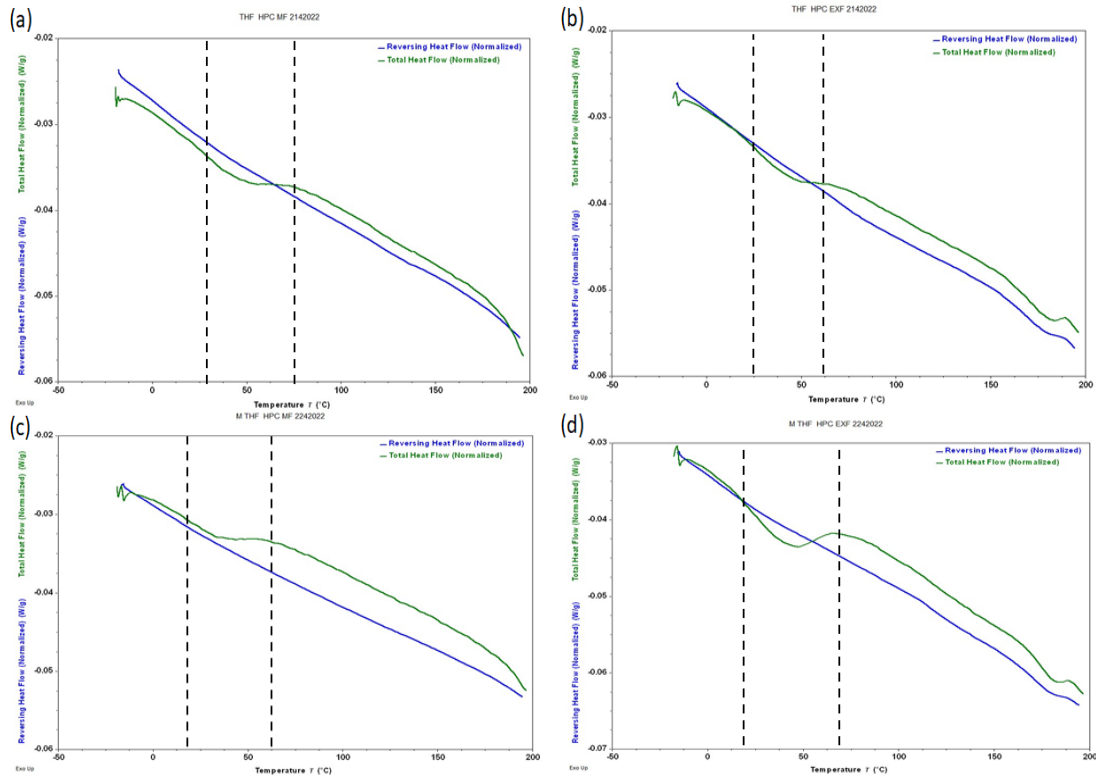
The two formulations with the highest product temperatures reached during significant granule growth both contained HPC MF. These two formulations had the higher coefficient of friction,  $f$  measured from the shear cell analysis 0.70 for the formulation with THF and 0.64 for the formulation with MTHF. A high coefficient of friction,  $f$  is necessary for FED to drive an increase in granule size. This may suggest that the polymer is softening at a temperature that is lower than the  $T_g$ .

The endothermic peak observed at temperatures lower than the  $T_g$  suggests that the polymer particles are forced to increase in temperature locally to overcome the polymer's thermal resistance. The power induced by local FED is the driver that forces the polymer

to reach this endotherm. The endotherm is a characteristic of the polymer that is revealed by the sum of all local interparticle velocity differences caused by the mixing, under normal pressure, in the batch mixer.



**4.5.1.1 Micronized and un-micronized theophylline formulations.** A significant endothermic event that could explain low onset of molecular mobility was observed in the following temperature ranges and are presented in Figure 4.102 from the total heat flow and Table 4.15.



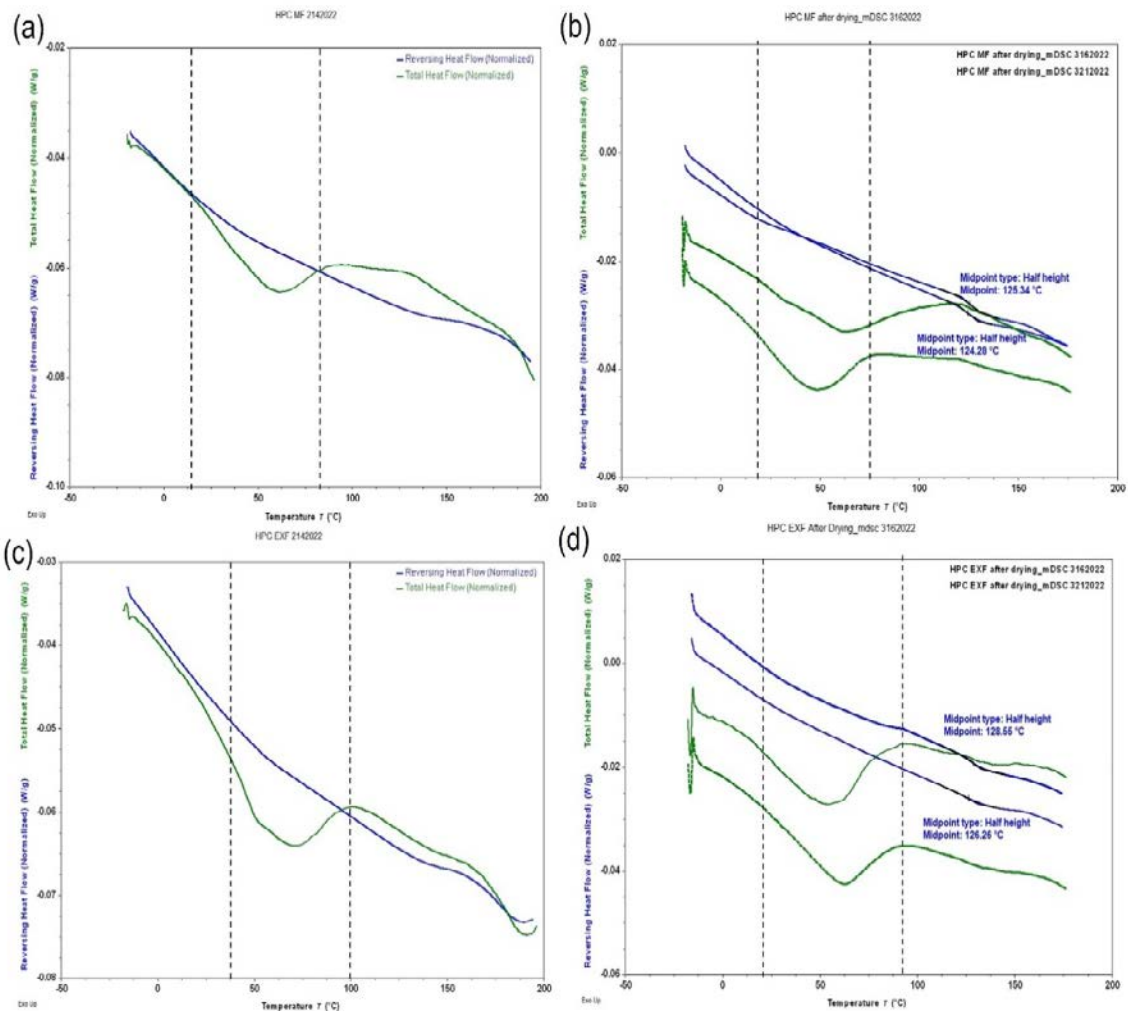
**Figure 4.102** Endothermic event measured by MDSC for As-is (a) 70% theophylline (THF): 30% hydroxypropylcellulose MF (HPC MF); (b) 70% theophylline (THF): 30% hydroxypropylcellulose EXF (HPC EXF); (c) 70% micronized theophylline (MTHF) : 30% hydroxypropylcellulose MF (HPC MF); (d) 70% micronized theophylline (MTHF): 30% hydroxypropylcellulose MF (HPC MF).  
*(Source: Pafiakis, Armenante, Gogos 2022)*

**Table 4.15** Estimated Endothermic Event Measured by MDSC for: (a) 70% Theophylline: 30% Hydroxypropylcellulose (HPC MF); (b) 70% Theophylline: 30% Hydroxypropylcellulose (HPC EXF) ; (c) 70% Micronized Theophylline: 30% Hydroxypropylcellulose (HPC MF); (d) 70% Micronized Theophylline: 30% Hydroxypropylcellulose (HPC MF).

Formulation	Endotherm range	Measured Tg
70% Theophylline: 30% HPC MF	28-75°C	Not Detected
70% Theophylline: 30% HPC EXF	25°C-62.5°C	Not Detected
70% Micronized Theophylline: 30% HPC MF	15°C-62.5°C	Not Detected
70% Micronized Theophylline: 30% HPC EXF	20°C-62.5°C	Not Detected

(Source: Pafiakis, Armenante, Gogos 2022)

**4.5.1.2 Hydroxypropylcellulose MF and EXF.** A more prominent endothermic event was observed for the neat polymers before and after drying with little difference between the two measurements as shown in Figure 4.103. This was to rule out any response typical with evaporation from the bulk material absorbing moisture while being stored.



**Figure 4.103** Endothermic event measured by MDSC for (a) as-is hydroxypropylcellulose MF (HPC MF); (b) Dried hydroxypropylcellulose (HPC MF); (c) as-is hydroxypropylcellulose EXF (HPC EXF); (d) dried hydroxypropylcellulose (HPC EXF). (Source: Pafiakis, Armenante, Gogos 2022)

Approximately 0.103 mg (0.934 % w/w) of water was removed for dried HPC MF (coarse polymer) and 0.056 mg of water (0.48% w/w) for dried HPC EXF (fine polymer).

The estimated endotherm temperature ranges and the  $T_g$  of dried HPC MF (coarse polymer) dried HPC EXF (fine polymer) are summarized in Table 4.16.

**Table 4.16** Estimated Endothermic Event Measured by MDSC for (a) As-is Hydroxypropylcellulose MF (HPC MF); (b) Dried Hydroxypropylcellulose MF (HPC MF); (c) As-is Hydroxypropylcellulose EXF (HPC EXF); (d) Dried Hydroxypropylcellulose EXF (HPC EXF)

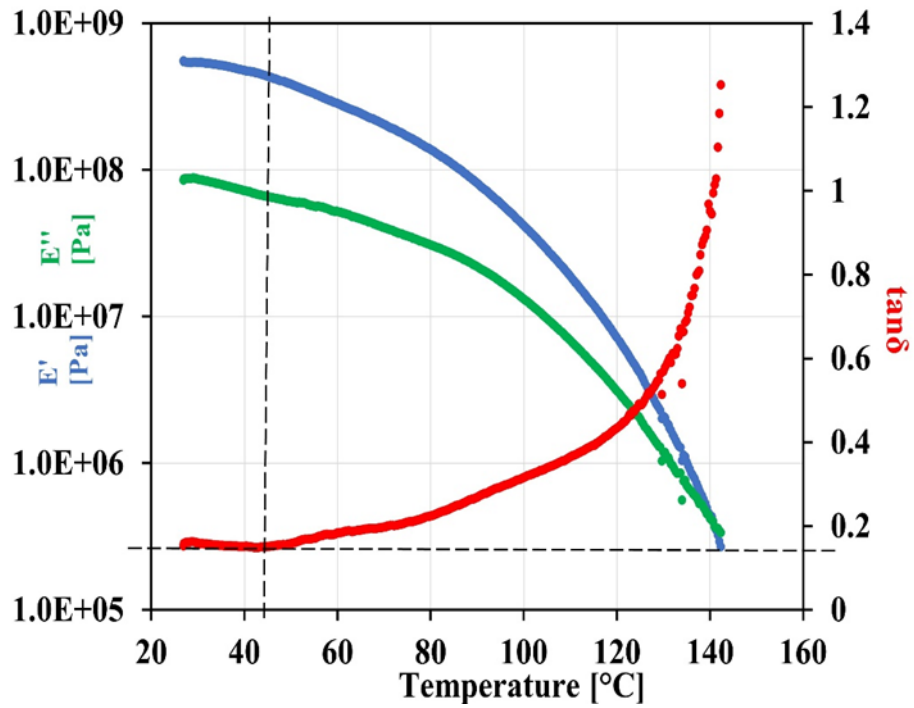
Sample	Endotherm range	Measured $T_g$
HPC MF	25°C-80°C	Not Detected
Dried HPC MF	25°C-75°C	124.81 ± 0.53°C
HPC EXF	30°C -100°C	Not Detected
Dried HPC EXF	25°C-95°C	127.41 ±1.15°C

(Source: Pafiakis, Armenante, Gogos 2022)

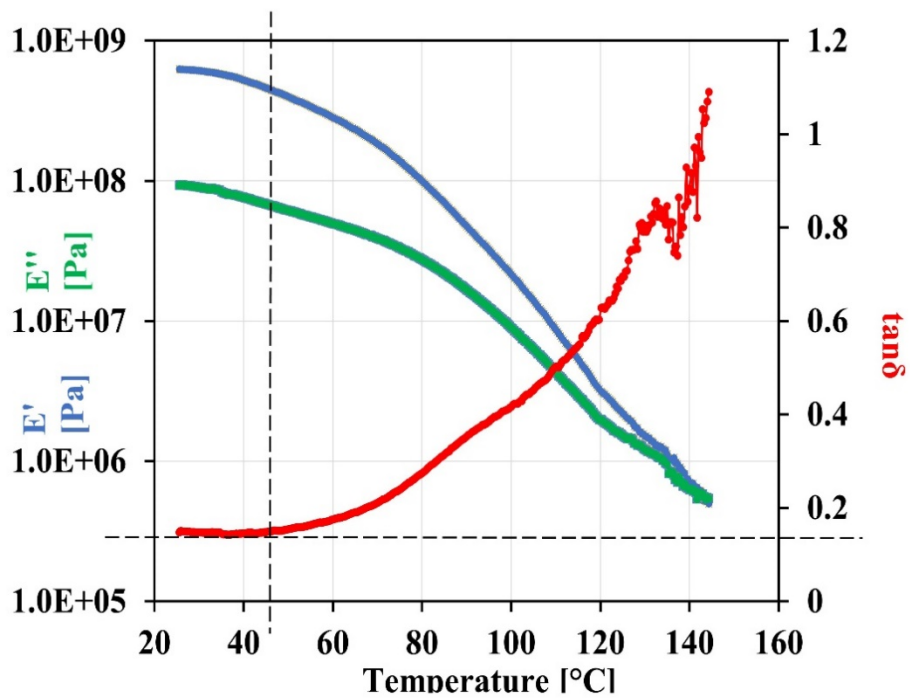
For HPC MF (coarse polymer) and HPC EXF (fine polymer) were measured and is approximately the same at 124.81 ± 0.53°C and 127.41 ±1.15°C, respectively (Pafiakis, Armenante, Gogos 2022).

#### 4.5.2 Dynamic Mechanical Thermal Analysis (DMTA) for Hydroxypropylcellulose (HPC) MF and EXF

At the endothermic peak the polymers may be the onset of molecular mobility within the temperature ranges measured. The polymer is not fully flowing within the endotherm temperature ranges, but it may be soft and “*tacky*” enough to facilitate granule growth. The moduli that make up the complex Young’s Modulus  $E^*$  are the storage (elastic) modulus  $E'$  and the loss (viscous) modulus  $E''$ . Both were measured along with the mechanical thermal energy or (loss tangent),  $\tan \delta$  for HPC MF and HPC EXF. Figures 4.104 and 4.105 for HPC MF and HPC EXF suggested the subtle changes of mechanical thermal energy ( $\tan \delta$ ) at low temperatures may be causing local molecular mobility.



**Figure 4.104** Dynamic temperature ramp of hydroxypropylcellulose MF (HPC MF).  
 (Source: Pafiakis, Armenante, Gogos 2022)



**Figure 4.105** Dynamic temperature ramp of hydroxypropylcellulose (HPC EXF).  
 (Source: Pafiakis, Armenante, Gogos 2022)

Both polymers are losing modulus and onset of flow from  $\tan \delta$  could be 50°C for HPC MF and 45°C for HPC EXF. The samples may not necessarily be in the glass transition region of viscous behavior, but it only takes 10 to 50 atoms for the molecule to be excited or in this case mobile (Sperling 2006, p. 364). As the powder blend rapidly heats up, the particle surfaces of the formulation absorb the frictional energy. The temperature locally may reach and exceed the  $T_g$  to start granule growth but cumulatively the temperature response measured much lower (Pafiakis, Armenante, Gogos 2022).

## CHAPTER 5

### CONCLUDING REMARKS

#### 5.1 Summary

Feasibility of twin screw granulation using theophylline and HPC was carried out on a 30 mm Twin Screw Mixing Element Evaluator (TSMEE). Trials successfully demonstrated that this formulation was amenable to being granulated. Furthermore, carcass analysis of granules collected across the mixing section were evaluated using SEM. The imaging helped to determine the extent of mixing and the screw configuration needed on the 27 mm co-rotating twin screw extruder trials. It was important to balance the magnitude of kneading without negating the contribution of the input material properties.

Four formulations were evaluated in large scale extrusion trials using the 27 mm co-rotating twin screw extruder. A method that enabled granulation in a counter-rotating batch mixer to emulate large scale dry twin screw granulation was also developed using the Brabender Batch mixer. Both sets of data from the extrusion and batch mixing trials agree that formulations containing the coarse polymer granulated more effectively due to the slightly higher friction coefficient,  $f$  between the API and Polymer. Particle size distribution analysis showed that the formulations that were granulated with the fine polymer deformed more efficiently in the extrusion trials. The *time dilation* provided by the batch mixer helped elucidate some of what was happening in the mixing zone.

The fine API formulations lasted a longer time in the batch mixer since it became more malleable than the formulation containing the coarse API. It was also observed that both APIs performed better in the twin screw granulation trials with the coarse polymer

(HPC MF) at lower processing temperatures. It seemed that the PED and FED were controlled by the material properties. More specifically, because of the interaction between the inherently high lubricity (i.e., low friction coefficient,  $f$ ) of the API coating the polymer. The onset of *glue-point temperature* was delayed because the API to Polymer contact was limited.

It was also found in the 27 mm TSG trials that the HPC EXF, the finer polymer, was influencing the mechanism. This led to undesirable over-granulation. The HPC EXF formulations worked well at low feed rate, temperatures and screw speeds in the twin screw granulation trials but missed on producing acceptable granulations at the higher parameters. This again could be because of how the fine polymer particles interact with the API particles. Since both API particle sizes were closer in size with the fine polymer, the interaction led a faster onset of granulation. Whereas the API protected the polymer by creating a lubricating effect for the formulations containing the larger polymer particles (HPC MF). The particle size difference reduced the extent of deformation and heat transfer. This mitigated, and in some instances eliminated, the transition from FED and PED to VED. However, since the fine material are closer in size, the heat transfer from FED and PED in the mixing section caused the polymer particle to soften more efficiently and granulate sooner because there are more available surfaces.

Furthermore, it was possible to divide each granulation into a series of stages of deformation, despite the duration of mixing in the batch mixer. The period and extent of each stage also varied between the four formulations. The stages identified were, Stage I: Consolidation, Stage II: Semi Compacted, Stage III: Compacted, Stage IV: Melt Bound Solid Particles, and Stage V: Solid Rich Suspension. Three of the four formulations stopped



at Stage III due to mixer limitations. These were both formulations containing THF (coarse API) and the MTHF:HPC MF (fine-coarse) formulation. The MTHF:HPC EXF (fine-fine) formulation reached Stage V; this is beyond the PED and FED melting mechanism and terminated with VED.

Mercury Intrusion Porosimetry, X-Ray Tomography and SEM microscopy were used to measure and show the rate of sintering, or densification for each formula, respectively. As a result of the combined effect of compaction and sintering, the pores measured and illustrated are indicative of the voids formed between the molten polymer pools and API particles. Both formulations containing THF (coarse API) and the MTHF:HPC MF (fine-coarse) formulation, densified much faster. The extent for all three granulations was approximately the same. The MTHF:HPC EXF (fine-fine) formulation showed the greatest extent of densification, due to its inherently high surface area. Because the polymer particle size was closest to in size with the API, the local heating and melting was the most efficient for this formulation.

SEM analysis across each deformation stage confirmed that PED and FED led to the activation of the *glue-point temperature* of the polymer. This facilitated local melting pools between the polymer and API, leading to sintering and agglomeration with more mixing. MDSC and DMTA were used to characterize the thermo-physical properties of the formulations and the polymers. Thermal events observed in MDSC suggest that the binding temperature is much lower for HPC MF and HPC EXF. DMTA also suggested that onset of molecular mobility is much lower than the  $T_g$ . The low temperatures measured correlate strongly with the temperature ranges that had significant granule growth in the Brabender

batch mixer studies and the observed local polymer melts from samples collected at low product temperatures.

## **5.2 Suggested Future Work**

### **5.2.1 Real-time measurement of heat (FED) generation during batch mixing**

The Brabender would first need to be fitted with a face cover that has a port for a window. The window would need to be made of Zinc Selenide (ZnSe) to have the emissivity needed to collect thermal spectra with a thermal imaging camera. The assessment would then be done on one formulation where different sieve cuts are taken of the neat API and the Polymer. Different blend ratio consisting of the different sieve cuts could be assessed and the sieve fraction that truly activates granulation may be determined from this work. The thermal imaging data could also be used to build PED and FED models for twin screw granulation.

### **5.2.2 Thermal shear cell experiments**

A critical piece of this work was the use of the iShear<sup>®</sup>: Powder Flow Analyzer to determine the coefficient of friction,  $f$ . These studies were performed at room temperature for all the formulations. It may be possible to design a shear cell that can be heated to a particular temperature during the analysis. The effect of temperature on the coefficient of friction,  $f$  could be used to identify other polymers that are more amenable to dry twin screw granulation.

### **5.2.3 Controlled Deformation Studies.**

The extent of deformation was key in generating the granulating melting mechanisms PED and FED. Understanding the propensity of deformation of these formulations can lead to a better understanding of what was happening in the mixing zones in the extrusion and batch mixing trials. The assessment would entail preparing flat faced compacts at a particular thickness of the different formulation and placing a weight on top of them while the compacts are in an oven at a specific temperature. The compacts would be set up such that the reduction of height can be determined by taking interval reading or recording through a sight glass. Formulations that "*flatten*" faster may be more amenable to deformation and perhaps may lead to undesirable granulation properties.

### **5.2.4 Down Stream Processing of Resulting Granules**

Ultimately, one would want to know if the resulting granulations are amenable to downstream pharmaceutical processing. This work would pick up from where the work presented in this dissertation left off. All granulation prepared in the 27mm TSG trials would first be milled. A profile of different milling screens would be investigated. Particle size distribution would be assessed along with several other powder properties. The granules from each milling study would be analyzed using the Drucker-Prager Cap Model for compaction simulation. The model will shed light on the differences of Cohesion, Hydrostatic compression yield stress, and Young's Modulus. The resulting milled granules would be blended with extra granular excipients such as microcrystalline cellulose and magnesium stearate. The resulting blend would be compressed into tablets using a tablet press. Content uniformity could be assessed for each formulation by taking stratified samples across the tableting run. Compression profiles of the tablets would be prepared,

and tablet hardness, assay, degradation, disintegration, and dissolution could be used to compare quality attributes. Granules from the Brabender could also be prepared into tablet on a small scale to see of the resulting quality attributes of the tablets from the two different granulating methods are the same.

## APPENDIX A

### BULK AND TAP DENSITY

The following data was used to generate Figures 4.3, 4.8, and 4.19. despite the differences in bulk density, each batch loaded in the Brabender studies was approximately 45 g.

**Table A.1** Bulk and Tap Density of Raw Material

<b>Raw Materials</b>				
	MTHF	THF	HPC MF	HPC EXF
Bulk Density	0.289	0.307	0.435	0.265
Tap Density	0.407	0.472	0.534	0.39

**Table A.2** Bulk and Tap Density of Theophylline Blends

<b>70% Theophylline Formulations</b>				
	THF:HPC MF	MTHF:HPC MF	THF:HPC EXF	MTHF:HPC EXF
Bulk Density	0.437	0.292	0.313	0.269
Tap Density	0.649	0.436	0.486	0.419

**APPENDIX B**  
**PARTICLE SIZE ANALYSES**

Tables B.1 through B.8 were used to create the particle size distribution data in section 4.1.3

**Table B.1** CamSizer Data for Hydroxypropylcellulose MF (HPC MF)

<b>x [µm] at Q3 = 10.0</b>	99.51								
<b>x [µm] at Q3 = 50.0</b>	306.28								
<b>x [µm] at Q3 = 90.0</b>	599.01								
<b>Mv3(x) [µm]</b>	330.13								
<b>Sigma3(x) [µm]</b>	190.58								
<b>SPAN3</b>	1.631								
<b>par3a [%]</b>	-3.43								
<b>xmax3a [µm]</b>	80								
<b>Q3 (Symm=0.9) [%]</b>	86.91								
<b>Q3 (b/l=0.9) [%]</b>	99.91								
<b>Mean value Symm3</b>	0.828								
<b>Mean value b/l3</b>	0.5055								
<b>Size class</b>	<b>[µm]</b>	<b>p3 [%]</b>	<b>Q3 [%]</b>	<b>Symm3</b>	<b>b/l3</b>	<b>Conv_A3</b>	<b>Ellipse3</b>	<b>RDNS_C</b>	<b>PDN</b>
0	1	0.003	0.003	0.87	0.727	0.994	0.04	-1	2582523
1	1.1	0	0.003	0.87	0.727	0.994	0.04	-1	0
1.1	1.21	0.001	0.004	0.87	0.727	0.994	0.04	-1	5813
1.21	1.33	0	0.004	0.87	0.727	0.994	0.04	-1	11001
1.33	1.46	0	0.004	0.87	0.727	0.994	0.04	-1	9132
1.46	1.61	0.001	0.005	0.87	0.727	0.994	0.04	-1	10283
1.61	1.77	0	0.005	0.87	0.727	0.994	0.04	-1	104025
1.77	1.95	0.001	0.006	0.87	0.727	0.994	0.04	-1	47667
1.95	2.14	0	0.006	0.87	0.727	0.994	0.04	-1	603224
2.14	2.36	0.001	0.007	0.87	0.727	0.994	0.04	-1	546632
2.36	2.59	0.002	0.009	0.862	0.679	0.99	0.048	-1	305420
2.59	2.85	0.003	0.012	0.861	0.679	0.99	0.048	-1	382640
2.85	3.14	0.003	0.015	0.861	0.679	0.99	0.048	-1	352500
3.14	3.45	0.003	0.018	0.861	0.679	0.99	0.048	-1	449207
3.45	3.8	0.004	0.022	0.861	0.679	0.99	0.048	-1	269693
3.8	4.18	0.004	0.026	0.861	0.679	0.99	0.048	-1	340149
4.18	4.59	0.004	0.03	0.861	0.679	0.99	0.048	-1	171892
4.59	5.05	0.006	0.036	0.861	0.665	0.987	0.06	-1	149009
5.05	5.56	0.006	0.042	0.861	0.659	0.986	0.065	-1	161332
5.56	6.12	0.007	0.049	0.861	0.659	0.986	0.065	-1	126273
6.12	6.73	0.008	0.057	0.861	0.659	0.986	0.065	-1	115626
6.73	7.4	0.007	0.064	0.866	0.653	0.985	0.065	-1	63341
7.4	8.14	0.009	0.073	0.874	0.643	0.983	0.065	-1	62125
8.14	8.95	0.009	0.082	0.874	0.643	0.983	0.065	-1	43869
8.95	9.85	0.011	0.093	0.871	0.635	0.983	0.068	-1	35427
9.85	10.83	0.013	0.106	0.868	0.624	0.982	0.073	-1	36715
10.83	11.93	0.015	0.121	0.868	0.626	0.982	0.074	-1	21209
11.93	13.11	0.018	0.139	0.868	0.648	0.981	0.08	-1	15561
13.11	14.42	0.019	0.158	0.859	0.614	0.979	0.083	-1	14056
14.42	15.86	0.018	0.176	0.815	0.46	0.968	0.096	-1	6685
15.86	17.45	0.026	0.202	0.836	0.522	0.968	0.098	0.39	4107
17.45	19.19	0.033	0.235	0.84	0.564	0.969	0.102	0.327	5246
19.19	21.11	0.043	0.278	0.817	0.557	0.97	0.108	0.203	14552
21.11	23.23	0.045	0.323	0.817	0.557	0.97	0.108	0.203	68
23.23	25.55	0.066	0.389	0.832	0.601	0.957	0.109	0.351	4890
25.55	28.1	0.128	0.517	0.927	0.769	0.983	0.039	0.681	8978
28.1	30.91	0.228	0.745	0.928	0.688	0.988	0.029	0.582	4405
30.91	34	0.184	0.939	0.915	0.638	0.986	0.047	0.425	6269
34	37.4	0.125	1.054	0.94	0.86	0.996	0.029	0.927	3763
37.4	41.14	0.337	1.361	0	0	0	0	-1	0
41.14	45.26	0.457	1.848	0.964	0.898	0.997	0.023	0.744	3560
45.26	49.79	0.645	2.493	0.847	0.551	0.984	0.059	-1	1279
49.79	54.76	0.586	3.079	0.824	0.522	0.975	0.077	-1	11854
54.76	60.24	0.52	3.599	0.828	0.51	0.98	0.076	-1	17910
60.24	66.26	0.765	4.364	0.816	0.498	0.972	0.091	-1	11943
66.26	72.89	1.064	5.427	0.826	0.51	0.974	0.086	-1	14425
72.89	80.18	1.431	6.857	0.823	0.504	0.971	0.093	-1	12283
80.18	88.2	1.362	8.218	0.82	0.512	0.964	0.101	-1	11492
88.2	97.02	1.395	9.612	0.819	0.502	0.965	0.101	-1	9391
97.02	106.72	1.778	11.389	0.821	0.503	0.964	0.102	-1	15071
106.72	117.39	2.139	13.527	0.821	0.508	0.962	0.104	-1	14545
117.39	129.13	2.378	15.904	0.82	0.509	0.961	0.106	-1	12651
129.13	142.04	2.639	18.542	0.818	0.516	0.958	0.109	-1	10146
142.04	156.25	2.906	21.447	0.819	0.512	0.957	0.109	-1	8468
156.25	171.87	3.147	24.592	0.819	0.517	0.955	0.11	-1	7045
171.87	189.06	3.446	28.036	0.817	0.516	0.953	0.111	-1	5784
189.06	207.97	3.797	31.831	0.816	0.514	0.951	0.112	0.22	4839
207.97	228.76	4.055	35.884	0.818	0.523	0.95	0.112	0.205	3877
228.76	251.64	4.207	40.089	0.818	0.522	0.95	0.111	0.206	2964
251.64	276.8	4.569	44.656	0.823	0.519	0.951	0.108	0.22	2495
276.8	304.28	4.995	49.649	0.823	0.521	0.951	0.107	0.204	2051
304.28	334.93	5.341	54.987	0.827	0.535	0.952	0.106	0.2	1667
334.93	368.42	5.821	60.805	0.829	0.535	0.953	0.103	0.254	1353
368.42	405.27	6.159	66.961	0.83	0.533	0.954	0.102	0.242	1133
405.27	445.79	6.291	73.249	0.838	0.551	0.958	0.097	0.232	860
445.79	490.37	5.865	79.111	0.836	0.555	0.956	0.097	0.257	630
490.37	539.41	5.561	84.669	0.849	0.577	0.963	0.089	0.219	458
539.41	593.37	4.881	89.548	0.839	0.596	0.957	0.095	0.248	318
593.37	652.68	3.852	93.398	0.85	0.62	0.964	0.088	0.249	200
652.68	717.95	2.946	96.343	0.851	0.652	0.963	0.085	0.237	123
717.95	789.76	2.315	98.657	0.843	0.678	0.959	0.09	0.226	75
789.76	868.72	0.908	99.565	0.858	0.673	0.963	0.085	0.218	23
868.72	955.59	0.435	100	0.783	0.678	0.949	0.123	0.217	8
955.59	1051.15	0	100	0	0	0	0	0	0
1051.15	1156.27	0	100	0	0	0	0	0	0
1156.27	1000000	0	100	0	0	0	0	0	0

**Table B.2** CamSizer Data for Hydroxypropylcellulose EXF (HPC EXF)

x [µm] at Q3 = 10.0 %	16.08									
x [µm] at Q3 = 50.0 %	45.82									
x [µm] at Q3 = 90.0 %	86.25									
Mv3(x) [µm]	49.89									
Sigma3(x) [µm]	30.28									
SPAN3	1.531									
par3a [%]	-105.03									
xmax3a [µm]	83.95									
Q3 (Symm=0.9) [%]	81.03									
Q3 (b/l=0.9) [%]	99.6									
Mean value Symm3	0.8444									
Mean value b/l3	0.5494									
<b>Size class</b>	<b>[µm]</b>	<b>p3 [%]</b>	<b>Q3 [%]</b>	<b>Symm3</b>	<b>b/l3</b>	<b>Conv_A3</b>	<b>Ellipse3</b>	<b>RDNS_C3</b>	<b>PDN</b>	
0	1	0.006	0.006	0.98	0.486	0.998	0.336	-1	1217930	
1	1.1	0.001	0.007	0.847	0.638	1	0	-1	0	
1.1	1.21	0.001	0.008	0.847	0.638	1	0	-1	0	
1.21	1.33	0.001	0.009	0.847	0.638	1	0	-1	0	
1.33	1.46	0.003	0.012	0.87	0.62	0.997	0.035	-1	0	
1.46	1.61	0.004	0.016	0.871	0.62	0.997	0.036	-1	20404	
1.61	1.77	0.004	0.02	0.871	0.62	0.997	0.036	-1	25775	
1.77	1.95	0.004	0.024	0.871	0.62	0.997	0.036	-1	24992	
1.95	2.14	0.01	0.034	0.87	0.713	0.992	0.031	-1	138612	
2.14	2.36	0.015	0.049	0.87	0.719	0.991	0.03	-1	116409	
2.36	2.59	0.015	0.064	0.87	0.719	0.991	0.03	-1	103004	
2.59	2.85	0.028	0.092	0.861	0.654	0.992	0.044	-1	159713	
2.85	3.14	0.037	0.129	0.86	0.645	0.992	0.046	-1	214914	
3.14	3.45	0.046	0.175	0.86	0.639	0.991	0.049	-1	293026	
3.45	3.8	0.068	0.243	0.861	0.63	0.99	0.053	-1	176103	
3.8	4.18	0.084	0.327	0.86	0.613	0.989	0.054	-1	250195	
4.18	4.59	0.106	0.433	0.86	0.592	0.987	0.056	-1	169766	
4.59	5.05	0.142	0.575	0.865	0.616	0.99	0.054	-1	143097	
5.05	5.56	0.173	0.748	0.866	0.602	0.989	0.056	-1	141647	
5.56	6.12	0.231	0.979	0.876	0.624	0.988	0.058	-1	138317	
6.12	6.73	0.301	1.28	0.867	0.56	0.985	0.057	-1	152991	
6.73	7.4	0.392	1.672	0.87	0.609	0.986	0.061	-1	153796	
7.4	8.14	0.477	2.149	0.873	0.579	0.986	0.064	-1	140053	
8.14	8.95	0.548	2.697	0.872	0.588	0.985	0.066	-1	104656	
8.95	9.85	0.637	3.334	0.87	0.539	0.985	0.066	-1	108435	
9.85	10.83	0.79	4.124	0.885	0.612	0.985	0.06	-1	63457	
10.83	11.93	1.025	5.149	0.875	0.57	0.984	0.064	-1	78050	
11.93	13.11	1.161	6.31	0.876	0.515	0.981	0.066	-1	56590	
13.11	14.42	1.486	7.796	0.874	0.544	0.982	0.065	-1	60961	
14.42	15.86	1.908	9.704	0.877	0.548	0.98	0.065	-1	56999	
15.86	17.45	2.13	11.834	0.885	0.585	0.982	0.063	-1	28998	
17.45	19.19	2.417	14.251	0.88	0.514	0.979	0.069	0.31	23842	
19.19	21.11	2.46	16.711	0.875	0.583	0.982	0.068	0.407	24525	
21.11	23.23	2.612	19.323	0.861	0.551	0.974	0.077	0.374	19969	
23.23	25.55	2.597	21.92	0.834	0.553	0.972	0.09	0.194	17601	
25.55	28.1	3.897	25.817	0.869	0.512	0.977	0.074	0.314	14018	
28.1	30.91	4.228	30.045	0.918	0.8	0.984	0.042	0.428	2414	
30.91	34	4.646	34.691	0.874	0.524	0.981	0.061	0.213	6733	
34	37.4	4.34	38.431	0.862	0.712	0.967	0.083	0.087	4025	
37.4	41.14	4.686	43.717	0.892	0.744	0.981	0.073	0.077	986	
41.14	45.26	5.533	49.25	0.886	0.64	0.985	0.06	0.233	7865	
45.26	49.79	7.328	56.578	0	0	0	0	-1	2123	
49.79	54.76	5.902	62.48	0.846	0.586	0.986	0.06	0.115	11095	
54.76	60.24	5.9	68.38	0.855	0.588	0.991	0.053	-1	13575	
60.24	66.26	6.586	74.966	0.848	0.589	0.986	0.064	-1	5914	
66.26	72.89	4.839	79.805	0.856	0.598	0.988	0.061	-1	5966	
72.89	80.18	6.633	86.438	0.855	0.618	0.986	0.068	-1	3444	
80.18	88.2	4.183	90.621	0.843	0.605	0.978	0.081	-1	1803	
88.2	97.02	3.292	93.913	0.848	0.624	0.979	0.08	-1	1184	
97.02	106.72	1.746	95.659	0.836	0.624	0.972	0.093	-1	1010	
106.72	117.39	1.48	97.139	0.82	0.602	0.96	0.108	-1	732	
117.39	129.13	0.969	98.108	0.83	0.609	0.963	0.101	-1	358	
129.13	142.04	0.633	98.741	0.809	0.593	0.945	0.121	-1	154	
142.04	156.25	0.468	99.209	0.8	0.542	0.941	0.129	-1	98	
156.25	171.87	0.295	99.504	0.768	0.523	0.911	0.15	-1	44	
171.87	189.06	0.199	99.703	0.772	0.591	0.931	0.136	-1	22	
189.06	207.97	0.106	99.809	0.831	0.656	0.957	0.101	0.019	9	
207.97	228.76	0.067	99.876	0.675	0.57	0.802	0.13	1	2	
228.76	251.64	0.093	99.969	0.849	0.661	0.959	0.092	0.233	6	
251.64	276.8	0.031	100	0.861	0.746	0.986	0.045	0.066	1	
276.8	304.28	0	100	0	0	0	0	0	0	
304.28	334.93	0	100	0	0	0	0	0	0	
334.93	368.42	0	100	0	0	0	0	0	0	
368.42	405.27	0	100	0	0	0	0	0	0	
405.27	445.79	0	100	0	0	0	0	0	0	
445.79	490.37	0	100	0	0	0	0	0	0	
490.37	539.41	0	100	0	0	0	0	0	0	
539.41	593.37	0	100	0	0	0	0	0	0	
593.37	652.68	0	100	0	0	0	0	0	0	
652.68	717.95	0	100	0	0	0	0	0	0	
717.95	789.76	0	100	0	0	0	0	0	0	
789.76	868.72	0	100	0	0	0	0	0	0	
868.72	955.59	0	100	0	0	0	0	0	0	
955.59	1051.15	0	100	0	0	0	0	0	0	
1051.15	1156.27	0	100	0	0	0	0	0	0	
1156.27	1000000	0	100	0	0	0	0	0	0	



**Table B.3** CamSizer Data for Micronized Theophylline (MTHF)

x [µm] at Q3 = 10.0 %	3.54									
x [µm] at Q3 = 50.0 %	6.97									
x [µm] at Q3 = 90.0 %	13.91									
Mv3(x) [µm]	10.47									
Sigma3(x) [µm]	21.43									
SPAN3	1.487									
par3a [%]	36.65									
xmax3a [µm]	189.17									
Q3 (Symm=0.9) [%]	56.49									
Q3 (b/l=0.9) [%]	98.96									
Mean value Symm3	0.8892									
Mean value b/l3	0.7149									
<b>Size class</b>	<b>[µm]</b>	<b>p3 [%]</b>	<b>Q3 [%]</b>	<b>Symm3</b>	<b>b/l3</b>	<b>Conv_A3</b>	<b>Ellipse3</b>	<b>RDNS_C3</b>	<b>PDN</b>	
0	1	0.113	0.113	0.981	0.495	0.992	0.228	-1	760840	
1	1.1	0.029	0.142	0.848	0.668	0.912	0.127	-1	0	
1.1	1.21	0.032	0.174	0.848	0.668	0.912	0.127	-1	0	
1.21	1.33	0.036	0.21	0.846	0.67	0.914	0.127	-1	3558	
1.33	1.46	0.095	0.305	0.8	0.721	0.943	0.125	-1	2677	
1.46	1.61	0.146	0.451	0.821	0.602	0.985	0.015	-1	7748	
1.61	1.77	0.207	0.658	0.874	0.679	0.996	0.004	-1	19784	
1.77	1.95	0.308	0.966	0.85	0.627	0.99	0.052	-1	12189	
1.95	2.14	0.44	1.406	0.866	0.688	0.99	0.033	-1	133574	
2.14	2.36	0.69	2.096	0.867	0.715	0.991	0.042	-1	184629	
2.36	2.59	0.961	3.057	0.861	0.708	0.991	0.049	-1	140632	
2.59	2.85	1.417	4.474	0.861	0.744	0.987	0.053	-1	250819	
2.85	3.14	2.025	6.499	0.872	0.696	0.989	0.043	-1	624934	
3.14	3.45	2.661	9.16	0.874	0.672	0.991	0.042	-1	712324	
3.45	3.8	3.514	12.674	0.87	0.746	0.987	0.053	-1	844694	
3.8	4.18	4.253	16.927	0.881	0.711	0.991	0.042	-1	1560025	
4.18	4.59	4.867	21.794	0.877	0.741	0.988	0.05	-1	1126746	
4.59	5.05	5.545	27.339	0.883	0.729	0.989	0.048	-1	1182129	
5.05	5.56	6.066	33.405	0.885	0.73	0.988	0.049	-1	959527	
5.56	6.12	6.595	40	0.887	0.728	0.989	0.047	-1	1096604	
6.12	6.73	7.191	47.191	0.887	0.737	0.988	0.05	-1	824592	
6.73	7.4	7.656	54.847	0.892	0.727	0.989	0.048	-1	742592	
7.4	8.14	7.626	62.473	0.895	0.735	0.989	0.048	-1	580154	
8.14	8.95	6.999	69.472	0.895	0.74	0.988	0.049	-1	376998	
8.95	9.85	6.126	75.598	0.899	0.737	0.989	0.048	-1	253866	
9.85	10.83	5.064	80.662	0.9	0.733	0.989	0.048	-1	174745	
10.83	11.93	4.271	84.933	0.901	0.719	0.988	0.05	-1	116337	
11.93	13.11	3.355	88.288	0.893	0.704	0.988	0.055	-1	49869	
13.11	14.42	2.655	90.943	0.903	0.734	0.989	0.055	-1	25888	
14.42	15.86	1.984	92.927	0.899	0.717	0.987	0.053	-1	14465	
15.86	17.45	1.461	94.388	0.891	0.753	0.986	0.057	0.242	6023	
17.45	19.19	0.905	95.293	0.861	0.672	0.984	0.073	0.231	3724	
19.19	21.11	0.86	96.153	0.917	0.56	0.988	0.056	0.371	1685	
21.11	23.23	0.516	96.669	0.903	0.827	0.981	0.052	0.259	1750	
23.23	25.55	0.365	97.034	0	0	0	0	-1	0	
25.55	28.1	0.285	97.319	0	0	0	0	-1	0	
28.1	30.91	0.291	97.61	0	0	0	0	-1	0	
30.91	34	0.032	97.642	0	0	0	0	-1	0	
34	37.4	0.589	98.231	0.9	0.817	0.99	0.053	0.571	1613	
37.4	41.14	0.055	98.286	0.882	0.759	0.987	0.063	0.435	63	
41.14	45.26	0	98.286	0	0	0	0	-1	0	
45.26	49.79	0	98.286	0.857	0.578	0.995	0.041	-1	0	
49.79	54.76	0.052	98.338	0.863	0.65	0.995	0.037	-1	30	
54.76	60.24	0.046	98.384	0.873	0.673	0.997	0.033	-1	56	
60.24	66.26	0.047	98.431	0.855	0.657	0.989	0.062	-1	25	
66.26	72.89	0.05	98.481	0.875	0.655	0.995	0.048	-1	30	
72.89	80.18	0.049	98.53	0.867	0.643	0.992	0.054	-1	16	
80.18	88.2	0.053	98.583	0.899	0.72	0.995	0.04	-1	15	
88.2	97.02	0.041	98.624	0.905	0.671	0.997	0.035	-1	8	
97.02	106.72	0.053	98.677	0.889	0.626	0.999	0.057	-1	9	
106.72	117.39	0.045	98.722	0.912	0.772	0.999	0.037	-1	5	
117.39	129.13	0.163	98.885	0.902	0.685	0.997	0.047	-1	16	
129.13	142.04	0.185	99.07	0.897	0.708	0.993	0.05	-1	17	
142.04	156.25	0.102	99.172	0.875	0.779	0.986	0.055	-1	4	
156.25	171.87	0.157	99.329	0.904	0.757	0.999	0.04	-1	7	
171.87	189.06	0.134	99.463	0.874	0.795	0.99	0.071	-1	4	
189.06	207.97	0.115	99.578	0.646	0.436	0.833	0.23	-1	3	
207.97	228.76	0.118	99.696	0.894	0.788	0.99	0.064	0.506	2	
228.76	251.64	0.18	99.876	0.925	0.781	0.995	0.04	0.475	3	
251.64	276.8	0.124	100	0.888	0.729	0.995	0.049	0.578	1	
276.8	304.28	0	100	0	0	0	0	0	0	
304.28	334.93	0	100	0	0	0	0	0	0	
334.93	368.42	0	100	0	0	0	0	0	0	
368.42	405.27	0	100	0	0	0	0	0	0	
405.27	445.79	0	100	0	0	0	0	0	0	
445.79	490.37	0	100	0	0	0	0	0	0	
490.37	539.41	0	100	0	0	0	0	0	0	
539.41	593.37	0	100	0	0	0	0	0	0	
593.37	652.68	0	100	0	0	0	0	0	0	
652.68	717.95	0	100	0	0	0	0	0	0	
717.95	789.76	0	100	0	0	0	0	0	0	
789.76	868.72	0	100	0	0	0	0	0	0	
868.72	955.59	0	100	0	0	0	0	0	0	
955.59	1051.15	0	100	0	0	0	0	0	0	
1051.15	1156.27	0	100	0	0	0	0	0	0	
1156.27	1000000	0	100	0	0	0	0	0	0	

**Table B.4** CamSizer Data for Theophylline (THF)

x [µm] at Q3 = 10.0 %	6.28										
x [µm] at Q3 = 50.0 %	15.49										
x [µm] at Q3 = 90.0 %	28.55										
Mv3(x) [µm]	16.91										
Sigma3(x) [µm]	10.84										
SPAN3	1.438										
par3a [%]	48.46										
xmax3a [µm]	243.02										
Q3 (Symm=0.9) [%]	57.23										
Q3 (b/l=0.9) [%]	99.18										
Mean value Symm3	0.8892										
Mean value b/l3	0.6409										
<b>Size class</b>	<b>[µm]</b>	<b>p3 [%]</b>	<b>Q3 [%]</b>	<b>Symm3</b>	<b>b/l3</b>	<b>Conv_A3</b>	<b>Ellipse3</b>	<b>RDNS_C3</b>	<b>PDN</b>		
0	1	0.019	0.019	0.981	0.49	0.997	0.272	-1	1462418		
1	1.1	0.004	0.023	0.863	0.674	0.965	0	-1	3616		
1.1	1.21	0.004	0.027	0.863	0.674	0.965	0	-1	0		
1.21	1.33	0.015	0.042	0.859	0.608	0.995	0.01	-1	0		
1.33	1.46	0.022	0.064	0.859	0.596	1	0.012	-1	2325		
1.46	1.61	0.026	0.09	0.859	0.596	1	0.012	-1	16320		
1.61	1.77	0.028	0.118	0.859	0.596	1	0.012	-1	14233		
1.77	1.95	0.047	0.165	0.864	0.678	0.995	0.029	-1	29810		
1.95	2.14	0.074	0.239	0.864	0.684	0.995	0.031	-1	153367		
2.14	2.36	0.123	0.362	0.873	0.675	0.996	0.03	-1	205935		
2.36	2.59	0.161	0.523	0.871	0.685	0.994	0.029	-1	182425		
2.59	2.85	0.254	0.777	0.862	0.707	0.989	0.042	-1	301974		
2.85	3.14	0.373	1.15	0.876	0.705	0.991	0.039	-1	562955		
3.14	3.45	0.506	1.656	0.874	0.665	0.992	0.042	-1	809223		
3.45	3.8	0.698	2.354	0.869	0.711	0.986	0.053	-1	810534		
3.8	4.18	0.894	3.248	0.879	0.7	0.99	0.043	-1	1526871		
4.18	4.59	1.099	4.347	0.879	0.715	0.989	0.048	-1	974720		
4.59	5.05	1.365	5.712	0.879	0.697	0.989	0.049	-1	1080353		
5.05	5.56	1.655	7.367	0.88	0.671	0.989	0.049	-1	1038742		
5.56	6.12	2.023	9.39	0.882	0.691	0.988	0.048	-1	959303		
6.12	6.73	2.458	11.848	0.885	0.685	0.989	0.049	-1	880798		
6.73	7.4	2.907	14.755	0.885	0.677	0.988	0.05	-1	823943		
7.4	8.14	3.277	18.032	0.886	0.687	0.987	0.052	-1	678435		
8.14	8.95	3.494	21.526	0.889	0.671	0.989	0.051	-1	494920		
8.95	9.85	3.764	25.29	0.893	0.663	0.988	0.052	-1	412334		
9.85	10.83	4.103	29.393	0.885	0.645	0.986	0.057	-1	299697		
10.83	11.93	4.748	34.141	0.897	0.656	0.989	0.051	-1	277673		
11.93	13.11	5.268	39.409	0.89	0.649	0.987	0.058	-1	180952		
13.11	14.42	6.023	45.432	0.889	0.654	0.985	0.056	-1	157166		
14.42	15.86	6.091	51.523	0.89	0.628	0.987	0.058	-1	111713		
15.86	17.45	6.644	58.167	0.895	0.638	0.987	0.056	0.591	92493		
17.45	19.19	6.833	65	0.892	0.634	0.989	0.06	0.44	69144		
19.19	21.11	6.775	71.775	0.889	0.637	0.988	0.061	0.503	32477		
21.11	23.23	5.843	77.618	0.904	0.683	0.989	0.049	0.572	32038		
23.23	25.55	5.483	83.101	0.886	0.705	0.989	0.064	0.484	25976		
25.55	28.1	5.938	89.039	0.878	0.68	0.986	0.064	0.401	13110		
28.1	30.91	4.928	93.967	0.919	0.689	0.992	0.044	0.54	9849		
30.91	34	2.963	96.93	0.915	0.66	0.989	0.049	0.403	5865		
34	37.4	0.979	97.909	0.903	0.611	0.99	0.056	0.532	2607		
37.4	41.14	0.539	98.448	0	0	0	0	-1	0		
41.14	45.26	0.516	98.964	0	0	0	0	-1	0		
45.26	49.79	0.184	99.148	0.869	0.673	0.995	0.035	-1	0		
49.79	54.76	0.494	99.642	0.875	0.682	0.996	0.032	-1	388		
54.76	60.24	0.158	99.8	0.873	0.668	0.996	0.037	-1	220		
60.24	66.26	0.041	99.841	0.876	0.653	0.996	0.038	-1	46		
66.26	72.89	0.019	99.86	0.854	0.6	0.983	0.056	-1	23		
72.89	80.18	0.008	99.868	0.836	0.685	0.984	0.063	-1	7		
80.18	88.2	0.008	99.876	0.833	0.455	0.97	0.096	-1	3		
88.2	97.02	0.007	99.883	0.899	0.74	0.996	0.041	-1	4		
97.02	106.72	0.013	99.896	0.854	0.36	0.982	0.072	-1	2		
106.72	117.39	0.014	99.91	0.859	0.784	0.991	0.063	-1	5		
117.39	129.13	0.002	99.912	0	0	0	0	-1	0		
129.13	142.04	0.005	99.917	0.881	0.873	1	0.063	-1	2		
142.04	156.25	0	99.917	0	0	0	0	-1	0		
156.25	171.87	0.007	99.924	0.923	0.808	0.994	0.042	-1	0		
171.87	189.06	0.008	99.932	0.923	0.808	0.994	0.042	-1	1		
189.06	207.97	0.027	99.959	0.792	0.647	0.94	0.089	-1	2		
207.97	228.76	0	99.959	0	0	0	0	-1	0		
228.76	251.64	0.041	100	0.877	0.739	0.987	0.068	0.075	2		
251.64	276.8	0	100	0	0	0	0	0	0		
276.8	304.28	0	100	0	0	0	0	0	0		
304.28	334.93	0	100	0	0	0	0	0	0		
334.93	368.42	0	100	0	0	0	0	0	0		
368.42	405.27	0	100	0	0	0	0	0	0		
405.27	445.79	0	100	0	0	0	0	0	0		
445.79	490.37	0	100	0	0	0	0	0	0		
490.37	539.41	0	100	0	0	0	0	0	0		
539.41	593.37	0	100	0	0	0	0	0	0		
593.37	652.68	0	100	0	0	0	0	0	0		
652.68	717.95	0	100	0	0	0	0	0	0		
717.95	789.76	0	100	0	0	0	0	0	0		
789.76	868.72	0	100	0	0	0	0	0	0		
868.72	955.59	0	100	0	0	0	0	0	0		
955.59	1051.15	0	100	0	0	0	0	0	0		
1051.15	1156.27	0	100	0	0	0	0	0	0		
1156.27	1000000	0	100	0	0	0	0	0	0		

**Table B.5** CamSizer Data for 70% Micronized Theophylline (MTHF) and 30% Hydroxypropylcellulose EXF (HPC EXF)

x [µm] at Q3 = 10.0 %	3.99								
x [µm] at Q3 = 50.0 %	9.49								
x [µm] at Q3 = 90.0 %	76.52								
Mv3(x) [µm]	24.95								
Sigma3(x) [µm]	31.15								
SPAN3	7.646								
par3a [%]	-113.47								
xmax3a [µm]	80								
Q3 (Symm=0.9) [%]	69.76								
Q3 (b/l=0.9) [%]	99.13								
Mean value Symm3	0.8713								
Mean value b/l3	0.6188								
<b>Size class</b>	<b>[µm]</b>	<b>p3 [%]</b>	<b>Q3 [%]</b>	<b>Symm3</b>	<b>b/l3</b>	<b>Conv_A3</b>	<b>Ellipse3</b>	<b>RDNS_C3</b>	<b>PDN</b>
0	1	0.063	0.061	0.982	0.497	0.998	0.216	-1	6557514
1	1.1	0.02	0.08	0.915	0.707	1	0.025	-1	23197
1.1	1.21	0.023	0.102	0.915	0.707	1	0.025	-1	3973
1.21	1.33	0.062	0.162	0.848	0.554	0.987	0.037	-1	0
1.33	1.46	0.07	0.23	0.848	0.553	0.987	0.037	-1	0
1.46	1.61	0.081	0.309	0.848	0.553	0.987	0.037	-1	176119
1.61	1.77	0.151	0.455	0.879	0.61	0.997	0.017	-1	264702
1.77	1.95	0.218	0.666	0.84	0.677	0.986	0.063	-1	247898
1.95	2.14	0.313	0.969	0.87	0.698	0.992	0.033	-1	2669285
2.14	2.36	0.488	1.442	0.874	0.682	0.994	0.035	-1	2691381
2.36	2.59	0.673	2.094	0.87	0.69	0.992	0.04	-1	2588069
2.59	2.85	0.993	3.057	0.861	0.73	0.988	0.048	-1	4426670
2.85	3.14	1.411	4.425	0.869	0.709	0.99	0.044	-1	10855477
3.14	3.45	1.85	6.219	0.876	0.681	0.992	0.041	-1	11716328
3.45	3.8	2.438	8.583	0.87	0.738	0.987	0.052	-1	12629582
3.8	4.18	2.953	11.446	0.879	0.724	0.991	0.043	-1	21754306
4.18	4.59	3.385	14.728	0.878	0.744	0.988	0.048	-1	13895268
4.59	5.05	3.868	18.478	0.882	0.733	0.989	0.047	-1	14078764
5.05	5.56	4.261	22.609	0.882	0.724	0.989	0.049	-1	11023360
5.56	6.12	4.656	27.123	0.886	0.734	0.989	0.048	-1	11424069
6.12	6.73	5.06	32.029	0.889	0.728	0.989	0.048	-1	8768663
6.73	7.4	5.382	37.247	0.891	0.731	0.989	0.047	-1	7513503
7.4	8.14	5.376	42.459	0.893	0.73	0.989	0.048	-1	5519953
8.14	8.95	4.989	47.296	0.894	0.731	0.989	0.049	-1	3710525
8.95	9.85	4.475	51.634	0.898	0.728	0.989	0.047	-1	2547947
9.85	10.83	3.838	55.355	0.897	0.718	0.989	0.049	-1	1559071
10.83	11.93	3.332	58.585	0.898	0.724	0.989	0.051	-1	974617
11.93	13.11	2.711	61.213	0.899	0.702	0.988	0.052	-1	563760
13.11	14.42	2.173	63.32	0.902	0.702	0.988	0.05	-1	304010
14.42	15.86	1.791	65.056	0.89	0.695	0.986	0.057	-1	147423
15.86	17.45	1.512	66.522	0.893	0.655	0.983	0.057	0.48	95527
17.45	19.19	1.134	67.621	0.877	0.627	0.982	0.065	0.384	49377
19.19	21.11	1.439	69.016	0.898	0.662	0.984	0.051	0.446	44187
21.11	23.23	1.313	70.289	0.879	0.678	0.979	0.073	0.264	19330
23.23	25.55	0.798	71.063	0.875	0.608	0.98	0.068	0.395	14474
25.55	28.1	1.175	72.202	0.911	0.534	0.987	0.054	0.288	10882
28.1	30.91	1.157	73.324	0.894	0.551	0.989	0.044	0.523	7189
30.91	34	1.733	75.004	0.85	0.662	0.958	0.09	0.406	9513
34	37.4	1.845	76.793	0.854	0.647	0.982	0.082	0.229	4764
37.4	41.14	1.476	78.224	0.854	0.828	0.989	0.055	0.521	2363
41.14	45.26	1.348	79.531	0.877	0.581	0.978	0.073	0.253	3458
45.26	49.79	1.805	81.281	0.885	0.564	0.982	0.069	0.256	3969
49.79	54.76	2.265	83.477	0.847	0.545	0.989	0.053	-1	7386
54.76	60.24	2.045	85.46	0.855	0.557	0.992	0.052	-1	11300
60.24	66.26	1.701	87.109	0.853	0.561	0.989	0.06	-1	5137
66.26	72.89	1.535	88.597	0.86	0.576	0.99	0.058	-1	5903
72.89	80.18	1.547	93.246	0.87	0.593	0.987	0.067	0.337	6138
80.18	88.2	1.611	94.808	0.858	0.59	0.985	0.069	-1	2219
88.2	97.02	1.422	96.187	0.863	0.599	0.985	0.067	-1	1729
97.02	106.72	1.188	97.339	0.86	0.596	0.983	0.073	-1	1639
106.72	117.39	0.982	98.291	0.856	0.61	0.982	0.078	-1	1156
117.39	129.13	0.681	98.951	0.851	0.603	0.978	0.084	-1	585
129.13	142.04	0.436	99.374	0.842	0.586	0.969	0.095	-1	272
142.04	156.25	0.258	99.624	0.809	0.553	0.947	0.118	-1	106
156.25	171.87	0.161	99.78	0.849	0.576	0.973	0.092	-1	65
171.87	189.06	0.096	99.873	0.804	0.528	0.947	0.121	-1	23
189.06	207.97	0.054	99.925	0.852	0.382	0.968	0.084	0.071	6
207.97	228.76	0.031	99.955	0.762	0.494	0.863	0.191	0.162	6
228.76	251.64	0.022	99.976	0.906	0.785	0.993	0.046	0.268	5
251.64	276.8	0.002	99.978	0	0	0	0	-1	0
276.8	304.28	0.002	99.98	0	0	0	0	-1	0
304.28	334.93	0.021	100	0.872	0.693	0.991	0.078	0.291	1
334.93	368.42	0	100	0	0	0	0	0	0
368.42	405.27	0	100	0	0	0	0	0	0
405.27	445.79	0	100	0	0	0	0	0	0
445.79	490.37	0	100	0	0	0	0	0	0
490.37	539.41	0	100	0	0	0	0	0	0
539.41	593.37	0	100	0	0	0	0	0	0
593.37	652.68	0	100	0	0	0	0	0	0
652.68	717.95	0	100	0	0	0	0	0	0
717.95	789.76	0	100	0	0	0	0	0	0
789.76	868.72	0	100	0	0	0	0	0	0
868.72	955.59	0	100	0	0	0	0	0	0
955.59	1051.15	0	100	0	0	0	0	0	0
1051.15	1156.27	0	100	0	0	0	0	0	0
1156.27	1000000	0	100	0	0	0	0	0	0

**Table B.6** CamSizer Data for 70% Micronized Theophylline and 30% Hydroxypropylcellulose MF (HPC MF)

x [µm] at Q3 = 10.0 %	4.29		
x [µm] at Q3 = 50.0 %	16.15		
x [µm] at Q3 = 90.0 %	440.61		
Mv3(x) [µm]	145.44		
Sigma3(x) [µm]	182.85		
SPAN3	27.015		
par3a [%]	-3.51		
xmax3a [µm]	86.75		
Q3 (Symm=0.9) [%]	76.94		
Q3 (b/l=0.9) [%]	99.48		
Mean value Symm3	0.858		
Mean value b/l3	0.5696		
Size class	[µm]	p3 [%]	Q3 [%]
0	1	0.046	0.046
1	1.1	0.021	0.067
1.1	1.21	0.023	0.09
1.21	1.33	0.026	0.116
1.33	1.46	0.053	0.169
1.46	1.61	0.077	0.246
1.61	1.77	0.112	0.358
1.77	1.95	0.176	0.534
1.95	2.14	0.235	0.769
2.14	2.36	0.379	1.148
2.36	2.59	0.527	1.675
2.59	2.85	0.78	2.455
2.85	3.14	1.117	3.572
3.14	3.45	1.467	5.039
3.45	3.8	1.935	6.974
3.8	4.18	2.339	9.313
4.18	4.59	2.669	11.982
4.59	5.05	3.026	15.008
5.05	5.56	3.291	18.299
5.56	6.12	3.568	21.867
6.12	6.73	3.866	25.733
6.73	7.4	4.077	29.81
7.4	8.14	4.029	33.839
8.14	8.95	3.656	37.495
8.95	9.85	3.152	40.647
9.85	10.83	2.564	43.211
10.83	11.93	2.226	45.437
11.93	13.11	1.883	47.32
13.11	14.42	1.459	48.779
14.42	15.86	1.049	49.828
15.86	17.45	0.8	50.628
17.45	19.19	0.626	51.254
19.19	21.11	0.623	51.877
21.11	23.23	0.356	52.233
23.23	25.55	0.146	52.379
25.55	28.1	0.212	52.591
28.1	30.91	0.153	52.744
30.91	34	0.164	52.908
34	37.4	0.127	53.035
37.4	41.14	0.131	53.166
41.14	45.26	0.24	53.406
45.26	49.79	0.12	53.526
49.79	54.76	0.286	53.812
54.76	60.24	0.485	54.297
60.24	66.26	0.726	55.023
66.26	72.89	0.549	55.572
72.89	80.18	0.813	56.385
80.18	88.2	0.747	57.132
88.2	97.02	0.467	57.599
97.02	106.72	0.823	58.422
106.72	117.39	1.099	59.521
117.39	129.13	1.22	60.741
129.13	142.04	1.343	62.084
142.04	156.25	1.513	63.597
156.25	171.87	1.588	65.185
171.87	189.06	1.633	66.818
189.06	207.97	1.788	68.606
207.97	228.76	1.993	70.599
228.76	251.64	2.384	72.983
251.64	276.8	2.69	75.673
276.8	304.28	2.867	78.54
304.28	334.93	2.945	81.485
334.93	368.42	2.792	84.277
368.42	405.27	2.781	87.058
405.27	445.79	3.528	90.586
445.79	490.37	3.576	94.162
490.37	539.41	2.04	96.202
539.41	593.37	0.938	97.14
593.37	652.68	1.899	99.039
652.68	717.95	0.961	100
717.95	789.76	0	100
789.76	868.72	0	100
868.72	955.59	0	100
955.59	1051.15	0	100
1051.15	1156.27	0	100
1156.27	1000000	0	100

**Table B.7** CamSizer Data for 70% Theophylline (THF) and 30% Hydroxypropylcellulose MF (HPC MF)

x [µm] at Q3 = 10.0 %	6.59									
x [µm] at Q3 = 50.0 %	17.54									
x [µm] at Q3 = 90.0 %	180.5									
Mv3(x) [µm]	57.09									
Sigma3(x) [µm]	118.99									
SPAN3	9.915									
par3a [%]	1.81									
xmax3a [µm]	126.63									
Q3 (Symm=0.9) [%]	66.79									
Q3 (b/l=0.9) [%]	99.62									
Mean value Symm3	0.8703									
Mean value b/l3	0.5931									
Size class	[µm]	p3 [%]	Q3 [%]	Symm3	b/l3	Conv_A3	Ellipse3	RDNS_C3	PDN	
0	1	0.089	0.089	0.883	0.632	0.991	0.084	-1	25165511	
1	1.1	0.009	0.098	0.883	0.632	0.991	0.084	-1	0	
1.1	1.21	0.01	0.108	0.883	0.632	0.991	0.084	-1	0	
1.21	1.33	0.011	0.119	0.883	0.632	0.991	0.084	-1	0	
1.33	1.46	0.012	0.131	0.883	0.632	0.991	0.084	-1	0	
1.46	1.61	0.013	0.144	0.883	0.632	0.991	0.084	-1	251944	
1.61	1.77	0.015	0.159	0.883	0.632	0.991	0.084	-1	469534	
1.77	1.95	0.016	0.175	0.883	0.632	0.991	0.084	-1	252173	
1.95	2.14	0.039	0.214	0.871	0.671	0.993	0.041	-1	3219914	
2.14	2.36	0.104	0.318	0.869	0.676	0.993	0.035	-1	3058847	
2.36	2.59	0.148	0.466	0.869	0.667	0.992	0.044	-1	3366272	
2.59	2.85	0.224	0.69	0.862	0.724	0.989	0.052	-1	4876791	
2.85	3.14	0.332	1.022	0.87	0.7	0.99	0.041	-1	12880935	
3.14	3.45	0.444	1.466	0.873	0.653	0.992	0.04	-1	15118964	
3.45	3.8	0.615	2.081	0.871	0.719	0.988	0.05	-1	15193259	
3.8	4.18	0.784	2.865	0.878	0.7	0.99	0.044	-1	28512859	
4.18	4.59	0.968	3.833	0.877	0.714	0.988	0.048	-1	18940497	
4.59	5.05	1.212	5.045	0.881	0.698	0.989	0.048	-1	19627184	
5.05	5.56	1.486	6.531	0.881	0.672	0.989	0.048	-1	17769371	
5.56	6.12	1.808	8.339	0.884	0.691	0.988	0.048	-1	19268350	
6.12	6.73	2.181	10.52	0.885	0.677	0.989	0.049	-1	16185422	
6.73	7.4	2.595	13.115	0.889	0.675	0.989	0.049	-1	16285149	
7.4	8.14	2.993	16.108	0.889	0.679	0.988	0.05	-1	12758321	
8.14	8.95	3.251	19.359	0.891	0.668	0.989	0.05	-1	10750375	
8.95	9.85	3.447	22.806	0.891	0.663	0.988	0.051	-1	7830441	
9.85	10.83	3.576	26.382	0.891	0.661	0.988	0.052	-1	6028426	
10.83	11.93	3.963	30.345	0.893	0.656	0.988	0.053	-1	4985173	
11.93	13.11	4.303	34.648	0.893	0.638	0.987	0.055	-1	3650554	
13.11	14.42	4.813	39.461	0.89	0.638	0.987	0.058	-1	2641966	
14.42	15.86	5.003	44.464	0.894	0.632	0.988	0.056	-1	2053064	
15.86	17.45	5.24	49.704	0.89	0.65	0.987	0.058	-1	1646497	
17.45	19.19	5.499	55.203	0.888	0.642	0.986	0.061	0.469	1124288	
19.19	21.11	5.614	60.817	0.892	0.654	0.987	0.059	0.437	879337	
21.11	23.23	5.634	66.451	0.897	0.66	0.987	0.058	0.465	699928	
23.23	25.55	4.918	71.369	0.894	0.701	0.986	0.062	0.509	413029	
25.55	28.1	4.415	75.784	0.897	0.664	0.987	0.058	0.424	199310	
28.1	30.91	3.649	79.433	0.909	0.698	0.988	0.049	0.601	162131	
30.91	34	2.791	82.224	0.905	0.753	0.988	0.054	0.576	83507	
34	37.4	1.531	83.755	0.921	0.8	0.993	0.046	0.623	32811	
37.4	41.14	0.758	84.513	0.887	0.803	0.982	0.06	0.4	6788	
41.14	45.26	0.5	85.013	0.935	0.764	0.996	0.032	0.512	6173	
45.26	49.79	0.52	85.533	0.869	0.625	0.993	0.037	-1	0	
49.79	54.76	0.427	85.96	0.851	0.641	0.979	0.072	-1	6916	
54.76	60.24	0.23	86.19	0.842	0.569	0.986	0.063	-1	4405	
60.24	66.26	0.305	86.495	0.828	0.549	0.978	0.081	-1	1960	
66.26	72.89	0.302	86.797	0.833	0.538	0.979	0.081	-1	2262	
72.89	80.18	0.351	87.148	0.828	0.531	0.975	0.089	-1	1728	
80.18	88.2	0.125	87.273	0.825	0.527	0.972	0.092	-1	1244	
88.2	97.02	0.137	87.41	0.823	0.524	0.968	0.098	-1	1094	
97.02	106.72	0.262	87.672	0.826	0.527	0.968	0.099	-1	1759	
106.72	117.39	0.342	88.014	0.831	0.532	0.97	0.096	-1	1697	
117.39	129.13	0.379	88.393	0.832	0.526	0.968	0.097	-1	1405	
129.13	142.04	0.415	88.808	0.829	0.526	0.964	0.099	-1	1151	
142.04	156.25	0.451	89.259	0.835	0.532	0.965	0.097	-1	923	
156.25	171.87	0.479	89.738	0.83	0.538	0.961	0.101	-1	760	
171.87	189.06	0.528	90.266	0.836	0.528	0.964	0.096	-1	628	
189.06	207.97	0.593	90.859	0.836	0.523	0.963	0.097	0.284	545	
207.97	228.76	0.586	91.445	0.83	0.548	0.96	0.1	0.248	396	
228.76	251.64	0.628	92.073	0.842	0.549	0.963	0.093	0.259	323	
251.64	276.8	0.713	92.786	0.852	0.555	0.967	0.087	0.28	281	
276.8	304.28	0.813	93.599	0.845	0.534	0.964	0.088	0.264	238	
304.28	334.93	0.865	94.464	0.851	0.526	0.966	0.085	0.274	170	
334.93	368.42	0.967	95.431	0.862	0.534	0.969	0.078	0.299	164	
368.42	405.27	0.93	96.361	0.86	0.558	0.97	0.081	0.34	119	
405.27	445.79	0.798	97.159	0.859	0.579	0.971	0.08	0.311	76	
445.79	490.37	0.638	97.797	0.861	0.64	0.972	0.078	0.369	52	
490.37	539.41	0.7	98.497	0.869	0.621	0.973	0.077	0.302	42	
539.41	593.37	0.61	99.107	0.879	0.641	0.979	0.066	0.38	28	
593.37	652.68	0.36	99.467	0.858	0.649	0.973	0.077	0.324	14	
652.68	717.95	0.223	99.69	0.886	0.644	0.98	0.062	0.412	6	
717.95	789.76	0.219	99.909	0.874	0.76	0.979	0.06	0.528	6	
789.76	868.72	0.091	100	0.752	0.554	0.972	0.103	0.394	1	
868.72	955.59	0	100	0	0	0	0	0	0	
955.59	1051.15	0	100	0	0	0	0	0	0	
1051.15	1156.27	0	100	0	0	0	0	0	0	
1156.27	1000000	0	100	0	0	0	0	0	0	

**Table B.8** CamSizer Data for 70% Theophylline (THF) and 30% Hydroxypropylcellulose EXF (HPC EXF) \*

x [µm] at Q3 = 10.0 %	7.4		
x [µm] at Q3 = 50.0 %	19.2		
x [µm] at Q3 = 90.0 %	60.24		
Mv3(x) [µm]	NA		
Sigma3(x) [µm]	NA		
SPAN3	NA		
par3a [%]	NA		
xmax3a [µm]	NA		
Q3 (Symm=0.9) [%]	NA		
Q3 (b/l=0.9) [%]	NA		
Mean value Symm3	NA		
Mean value b/l3	NA		
Size class	[µm]	p3 [%]	Q3 [%]
0	1	0.0151	0.0151
1	1.1	0.0031	0.0182
1.1	1.21	0.0031	0.0213
1.21	1.33	0.0108	0.0321
1.33	1.46	0.0163	0.0484
1.46	1.61	0.0194	0.0678
1.61	1.77	0.0208	0.0886
1.77	1.95	0.0341	0.1227
1.95	2.14	0.0548	0.1775
2.14	2.36	0.0906	0.2681
2.36	2.59	0.1172	0.3853
2.59	2.85	0.1862	0.5715
2.85	3.14	0.2722	0.8437
3.14	3.45	0.368	1.2117
3.45	3.8	0.509	1.7207
3.8	4.18	0.651	2.3717
4.18	4.59	0.8011	3.1728
4.59	5.05	0.9981	4.1709
5.05	5.56	1.2104	5.3813
5.56	6.12	1.4854	6.8667
6.12	6.73	1.8109	8.6776
6.73	7.4	2.1525	10.8301
7.4	8.14	2.437	13.2671
8.14	8.95	2.6102	15.8773
8.95	9.85	2.8259	18.7032
9.85	10.83	3.1091	21.8123
10.83	11.93	3.6311	25.4434
11.93	13.11	4.0359	29.4793
13.11	14.42	4.6619	34.1412
14.42	15.86	4.8361	38.9773
15.86	17.45	5.2898	44.2671
17.45	19.19	5.5082	49.7753
19.19	21.11	5.4805	55.2558
21.11	23.23	4.8737	60.1295
23.23	25.55	4.6172	64.7467
25.55	28.1	5.3257	70.0724
28.1	30.91	4.718	74.7904
30.91	34	3.4679	78.2583
34	37.4	1.9873	80.0656
37.4	41.14	1.7831	82.0287
41.14	45.26	2.0211	84.0498
45.26	49.79	2.3272	86.377
49.79	54.76	2.1164	88.4934
54.76	60.24	1.8806	90.374
60.24	66.26	2.0045	92.3785
66.26	72.89	1.465	93.8435
72.89	80.18	1.9955	95.839
80.18	88.2	1.2605	97.0995
88.2	97.02	0.9925	98.092
97.02	106.72	0.5329	98.6249
106.72	117.39	0.4538	99.0787
117.39	129.13	0.2921	99.3708
129.13	142.04	0.1934	99.5642
142.04	156.25	0.1404	99.7046
156.25	171.87	0.0934	99.798
171.87	189.06	0.0653	99.8633
189.06	207.97	0.0507	99.914
207.97	228.76	0.0201	99.9341
228.76	251.64	0.0566	99.9907
251.64	276.8	0.0093	30
276.8	304.28	0	30
304.28	334.93	0	30
334.93	368.42	0	30
368.42	405.27	0	30
405.27	445.79	0	30
445.79	490.37	0	30
490.37	539.41	0	30
539.41	593.37	0	30
593.37	652.68	0	30
652.68	717.95	0	30
717.95	789.76	0	30
789.76	868.72	0	30
868.72	955.59	0	30
955.59	1051.15	0	30
1051.15	1156.27	0	30
1156.27	1000000	0	30

\*THF:HPC EXF Sample was compromised, and values were calculated from raw material

Tables B.9 through B.12 Shows the methodology used for sieve particle size analysis for the 27 mm twin screw granulation experiments in section 4.2 and the Brabender batch mixing experiments in section 4.4.

**Table B.9** Sieve Analysis Data for 70% Micronized Theophylline (MTHF) and 30% Hydroxypropylcellulose EXF (HPC EXF)

<b>SIEVE PARTICLE SIZE ANALYSIS</b>											
Sieve analyzer used:											
Sieve settings: Sift = 5, Pulse = 5, Time = 5 minutes											
Balance Used: <b>Scale -2364</b>											
Date: Apr. 21, 2011											
Analyst: Gary Kovac											
<b>Batch</b> MTHF_HPC EXF											
Sample weight: g											
ATM SONIC SIFTER: AMPL 5 ; TIME- 5 min; MODE -sift/pulse											
US Sieve Series	Size	Mean Size (microns)	Tare Wgt	Retained+ Tare Wgt	Wgt Retained	% Wgt Retained					
Mesh #	(microns)	(d)	(gm)	(gm)	(gm)	(n)	n(log d)	n(log d- log d(gw))^2	n*d	n(d-d(a))^2	
8	2360	3,540	0.0000	0.0000	0.00	0	0.00	0.00	0.00	0.00	
20	840	1,260	43.9130	45.8830	1.97	39	113.72	25.95	32664.82	6647423.96	
40	420	630	40.7260	41.4620	0.74	15	38.11	3.87	6101.86	622.72	
60	250	335	36.0240	36.4700	0.45	9	21.11	0.74	2200.95	274403.89	
80	180	215	35.8730	36.0220	0.15	3	6.63	0.06	529.41	178780.63	
140	105	143	33.5230	33.7590	0.24	5	9.42	0.03	489.14	481654.57	
270	53	79	35.9270	36.5660	0.64	13	21.75	1.85	668.52	1760054.56	
pan	0	27	167.3570	168.2470	0.89	18				3196381.17	
					5.07	100.0	210.7	32.5	42654.7	12539321.5	
<u>Assuming Log-Normal Distribution:</u>											
Geometric Mean Diameter by Wgt, d(gw) =					128	= antilog [Sum (n*log d)/Sum n]					
Geometric Std Deviation, sd(g) =					3.72	= antilog [(Sum n(log d-log d(gw))^2)/Sum n]					
Geometric Mean Diameter by Nu., d(gn) =					0.73	= antilog [log d(gw)-6.908(log sd(g))^2]					
Mean Volume Surface Diameter, d(vs) =					54.09	= antilog [log d(gw)-1.151(log sd(g))^2]					
<u>Assuming Normal Distribution:</u>											
Arithmetic Mean Diameter, d(a) =					426.5	Microns	= Sum (n*d) / Sum n				
Arithmetic Std Deviation, sd(a) =					354.1	Microns	= Sum n(d-X(a))^2/Sum n				

**Table B.10 Sieve Analysis Data for 70% Micronized Theophylline (MTHF) and 30% Hydroxypropylcellulose MF (HPC MF)**

SIEVE PARTICLE SIZE ANALYSIS										
Sieve settings: Sift = 5, Pulse = 5, Time = 5 minutes										
Batch: MTHF_HPC MF										
ATM SONIC SIFTER: AMPL 5 ; TIME- 5 min; MODE -sift/pulse										
US Sieve Series	Size	Mean Size (microns)	Tare Wgt	Retained+ Tare Wgt	Wgt Retained	% Wgt Retained				
Mesh #	(microns)	(d)	(gm)	(gm)	(gm)	(n)	n(log d)	n(log d-log d(gw))^2	n*d	n(d-d(a))^2
8	666	999	0.0000	0.0000	0.00	0	0.00	0.00	0.00	0.00
20	840	1,260	43.9120	44.4650	0.55	10	29.61	9.38	8506.13	3566757.90
40	420	630	40.7260	41.5010	0.77	14	37.23	6.21	5960.45	427127.40
60	250	335	36.0240	37.2670	1.24	23	54.58	4.33	5690.35	276.57
80	180	215	35.8680	36.6250	0.76	14	31.26	1.19	2495.15	61327.09
140	105	143	33.5230	34.3670	0.84	15	31.24	0.05	1622.78	309506.85
270	53	79	35.9270	36.3150	0.39	7	12.25	0.40	376.56	266063.43
pan	0	27	167.3570	168.2580	0.90	16				1002620.24
					5.46	100.0	196.2	21.6	24651.4	5633679.5
Assuming Log-Normal Distribution:										
Geometric Mean Diameter by Wgt, d(gw) =				92	= antilog [Sum (n*log d)/Sum n]					
Geometric Std Deviation, sd(g) =				2.91	= antilog [(Sum n(log d-log d(gw))^2)/Sum n]					
Geometric Mean Diameter by Nu., d(gn) =				2.96	= antilog [log d(gw)-6.908(log sd(g))^2]					
Mean Volume Surface Diameter, d(vs) =				51.69	= antilog [log d(gw)-1.151(log sd(g))^2]					
Assuming Normal Distribution:										
Arithmetic Mean Diameter, d(a) =				246.5	Microns	= Sum (n*d) / Sum n				
Arithmetic Std Deviation, sd(a) =				237.4	Microns	= Sum n(d-X(a))^2/Sum n				

**Table B.11 Sieve Analysis Data for 70% Theophylline (THF) and 30% Hydroxypropylcellulose MF (HPC MF)**

SIEVE PARTICLE SIZE ANALYSIS										
Sieve settings: Sift = 5, Pulse = 5, Time = 5 minutes										
Batch: THF_HPC MF										
ATM SONIC SIFTER: AMPL 5 ; TIME- 5 min; MODE -sift/pulse										
US Sieve Series	Size	Mean Size (microns)	Tare Wgt	Retained+ Tare Wgt	Wgt Retained	% Wgt Retained				
Mesh #	(microns)	(d)	(gm)	(gm)	(gm)	(n)	n(log d)	n(log d-log d(gw))^2	n*d	n(d-d(a))^2
8	2360	3,540	0.0000	0.0000	0.00	0	0.00	0.00	0.00	0.00
20	840	1,260	43.9140	44.1320	0.22	4	13.03	8.55	3741.72	2064549.57
40	420	630	40.7260	41.1130	0.39	8	20.74	9.30	3321.21	537830.84
60	250	335	36.0250	36.8570	0.83	17	40.77	12.55	4250.10	140146.98
80	180	215	35.8720	36.5400	0.67	14	30.78	7.01	2456.89	5902.45
140	105	143	33.5260	34.2770	0.75	15	31.02	3.57	1611.26	45087.25
270	53	79	35.9290	36.4270	0.50	10	17.55	0.35	539.31	114777.00
pan	0	27	167.3570	168.8970	1.54	31				797571.93
					4.89	100.0	153.9	41.3	15920.5	3705866.0
Assuming Log-Normal Distribution:										
Geometric Mean Diameter by Wgt, d(gw) =				35	= antilog [Sum (n*log d)/Sum n]					
Geometric Std Deviation, sd(g) =				4.39	= antilog [(Sum n(log d-log d(gw))^2)/Sum n]					
Geometric Mean Diameter by Nu., d(gn) =				0.05	= antilog [log d(gw)-6.908(log sd(g))^2]					
Mean Volume Surface Diameter, d(vs) =				11.56	= antilog [log d(gw)-1.151(log sd(g))^2]					
Assuming Normal Distribution:										
Arithmetic Mean Diameter, d(a) =				159.2	Microns	= Sum (n*d) / Sum n				
Arithmetic Std Deviation, sd(a) =				192.5	Microns	= Sum n(d-X(a))^2/Sum n				



**Table B.12** Sieve Analysis Data for 70% Theophylline (THF) and 30% Hydroxypropylcellulose EXF (HPC EXF)

SIEVE PARTICLE SIZE ANALYSIS										
Sieve settings: Sift = 5, Pulse = 5, Time = 5 minutes										
Batch 70:30 THF:HPC EXF										
Sample weight: g										
ATM SONIC SIFTER: AMPL _5_ ; TIME- _5_ min; MODE -sift/pulse										
US Sieve Series	Size	Mean Size (microns)	Tare Wgt	Retained+ Tare Wgt	Wgt Retained	% Wgt Retained				
Mesh #	(microns)	(d)	(gm)	(gm)	(gm)	(n)	n(log d)	n(log d- log d(gw))^2	n*d	n(d-d(a))^2
8	2360	3,540	0.0000	0.0000	0.00	0	0.00	0.00	0.00	0.00
20	840	1,260	43.9130	44.816	0.90	17	49.61	47.90	14249.86	6870891.85
40	420	630	40.7260	41.15	0.42	8	20.65	14.98	3306.03	368667.84
60	250	335	36.0240	36.22	0.19	4	8.60	4.78	897.05	7730.50
80	180	215	35.8690	35.99	0.12	2	4.91	2.23	392.26	1212.12
140	105	143	33.5240	33.85	0.33	6	12.49	3.73	648.98	60069.58
270	53	79	35.9290	36.80	0.87	16	28.12	3.76	864.25	369762.10
pan	0	27	167.3720	169.87	2.50	47				1944242.62
					5.32	100.0	124.4	77.4	20358.4	9622576.6
<u>Assuming Log-Normal Distribution:</u>										
Geometric Mean Diameter by Wgt, d(gw) =				18	= antilog [Sum (n*log d)/Sum n]					
Geometric Std Deviation, sd(g) =				7.58	= antilog [(Sum n(log d-log d(gw))^2)/Sum n]					
Geometric Mean Diameter by Nu., d(gn) =				0.00	= antilog [log d(gw)-6.908(log sd(g))^2]					
Mean Volume Surface Diameter, d(vs) =				2.25	= antilog [log d(gw)-1.151(log sd(g))^2]					
<u>Assuming Normal Distribution:</u>										
Arithmetic Mean Diameter, d(a) =				203.6	Microns	= Sum (n*d) / Sum n				
Arithmetic Std Deviation, sd(a) =				310.2	Microns	= Sum n(d-X(a))^2/Sum n				

## **APPENDIX C**

### **CONVEYING AND KNEADING BLOCK NOMANCLATURE FOR THE 27 mm CO-ROTATING TWIN SCREW EXTRUDER**

The nomanclature listed in figures C.1 through C.3 shows illustrations of the the conveying and kneading elements used for the screw configuration described in section 4.2.2 Parametric effects using three 5 mm kneading blocks to granulate in a 27 mm co-rotating twin screw extruder.

# MICRO 27 GL



## Function of screw elements and combinations of kneading disks with different twisting angles

Kombination of kneading discs 30° conveying



KB5-2-30-30°RE

Kombination of kneading discs 60° conveying



KB5-2-30-60°RE

Kombination of kneading discs 90°



KB5-2-30-90°

Kombination of kneading discs 60° back-conveying



KB5-2-30-30°LI



GFA-2-20R



GFA-2-20L

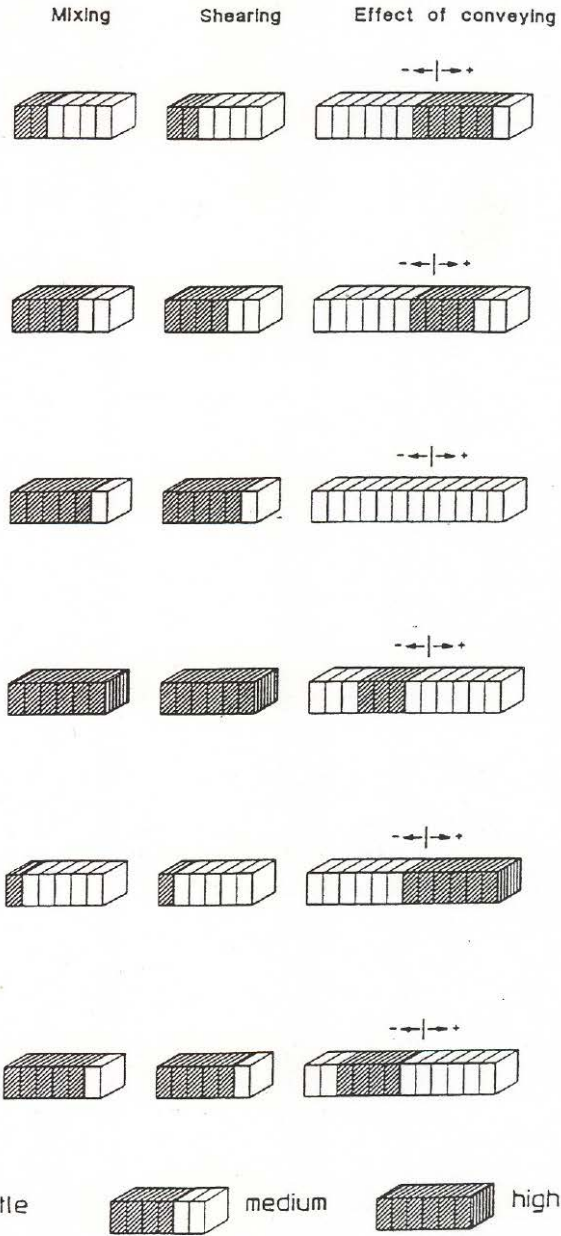


Figure C.1 Screw elements and kneading block names

# Micro 27 GL



## Function of screw elements with different helix angles

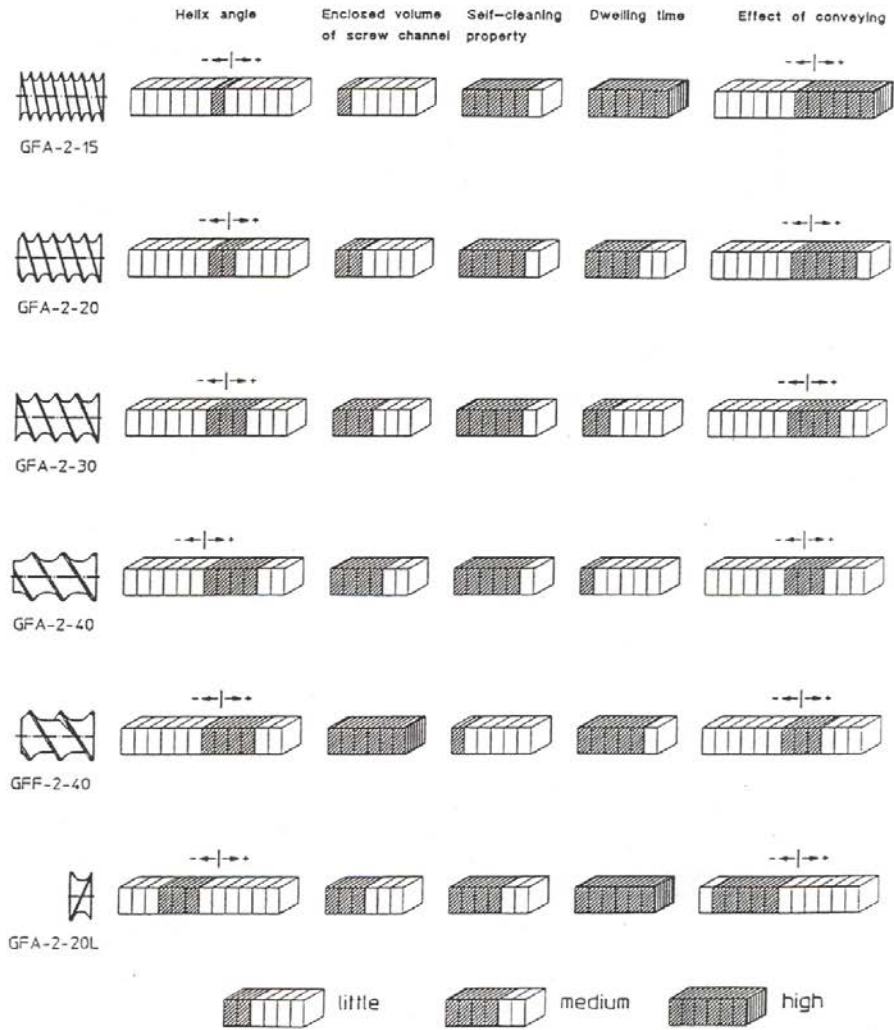


Figure C.2 Screw conveying element names

## 11.0 UNDERSTANDING THE LEISTRITZ SCREW NOMENCLATURE

The Leistritz screw terminology and designations are logical and fairly well organized. The attached sheets from the 27mm extruder manual make a good example that applies to all the extruder sizes.

Please keep in mind that these sheets only list the common element types. There are many other special elements we've made over the years which have unique designations that are too numerous to mention here.

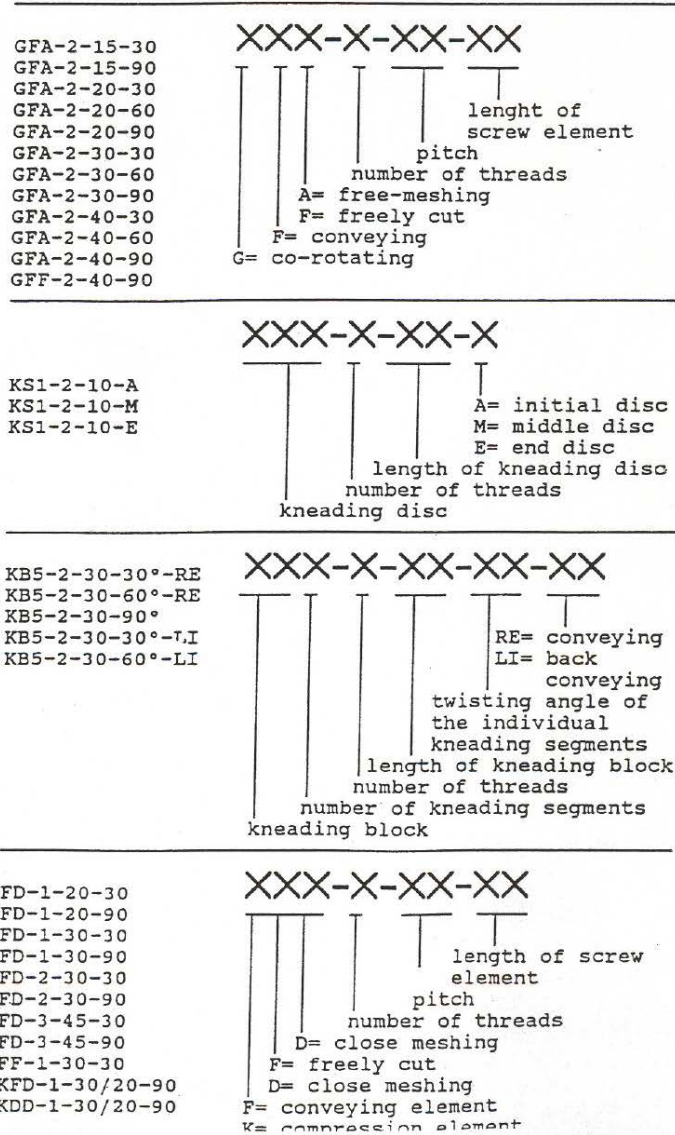


Figure C.3 Conveying and kneading block naming convention

## **APPENDIX D**

### **iShear: POWDER FLOW RHEOMETER REPORTS**

Tables D.1 through D.4 are used to build the profiles in Figure 4.75 illustrating the coefficient of friction,  $f$ , as a function of drug load for all four formulations.

**Table D.1** iShear Data for Theophylline (THF): Hydroxypropylcellulose EXF (HPC EXF)

	Yield locus slope, TanFI [-]	Internal angle of friction, FI [deg]	Cohesion intercept, c [gm/cm <sup>2</sup> ]	Effective angle of friction, FIE [deg]	Average consolid. stress, $\sigma$ (avg) [gm/cm <sup>2</sup> ]	Deviatoric consolid. stress, $\sigma$ (dev) [gm/cm <sup>2</sup> ]	Uniaxial compressive strength, fc [gm/cm <sup>2</sup> ]	Major consolidation stress, $\sigma_1$ [gm/cm <sup>2</sup> ]	Minor consolidation stress, $\sigma_2$ [gm/cm <sup>2</sup> ]	Relative flowability index, RI [-]	Absolute flowability index, AI [-]	Regression coefficient, [-]	Std. error [gm/cm <sup>2</sup> ]
HPC EXF A	0.68	34.09	12.95	52.91	45.21	36.07	48.80	81.28	9.15	1.48	0.51	0.95	1.37
HPC EXF B	0.96	43.82	10.36	55.22	57.96	47.61	48.59	105.57	10.36	1.96	0.67	0.99	0.92
HPC EXF C	0.84	40.15	18.00	61.90	57.98	51.15	77.48	109.13	6.83	1.32	0.45	0.93	2.06
<b>Average</b>	<b>0.83</b>	<b>39.35</b>	<b>13.77</b>	<b>56.68</b>	<b>53.72</b>	<b>44.94</b>	<b>58.29</b>	<b>98.66</b>	<b>8.78</b>	<b>1.59</b>	<b>0.55</b>	<b>0.96</b>	<b>1.45</b>
<b>Min</b>	<b>0.68</b>	<b>34.09</b>	<b>10.36</b>	<b>52.91</b>	<b>45.21</b>	<b>36.07</b>	<b>48.59</b>	<b>81.28</b>	<b>6.83</b>	<b>1.32</b>	<b>0.45</b>	<b>0.93</b>	<b>0.92</b>
<b>Max</b>	<b>0.96</b>	<b>43.82</b>	<b>18.00</b>	<b>61.90</b>	<b>57.98</b>	<b>51.15</b>	<b>77.48</b>	<b>109.13</b>	<b>10.36</b>	<b>1.96</b>	<b>0.67</b>	<b>0.99</b>	<b>2.06</b>
<b>Standard Deviation</b>	<b>0.14</b>	<b>4.91</b>	<b>3.89</b>	<b>4.67</b>	<b>7.37</b>	<b>7.89</b>	<b>16.62</b>	<b>15.16</b>	<b>7.37</b>	<b>0.33</b>	<b>0.11</b>	<b>0.03</b>	<b>0.57</b>
25 THF_75HPC EXF A	0.83	39.65	9.45	51.59	50.00	39.18	40.21	89.18	10.82	1.95	0.74	0.98	1.16
25 THF_75HPC EXF B	0.89	41.55	8.30	51.51	52.00	40.70	36.89	92.70	11.30	2.21	0.84	0.99	0.94
25 THF_75HPC EXF C	0.91	42.18	10.33	54.19	54.89	44.51	46.59	99.40	10.38	1.91	0.73	0.98	1.19
<b>Average</b>	<b>0.87</b>	<b>41.13</b>	<b>9.36</b>	<b>52.43</b>	<b>52.30</b>	<b>41.47</b>	<b>41.23</b>	<b>93.76</b>	<b>10.83</b>	<b>2.02</b>	<b>0.77</b>	<b>0.98</b>	<b>1.10</b>
<b>Min</b>	<b>0.83</b>	<b>39.65</b>	<b>8.30</b>	<b>51.51</b>	<b>50.00</b>	<b>39.18</b>	<b>36.89</b>	<b>89.18</b>	<b>10.38</b>	<b>1.91</b>	<b>0.73</b>	<b>0.98</b>	<b>0.94</b>
<b>Max</b>	<b>0.91</b>	<b>42.18</b>	<b>10.33</b>	<b>54.19</b>	<b>54.89</b>	<b>44.51</b>	<b>46.59</b>	<b>99.40</b>	<b>11.30</b>	<b>2.21</b>	<b>0.84</b>	<b>0.99</b>	<b>1.19</b>
<b>Standard Deviation</b>	<b>0.04</b>	<b>1.32</b>	<b>1.02</b>	<b>1.52</b>	<b>2.46</b>	<b>2.75</b>	<b>4.93</b>	<b>5.19</b>	<b>0.46</b>	<b>0.16</b>	<b>0.06</b>	<b>0.00</b>	<b>0.13</b>
50 THF_75HPC EXF A	0.83	39.57	9.33	51.41	49.79	38.92	39.65	88.71	10.88	1.96	0.84	0.98	0.93
50 THF_75HPC EXF B	0.78	38.03	9.25	50.30	47.54	36.58	37.97	84.11	10.96	1.93	0.83	0.98	1.08
50 THF_75HPC EXF C	0.70	34.86	8.46	47.13	43.02	31.53	32.39	74.55	11.49	1.95	0.84	0.98	0.80
<b>Average</b>	<b>0.77</b>	<b>37.49</b>	<b>9.01</b>	<b>49.61</b>	<b>46.78</b>	<b>35.67</b>	<b>36.67</b>	<b>82.46</b>	<b>11.11</b>	<b>1.95</b>	<b>0.84</b>	<b>0.98</b>	<b>0.94</b>
<b>Min</b>	<b>0.70</b>	<b>34.86</b>	<b>8.46</b>	<b>47.13</b>	<b>43.02</b>	<b>31.53</b>	<b>32.39</b>	<b>74.55</b>	<b>10.88</b>	<b>1.93</b>	<b>0.83</b>	<b>0.98</b>	<b>0.80</b>
<b>Max</b>	<b>0.83</b>	<b>39.57</b>	<b>9.33</b>	<b>51.41</b>	<b>49.79</b>	<b>38.92</b>	<b>39.65</b>	<b>88.71</b>	<b>11.49</b>	<b>1.96</b>	<b>0.84</b>	<b>0.98</b>	<b>1.08</b>
<b>Standard Deviation</b>	<b>0.07</b>	<b>2.40</b>	<b>0.49</b>	<b>2.22</b>	<b>3.45</b>	<b>3.77</b>	<b>3.80</b>	<b>7.22</b>	<b>0.33</b>	<b>0.02</b>	<b>0.01</b>	<b>0.00</b>	<b>0.14</b>
70 THF_30HPC EXF A	0.68	34.06	18.91	61.46	49.21	43.23	71.23	92.43	5.98	1.21	0.53	0.96	1.26
70 THF_30HPC EXF B	0.70	34.85	20.88	64.57	51.66	46.66	79.97	98.32	5.00	1.17	0.52	0.98	0.89
70 THF_30HPC EXF C	0.64	32.70	23.04	68.01	50.10	46.45	84.34	96.55	3.64	1.10	0.49	1.00	0.32
<b>Average</b>	<b>0.67</b>	<b>33.87</b>	<b>20.95</b>	<b>64.68</b>	<b>50.32</b>	<b>45.45</b>	<b>78.51</b>	<b>95.77</b>	<b>4.88</b>	<b>1.16</b>	<b>0.52</b>	<b>0.98</b>	<b>0.82</b>
<b>Min</b>	<b>0.64</b>	<b>32.70</b>	<b>18.91</b>	<b>61.46</b>	<b>49.21</b>	<b>43.23</b>	<b>71.23</b>	<b>92.43</b>	<b>3.64</b>	<b>1.10</b>	<b>0.49</b>	<b>0.96</b>	<b>0.32</b>
<b>Max</b>	<b>0.70</b>	<b>34.85</b>	<b>23.04</b>	<b>68.01</b>	<b>51.66</b>	<b>46.66</b>	<b>84.34</b>	<b>98.32</b>	<b>5.98</b>	<b>1.21</b>	<b>0.53</b>	<b>1.00</b>	<b>1.26</b>
<b>Standard Deviation</b>	<b>0.03</b>	<b>1.09</b>	<b>2.06</b>	<b>3.28</b>	<b>1.24</b>	<b>1.92</b>	<b>6.68</b>	<b>3.02</b>	<b>1.17</b>	<b>0.06</b>	<b>0.02</b>	<b>0.02</b>	<b>0.48</b>
75 THF_25HPC EXF A	0.73	36.09	8.84	48.48	44.73	33.49	34.76	78.23	11.24	1.93	1.07	0.95	1.54
75 THF_25HPC EXF B	0.61	31.42	9.57	46.44	40.17	29.11	34.13	69.29	11.06	1.71	0.95	0.93	1.50
75 THF_25HPC EXF C	0.79	38.32	9.71	51.06	48.30	37.57	40.10	85.86	10.73	1.87	1.05	0.94	1.86
<b>Average</b>	<b>0.71</b>	<b>35.28</b>	<b>9.37</b>	<b>48.66</b>	<b>44.40</b>	<b>33.39</b>	<b>36.33</b>	<b>77.79</b>	<b>11.01</b>	<b>1.84</b>	<b>1.02</b>	<b>0.94</b>	<b>1.63</b>
<b>Min</b>	<b>0.61</b>	<b>31.42</b>	<b>8.84</b>	<b>46.44</b>	<b>40.17</b>	<b>29.11</b>	<b>34.13</b>	<b>69.29</b>	<b>10.73</b>	<b>1.71</b>	<b>0.95</b>	<b>0.93</b>	<b>1.50</b>
<b>Max</b>	<b>0.79</b>	<b>38.32</b>	<b>9.71</b>	<b>51.06</b>	<b>48.30</b>	<b>37.57</b>	<b>40.10</b>	<b>85.86</b>	<b>11.24</b>	<b>1.93</b>	<b>1.07</b>	<b>0.95</b>	<b>1.86</b>
<b>Standard Deviation</b>	<b>0.09</b>	<b>3.53</b>	<b>0.47</b>	<b>2.32</b>	<b>4.07</b>	<b>4.23</b>	<b>3.28</b>	<b>8.30</b>	<b>0.26</b>	<b>0.12</b>	<b>0.06</b>	<b>0.01</b>	<b>0.20</b>
THF A	0.90	42.08	7.98	51.52	52.59	41.17	35.93	93.75	11.42	2.29	1.03	0.94	2.09
THF B	0.96	43.95	6.73	51.50	54.73	42.83	31.68	97.56	11.90	2.70	1.22	0.99	0.75
THF C	0.78	37.98	9.85	51.03	47.93	37.26	40.39	85.20	10.67	1.85	0.83	0.94	1.78
<b>Average</b>	<b>0.88</b>	<b>41.34</b>	<b>8.19</b>	<b>51.35</b>	<b>51.75</b>	<b>40.42</b>	<b>36.00</b>	<b>92.17</b>	<b>11.33</b>	<b>2.28</b>	<b>1.02</b>	<b>0.96</b>	<b>1.54</b>
<b>Min</b>	<b>0.78</b>	<b>37.98</b>	<b>6.73</b>	<b>51.03</b>	<b>47.93</b>	<b>37.26</b>	<b>31.68</b>	<b>85.20</b>	<b>10.67</b>	<b>1.85</b>	<b>0.83</b>	<b>0.94</b>	<b>0.75</b>
<b>Max</b>	<b>0.96</b>	<b>43.95</b>	<b>9.85</b>	<b>51.52</b>	<b>54.73</b>	<b>42.83</b>	<b>40.39</b>	<b>97.56</b>	<b>11.90</b>	<b>2.70</b>	<b>1.22</b>	<b>0.99</b>	<b>2.09</b>
<b>Standard Deviation</b>	<b>0.09</b>	<b>3.06</b>	<b>1.57</b>	<b>0.28</b>	<b>3.48</b>	<b>2.86</b>	<b>4.35</b>	<b>6.33</b>	<b>0.62</b>	<b>0.43</b>	<b>0.19</b>	<b>0.03</b>	<b>0.70</b>
HPC MF A	0.76	37.25	4.81	43.95	43.11	29.92	19.39	73.03	13.19	3.09	1.30	0.99	0.59
HPC MF B	0.81	38.94	5.11	45.72	46.45	32.54	21.41	77.99	12.91	3.04	1.30	1.00	0.27
HPC MF C	0.86	40.75	5.22	47.31	48.06	35.33	22.79	83.39	12.73	3.10	1.27	1.00	0.36
<b>Average</b>	<b>0.81</b>	<b>38.98</b>	<b>5.05</b>	<b>45.66</b>	<b>45.54</b>	<b>32.60</b>	<b>21.20</b>	<b>78.14</b>	<b>12.94</b>	<b>3.08</b>	<b>1.29</b>	<b>1.00</b>	<b>0.41</b>
<b>Min</b>	<b>0.76</b>	<b>37.25</b>	<b>4.81</b>	<b>43.95</b>	<b>43.11</b>	<b>29.92</b>	<b>19.39</b>	<b>73.03</b>	<b>12.73</b>	<b>3.04</b>	<b>1.27</b>	<b>0.99</b>	<b>0.27</b>
<b>Max</b>	<b>0.86</b>	<b>40.75</b>	<b>5.22</b>	<b>47.31</b>	<b>48.06</b>	<b>35.33</b>	<b>22.79</b>	<b>83.39</b>	<b>13.19</b>	<b>3.10</b>	<b>1.30</b>	<b>1.00</b>	<b>0.59</b>
<b>Standard Deviation</b>	<b>0.05</b>	<b>1.75</b>	<b>0.21</b>	<b>1.68</b>	<b>2.48</b>	<b>2.70</b>	<b>1.71</b>	<b>5.18</b>	<b>0.23</b>	<b>0.03</b>	<b>0.02</b>	<b>0.00</b>	<b>0.16</b>

**Table D.2** iShear Data for Theophylline (THF): Hydroxypropylcellulose MF (HPC MF)

	Yield locus slope, TanFI [-]	Internal angle of friction, FI [deg]	Cohesion intercept, c [gm/cm <sup>2</sup> ]	Effective angle of friction, FIE [deg]	Average consolid. stress, $\sigma$ (avg) [gm/cm <sup>2</sup> ]	Deviatoric consolid. stress, $\sigma$ (dev) [gm/cm <sup>2</sup> ]	Uniaxial compressive strength, $f_c$ [gm/cm <sup>2</sup> ]	Major consolidation stress, $\sigma_1$ [gm/cm <sup>2</sup> ]	Minor consolidation stress, $\sigma_2$ [gm/cm <sup>2</sup> ]	Relative flowability index, RI [-]	Absolute flowability index, AI [-]	Regression coefficient, [-]	Std.error [gm/cm <sup>2</sup> ]
HPC MF A	0.76	37.25	4.81	43.95	43.11	29.92	19.39	73.03	13.19	3.09	1.30	0.99	0.59
HPC MF B	0.81	38.94	5.11	45.72	45.45	32.54	21.41	77.99	12.91	3.04	1.30	1.00	0.27
HPC MF C	0.86	40.75	5.22	47.31	48.06	35.33	22.79	83.39	12.73	3.10	1.27	1.00	0.36
<b>Average</b>	<b>0.81</b>	<b>38.98</b>	<b>5.05</b>	<b>45.66</b>	<b>45.54</b>	<b>32.60</b>	<b>21.20</b>	<b>78.14</b>	<b>12.94</b>	<b>3.08</b>	<b>1.29</b>	<b>1.00</b>	<b>0.41</b>
<b>Min</b>	<b>0.76</b>	<b>37.25</b>	<b>4.81</b>	<b>43.95</b>	<b>43.11</b>	<b>29.92</b>	<b>19.39</b>	<b>73.03</b>	<b>12.73</b>	<b>3.04</b>	<b>1.27</b>	<b>0.99</b>	<b>0.27</b>
<b>Max</b>	<b>0.86</b>	<b>40.75</b>	<b>5.22</b>	<b>47.31</b>	<b>48.06</b>	<b>35.33</b>	<b>22.79</b>	<b>83.39</b>	<b>13.19</b>	<b>3.10</b>	<b>1.30</b>	<b>1.00</b>	<b>0.59</b>
<b>Standard Deviation</b>	<b>0.05</b>	<b>1.75</b>	<b>0.21</b>	<b>1.68</b>	<b>2.48</b>	<b>2.70</b>	<b>1.71</b>	<b>5.18</b>	<b>0.23</b>	<b>0.03</b>	<b>0.02</b>	<b>0.00</b>	<b>0.16</b>
25 THF_75HPC MF A	0.82	39.28	5.19	46.09	45.97	33.12	21.90	79.08	12.85	3.02	1.61	0.99	0.88
25 THF_75HPC MF B	0.80	38.56	5.84	46.36	45.54	32.96	24.26	78.50	12.59	2.72	1.47	0.98	1.04
25 THF_75HPC MF C	0.81	38.90	5.96	46.77	46.09	33.58	24.94	79.67	12.51	2.69	1.46	0.99	0.79
<b>Average</b>	<b>0.81</b>	<b>38.91</b>	<b>5.67</b>	<b>46.41</b>	<b>45.87</b>	<b>33.22</b>	<b>23.70</b>	<b>79.09</b>	<b>12.65</b>	<b>2.81</b>	<b>1.51</b>	<b>0.98</b>	<b>0.91</b>
<b>Min</b>	<b>0.80</b>	<b>38.56</b>	<b>5.19</b>	<b>46.09</b>	<b>45.54</b>	<b>32.96</b>	<b>21.90</b>	<b>78.50</b>	<b>12.51</b>	<b>2.69</b>	<b>1.46</b>	<b>0.98</b>	<b>0.79</b>
<b>Max</b>	<b>0.82</b>	<b>39.28</b>	<b>5.96</b>	<b>46.77</b>	<b>46.09</b>	<b>33.58</b>	<b>24.94</b>	<b>79.67</b>	<b>12.85</b>	<b>3.02</b>	<b>1.61</b>	<b>0.99</b>	<b>1.04</b>
<b>Standard Deviation</b>	<b>0.01</b>	<b>0.36</b>	<b>0.42</b>	<b>0.34</b>	<b>0.29</b>	<b>0.32</b>	<b>1.60</b>	<b>0.58</b>	<b>0.18</b>	<b>0.18</b>	<b>0.08</b>	<b>0.00</b>	<b>0.13</b>
50 THF_75HPC MF A	0.73	36.01	7.38	46.47	43.58	31.59	29.00	75.17	11.98	2.18	1.40	0.98	0.92
50 THF_75HPC MF B	0.82	39.48	6.19	47.51	47.07	34.71	26.25	81.78	12.36	2.64	1.63	0.99	0.76
50 THF_75HPC MF C	0.78	37.99	5.80	45.87	44.79	32.14	23.80	76.93	12.64	2.70	1.68	0.99	0.73
<b>Average</b>	<b>0.78</b>	<b>37.83</b>	<b>6.46</b>	<b>46.62</b>	<b>45.14</b>	<b>32.82</b>	<b>26.35</b>	<b>77.96</b>	<b>12.33</b>	<b>2.51</b>	<b>1.57</b>	<b>0.99</b>	<b>0.80</b>
<b>Min</b>	<b>0.73</b>	<b>36.01</b>	<b>5.80</b>	<b>45.87</b>	<b>43.58</b>	<b>31.59</b>	<b>23.80</b>	<b>75.17</b>	<b>11.98</b>	<b>2.18</b>	<b>1.40</b>	<b>0.98</b>	<b>0.73</b>
<b>Max</b>	<b>0.82</b>	<b>39.48</b>	<b>7.38</b>	<b>47.51</b>	<b>47.07</b>	<b>34.71</b>	<b>29.00</b>	<b>81.78</b>	<b>12.64</b>	<b>2.70</b>	<b>1.68</b>	<b>0.99</b>	<b>0.92</b>
<b>Standard Deviation</b>	<b>0.05</b>	<b>1.74</b>	<b>0.82</b>	<b>0.83</b>	<b>1.77</b>	<b>1.66</b>	<b>2.60</b>	<b>3.42</b>	<b>0.33</b>	<b>0.29</b>	<b>0.15</b>	<b>0.00</b>	<b>0.10</b>
70 THF_30HPC MF A	0.64	32.75	8.57	45.84	40.86	29.31	31.41	70.17	11.54	1.87	1.00	0.95	1.33
70 THF_30HPC MF B	0.75	36.82	7.88	47.72	44.92	33.23	31.50	78.15	11.69	2.11	1.13	0.98	0.92
70 THF_30HPC MF C													
<b>Average</b>	<b>0.70</b>	<b>34.79</b>	<b>8.23</b>	<b>46.78</b>	<b>42.89</b>	<b>31.27</b>	<b>31.45</b>	<b>74.16</b>	<b>11.62</b>	<b>1.99</b>	<b>1.06</b>	<b>0.97</b>	<b>1.13</b>
<b>Min</b>	<b>0.64</b>	<b>32.75</b>	<b>7.88</b>	<b>45.84</b>	<b>40.86</b>	<b>29.31</b>	<b>31.41</b>	<b>70.17</b>	<b>11.54</b>	<b>1.87</b>	<b>1.00</b>	<b>0.95</b>	<b>0.92</b>
<b>Max</b>	<b>0.75</b>	<b>36.82</b>	<b>8.57</b>	<b>47.72</b>	<b>44.92</b>	<b>33.23</b>	<b>31.50</b>	<b>78.15</b>	<b>11.69</b>	<b>2.11</b>	<b>1.13</b>	<b>0.98</b>	<b>1.33</b>
<b>Standard Deviation</b>	<b>0.07</b>	<b>2.88</b>	<b>0.49</b>	<b>1.32</b>	<b>2.87</b>	<b>2.77</b>	<b>0.06</b>	<b>5.64</b>	<b>0.10</b>	<b>0.17</b>	<b>0.09</b>	<b>0.02</b>	<b>0.29</b>
75 THF_25HPC MF A	0.73	36.09	8.84	48.48	44.73	33.49	34.76	78.23	11.24	1.93	1.07	0.95	1.54
75 THF_25HPC MF B	0.61	31.42	9.57	46.44	40.17	29.11	34.13	69.29	11.06	1.71	0.95	0.93	1.50
75 THF_25HPC MF C	0.79	38.32	9.71	51.06	48.30	37.57	40.10	85.86	10.73	1.87	1.05	0.94	1.86
<b>Average</b>	<b>0.71</b>	<b>35.28</b>	<b>9.37</b>	<b>48.66</b>	<b>44.40</b>	<b>33.39</b>	<b>36.33</b>	<b>77.79</b>	<b>11.01</b>	<b>1.84</b>	<b>1.02</b>	<b>0.94</b>	<b>1.63</b>
<b>Min</b>	<b>0.61</b>	<b>31.42</b>	<b>8.84</b>	<b>46.44</b>	<b>40.17</b>	<b>29.11</b>	<b>34.13</b>	<b>69.29</b>	<b>10.73</b>	<b>1.71</b>	<b>0.95</b>	<b>0.93</b>	<b>1.50</b>
<b>Max</b>	<b>0.79</b>	<b>38.32</b>	<b>9.71</b>	<b>51.06</b>	<b>48.30</b>	<b>37.57</b>	<b>40.10</b>	<b>85.86</b>	<b>11.24</b>	<b>1.93</b>	<b>1.07</b>	<b>0.95</b>	<b>1.86</b>
<b>Standard Deviation</b>	<b>0.09</b>	<b>3.53</b>	<b>0.47</b>	<b>2.32</b>	<b>4.07</b>	<b>4.23</b>	<b>3.28</b>	<b>8.30</b>	<b>0.26</b>	<b>0.12</b>	<b>0.06</b>	<b>0.01</b>	<b>0.20</b>
THF A	0.90	42.08	7.98	51.52	52.59	41.17	35.93	93.75	11.42	2.29	1.03	0.94	2.09
THF B	0.96	43.95	6.73	51.50	54.73	42.83	31.68	97.56	11.90	2.70	1.22	0.99	0.75
THF C	0.78	37.98	9.85	51.03	47.93	37.26	40.39	85.20	10.67	1.85	0.83	0.94	1.78
<b>Average</b>	<b>0.88</b>	<b>41.34</b>	<b>8.19</b>	<b>51.35</b>	<b>51.75</b>	<b>40.42</b>	<b>36.00</b>	<b>92.17</b>	<b>11.33</b>	<b>2.28</b>	<b>1.02</b>	<b>0.96</b>	<b>1.54</b>
<b>Min</b>	<b>0.78</b>	<b>37.98</b>	<b>6.73</b>	<b>51.03</b>	<b>47.93</b>	<b>37.26</b>	<b>31.68</b>	<b>85.20</b>	<b>10.67</b>	<b>1.85</b>	<b>0.83</b>	<b>0.94</b>	<b>0.75</b>
<b>Max</b>	<b>0.96</b>	<b>43.95</b>	<b>9.85</b>	<b>51.52</b>	<b>54.73</b>	<b>42.83</b>	<b>40.39</b>	<b>97.56</b>	<b>11.90</b>	<b>2.70</b>	<b>1.22</b>	<b>0.99</b>	<b>2.09</b>
<b>Standard Deviation</b>	<b>0.09</b>	<b>3.06</b>	<b>1.57</b>	<b>0.28</b>	<b>3.48</b>	<b>2.86</b>	<b>4.35</b>	<b>6.33</b>	<b>0.62</b>	<b>0.43</b>	<b>0.19</b>	<b>0.03</b>	<b>0.70</b>



**Table D.3** iShear Data for Micronized Theophylline (MTHF): Hydroxypropylcellulose EXF (HPC EXF)

	Yield locus slope, TanFI [-]	Internal angle of friction, FI [deg]	Cohesion intercept, c [gm/cm <sup>2</sup> ]	Effective angle of friction, FIE [deg]	Average consolid. stress, $\sigma$ (avg)	Deviatoric consolid. stress, $\sigma$ (dev) [gm/cm <sup>2</sup> ]	Unaxial compressive strength, fc [gm/cm <sup>2</sup> ]	Major consolidation stress, $\sigma$ 1 [gm/cm <sup>2</sup> ]	Minor consolidation stress, $\sigma$ 2 [gm/cm <sup>2</sup> ]	Relative flowability index, RI [-]	Absolute flowability index, AI [-]	Regression coefficient, [-]	Std. error [gm/cm <sup>2</sup> ]
HPC EXF A	0.68	34.09	12.95	52.91	45.21	36.07	48.80	81.28	9.15	1.48	0.51	0.95	1.37
HPC EXF B	0.96	43.82	10.36	55.22	57.96	47.61	48.59	105.57	10.36	1.96	0.67	0.99	0.92
HPC EXF C	0.84	40.15	18.00	61.90	57.98	51.15	77.48	109.13	6.83	1.32	0.45	0.93	2.06
<b>Average</b>	<b>0.83</b>	<b>39.35</b>	<b>13.77</b>	<b>56.68</b>	<b>53.72</b>	<b>44.94</b>	<b>58.29</b>	<b>98.66</b>	<b>8.78</b>	<b>1.59</b>	<b>0.55</b>	<b>0.96</b>	<b>1.45</b>
<b>Min</b>	<b>0.68</b>	<b>34.09</b>	<b>10.36</b>	<b>52.91</b>	<b>45.21</b>	<b>36.07</b>	<b>48.59</b>	<b>81.28</b>	<b>6.83</b>	<b>1.32</b>	<b>0.45</b>	<b>0.93</b>	<b>0.92</b>
<b>Max</b>	<b>0.96</b>	<b>43.82</b>	<b>18.00</b>	<b>61.90</b>	<b>57.98</b>	<b>51.15</b>	<b>77.48</b>	<b>109.13</b>	<b>10.36</b>	<b>1.96</b>	<b>0.67</b>	<b>0.99</b>	<b>2.06</b>
<b>Standard Deviation</b>	<b>0.14</b>	<b>4.91</b>	<b>3.89</b>	<b>4.67</b>	<b>7.37</b>	<b>7.89</b>	<b>16.62</b>	<b>15.16</b>	<b>1.79</b>	<b>0.33</b>	<b>0.11</b>	<b>0.03</b>	<b>0.57</b>
25 MTHF_75HPC EXF A	0.64	32.67	11.25	49.70	42.50	32.41	41.17	74.91	10.08	1.57	0.59	0.97	1.08
25 MTHF_75HPC EXF B	0.79	38.20	12.44	54.38	50.27	40.86	51.24	91.13	9.41	1.59	0.60	0.93	1.91
25 MTHF_75HPC EXF C													
<b>Average</b>	<b>0.71</b>	<b>35.43</b>	<b>11.85</b>	<b>52.04</b>	<b>46.38</b>	<b>36.64</b>	<b>46.20</b>	<b>83.02</b>	<b>9.74</b>	<b>1.58</b>	<b>0.59</b>	<b>0.95</b>	<b>1.50</b>
<b>Min</b>	<b>0.64</b>	<b>32.67</b>	<b>11.25</b>	<b>49.70</b>	<b>42.50</b>	<b>32.41</b>	<b>41.17</b>	<b>74.91</b>	<b>9.41</b>	<b>1.57</b>	<b>0.59</b>	<b>0.93</b>	<b>1.08</b>
<b>Max</b>	<b>0.79</b>	<b>38.20</b>	<b>12.44</b>	<b>54.38</b>	<b>50.27</b>	<b>40.86</b>	<b>51.24</b>	<b>91.13</b>	<b>10.08</b>	<b>1.59</b>	<b>0.60</b>	<b>0.97</b>	<b>1.91</b>
<b>Standard Deviation</b>	<b>0.10</b>	<b>3.91</b>	<b>0.84</b>	<b>3.31</b>	<b>5.49</b>	<b>5.97</b>	<b>7.12</b>	<b>11.47</b>	<b>0.48</b>	<b>0.01</b>	<b>0.01</b>	<b>0.02</b>	<b>0.58</b>
50 MTHF_50HPC EXF A	0.49	25.97	14.59	51.51	38.04	29.77	46.66	67.81	8.27	1.28	0.50	0.95	1.06
50 MTHF_50HPC EXF B	0.91	42.29	8.71	52.47	53.60	42.51	39.38	96.11	11.09	2.16	0.86	0.99	0.77
50 MTHF_50HPC EXF C	0.73	36.31	11.47	52.10	46.93	37.03	45.33	83.96	9.90	1.63	0.66	0.96	1.28
<b>Average</b>	<b>0.71</b>	<b>34.86</b>	<b>11.59</b>	<b>52.03</b>	<b>46.19</b>	<b>36.44</b>	<b>43.79</b>	<b>82.63</b>	<b>9.75</b>	<b>1.69</b>	<b>0.67</b>	<b>0.97</b>	<b>1.04</b>
<b>Min</b>	<b>0.49</b>	<b>25.97</b>	<b>8.71</b>	<b>51.51</b>	<b>38.04</b>	<b>29.77</b>	<b>39.38</b>	<b>67.81</b>	<b>8.27</b>	<b>1.28</b>	<b>0.50</b>	<b>0.95</b>	<b>0.77</b>
<b>Max</b>	<b>0.91</b>	<b>42.29</b>	<b>14.59</b>	<b>52.47</b>	<b>53.60</b>	<b>42.51</b>	<b>46.66</b>	<b>96.11</b>	<b>11.09</b>	<b>2.16</b>	<b>0.86</b>	<b>0.99</b>	<b>1.28</b>
<b>Standard Deviation</b>	<b>0.21</b>	<b>8.25</b>	<b>2.94</b>	<b>0.48</b>	<b>7.81</b>	<b>6.39</b>	<b>3.88</b>	<b>14.19</b>	<b>1.42</b>	<b>0.44</b>	<b>0.18</b>	<b>0.02</b>	<b>0.25</b>
70MTHF_30HPC EXF A	0.57	29.71	10.96	47.50	39.39	29.04	37.74	68.44	10.35	1.54	0.60	0.98	0.64
70 MTHF_30HPC EXF B	0.61	31.33	8.90	45.37	39.69	28.24	31.68	67.93	11.44	1.78	0.70	0.96	1.07
70 MTHF_30HPC EXF C	0.67	33.91	8.96	47.19	42.32	31.04	33.64	73.36	11.27	1.85	0.73	0.96	1.29
<b>Average</b>	<b>0.62</b>	<b>31.65</b>	<b>9.61</b>	<b>46.68</b>	<b>40.47</b>	<b>29.44</b>	<b>34.35</b>	<b>69.91</b>	<b>11.02</b>	<b>1.72</b>	<b>0.67</b>	<b>0.97</b>	<b>1.00</b>
<b>Min</b>	<b>0.57</b>	<b>29.71</b>	<b>8.90</b>	<b>45.37</b>	<b>39.39</b>	<b>28.24</b>	<b>31.68</b>	<b>67.93</b>	<b>10.35</b>	<b>1.54</b>	<b>0.60</b>	<b>0.96</b>	<b>0.64</b>
<b>Max</b>	<b>0.67</b>	<b>33.91</b>	<b>10.96</b>	<b>47.50</b>	<b>42.32</b>	<b>31.04</b>	<b>37.74</b>	<b>73.36</b>	<b>11.44</b>	<b>1.85</b>	<b>0.73</b>	<b>0.98</b>	<b>1.29</b>
<b>Standard Deviation</b>	<b>0.05</b>	<b>2.12</b>	<b>1.17</b>	<b>1.15</b>	<b>1.61</b>	<b>1.44</b>	<b>3.09</b>	<b>3.00</b>	<b>0.59</b>	<b>0.16</b>	<b>0.07</b>	<b>0.01</b>	<b>0.33</b>
75MTHF_25HPC EXF A	0.81	39.08	10.77	52.83	50.23	40.03	45.26	90.26	10.20	1.77	0.62	0.92	2.22
75MTHF_25HPC EXF B	0.50	26.67	9.20	42.66	35.93	24.35	29.84	60.28	11.58	1.63	0.57	0.90	1.54
75MTHF_25HPC EXF C													
<b>Average</b>	<b>0.66</b>	<b>32.87</b>	<b>9.99</b>	<b>47.75</b>	<b>43.08</b>	<b>32.19</b>	<b>37.55</b>	<b>75.27</b>	<b>10.89</b>	<b>1.70</b>	<b>0.59</b>	<b>0.91</b>	<b>1.88</b>
<b>Min</b>	<b>0.50</b>	<b>26.67</b>	<b>9.20</b>	<b>42.66</b>	<b>35.93</b>	<b>24.35</b>	<b>29.84</b>	<b>60.28</b>	<b>10.20</b>	<b>1.63</b>	<b>0.57</b>	<b>0.90</b>	<b>1.54</b>
<b>Max</b>	<b>0.81</b>	<b>39.08</b>	<b>10.77</b>	<b>52.83</b>	<b>50.23</b>	<b>40.03</b>	<b>45.26</b>	<b>90.26</b>	<b>11.58</b>	<b>1.77</b>	<b>0.62</b>	<b>0.92</b>	<b>2.22</b>
<b>Standard Deviation</b>	<b>0.22</b>	<b>8.77</b>	<b>1.11</b>	<b>7.19</b>	<b>10.12</b>	<b>11.09</b>	<b>10.90</b>	<b>21.20</b>	<b>0.97</b>	<b>0.10</b>	<b>0.04</b>	<b>0.01</b>	<b>0.48</b>
MTHF A	0.53	27.97	13.30	50.30	39.12	30.10	44.25	69.21	9.02	1.36	0.47	0.86	1.97
MTHF B	0.83	39.56	8.53	50.43	37.85	27.85	36.22	86.96	11.25	2.09	0.72	0.98	1.04
MTHF C	0.94	43.27	6.58	50.83	53.36	41.37	30.47	94.73	11.99	2.72	0.94	0.97	1.47
<b>Average</b>	<b>0.77</b>	<b>36.94</b>	<b>9.47</b>	<b>50.52</b>	<b>47.19</b>	<b>36.44</b>	<b>36.98</b>	<b>83.63</b>	<b>10.76</b>	<b>2.06</b>	<b>0.71</b>	<b>0.94</b>	<b>1.50</b>
<b>Min</b>	<b>0.53</b>	<b>27.97</b>	<b>6.58</b>	<b>50.30</b>	<b>39.12</b>	<b>30.10</b>	<b>30.47</b>	<b>69.21</b>	<b>9.02</b>	<b>1.36</b>	<b>0.47</b>	<b>0.86</b>	<b>1.04</b>
<b>Max</b>	<b>0.94</b>	<b>43.27</b>	<b>13.30</b>	<b>50.83</b>	<b>53.36</b>	<b>41.37</b>	<b>44.25</b>	<b>94.73</b>	<b>11.99</b>	<b>2.72</b>	<b>0.94</b>	<b>0.98</b>	<b>1.97</b>
<b>Standard Deviation</b>	<b>0.21</b>	<b>7.98</b>	<b>3.46</b>	<b>0.28</b>	<b>7.31</b>	<b>5.77</b>	<b>6.92</b>	<b>13.08</b>	<b>1.55</b>	<b>0.68</b>	<b>0.24</b>	<b>0.07</b>	<b>0.47</b>

**Table D.4** iShear Data for Micronized Theophylline (MTHF): Hydroxypropylcellulose MF (HPC MF)

	Yield locus slope, TanFI [-]	Internal angle of friction, FI [deg]	Cohesion intercept, c [gm/cm <sup>2</sup> ]	Effective angle of friction, FIE [deg]	Average consolid. stress, $\sigma$ (avg) [gm/cm <sup>2</sup> ]	Deviatoric consolid. stress $\sigma$ (dev) [gm/cm <sup>2</sup> ]	Uniaxial compressive strength, fc [gm/cm <sup>2</sup> ]	Major consolidation stress, $\sigma$ 1 [gm/cm <sup>2</sup> ]	Minor consolidation stress, $\sigma$ 2 [gm/cm <sup>2</sup> ]	Relative flowability index, RI [-]	Absolute flowability index, AI [-]	Regression coefficient, [-]	Std. error [gm/cm <sup>2</sup> ]
HPC MF A	0.76	37.25	4.81	43.95	43.11	29.92	19.39	73.03	13.19	3.09	1.30	0.99	0.59
HPC MF B	0.81	38.94	5.11	45.72	45.45	32.54	21.41	77.99	12.91	3.04	1.30	1.00	0.27
HPC MF C	0.86	40.75	5.22	47.31	48.06	35.33	22.79	83.39	12.73	3.10	1.27	1.00	0.36
Average	0.81	38.98	5.05	45.66	45.54	32.60	21.20	78.14	12.94	3.08	1.29	1.00	0.41
Min	0.76	37.25	4.81	43.95	43.11	29.92	19.39	73.03	12.73	3.04	1.27	0.99	0.27
Max	0.86	40.75	5.22	47.31	48.06	35.33	22.79	83.39	13.19	3.10	1.30	1.00	0.59
Standard Deviation	0.05	1.75	0.21	1.68	2.48	2.70	1.71	5.18	0.23	0.03	0.02	0.00	0.16
25 MTHF_75HPC MF A	0.71	35.43	5.61	43.59	41.64	28.71	21.76	70.36	12.93	2.64	1.30	0.97	1.08
25 MTHF_75HPC MF B	0.78	37.88	5.42	45.28	44.35	31.51	22.17	75.87	12.84	2.84	1.42	0.98	0.89
25 MTHF_75HPC MF C													
Average	0.74	36.66	5.52	44.43	43.00	30.11	21.96	73.11	12.88	2.74	1.36	0.98	0.98
Min	0.71	35.43	5.42	43.59	41.64	28.71	21.76	70.36	12.84	2.64	1.30	0.97	0.89
Max	0.78	37.88	5.61	45.28	44.35	31.51	22.17	75.87	12.93	2.84	1.42	0.98	1.08
Standard Deviation	0.05	1.74	0.13	1.20	1.91	1.98	0.30	3.89	0.07	0.14	0.08	0.01	0.13
50 MTHF_50HPC MF A	0.70	34.94	7.90	46.41	42.73	30.95	30.32	73.68	11.78	2.04	1.07	0.96	1.35
50 MTHF_50HPC MF B	0.66	33.57	7.61	45.02	41.06	29.04	28.36	70.10	12.02	2.05	1.08	0.98	0.92
50 MTHF_50HPC MF C													
Average	0.68	34.26	7.75	45.72	41.89	29.99	29.34	71.89	11.90	2.05	1.08	0.97	1.13
Min	0.66	33.57	7.61	45.02	41.06	29.04	28.36	70.10	11.78	2.04	1.07	0.96	0.92
Max	0.70	34.94	7.90	46.41	42.73	30.95	30.32	73.68	12.02	2.05	1.08	0.98	1.35
Standard Deviation	0.02	0.97	0.21	0.99	1.18	1.35	1.39	2.53	0.17	0.00	0.01	0.01	0.30
70MTHF_30HPC MF A	0.52	27.61	11.08	46.42	37.64	27.27	36.61	64.90	10.37	1.49	0.59	0.93	1.27
70 MTHF_30HPC MF B	0.75	37.02	6.02	45.39	43.76	31.15	24.15	74.91	12.61	2.58	1.04	0.97	1.16
70 MTHF_30HPC MF C													
Average	0.64	32.32	8.55	45.91	40.70	29.21	30.38	69.90	11.49	2.03	0.81	0.95	1.21
Min	0.52	27.61	6.02	45.39	37.64	27.27	24.15	64.90	10.37	1.49	0.59	0.93	1.16
Max	0.75	37.02	11.08	46.42	43.76	31.15	36.61	74.91	12.61	2.58	1.04	0.97	1.27
Standard Deviation	0.16	6.65	3.58	0.73	4.33	2.75	8.81	7.07	1.58	0.77	0.31	0.03	0.08
75MTHF_25HPC MF A													
75MTHF_25HPC MF B	0.74	36.53	13.80	55.26	48.94	40.22	54.78	89.16	8.72	1.47	0.64	0.86	2.76
75MTHF_25HPC MF C	0.63	32.31	12.00	50.59	42.59	32.91	43.58	75.50	9.68	1.51	0.63	0.98	0.82
Average	0.69	34.42	12.90	52.93	45.77	36.56	49.18	82.33	9.20	1.49	0.64	0.92	1.79
Min	0.63	32.31	12.00	50.59	42.59	32.91	43.58	75.50	8.72	1.47	0.63	0.86	0.82
Max	0.74	36.53	13.80	55.26	48.94	40.22	54.78	89.16	9.68	1.51	0.64	0.98	2.76
MTHF A	0.53	27.97	13.30	50.30	39.12	30.10	44.25	69.21	9.02	1.36	0.47	0.86	1.97
MTHF B	0.83	39.56	8.53	50.43	49.11	37.85	36.22	86.96	11.25	2.09	0.72	0.98	1.04
MTHF C	0.94	43.27	6.58	50.83	53.36	41.37	30.47	94.73	11.99	2.72	0.94	0.97	1.47
Average	0.77	36.94	9.47	50.52	47.19	36.44	36.98	83.63	10.76	2.06	0.71	0.94	1.50
Min	0.53	27.97	6.58	50.30	39.12	30.10	30.47	69.21	9.02	1.36	0.47	0.86	1.04
Max	0.94	43.27	13.30	50.83	53.36	41.37	44.25	94.73	11.99	2.72	0.94	0.98	1.97
Standard Deviation	0.21	7.98	3.46	0.28	7.31	5.77	6.92	13.08	1.55	0.68	0.24	0.07	0.47

## APPENDIX E

### MERCURY INTRUSION POROSIMETRY: SUMMARY TABLES

The mercury intrusion porosimetry (MIP) data presented in Tables E.1 through E.9 was used as an alternate method to assess the sintering and binding that was occurring in the granules prepared using the Brabender batch mixer in section 4.4.2.

**Table E.1** Mercury Intrusion Data Summary for Raw Materials

	HPC EXF	HPC MF	MTHF	THF
Total Intrusion Volume (mL/g)	0.0289	0.0598	0.8814	0.8951
Total Pore Area (m <sup>2</sup> /g)	0.012	0.408	1.193	0.727
Median Pore Diameter (Volume) (μm)	9.6019	3.5511	2.7097	5.2484
Median Pore Diameter (Area) (μm)	10.0000	0.0456	2.4863	4.8332
Average Pore Diameter (4V/A) (μm)	9.2974	0.5856	2.9548	4.9229
Bulk Density at 18.09 psia (g/mL)	0.3236	0.4113	0.3568	0.4019
Apparent (skeletal) Density (g/mL)	0.3267	0.4217	0.5206	0.6278
Porosity (%)	0.9351	2.4584	31.4525	35.9778
Stem Volume Used (%)	93	76	93	93

**Table E.2** Mercury Intrusion Data Summary for Theophylline and Hydroxypropylcellulose Blends Prior to Batch Mixing (t=0).

Initial t=0	THF_HPC EXF	THF_HPC MF	MTHF_HPC EXF	MTHF_HPC MF
Total Intrusion Volume (mL/g)	0.9842	0.7617	0.7676	0.9261
Total Pore Area (m <sup>2</sup> /g)	0.889	0.719	0.843	1.405
Median Pore Diameter (Volume) (μm)	6.3117	5.5386	3.5824	2.9854
Median Pore Diameter (Area) (μm)	4.3709	4.2460	3.2636	2.3545
Average Pore Diameter (4V/A) (μm)	4.4305	4.2368	3.6418	2.6368
Bulk Density at 18.09 psia (g/mL)	0.4140	0.4892	0.3531	0.3968
Apparent (skeletal) Density (g/mL)	0.6988	0.7797	0.4844	0.6272
Porosity (%)	40.7518	37.2580	27.1030	36.7448
Stem Volume Used (%)	88	66	92	89

**Table E.3** Mercury Intrusion Data Summary for Applicable Theophylline and Hydroxypropylcellulose Blends at t=0.30 sec.

t=30 sec	THF_HPC EXF	THF_HPC MF	MTHF_HPC EXF	MTHF_HPC MF
Total Intrusion Volume (mL/g)	0.4697	0.3173	NA	NA
Total Pore Area (m <sup>2</sup> /g)	3.308	2.317	NA	NA
Median Pore Diameter (Volume) (μm)	1.3695	10863	NA	NA
Median Pore Diameter (Area) (μm)	0.2507	3533	NA	NA
Average Pore Diameter (4V/A) (μm)	0.5681	5478	NA	NA
Bulk Density at 18.09 psia (g/mL)	0.7485	0.8958	NA	NA
Apparent (skeletal) Density (g/mL)	1.1543	1.2515	NA	NA
Porosity (%)	35.1572	28.4246	NA	NA
Stem Volume Used (%)	30	20	NA	NA

**Table E.4** Mercury Intrusion Data Summary for Applicable Theophylline and Hydroxypropylcellulose Blends at  $t=1$  min.

$t=1$ min	THF_HPC EXF	THF_HPC MF	MTHF_HPC EXF	MTHF_HPC MF
Total Intrusion Volume (mL/g)	0.4436	0.2923	0.3032	0.5677
Total Pore Area (m <sup>2</sup> /g)	3.006	3.290	3.045	1.843
Median Pore Diameter (Volume) ( $\mu\text{m}$ )	0.9036	6924	0.6775	17911
Median Pore Diameter (Area) ( $\mu\text{m}$ )	0.4569	2166	0.2749	13108
Average Pore Diameter (4V/A) ( $\mu\text{m}$ )	0.5902	3553	0.3983	12323
Bulk Density at 18.09 psia (g/mL)	0.7925	0.8951	0.9053	0.6719
Apparent (skeletal) Density (g/mL)	1.2220	1.2123	1.2478	1.0863
Porosity (%)	35.1513	26.1637	27.4492	38.1435
Stem Volume Used (%)	26	19	20	39

**Table E.5** Mercury Intrusion Data Summary for Applicable Theophylline and Hydroxypropylcellulose Blends at  $t=1.5$  min.

$t=1.5$ min	THF_HPC EXF	THF_HPC MF	MTHF_HPC EXF	MTHF_HPC MF
Total Intrusion Volume (mL/g)	0.4089	0.3166	NA	NA
Total Pore Area (m <sup>2</sup> /g)	3.925	4.027	NA	NA
Median Pore Diameter (Volume) ( $\mu\text{m}$ )	0.7973	5680	NA	NA
Median Pore Diameter (Area) ( $\mu\text{m}$ )	0.2541	1965	NA	NA
Average Pore Diameter (4V/A) ( $\mu\text{m}$ )	0.4167	3145	NA	NA
Bulk Density at 18.09 psia (g/mL)	0.8059	0.8377	NA	NA
Apparent (skeletal) Density (g/mL)	1.2019	1.1402	NA	NA
Porosity (%)	32.9508	26.5257	NA	NA
Stem Volume Used (%)	26	21	NA	NA

**Table E.6** Mercury Intrusion Data Summary for Applicable Theophylline and Hydroxypropylcellulose Blends at  $t=2$  min.

Initial $t=2$ min	THF_HPC EXF	THF_HPC MF	MTHF_HPC EXF	MTHF_HPC MF
Total Intrusion Volume (mL/g)	0.2621	0.2390	0.0823	0.3203
Total Pore Area (m <sup>2</sup> /g)	5.331	4.933	3.378	2.765
Median Pore Diameter (Volume) ( $\mu\text{m}$ )	4319	3884	0.3231	9210
Median Pore Diameter (Area) ( $\mu\text{m}$ )	885	936	0.0178	2384
Average Pore Diameter (4V/A) ( $\mu\text{m}$ )	1966	1938	0.0975	4633
Bulk Density at 18.09 psia (g/mL)	0.9073	0.8779	1.0162	0.7701
Apparent (skeletal) Density (g/mL)	1.1903	1.1110	1.1090	1.0223
Porosity (%)	23.7764	20.9844	8.3660	24.6640
Stem Volume Used (%)	20	19	10	22

**Table E.7** Mercury Intrusion Data Summary for Applicable Theophylline and Hydroxypropylcellulose Blends at  $t=3$  min.

$t=3$ min	THF_HPC EXF	THF_HPC MF	MTHF_HPC EXF	MTHF_HPC MF
Total Intrusion Volume (mL/g)	NA	NA	0.0457	0.3016
Total Pore Area (m <sup>2</sup> /g)	NA	NA	4.587	3.541
Median Pore Diameter (Volume) ( $\mu\text{m}$ )	NA	NA	0.0541	7111
Median Pore Diameter (Area) ( $\mu\text{m}$ )	NA	NA	0.0206	1680
Average Pore Diameter (4V/A) ( $\mu\text{m}$ )	NA	NA	0.0399	3407
Bulk Density at 18.09 psia (g/mL)	NA	NA	1.1491	0.8549
Apparent (skeletal) Density (g/mL)	NA	NA	1.2128	1.1519
Porosity (%)	NA	NA	5.2527	25.7851
Stem Volume Used (%)	NA	NA	6	22

**Table E.8** Mercury Intrusion Data Summary for Applicable Theophylline and Hydroxypropylcellulose Blends at t=4 min.

t=4 min	THF_HPC EXF	THF_HPC MF	MTHF_HPC EXF	MTHF_HPC MF
Total Intrusion Volume (mL/g)	NA	NA	0.0655	0.2388
Total Pore Area (m <sup>2</sup> /g)	NA	NA	3.944	3.935
Median Pore Diameter (Volume) (μm)	NA	NA	0.3297	0.5907
Median Pore Diameter (Area) (μm)	NA	NA	0.0184	0.0942
Average Pore Diameter (4V/A) (μm)	NA	NA	0.0665	0.2427
Bulk Density at 18.09 psia (g/mL)	NA	NA	1.0939	0.8493
Apparent (skeletal) Density (g/mL)	NA	NA	1.1784	1.0653
Porosity (%)	NA	NA	7.1702	20.2814
Stem Volume Used (%)	NA	NA	8	21

**Table E.9** Mercury Intrusion Data Summary for Applicable Theophylline and Hydroxypropylcellulose Blends at t=5 min.

t=5 min	THF_HPC EXF	THF_HPC MF	MTHF_HPC EXF	MTHF_HPC MF
Total Intrusion Volume (mL/g)	NA	NA	0.0293	0.2506
Total Pore Area (m <sup>2</sup> /g)	NA	NA	3.071	4.308
Median Pore Diameter (Volume) (μm)	NA	NA	0.0510	0.8836
Median Pore Diameter (Area) (μm)	NA	NA	0.0204	0.0671
Average Pore Diameter (4V/A) (μm)	NA	NA	0.0382	0.2326
Bulk Density at 18.09 psia (g/mL)	NA	NA	1.2065	0.8649
Apparent (skeletal) Density (g/mL)	NA	NA	1.2508	1.1041
Porosity (%)	NA	NA	3.5406	21.6691
Stem Volume Used (%)	NA	NA	5	20

## REFERENCES

- Agassant JF, Baaijens F, Bastian H, Bernnat A, Bogaerds ACB, Coupeuz T, Debbaut B, Gavrus AL, Goublomme A, and van Gurp M, et al. 2002. The matching of experimental polymer processing flows to viscoelastic numerical simulation. *International Polymer Processing*; **17**(1):3- 10
- Alvarez JE, Snijder H, Vaneker T, Cheng H, Thornton AR, Luding S, and Weinhart T. 2022. Visco-elastic sintering kinetics in virgin and aged polymer powders. *Powder technology.*, 397.
- Bhugra C. and Pikal MJ. 2008. Role of thermodynamic, molecular, and kinetic factors in crystallization from the amorphous state. *Journal of Pharmaceutical Sciences*; **97**(4):p. 1329-1349.
- Cohen SC and Tabor D. 1966. The friction and lubrication of polymers. *Proceedings of the Royal Society of London Series A. Mathematical and Physical Sciences*; **291**(1425):186-207.
- Bravo VI, Hrymak AN, and Wright JD. 2000. Numerical simulation of pressure and velocity profiles in kneading elements of a Co-TSE. *Polymer Engineering and Science*; **40**(1):525-541
- Breitenbach J. 2002. Melt extrusion: from process to drug delivery technology. *European Journal of Pharmaceutics and Biopharmaceutics*; **54**(2):107-117.
- Breitenbach, J., 2006. Melt extrusion can bring new benefits to HIV therapy: the example of Kaletra tablets. *American Journal of Drug Delivery*; 4, 61-64.
- Carson, JW and Pittenger, BH. 1998. Bulk properties of powders. In: Lee PW, Trudel Y, Iacocca R, German RM, Ferguson BL, Eisen WB, Moyer K, Madan D, and Sanderow H editors. *Powder metal technology and applications*. Association of Materials-Centric Engineers and Scientists (ASM) International 7:p. 287-301
- Chokshi RJ, Sandhu HK, Iyer RM, Shah NH, Malick AW, and Zia H. 2005. Characterization of physico-mechanical properties of indomethacin and polymers to assess their suitability for hot-melt extrusion processes as a means to manufacture solid dispersion/solution. *Journal of Pharmaceutical. Sciences*; **94**(11): p. 2463-2474.
- Dankwerts, PV.1953. Mixing of thick liquids, pastes, and slurries. *Nature*.172, p. 846-877
- Dreiblatt, A. 2007. Process design. In: Ghebre-Sellassie, I., Martin C. editors. *Pharm. Extrusion Technical*. Informa Healthcare, New York, NY, p.153-169.
- Dreiblatt, A. 2013. Training Presentation Prepared for Polymer Center of Excellence. *Twin Screw Compounding*. Century Extrusion.



Ebube NK, Hikal AH, Wyandt CM, Beer DC, Miller LG, and Jones AB, Effect of drug, formulation and process variables on granulation and compaction characteristics of heterogeneous matrices Part 1: HPMC and HPC systems. 1997. *International Journal of Pharmaceutics*, **156**(1), p. 49-57

Ennis BJ, Witt W, Weinekötter R, Sphar D, Gommeran E, Snow R, Allen T, Raymus GJ, and Lister JD, 2008. Section 21, Control and design of granulation processes In: Don WG, Robert HP. editors. *Perry's Chemical Engineers' Handbook*. 8th ed. NY New York (NY): McGraw-Hill; p. 110-117.

Ennis BJ. 1996. Agglomeration and size enlargement session summary paper. *Powder Technol.*, 88(3):p. 203-225.

Esseghir M, Yu DW, Gogos CG, and Todd DB, 1997. Melting mechanisms of single-component polymers in co-rotating twin-screw kneading blocks through visual and microscopic analysis. Society of Plastic Engineers (SPE) Annual Technical Conference (ANTEC) Technical Papers. 3684-3689.

Freeman R. 2007. Measuring the flow properties of consolidated, conditioned and aerated powders - A comparative study using a powder rheometer and a rotational shear cell, *Powder Technology*; **174**(1-2):p. 25-33

Freeman T, Bey HV, Hanish M, Brockbank K, and Armstrong B, The influence of roller compaction processing variables on the rheological properties of granules. 2016. *Asian Journal of Pharmaceutical Sciences (AJPS)* **11**(4) p. 516-527.

Freeman technology: a micromeritics company. Powder Rheology: Why are powders complex, <https://www.freemantech.co.uk/learn/powder-rheology>, April 01, 2017.

Gogos CG, Esseghir M, Yu DW, Todd DB, and Curry J, 1994. The twin -screw mixing element evaluator: on-line performance evaluation of modular twin-screw mixing elements. Society of Plastic Engineers (SPE) Annual Technical Conference (ANTEC) Technical Papers. 270-276.

Gogos CG. 2012. Fundamentals of Dispersive and Distributive Mixing with Dissolution and Applications to Hot Melt Extrusion. Paper presented at: American Leistritz Hot Melt Extrusion Workshop; June 6-7; Somerville, NJ USA.

Hancock BC, York P, and Rowe RC. 1997. The use of solubility parameters in pharmaceutical dosage form design. *International Journal of Pharmaceutics*; **148**(1):1-21.

Hu Xinhui, Cunningham J, and Winstead D. 2008. Understanding and Predicting Bed Humidity in Fluidized Bed Granulation. *Journal of Pharmaceutical Sciences*. 97.4 : 1564-577.

iPowder Systems: Instruments for Powder Characterization,  
[http://www.powdernotes.com/innerframeset\\_ipowder/framemain\\_ipowdermain.html](http://www.powdernotes.com/innerframeset_ipowder/framemain_ipowdermain.html),  
May 06, 2022.

Ioannidis N. 2016. Polymer processing aspects of hot-melt extrusion. Polymer Processing Institute (PPI) capability presentation New Brunswick, NJ.

Kallakunta VR, Patil H, Tiwari R, Ye X, Upadhye S, Vladyka RS, Sarabu S, Kim DW, Bandari S, and Repka MA. 2019. Exploratory studies in heat-assisted continuous twin-screw dry granulation: A novel alternative technique to conventional dry granulation. *International Journal of Pharmaceutics*; 555:380-393.

Kim MH. 1999. Melting phenomena and mechanisms in polymer processing [dissertation]. Hoboken (NJ): Stevens Institute of Technology

Kim J-M, Lee U-H, Chang S-M, and Park JY. 2014. Gravimetric detection of theophylline on pore-structured molecularly imprinted conducting polymer. *Sensors and Actuators B: Chemical*. 200:25-30.

Klucel™ Hydroxypropylcellulose Physical and Chemical Properties. 2017. Ashland. p.1- 24

Kolter K, Kari M, Nalawade S, and Rottmann N, 2010. Hot-melt extrusion with BASF Pharma Polymers: Extrusion Compendium. BASF, Ludwigshafen, Germany.

Liu H. 2010. Hot melt mixing/extrusion and dissolution of drug (indomethacin) in acrylic copolymer matrices [dissertation]. Newark (NJ): New Jersey Institute of Technology.

Liu Y, Thompson MR, O'Donnell, KP, Ali S. 2017. Heat assisted twin screw dry granulation. *AIChE Journal*; **63**(11):4748-4760.

Martin C. 2011. Understanding Hot Melt Extrusion and Developments for Pharmaceutical Applications. Paper presented at: American Leistritz Hot Melt Extrusion Workshop; June 15-16; Somerville, NJ USA.

Maddock, BH. 1959. A visual analysis of flow and mixing in extruder screws. Society of Plastic Engineers (SPE) Annual Technical Conference (ANTEC) Technical Papers. 383- 389

Mahlin D and Bergström CAS. 2013. Early drug development predictions of glass-forming ability and physical stability of drugs. *European Journal of Pharmaceutical Sciences*; **49**(2) p.323-332.

Masuda H, Gotoh K. 1997. Adhesive Force of a Single Particle. In: Gotoh K, Masuda H, Higashitani K. editors. *Powder technology handbook*. 2nd ed. Basel (NY): Marcel Dekker; p. 133-142.

Mohammed N, Majumdar S., Singh A, Deng W, Murthy NS, Pinto E, and Repka MA. 2012. Klucel™ EF and ELF polymers for immediate-release oral dosage forms prepared by melt extrusion technology. *American Association of Pharmaceutical Scientists (AAPS) PharmSciTech*; **13**(4), 1158-1169.

Monteyne T, Heeze L, Mortier ST, Oldorp K, Nopens I, Remon JP, Vervaet C, and De Beer T. 2016. The use of rheology to elucidate the granulation mechanisms of a miscible and immiscible system during continuous twin-screw melt granulation. *International Journal of Pharmaceutics*; **510**(1):271-284.

Narang AS, Tao L, Zhao J, Keluskar R, Gour S, Stevens T, Macias K, Remy B, Pandey P, LaRoche RD et al. 2019. Chapter 10 - Effect of binder attributes on granule growth and densification. In: Narang AS, Badawy SIF, editors. *Handbook of Pharmaceutical Wet Granulation*. Academic Press; p. 351-386.

Okuyama K. 1997. Sintering. In: Gotoh K, Masuda H, and Higashitani K. editors. *Powder Technology HB*. 2nd ed. Basel (NY): Marcel Dekker; p. 193-200.

Okuyama K and Higashitani K. 1997. Agglomeration (Coagulation). In: Gotoh K, Masuda H, and Higashitani K. editors. *Powder Technology*. HB. 2nd ed. Basel (NY): Marcel Dekker; p. 155-174.

Pafiakis S, Jones J, Escotet M, Ioannidis N, Chan S, Won B, Macias K, Keluskar R, Martin K, and Trinh J, et al. 2015. Investigation of a suitable lubricant for increasing slip in a continuous, co-rotating twin screw dry granulation process. Poster session presented at: American Institute of Chemical Engineers (AIChE) Annual Meeting; Nov 7-11; Salt Lake City, UT.

Pafiakis S, Trinh J, Martin K, Keluskar R; Levins C, Jones J, Allenspach C, Stamato H, and Raghavan K. 2016. Twin Screw Granulation: A case study for enabling an adaptive Study plan to ensure process robustness and on-time clinical supplies manufacture for a product with break-through designation. Paper presented at: American Association of Pharmaceutical Scientist (AAPS) Annual Meeting and Exposition; Nov 13-17; Denver, CO.

Pafiakis S, Armenante P, and Gogos C. 2022. The influence of input material properties on hot melt granules prepared using a counter-rotating batch mixer. *Pharmaceutical Development and Technology*; **27**(9):1-17.

Palzer S. 2011. Agglomeration of pharmaceutical, detergent, chemical and food powders - Similarities and differences of materials and processes. *Powder Technology* **206** (1- 2):2- 17.

Peeters E, Fonteyne M, Cappuyens P, Delaet U, Van Assche I, De Beer T, Remon J.P, and Vervaet C. 2015 Use of a continuous twin screw granulation and drying system during formulation development and process optimization, *European Journal of Pharmaceutics and Biopharmaceutics*; (89) p. 239-247.

Picker-Freyer K M and Dürig T, 2007. Physical mechanical and tablet formation properties of hydroxypropyl cellulose: In pure form and in mixtures. *American Associates of Pharmaceutical Scientists (AAPS) PharmSciTech*; **8**(4) Article 92.

Roberts AW. 2005. Characterization for hopper and stockpile design. In: McGlinchey D, editor. *Characterization Bulk Solids*. Oxford (UK): Blackwell Publishing; p. 85–131.

Shah UV, Karde V, Ghoroi C, and Heng JYY. 2017. Influence of particle properties on powder bulk behavior and processability. *International Journal of Pharmaceutics*. **518**(1):138-154.

Snow RH, Allen T, Ennis BJ, and Litster JD. 1997. Section 20, Size reduction and size enlargement. In: Green D and Perry RH, editors. *Perry's Chemical Engineers' Handbook*. 7th ed. New York (NY): McGraw-Hill; p. 1-89.

Sirasitthichoke C, Salloum S, and Armenante PM. 2022. Power number and hydrodynamic characterization of a stirred vessel equipped with a Retreat-Blade Impeller and different types of pharmaceutical single baffles. *Chemical Engineering Science*; 257 p. 1-26.

Sperling LH. 2006. *Introduction to Physical Polymer Science*. Hoboken (NJ): Wiley-Interscience. Chapter 8, Glass-Rubber Transition Behavior; p.349-425.

Steiner R. 2007. Extruder Design. In: Ghebre-Sellassie, I and Martin C. editors. *Pharmaceutical Extrusion Technology*. Informa Healthcare, New York, NY, p.19-38.

Sullad AG, Manjeshwar LS, and Aminabhavi TM. 2010. Polymeric blend microspheres for controlled release of theophylline, *Journal of Applied Polymer Science* 117 1361– 1370.

Suzuki M. 1997. Description of particulate assemblies. In: Gotoh K, Masuda H, and Higashitani K. editors. *Powder technology handbook*. 2nd ed. Basel (NY): Marcel Dekker; p. 305-320.

Tadmor Z and Gogos CG. 2006. *Principles of Polymer Processing*. Hoboken (NJ): Wiley-Interscience. Chapter 4, The handling and transporting of polymer particulate solids; p. 144-177.

Tadmor Z and Gogos CG. 2006. *Principles of Polymer Processing*. Hoboken (NJ): Wiley-Interscience. Chapter 5, Melting; p. 178-234.

Tadmor Z and Gogos CG. 2006. Principles of Polymer Processing. Hoboken (NJ): Wiley-Interscience. Chapter 7, Mixing; p. 322-408.

Tadmor Z and Gogos CG. 2006. Principles of Polymer Processing. Hoboken (NJ): Wiley-Interscience. Chapter 10, Twin Screw and Twin Rotor Processing Equipment; p. 523-602

Terife G. 2013. Foaming of amorphous drug delivery systems prepared by hot met mixing and extrusion [dissertation] Newark (NJ): New Jersey Institute of Technology.

Thiel W. 2007. Twin-screw extrusion and Screw design. In: Ghebre-Sellassie, I and Martin C. editors. Pharmaceutical Extrusion Technology. Informa Healthcare, New York, NY, p.69-98.

Theophylline Anhydrous Ph. Eur., USP, JP Technical Information. 2009. Care Chemicals Division - Pharma Ingredients and Services - 67117 Limburgerhof - [www.pharma-ingredients.basf.com](http://www.pharma-ingredients.basf.com).

Trinh J, Pafiakis S, Keluskar R, Martin K, Levins C, Jones J, Stamato H, Ioannidis N, Peng C, and Gogos C. 2015. The development of a suitable screw configuration for the use in a continuous, co-rotating twin screw dry granulation process. Poster session presented at: American Institute of Chemical Engineers (AIChE) Annual Meeting; Nov 7-11; Salt Lake City, UT.

Valsamis LN and Canedo EL. 1991. Effect of rotor geometry and operating conditions on mixing performance in continuous mixers: an experimental study, Society of Plastic Engineers (SPE) Annual Technical Conference (ANTEC) Technical Papers. 629-632.

Valsamis LN and Canedo EL. 1994. Mixing in the Farrel continuous mixer. In: Manas-Zloczower I, and Tadmor Z, editors. Mixing and compounding: theory and practice. Munich (DE): Hanser, p. 1-89.

Vanhoorne V, Janssens L, Vercruyse J, De Beer T, Remon JP, and Vervaet C. 2016. Continuous twin screw granulation of controlled release formulations with various HPMC grades. International Journal of Pharmaceutics; **511**(2):1048-1057.

Vercruyse J, Peeters E, Fonteyne M, Cappuyns P, Delaet U, Van Assche I, De Beer T, Remon JP, and Vervaet C. 2015. Use of a continuous twin screw granulation and drying system during formulation development and process optimization, European Journal of Pharmaceutics and Biopharmaceutics; **89**(1):239-247.

Wang T, Randviir EP, and Banks CE. 2014. Detection of theophylline utilizing portable electrochemical sensors. Royal Society of Chemistry (RSC). 139 p.2000-2003

Wilcox RA, Deyoe CW, Pfost HB. 1970. A Method for determining and expressing the Size of feed particles by sieving. Poultry Science. **49**(1):9-13.